

LOCKHEED MARTIN ENERGY RESEARCH LIBRARIES



3 4456 0515775 4

CENTRAL RESEARCH LIBRARY
DOCUMENT COLLECTION

2y. 193

ORNL-4592
UC-34 -- Physics

OAK RIDGE NATIONAL LABORATORY
CENTRAL RESEARCH LIBRARY
DOCUMENT COLLECTION

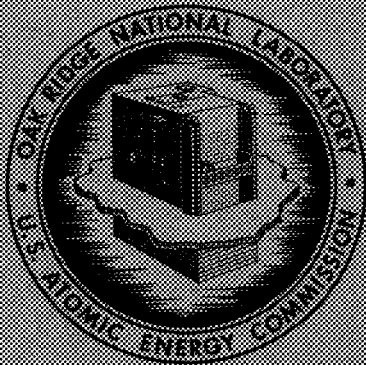
LIBRARY LOAN COPY

DO NOT TRANSFER TO ANOTHER PERSON

If you wish someone else to see this document, send in name with document and the library will arrange a loan

15-72207
15-72208

NEUTRON PHYSICS DIVISION
ANNUAL PROGRESS REPORT
FOR PERIOD ENDING MAY 31, 1970



OAK RIDGE NATIONAL LABORATORY

operated by

UNION CARBIDE CORPORATION

for the

U.S. ATOMIC ENERGY COMMISSION

Printed in the United States of America. Available from Clearinghouse for Federal
Scientific and Technical Information, National Bureau of Standards,
U.S. Department of Commerce, Springfield, Virginia 22151
Price: Printed Copy \$3.00; Microfiche \$0.65

LEGAL NOTICE

This report was prepared as an account of Government sponsored work. Neither the United States, nor the Commission, nor any person acting on behalf of the Commission:

- A. Makes any warranty or representation, expressed or implied, with respect to the accuracy, completeness, or usefulness of the information contained in this report, or that the use of any information, apparatus, method, or process disclosed in this report may not infringe privately owned rights; or
 - B. Assumes any liabilities with respect to the use of, or for damages resulting from the use of any information, apparatus, method, or process disclosed in this report.
- As used in the above, "person acting on behalf of the Commission" includes any employee or contractor of the Commission, or employee of such contractor, to the extent that such employee or contractor of the Commission, or employee of such contractor prepares, disseminates, or provides access to, any information pursuant to his employment or contract with the Commission, or his employment with such contractor.

ORNL-4592
UC-34 -- Physics

Contract No. W-7405-eng-26

**NEUTRON PHYSICS DIVISION
ANNUAL PROGRESS REPORT
For Period Ending May 31, 1970**

F. C. Maienschein, Director
R. G. Alsmiller, Associate Director
C. E. Clifford, Associate Director
R. W. Peelle, Associate Director

SEPTEMBER 1970

OAK RIDGE NATIONAL LABORATORY
Oak Ridge, Tennessee
operated by
UNION CARBIDE CORPORATION
for the
U. S. ATOMIC ENERGY COMMISSION

LOCKHEED MARTIN ENERGY RESEARCH LIBRARIES



3 4456 0515775 4

Reports previously issued in this series are as follows:

ORNL-2081	Period Ending September 10, 1956
ORNL-2389	Period Ending September 1, 1957
ORNL-2609	Period Ending September 1, 1958
ORNL-2842	Period Ending September 1, 1959
ORNL-3016	Period Ending September 1, 1960
ORNL-3193	Period Ending September 1, 1961
ORNL-3360	Period Ending September 1, 1962
ORNL-3499, Vols. I and II	Period Ending August 1, 1963
ORNL-3714, Vols. I and II	Period Ending August 1, 1964
ORNL-3858, Vols. I and II	Period Ending August 1, 1965
ORNL-3973, Vols. I and II	Period Ending May 31, 1966
ORNL-4134	Period Ending May 31, 1967
ORNL-4280	Period Ending May 31, 1968
ORNL-4433	Period Ending May 31, 1969

Contents

1. NEUTRON CROSS SECTIONS	1
1.0 Introduction — F. C. Maienschein	1
1.1 Measurements of the Neutron Fission and Absorption Cross Sections of ^{239}Pu Over the Energy Region 0.02 eV to 30 keV, Part II — R. Gwin, L. W. Weston, G. de Saussure, R. W. Ingle, J. H. Todd, F. E. Gillespie, R. W. Hockenbury, and R. C. Block	1
1.2 Measurements of the Neutron Capture and Fission Cross Sections for ^{239}Pu at ORELA — R. Gwin, L. W. Weston, R. W. Ingle, and H. Weaver	2
1.3 Measurement of the Capture Cross Section of ^{238}U up to 100 keV — G. de Saussure, E. G. Silver, R. W. Ingle, R. B. Perez, and H. Weaver	6
1.4 Measurement of Eta and the Fission and Total Cross Sections for ^{233}U Below 1 eV — L. W. Weston and J. H. Todd	11
1.5 Analytical Description of the Neutron Cross Sections of ^{233}U Below 60 eV — G. de Saussure	12
1.6 Autocorrelation Technique for Determining the Average Level Spacing of the Intermediate Subthreshold Structure in the Fission Cross Section of ^{235}U and ^{239}Pu — G. de Saussure, R. B. Perez, and M. N. Moore	13
1.7 Multilevel Effects in Fissile Cross Sections — R. B. Perez and G. de Saussure	13
1.8 SUPERPOLLA, A Program to Generate the Statistical Distribution of the <i>S</i> -Matrix Parameters — R. B. Perez and G. de Saussure	15
1.9 MSC, A Program to Evaluate Multiple Scattering Corrections in Thick Samples — N. M. Greene, R. B. Perez, G. de Saussure, and S. K. Penny	18
1.10 Determination of Heterogeneous Parameters by the Neutron Wave Technique — E. A. Bernard and R. B. Perez	21
1.11 A General Formalism for the <i>T</i> Matrix of Nuclear Reaction Theory — R. B. Perez and J. Mockel	22
1.12 The Absolute Spectrum of Photons Emitted in Coincidence with Thermal-Neutron Fission of ^{235}U — R. W. Peelle and F. C. Maienschein	23
1.13 Oak Ridge Electron Linear Accelerator (ORELA) — N. A. Betz, A. L. Boch, J. A. Harvey, T. A. Lewis, F. C. Maienschein, J. W. Reynolds, and H. A. Todd	24
1.14 Pulse-Shape Measurements for the Oak Ridge Electron Linear Accelerator with Gamma-Ray Detection Techniques — L. W. Weston and J. H. Todd	27
1.15 Fast Fission Chamber Amplifier-Discriminator System — R. W. Ingle, F. E. Gillespie, and L. W. Weston	27
1.16 11-MeV Proton Inelastic Scattering from Even-Even Medium-Weight Nuclei — C. M. Perey, R. J. Silva, J. K. Dickens, and F. G. Perey	28

1.17	Isobaric Spin Dependence in Proton Transfer Reactions — R. G. Couch, F. G. Perey, J. A. Biggerstaff, and K. K. Seth	28
1.18	Measurements of (d,n) Reactions on ^{58}Ni , ^{60}Ni , ^{62}Ni , and ^{64}Ni at 5 and 10 MeV — A. L. Marusak	28
1.19	Spectroscopy of $^{65,67,69}\text{Ga}$ by (d,n) Reaction — R. G. Couch, J. A. Biggerstaff, F. G. Perey, S. Raman, and K. K. Seth	29
1.20	Finite-Sample Corrections to Neutron Scattering Data — W. E. Kinney	29
1.21	Neutron Elastic- and Inelastic-Scattering Cross Sections for Sodium in the Range of 5.4 to 8.5 MeV — F. G. Perey and W. E. Kinney	29
1.22	Calcium Neutron Elastic- and Inelastic-Scattering Cross Sections from 4.0 to 8.5 MeV — F. G. Perey and W. E. Kinney	29
1.23	Sulfur Neutron Elastic- and Inelastic-Scattering Cross Sections from 4.0 to 8.5 MeV — F. G. Perey and W. E. Kinney	30
1.24	Neutron Elastic- and Inelastic-Scattering Cross Sections for Cobalt in the Energy Range 4.19 to 8.56 MeV — W. E. Kinney and F. G. Perey	30
1.25	Neutron Elastic- and Inelastic-Scattering Cross Sections for Magnesium in the Energy Range 4.19 to 8.56 MeV — W. E. Kinney and F. G. Perey	30
1.26	Carbon Neutron Elastic- and Inelastic-Scattering Cross Sections from 4.5 to 8.5 MeV — F. G. Perey and W. E. Kinney	30
1.27	^{60}Ni Neutron Elastic- and Inelastic-Scattering Cross Sections from 6.5 to 8.5 MeV — F. G. Perey, C. O. Le Rigoleur, and W. E. Kinney	30
1.28	Neutron Elastic- and Inelastic-Scattering Cross Sections for Silicon in the Energy Range 4.19 to 8.56 MeV — W. E. Kinney and F. G. Perey	31
1.29	Neutron Elastic- and Inelastic-Scattering Cross Sections for ^{56}Fe in the Energy Range 4.19 to 8.56 MeV — W. E. Kinney and F. G. Perey	31
1.30	A Monoenergetic 6130-keV Gamma-Ray Source for Detector Calibration — J. K. Dickens and R. D. Baybarz	31
1.31	Comparison of a Method for Measuring $(n,x\gamma)$ Cross Sections Using a Pulsed Van de Graaff Accelerator with a Method Using an Electron Linac — J. K. Dickens and F. G. Perey	31
1.32	The $^{14}\text{N}(n,x\gamma)$ Reaction for $8.5 \leq E_n \leq 11$ MeV — J. K. Dickens and F. G. Perey	31
1.33	The $^{16}\text{O}(n,x\gamma)$ Reaction for $6.7 \leq E_n \leq 11$ MeV — J. K. Dickens and F. G. Perey	32
1.34	$^{28-30}\text{Si}(n,x\gamma)$ Reactions for $5.3 \leq E_n \leq 9.0$ MeV — J. K. Dickens	32
1.35	The $\text{Fe}(n,x\gamma)$ Reaction for $5.35 \leq E_n \leq 9.0$ MeV — J. K. Dickens and F. G. Perey	32
1.36	Calculated ^{56}Fe Neutron Elastic and Inelastic Scattering and Gamma-Ray Production Cross Sections from 1.0 to 7.6 MeV — W. E. Kinney and F. G. Perey	35
1.37	A Reevaluation of Natural Iron Neutron and Gamma-Ray Production Cross Sections, ENDF/B Material 1124 — S. K. Penny and W. E. Kinney	35
2.	REACTOR AND WEAPONS RADIATION SHIELDING	36
2.0	Introduction — C. E. Clifford	36

2.1	The MORSE Code --- A Multigroup Neutron and Gamma-Ray Monte Carlo Transport Code -- E. A. Straker, P. N. Stevens, V. R. Cain and D. C. Irving	37
2.2	SAMBO, A Collision Analysis Package for Monte Carlo Codes -- V. R. Cain	37
2.3	A Review of Some Recent Multidimensional Discrete Ordinates Shielding Calculations -- F. R. Mynatt	37
2.4	A Study of the Overlap Conditions and Resulting Accuracy Obtained in Sequential Discrete Ordinates Transport Calculations for a Point Source in a 5000-m Radius Sphere of Air -- J. V. Pace and F. R. Mynatt	38
2.5	O6R-ACTIFK, Monte Carlo Neutron Transport Code -- C. L. Thompson and E. A. Straker	39
2.6	O6R-D, A Discrete Scattering Version of O6R with Importance Sampling of the Angle of Scatter -- C. E. Burgart	39
2.7	A General Method of Importance Sampling the Angle of Scattering in Monte Carlo Calculations -- C. E. Burgart and P. N. Stevens	39
2.8	Treatment of ${}^6\text{Li}(n, dn)\alpha$, ${}^7\text{Li}(n, tn)\alpha$ Reactions in O6R Random Walk and Analysis -- C. E. Burgart	40
2.9	The Adjoint Boltzmann Equation and Its Simulation by Monte Carlo -- D. C. Irving	40
2.10	PLOTTER, A General-Purpose Plotting Routine -- D. C. Irving and H. S. Moran	40
2.11	PICTURE: An Aid in Debugging Geom Input Data -- D. C. Irving and G. W. Morrison	40
2.12	Neutron-Energy-Dependent Capture Gamma-Ray Yields in ${}^{238}\text{U}$ -- R. S. Booth, K. J. Yost, F. J. Muckenthaler, J. E. White, and S. K. Penny	41
2.13	The Total Gamma-Ray Energy Spectrum Above 1 MeV from Neutron Interactions in ${}^{235}\text{U}$ and ${}^{238}\text{U}$ -- R. S. Booth and F. J. Muckenthaler	41
2.14	A Comparison of Folding and Unfolding Techniques for Determining the Gamma Spectrum from Thermal-Neutron Capture in Aluminum -- R. S. Booth	41
2.15	Analysis of Proportional Counter Pulse-Height Spectra -- R. M. Freestone, Jr.	41
2.16	The Calculation of Gamma-Ray Transition Probabilities in Odd- <i>A</i> Nuclei -- K. J. Yost, P. H. Pitkanen, and C. Y. Fu	42
2.17	A Unified Model of Deformed Odd-Odd Nuclei for Nuclear Data Generation and Analysis -- C. Y. Fu and K. J. Yost	42
2.18	The Application of Extended <i>R</i> -Matrix Theory to Elastic Scattering of Neutrons by ${}^{12}\text{C}$ -- K. J. Yost and P. H. Pitkanen	43
2.19	Neutron Energy-Dependent Capture Gamma-Ray Yields for ${}^{181}\text{Ta}$ -- K. J. Yost, J. E. White, and C. Y. Fu	44
2.20	A Bootstrap Method for the Calculation of High-Lying Nuclear Levels and Electromagnetic Moments (I). Theory -- K. Kumar	46
2.21	A Bootstrap Method for the Calculation of High-Lying Nuclear Levels and Electromagnetic Moments (II). Application to ${}^{13}\text{C}$ and ${}^{209}\text{Pb}$ -- K. Kumar, K. J. Yost, and C. Y. Fu	46
2.22	Collective Treatment of the Pairing Hamiltonian (I). Formulation of the Model -- D. R. Bès, R. A. Broglia, R. P. J. Perazzo, and K. Kumar	48
2.23	The Prolate-Oblate Difference and Its Effect on Energy Levels and Quadrupole Moments -- K. Kumar	48

2.24	UKE -- A Computer Program for Translating Neutron Cross-Section Data from the UKAEA Nuclear Data Library to the Evaluated Nuclear Data File Format -- R. Q. Wright, S. N. Cramer, and D. C. Irving	50
2.25	Reactor Radiation Shielding Program at the Tower Shielding Facility -- C. E. Clifford, F. J. Muckenthaler, K. M. Henry, J. L. Hull, and L. B. Holland	50
2.26	LMFBR Shielding Development Program -- Interim Report: Preliminary Evaluation of Techniques for Predicting the Spectra of Neutrons Transmitted by Grid Plate Shields -- C. E. Clifford, F. R. Mynatt, and H. C. Claiborne	51
2.27	Neutron Transport in Iron -- F. R. Mynatt, F. J. Muckenthaler, M. L. Gritzner, E. A. Straker, R. Q. Wright, L. R. Williams, and R. M. Freestone, Jr.	52
2.28	Comparisons of Monte Carlo Calculations with Measurements of Neutron Leakage from the TSF-SNAP Reactor -- V. R. Cain	52
2.29	The Importance Distribution of Neutron Reactions Relative to Their Contribution to the Secondary Gamma-Ray Dose Transmitted by Tungsten and Laminated Lithium Hydride and Tungsten Shields -- J. V. Pace and F. R. Mynatt	52
2.30	Gamma-Ray Spectra Arising from Fast-Neutron Interactions in Elements Found in Soils, Concretes, and Structural Materials -- R. E. Maerker and F. J. Muckenthaler	53
2.31	Gamma-Ray Spectra Arising from Thermal-Neutron Capture in Elements Found in Soils, Concretes, and Structural Materials -- R. E. Maerker and F. J. Muckenthaler	53
2.32	Gamma-Ray Spectra Arising from Fast-Neutron Interactions in Iron, Aluminum, Copper, Zinc, and Titanium -- R. E. Maerker and F. J. Muckenthaler	53
2.33	The POPOP4 Library of Secondary Gamma-Ray Data -- W. E. Ford III	54
2.34	The Use and "Testing" of Al, Fe, Ni, Cu, and Pb Secondary Gamma-Ray Production Data Sets from the POPOP4 Library -- W. E. Ford III and D. H. Wallace	54
2.35	Simultaneous Fast-Neutron Spectral Measurements by Time-of-Flight and Pulse-Height Unfolding Techniques -- E. A. Straker, C. E. Burgart, T. A. Love, and R. M. Freestone, Jr.	55
2.36	Measurement of Time-Dependent Gamma-Ray Spectra from Polyethylene -- C. E. Burgart, T. A. Love, R. M. Freestone, Jr., and E. A. Straker	56
2.37	The Energy Spectrum of Photoneutrons Produced by 140-MeV Electrons Incident on Tantalum -- C. E. Burgart, E. A. Straker, T. A. Love, and R. M. Freestone, Jr.	58
2.38	Time-Dependent Coupled Neutron-Gamma Calculations in Polyethylene -- C. E. Burgart and W. W. Engle, Jr.	58
2.39	On-Line Data-Acquisition and Treatment Programs for a PDP-9 Computer -- R. M. Freestone, Jr., and C. E. Burgart	59
2.40	Design Considerations for an ORELA Target Using Tantalum Followed by Beryllium -- R. S. Booth	59
2.41	A Tantalum-Beryllium Target for ORELA -- J. Lewin	60
2.42	Time-Dependent Neutron and Secondary Gamma-Ray Transport in Infinite Air and in Air over Ground -- E. A. Straker	60

2.43	Neutron and Secondary Gamma-Ray-Induced Heat in the Ground Due to Point 12.2-to-15-MeV and Fission Sources at an Altitude of 50 ft -- E. A. Straker, M. B. Emmett, and M. L. Gritzner	60
2.44	Ground Heating Due to a Point Source of 12.2-to-15-MeV Neutrons at an Altitude of 50 ft -- E. A. Straker, M. B. Emmett, and C. L. Thompson	62
2.45	Sensitivity of Secondary Gamma-Ray Dose to Angular Distribution of Gamma Rays from Neutron Inelastic Scattering -- E. A. Straker	62
2.46	Status of Neutron Transport in the Atmosphere -- E. A. Straker	62
2.47	A FORTRAN-360 Subroutine Package for Producing Printed Linear, Semilogarithmic or Logarithmic Graphs -- C. L. Thompson	62
2.48	Dose Rates in a Slab Phantom from Monoenergetic Gamma Rays -- H. C. Claiborne and D. K. Trubey	63
2.49	Project Safeguard -- H. C. Claiborne	63
2.50	The Calculation of Neutron-Induced Physical Doses in Human Tissues -- J. J. Ritts, M. Solomito, and P. N. Stevens	63
2.51	Differential Neutron and Secondary Gamma-Ray Albedos for Steel-Covered Concrete Slabs: Vols. I--VI -- M. B. Wells and J. D. Marshall	63
2.52	Analysis of Initial Radiation Protection Aboard Ship -- R. L. French and J. M. Newell	64
2.53	Prediction of Nuclear Weapon Neutron Radiation Environments -- R. L. French and L. G. Mooney	64
2.54	Calculations of Weapon Radiation Doses in Single-Compartment Above-Ground Concrete Structures -- L. G. Mooney	65
2.55	Analysis of Initial Radiation Protection Aboard the CVA-66 -- R. L. French, L. G. Mooney, J. M. Newell, and N. M. Schaeffer	65
2.56	System of Ship Shielding Codes -- J. M. Newell, R. L. French, R. Kimmell, and J. K. Warkentin	65
2.57	Weapons Radiation Shielding Handbook: Status Report -- L. S. Abbott, H. C. Claiborne, and C. E. Clifford, Editors	66
3.	RADIATION SHIELDING INFORMATION CENTER	67
3.1	Recent Developments in RSIC Operations -- D. K. Trubey, Betty F. Maskewitz, and R. W. Roussin	67
3.2	The Radiation Shielding Information Center -- A Technical Information Service for Nuclear Engineers -- D. K. Trubey	72
3.3	Computer Codes for Shielding Calculations -- 1969 -- D. K. Trubey and Betty F. Maskewitz	72
3.4	The Information Analysis Center Concept as Developed by the Radiation Shielding Information Center in Its Computer Codes Activities -- B. F. Maskewitz, D. K. Trubey, H. E. Comolander, H. R. Hendrickson, I. J. Brown, R. W. Roussin, V. A. Jacobs, C. M. Anthony, J. Gurney, M. W. Landay, and A. B. Gustin	72

3.5	The 1969 RSIC Computer-Based Information Retrieval System in Brief -- J. G. Jones, D. K. Trubey, and J. Gurney	74
3.6	Abstracts of Digital Computer Code Packages Assembled by the Radiation Shielding Information Center -- Betty F. Maskewitz	75
3.7	Shielding Benchmark Problems -- A. E. Profio (Editor)	75
3.8	The Attenuation Properties of Concrete for Shielding of Neutrons of Energy Less than 15 MeV -- F. A. R. Schmidt	75
3.9	A Review of Multigroup Nuclear Cross-Section Preparation -- Theory, Techniques, and Computer Codes -- D. K. Trubey and Jane Gurney, Compilers	76
3.10	Comparisons of the Results Obtained with Several Electron-Penetration Codes -- W. Wayne Scott	76
3.11	Kernel Methods for Radiation Shielding Calculations -- D. K. Trubey	77
3.12	Adjoint S_N Calculations of Coupled Neutron, Gamma-Ray Transport Through Concrete Slabs -- R. W. Roussin and F. A. R. Schmidt	77
3.13	Gamma-Ray Buildup Factor Coefficients for Concrete and Other Materials -- D. K. Trubey	78
3.14	UKE -- A Computer Program for Translating Neutron Cross-Section Data from the UKAEA Nuclear Data Library to the Evaluated Nuclear Data File Format -- R. O. Wright, S. N. Cramer, and D. C. Irving	78
3.15	OGRE Cross-Section Package for Using Photon Interaction Data in ENDF/B Format -- D. K. Trubey and J. R. Stockton	78
3.16	OGRE Mastape -- Photon Interaction Cross-Section Library and Data Handling Code -- D. K. Trubey and H. E. Francis	79
3.17	Using ANISN to Reduce the DLC-2 100-Group Cross-Section Data to a Smaller Number of Groups -- R. W. Roussin	79
3.18	JRMACRO: A Program for Converting Microscopic Multigroup, P_n Expansion Cross-Section Data into Corresponding Macroscopic Data for Mixtures or Compounds -- J. J. Ritts, R. W. Roussin, and I. J. Brown	79
3.19	Calculated Data for Inclusion in the Space Shielding Handbook -- R. T. Santoro, H. C. Claiborne, F. S. Alsmiller, and R. G. Alsmiller, Jr.	80
4.	THEORETICAL STUDIES FOR MEDIUM- AND HIGH-ENERGY RADIATION SHIELDING	82
4.0	Introduction -- R. G. Alsmiller, Jr.	82
4.1	Calculation of Nuclear Reactions for Incident Nucleons and π -Mesons in the Energy Range 30 to 2700 MeV -- H. W. Bertini	82
4.2	Results from Medium- and High-Energy Intranuclear-Cascade Calculation -- H. W. Bertini and M. P. Guthrie	83
4.3	The Masking Effect of Multiple Scattering on the Determination of the Two-Nucleon Correlation from π^- -Absorption Experiments -- H. W. Bertini	83
4.4	Absorption, Charge-Exchange, and Double-Charge-Exchange Reactions of π -Mesons with Complex Nuclei: Comparison of Theoretical Predictions with Experimental Results -- H. W. Bertini	83

4.5	An Extrapolation Method for Predicting Nucleon and Pion Differential Production Cross Sections from High-Energy (>3 GeV) Nucleon-Nucleus Collisions -- T. A. Gabriel, R. G. Alsmiller, Jr., and M. P. Guthrie	84
4.6	Calculation of the Neutron Spectra from Proton-Nucleus Nonelastic Collisions in the Energy Range 15--18 MeV and Comparison with Experiment -- R. G. Alsmiller, Jr., and O. W. Hermann	84
4.7	Calculation of the Photon-Production Spectrum from Proton-Nucleus Collisions in the Energy Range 15 to 150 MeV and Comparison with Experiment -- Y. Shima and R. G. Alsmiller, Jr.	84
4.8	Electromagnetic- and Nuclear-Cascade Calculations and Their Application in Shielding and Dosimetry -- R. G. Alsmiller, Jr.	85
4.9	Electron Transport with the Method of Discrete Ordinates -- D. E. Bartine, R. G. Alsmiller, Jr., F. R. Mynatt, W. W. Engle, Jr., and J. Barish	85
4.10	The Lateral Spread of High-Energy (≤ 400 -MeV) Neutron Beams and Earthshine -- R. G. Alsmiller, Jr., F. R. Mynatt, M. L. Gritzner, J. V. Pace, and J. Barish	86
4.11	Photon Leakage from the Moon Due to Solar-Flare Bombardment -- T. W. Armstrong, R. G. Alsmiller, Jr., and H. S. Moran	87
4.12	The Absorbed Dose and Dose Equivalent from Neutrons in the Energy Range 60 to 3000 MeV and Protons in the Energy Range 400 to 3000 MeV -- R. G. Alsmiller, Jr., T. W. Armstrong, and W. A. Coleman	88
4.13	The Absorbed Dose and Dose Equivalent from Negatively and Positively Charged Pions in the Energy Range 10 to 2000 MeV -- R. G. Alsmiller, Jr., T. W. Armstrong, and B. L. Bishop	88
4.14	Calculation of the Radiation Hazard at Supersonic Aircraft Altitudes Produced by an Energetic Solar Flare -- II. -- T. W. Armstrong and H. S. Moran	89
4.15	Calculation of the Radionuclide Production in Tissue by Solar-Flare Bombardment -- T. W. Armstrong and K. C. Chandler	89
4.16	Calculation of the Nucleon-Meson Cascade Induced in Iron by 19.2 GeV/c Protons and Comparison with Experiment -- T. W. Armstrong and B. L. Bishop	91
4.17	An Approximate Density-Effect Correction for the Ionization Loss of Charged Particles -- T. W. Armstrong and R. G. Alsmiller, Jr.	92
4.18	Calculations Evaluating Several Methods for Reducing the Residual Photon Dose Rate Around High-Energy Proton Accelerators -- T. W. Armstrong and J. Barish	92
4.19	Calculated Activation of Copper and Iron by 3-GeV Protons -- T. W. Armstrong and J. Barish	93
4.20	Calculation of the Long-Lived Induced Activity in Soil Produced by 200-MeV Protons -- T. A. Gabriel	93
4.21	Calculation of the Long-Lived Induced Activity in the Soil Around High-Energy Accelerator Target Areas -- T. A. Gabriel and R. G. Alsmiller, Jr.	93
4.22	High-Energy (<18 GeV) Muon Transport Calculations and Comparison with Experiment -- II. -- R. G. Alsmiller, Jr., and J. Barish	93
4.23	Calculation of the Energy Deposited in Thick Targets by High-Energy (1 GeV) Electron-Photon Cascades and Comparison with Experiment -- II. -- R. G. Alsmiller, Jr., and H. S. Moran	94

4.24	Photonucleon and Photopion Production from High-Energy (50 to 400 MeV) Electrons in Thick Copper Targets — T. A. Gabriel and R. G. Alsmiller, Jr.	94
4.25	Analytic Representation of Photonucleon and Photopion Differential Yields Resulting from High-Energy Electrons ($50 \leq E_0 \leq 400$ MeV) Incident on an Infinite Copper Target — T. A. Gabriel	94
4.26	The Energy Distribution of Photoneutrons Produced by 150-MeV Electrons in Thick Beryllium and Tantalum Targets — R. G. Alsmiller, Jr., T. A. Gabriel, and M. P. Guthrie	94
5.	MEDIUM-ENERGY NUCLEON SPECTROSCOPIC STUDIES	95
5.0	Introduction — R. W. Peelle	95
5.1	Measurement of Neutron Spectra in the Energy Range 2 to 60 MeV in the Upper Atmosphere — W. Zobel, T. A. Love, J. T. Delorenzo, and C. O. McNew	95
5.2	Differential Cross Sections for Hydrogen and Helium Particles from 30- to 60-MeV Protons on Nuclei — R. W. Peelle and F. E. Bertrand	98
5.3	Tabulated Cross Sections for Hydrogen and Helium Particles Produced by 62- and 29-MeV Protons on ^{197}Au — F. E. Bertrand and R. W. Peelle	102
5.4	Tabulated Cross Sections for Hydrogen and Helium Particles Produced by 62- and 29-MeV Protons on ^{120}Sn — F. E. Bertrand and R. W. Peelle	102
5.5	Tabulated Cross Sections for Hydrogen and Helium Particles Produced by 62-MeV Protons on ^{89}Y — F. E. Bertrand and R. W. Peelle	103
5.6	Tabulated Cross Sections for Hydrogen and Helium Particles Produced by 61-MeV Protons on ^{56}Fe — F. E. Bertrand and R. W. Peelle	103
5.7	Tabulated Cross Sections for Hydrogen and Helium Particles Produced by 62-, 39-, and 29-MeV Protons on ^{54}Fe — F. E. Bertrand and R. W. Peelle	103
5.8	Tabulated Cross Sections for Hydrogen and Helium Particles Produced by 62- and 29-MeV Protons on ^{27}Al — F. E. Bertrand and R. W. Peelle	103
5.9	Differential Cross Sections for Neutrons from 40- and 60-MeV Protons on Nuclei — J. W. Wachter, R. T. Santoro, T. A. Love, and W. Zobel	104
5.10	IBM-360 Routines to Read and Write PDP-8 Magnetic Tapes — J. W. Wachter and T. J. Tyrrell	106
5.11	TEDIT — Tape Editing Program for the PDP-8 — J. W. Wachter	106
	PUBLICATIONS AND PAPERS PRESENTED AT SCIENTIFIC MEETINGS	107

1. Neutron Cross Sections

1.0 INTRODUCTION

F. C. Maienschein

In the continuing effort to determine neutron cross sections needed for reactor development and related programs, attention has shifted to ORELA (the Oak Ridge Electron Linear Accelerator) as a source of pulsed neutrons. The Linac was accepted from the manufacturer in August 1969, after performing substantially in accordance with the specifications during acceptance tests. Since August the Linac has been operated for experiments with an availability (~74%) which we consider very good for a new accelerator.

The measurements at ORELA are designed to provide those data of greatest importance to the LMFBR (Liquid Metal Fast Breeder Reactor). The largest single effort is being invested in studies which use the large scintillation tank, ORELAST, at the 40-m station to measure the capture cross section of ^{238}U . Later, these measurements will be extended to higher energies (>100 keV) in a new flight station to be built at 150 m.

A final report of the earlier ORNL-RPI measurements of $\alpha(E)$ for ^{239}Pu has been prepared. Further experiments at ORELA also using ORELAST will be aimed at the very high accuracies which are requested for this parameter. Extensions of capture and fission cross sections and their ratios, α , have also been initiated for ^{241}Pu , ^{233}U , and ^{235}U . Clearly, in view of the high accuracies required, each of these measurements will require many man-years to complete. The overall rate of progress is expected to be consistent with the requirements of the LMFBR development, however.

The theoretical support for the measurement program at ORELA is represented here largely by studies of the multilevel formalisms for describing the behavior of neutron cross sections in the resonance region and a new and quicker method of converting from R -matrix to Kapur-Peierls parameters. This effort will likely shift to support primarily the ^{238}U measurements for the next year or so.

In studies of fast-neutron scattering at the Van de Graaffs, a breakthrough was claimed last year in the analysis of data which had been obtained earlier. This assertion is verified this year by the large volume of

results which have been published. In particular, cross sections for elastically and inelastically scattered neutrons over the incident neutron energy range from ~5 to 8.5 MeV are published (as of June 1, 1970) for approximately nine additional materials, and more reports are nearing completion. The $n, x\gamma$ measurements, analyses, and publications continue at a steady pace. An interesting development connected with these experiments has been the manufacture of a convenient monoenergetic gamma-ray source of high energy (6.13 MeV) which uses ^{244}Cm as a source of alpha particles for the reaction $^{13}\text{C}(\alpha, n)^{16}\text{O}$.

In a cooperative effort, physicists who made neutron scattering and $n, x\gamma$ measurements for iron are participating directly in an evaluation of the cross section for this material for the ENDF/B file.

1.1 MEASUREMENTS OF THE NEUTRON FISSION AND ABSORPTION CROSS SECTIONS OF ^{239}Pu OVER THE ENERGY REGION 0.02 eV TO 30 keV, PART II¹

R. Gwin	J. H. Todd ²
L. W. Weston	F. E. Gillespie ²
G. de Saussure	R. W. Hockenbury ³
R. W. Ingle ²	R. C. Block ³

The analysis of the measurements of the neutron capture (σ_c) and fission (σ_f) cross sections of ^{239}Pu performed at Rensselaer Polytechnic Institute has been completed.

The results of the detailed analysis confirm the α values (σ_c/σ_f) published previously, although for the energy region from 10 to 30 keV, the revised values of α are near the upper uncertainty limit of the early values.⁴

Figure 1.1.1 shows a histogram of values of $\bar{\alpha}$ derived in the present measurements as compared with values obtained by Sowerby *et al.*⁵ and Czirr and Lindsey⁶ and with values from the ENDF/B file for ^{239}Pu material 1104.⁷ An important feature to note in Fig. 1.1.1 is the general agreement of the various differential measurements above 4 keV and the merging of these values with the Van de Graaff measurements of Lottin

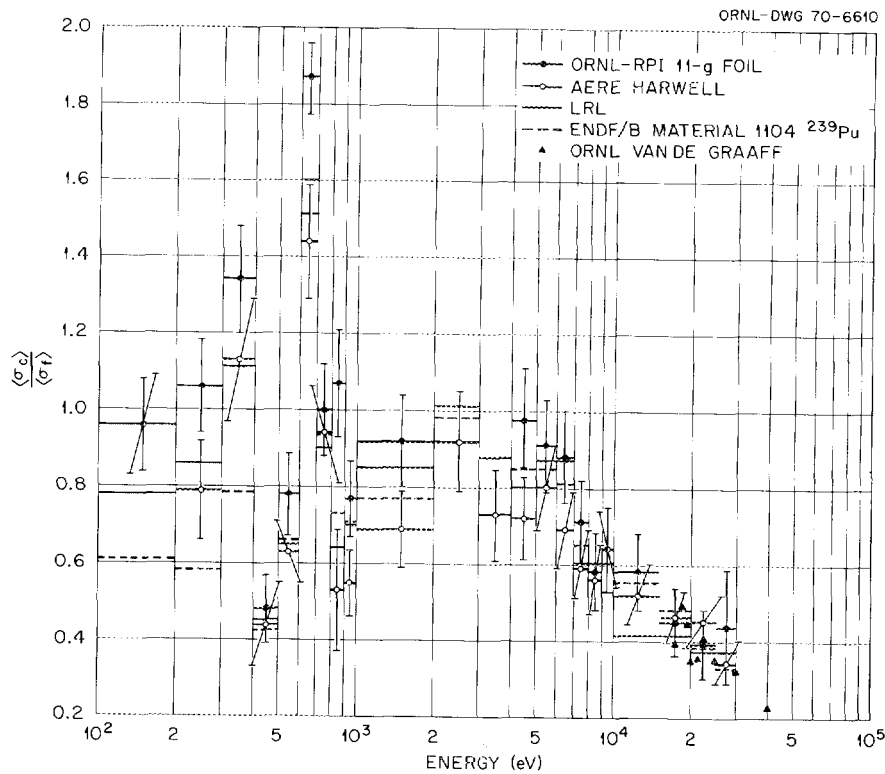


Fig. 1.1.1. $\bar{\alpha}$ for ^{239}Pu vs Energy.

*et al.*⁸ at about 20 keV. Since the accuracy of the Van de Graaff measurements is about $\pm 10\%$ of α and since a large part of the uncertainty in the present experiments derives from the process of normalization ($\sim 4\%$ in σ_f/σ_a), confidence in the differential measurements is enhanced.

References

- ¹ Summary of paper to be submitted for publication in *Nuclear Science and Engineering*.
- ² Instrumentation and Controls Division.
- ³ Rensselaer Polytechnic Institute, Troy, N.Y.
- ⁴ R. Gwin *et al.*, *Nucl. Sci. Eng.* **40**, 306 (1970).
- ⁵ M. G. Sowerby *et al.*, "The Ratio of the Capture and Fission Cross Sections of ^{239}Pu in the Energy Range 100 eV to 30 keV," to be published as paper CN-26/33 in *IAEA Intern. Conf. on Nuclear Data for Reactors, Helsinki, Finland, June 15-19, 1970*.
- ⁶ J. B. Czirr and J. S. Lindsey, *A Measurement of the Capture-to-Fission Ratio for ^{239}Pu* , UCRL-72080 (November 1969).
- ⁷ J. T. Hitchcock and B. A. Hutchins, *^{239}Pu Unresolved Resonance Data for ENDF/B, Version II*, GEAP-13591, General Electric Co., Sunnyvale, Calif.

⁸ A. Lottin *et al.*, "Ratio of Capture to Fission in ^{239}Pu at keV Neutron Energies," *Proc. Intern. Conf. on Fast Critical Experiments and Their Analysis*, ANL-7320, p. 22 (October 1966).

1.2 MEASUREMENTS OF THE NEUTRON CAPTURE AND FISSION CROSS SECTIONS FOR ^{239}Pu AT ORELA

R. Gwin R. W. Ingle¹
L. W. Weston H. Weaver

Experiments to more accurately determine the neutron capture and fission cross sections of ^{239}Pu over a wide energy range have been initiated at the Oak Ridge Electron Linear Accelerator (ORELA) with current emphasis on checking out the detector system and identifying and measuring the background sources. In these experiments the capture and fission cross sections are measured simultaneously with a detector system² similar to that used in earlier Linac time-of-flight measurements at Rensselaer Polytechnic Institute.³ The fissile sample is centered in a large tank of liquid scintillator that detects fission and capture events in the

sample by absorbing the prompt gamma rays emitted when these events occur. The two types of events are distinguished from one another by the difference in the pulse-height response of the scintillator to the gamma rays from fission and the response to gamma rays from neutron capture. This method, called the high-bias method, has been selected for these studies in preference to the ionization chamber technique because of the poor signal-to-background ratios obtained in the keV region with the ionization chamber.³

The sample used in these first test measurements consisted of an aluminum-wrapped metal foil containing a total ^{239}Pu mass of 11.2 g. In its position at the center of the scintillator tank, called ORELAST,² the sample was 40 m from the accelerator's tantalum target in which neutrons were produced by bursts of electrons. A burst width of 38 nsec and a burst repetition rate of 38 pulses/sec were used. The neutron energy range was from about 0.4 eV to about 100 keV. The minimum time-of-flight channel width was 40 nsec, and the dead time associated with the time-of-flight measurements was set at 16 μsec .

A major problem in such measurements is the proper determination of the large time-dependent background included in the pulses from the scintillator tank. Gamma rays contributing to this background can be due to several sources, some of which are correlated with fissions in the sample: delayed gamma rays produced by fission events and gamma rays produced by fission neutrons that slow down and are absorbed in and around the scintillator tank are such sources. Another background source is due to gamma rays emitted when neutrons elastically scattered from the sample are slowed and captured in and around the tank. In an attempt to reduce the background resulting from neutrons captured in the scintillator, boron was added to the tank.

The capability for dividing the scintillator tank into optically separate sections is being utilized to help identify the background sources. In these test experiments the tank was divided into two sections, the divider being in the vertical plane containing the center line of the neutron path. Pulses were recorded as coming from only one section of the tank or as coming from both sections simultaneously. Pulses from both sections are more likely to be due to gamma rays with a high multiplicity, while those from only one section probably would be due to those with a low multiplicity. The high-bias technique employed required that pulses from each of these two sections also be divided. All events which had pulse heights equivalent to gamma-ray energies between 3 and 10 MeV (low bias) were stored

in one "subsection," while those which had pulse heights equivalent to energies from 10 to 16 MeV (high bias) were stored in another subsection. Theoretically, about 10% of the fission events are recorded as high-bias pulses, with the remaining fission events and all the capture events recorded as low-bias pulses. In reality, however, about 1% of the capture events are detected in the high-bias pulses.

In one series of measurements to investigate the time-dependent background, "notch" filters were inserted in the neutron beam ahead of the detector tank. The materials and thicknesses for the notch filters were so chosen that they effectively filtered out all neutrons in the beam which corresponded to prominent neutron resonances for these materials. Thus the flux of neutrons at the resonance energies was essentially zero at the ^{239}Pu sample and any count rates observed at those energies could be assumed to be due to background sources. The materials chosen for the notch filters were Al, Na, Co, and Au, which have prominent neutron resonances at 35 keV, 2.85 keV, 132 eV, and 5 eV respectively. The 16- μsec dead time employed in the measurements served to substantially reduce that portion of the time-dependent background due to the background sources specified above.

In another series of measurements, with the notch filters still in the beam, a 0.01-in.-thick lead sample packaged the same as the ^{239}Pu sample was substituted for it to mock up the neutron scattering from the sample. Corresponding data from the two series, with corrections for the instrumental dead time and with the constant background subtracted, were then compared. The "mock" background results (those with the lead sample) were normalized to the foreground results (those with the plutonium sample) at 2.85 keV, the energy of the sodium resonance. The comparison of the low-bias data for events detected by only one section of the scintillator tank is shown in Fig. 1.2.1, and the comparison of low-bias events detected by both sections is shown in Fig. 1.2.2. It is noted that while the mock background and foreground curves in Fig. 1.2.2 agree at all resonance energies of the filters, the two curves in Fig. 1.2.1 differ at 35 keV as well as at other resonances. If the differences were due to electronic difficulties, they would appear in Fig. 1.2.2 also. The fact that they do not exist in Fig. 1.2.2 implies that they are due either to gamma rays with low multiplicities or to gamma rays originating at positions that favor one section of the tank. The possible time-dependent background sources mentioned above (i.e., delayed gamma rays from fission, gamma rays produced by the capture of fission neutrons, and gamma rays

produced by the capture of sample-scattered neutrons in the scintillator hydrogen) are all expected to have low multiplicities, and thus the difference is probably due to these three sources. At this point the relative magnitudes of the individual sources are unknown, but their total effect is about 10% of the mock background at 35 keV.

The high-bias data obtained with the ^{239}Pu sample and notch filters are presented in Fig. 1.2.3 for events detected by only one section of the tank and in Fig. 1.2.4 for events detected by both sections. These data, together with the low-bias data, were analyzed for α values of isolated resonances in the energy region below 100 eV by the technique reported in ref. 3. The analysis

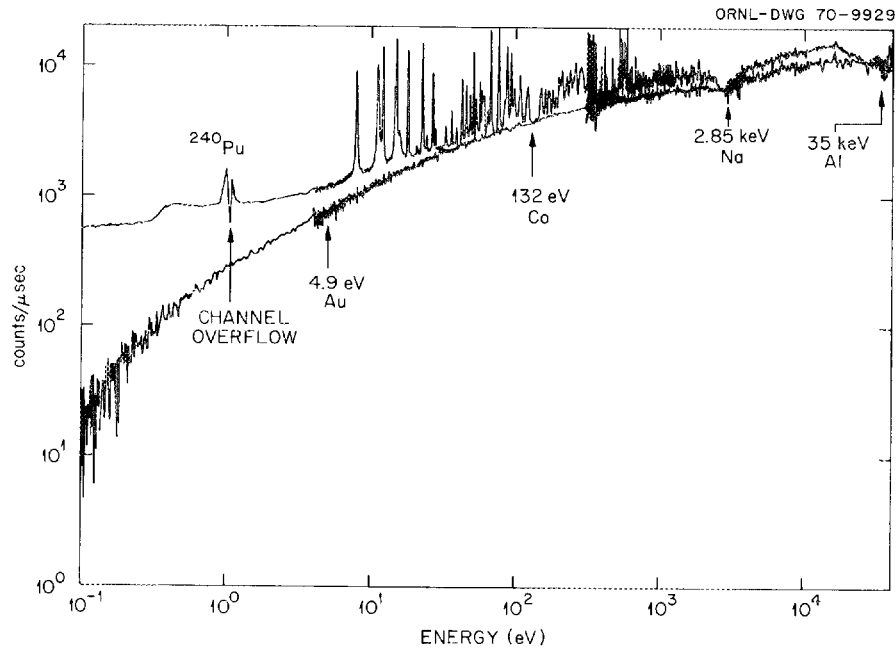


Fig. 1.2.1. ^{239}Pu Low-Bias Count Rate vs Energy for Events Detected by Only One Section of Detector.

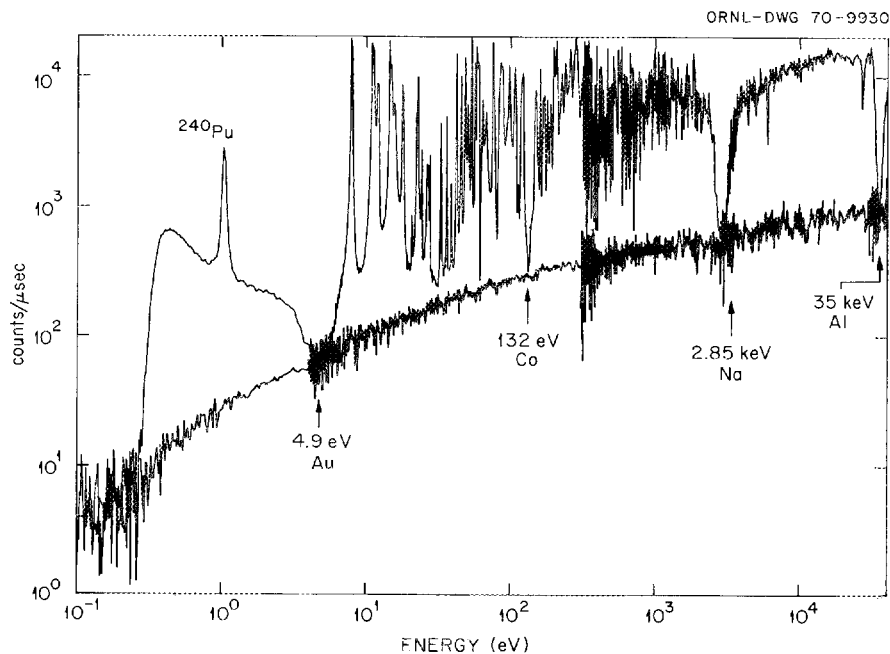


Fig. 1.2.2. ^{239}Pu Low-Bias Count Rate vs Energy for Events Detected by Both Sections of Detector.

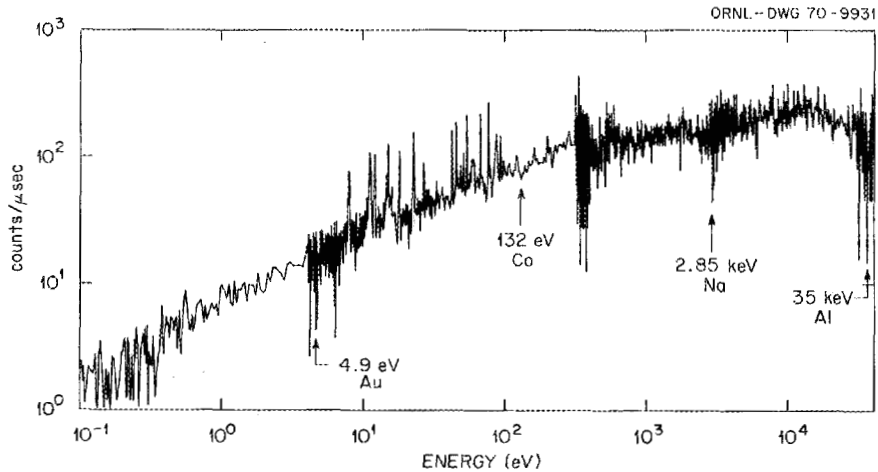


Fig. 1.2.3. ^{239}Pu High-Bias Count Rate vs Energy for Events Detected by Only One Section of Detector.

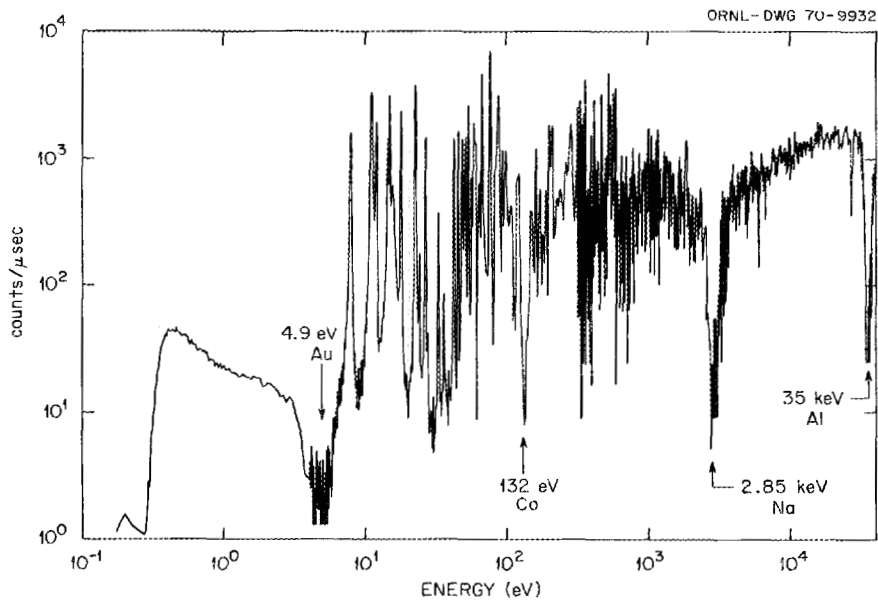


Fig. 1.2.4. ^{239}Pu High-Bias Count Rate vs Energy for Events Detected by Both Sections of Detector.

was performed first for the sum of all the events recorded in both sections and second for only those events recorded simultaneously by both sections. (The first case is the normal mode of operating a large liquid scintillator.) The results were consistent for both cases, but the standard errors of the derived values of σ_f/σ_a were about 8%, which is approximately twice that found for the experiments reported in ref. 3.

The use of the scintillator tank in the mode requiring coincidences from the two sections has not yet been proven to be the best technique. Possible changes in the gamma-ray average multiplicities and the resulting effect on the efficiency of the system must be

examined before this method is generally applied in future measurements.

References

- ¹ Instrumentation and Controls Division.
- ² E. G. Silver, J. H. Todd, and J. Lewin, "Assembly and Initial Operation of the ORELAST," sect. 1.11 in *Neutron Phys. Div. Ann. Progr. Rept. May 31, 1969*, ORNL-4443.
- ³ R. Gwin, L. W. Weston, G. de Saussure, R. W. Ingle, J. H. Todd, F. E. Gillespie, R. W. Hockenbury, and R. C. Block, *Nucl. Sci. Eng.* **40**, 306 (1970); see also sect. 1.1 in this report.

1.3 MEASUREMENT OF THE CAPTURE CROSS SECTION OF ^{238}U UP TO 100 keV

G. de Saussure R. W. Ingle¹
 E. G. Silver R. B. Perez
 H. Weaver

The accurate knowledge of the capture cross section of ^{238}U is of great importance to the breeder reactor program. Available measurements of this cross section show significant discrepancies both in averaged cross sections and in the resonance parameters.²⁻⁴ Hence a precision measurement of the capture cross section of ^{238}U has been assigned the highest priority by both the EANDC and LMFBR program plans.⁵

We are therefore measuring the ^{238}U capture cross section with good energy resolution and high precision up to a few hundred keV. Resonance parameters will also be determined from the results used in conjunction with transmission and self-indication measurements. This report describes our progress to date.

1.3.1 Method of Measurements

Our experiments utilize the ORELAST⁶ as a capture detector at the 40-m station of flight path No. 6 of ORELA.⁷ Measurements have been performed on ^{238}U samples of 1, 3, and 25 mils nominal thickness.⁸ With the thick samples the signal-to-background ratio is better, particularly at the high-energy end of the energy range investigated. With the thin samples, on the other hand, the corrections due to resonance self-shielding and multiple scattering are much smaller, in particular for the low-energy resonances where the 25-mil sample can be several mean free paths thick. The data from the three thicknesses will also be used to test various techniques now under development to account properly for sample thickness effects in obtaining resonance parameters from experimental capture rates.⁹

For each sample, measurements were done with and without a set of resonance absorbers in the beam. The resonance absorbers serve to monitor the background at time-of-flight intervals corresponding to the absorber black resonances. In addition, an "overlap filter" of ^{10}B to prevent "pulse overlap" between successive pulses of the Linac was used in most runs. Measurements were also performed, with and without the absorbers, with the ^{238}U replaced by an equivalent thickness of lead. These measurements serve the purpose of allowing the interpolation of the background between the resonance filter notches. All the measurements were done using 5-nsec Linac pulse widths and samples containing less than 5 ppm of uranium isotopes other than ^{238}U (ref. 8).

For this work the liquid scintillator tank is separated optically into halves (with the vertical separation plane containing the beam axis). A parallel plate beryllium-walled BF_3 chamber¹⁰ was placed across the beam at a distance of around 38 m from the neutron source and served to measure the neutron spectrum incident upon the ^{238}U sample.

Five count rates vs time of flight were recorded simultaneously during each measurement. One of the count rates gave the pulses from the BF_3 monitor, and the other four were associated with pulses from the liquid scintillator. The pulses from the liquid scintillator were divided into two pulse-height groups corresponding to equivalent gamma-ray energies between 2.8 and 4.5 MeV and between 4.5 and 10 MeV respectively. (Pulses below 2.8 or above 10 MeV were rejected.) In turn each of these pulse-height groups was subdivided into two subgroups according to whether or not a fast coincidence occurred between the halves of the tank. The four types of events from the scintillator were recorded separately in order to observe whether appreciable changes in pulse-height distribution or in multiplicity occurred as a function of time of flight. Such changes could be caused by electronic bias shifts or by changes in some of the average properties of the gamma-ray cascade following neutron capture. Preliminary reduction of the data indicates that such changes are not observed within the accuracy of the measurements.

The width of the time-of-flight channels varied from 5 nsec (for the first 80 μsec) to 2.56 μsec (at 2 msec). Table 1.3.1 shows the structure of the channel widths. The 122,880 channels of data were stored on disks during accumulation and then read on magnetic tape for batch processing.¹¹ Figure 1.3.1 shows a simplified block diagram of the electronics utilized in the present experiment.¹² An example of some of the raw data obtained is shown in Fig. 1.3.2. The count rate vs channel number curves for the 25-mil-thick ^{238}U sample exhibits the "notches" due to the filters' black resonances.

1.3.2 Data Analysis

Figure 1.3.3 shows the count rate of the BF_3 neutron monitor as a function of energy, both without resonance filters in the beam (upper curve) and with resonance filters (lower curve). The relation between the count rate per unit time, $C(E)$, shown on the figure and the neutron flux per unit energy, $\Phi(E)$, incident upon the BF_3 detector is given by¹³

$$C(E) = KE \Phi(E) dE ,$$

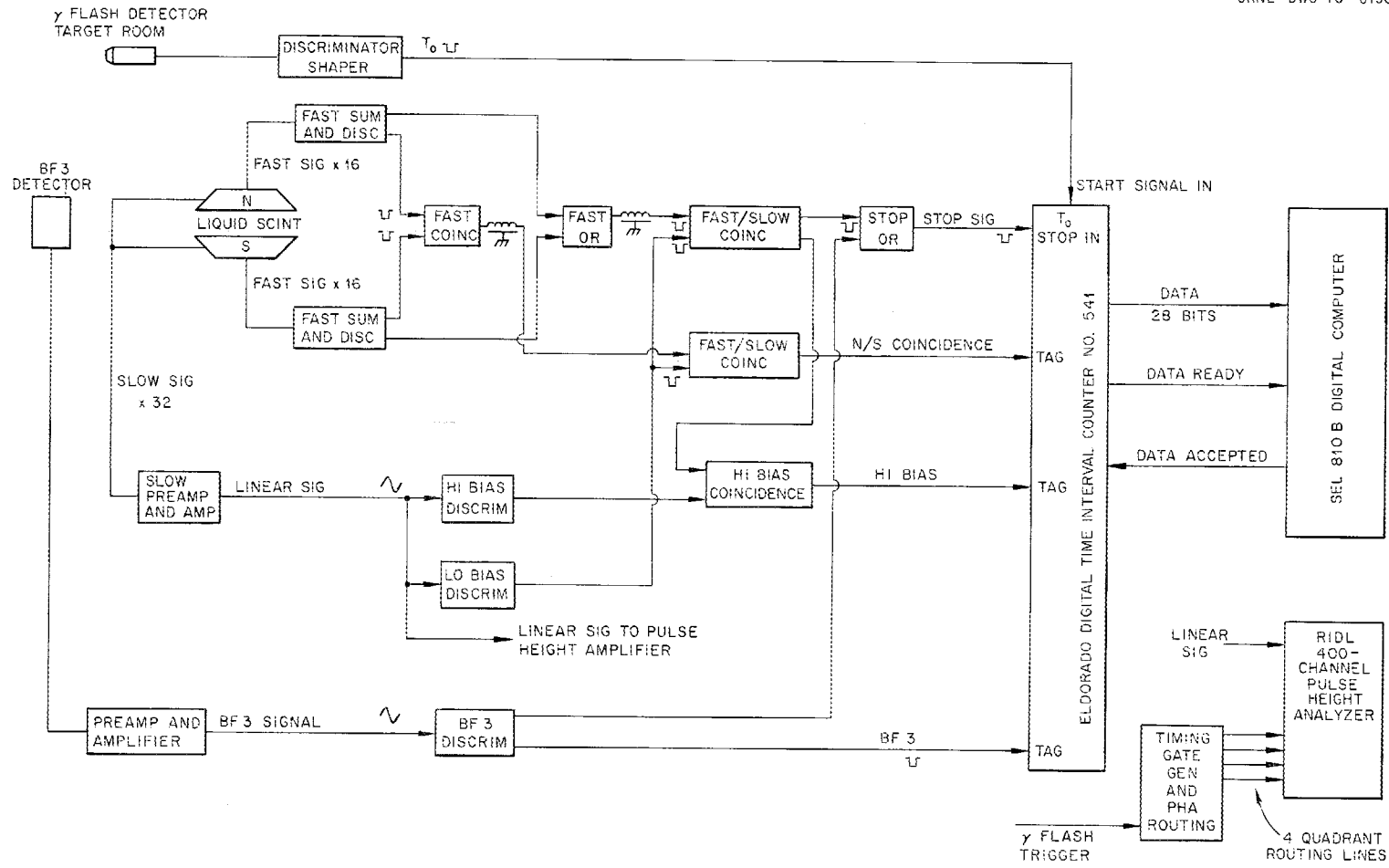


Fig. 1.3.1. Simplified Block Diagram of the Electronic Circuitry Used in the Measurements of the $^{238}\text{U}(n,\gamma)^{239}\text{U}$ Cross Section.

where K is an arbitrary constant, and where the efficiency of the detector is assumed to be proportional to $E^{-1/2}$. The solid line in Fig. 1.3.3 is an analytical fit to $C(E)$. Below 5 keV this fit has the form

$$C(E) = kE^\alpha e^{-\beta/\sqrt{E}},$$

where k is a constant, $\alpha = 0.16$ represents the "hardening" of the neutron flux due to the finite size of the neutron moderator (it corresponds to a flux $\Phi(E) dE = E^{-0.84} dE$), and β is the macroscopic capture cross section of the ^{10}B overlap filter at 1 eV. In the vicinity of 6 keV and above 20 keV, the neutron spectrum has a marked structure caused by the reso-

nances in the aluminum in which the neutron moderator is canned. The solid line is shown also through the spectrum with resonance filters to illustrate that below 1 keV the shape of the neutron spectrum is not appreciably distorted by the resonance filters.

Figure 1.3.4 shows the ORELAST count rate with the ^{238}U specimen replaced by a lead sample of equivalent thickness. From this curve the shape of the background as a function of time of flight can be obtained. The solid line shows a polynomial fit to this background shape in the energy region below 20 keV. In the measurement without filters, the background level is normalized in the energy region below 1 keV, where the filters do not appreciably distort the shape of the

Table 1.3.1. Time-of-Flight Program for Measurement of σ_c for ^{238}U

Number of Channels	Channel Width	Time of Flight	Energy
16384	5 nsec	0–81.92 μsec	>1.3 keV
2048	10 nsec	81.92–102.4 μsec	1.3 keV–800 eV
2048	20 nsec	102.4–143.36 μsec	800–400 eV
1024	40 nsec	143.36–184.32 μsec	400–250 eV
1024	80 nsec	184.32–266.24 μsec	250–120 eV
512	160 nsec	266.24–348.16 μsec	120–70 eV
512	320 nsec	348.16–512 μsec	70–32 eV
512	640 nsec	512–840 μsec	32–12.5 eV
256	1.28 μsec	840 μsec –1.167 msec	12.5–8 eV
256	2.56 μsec	1.167–1.823 msec	8–2.5 eV

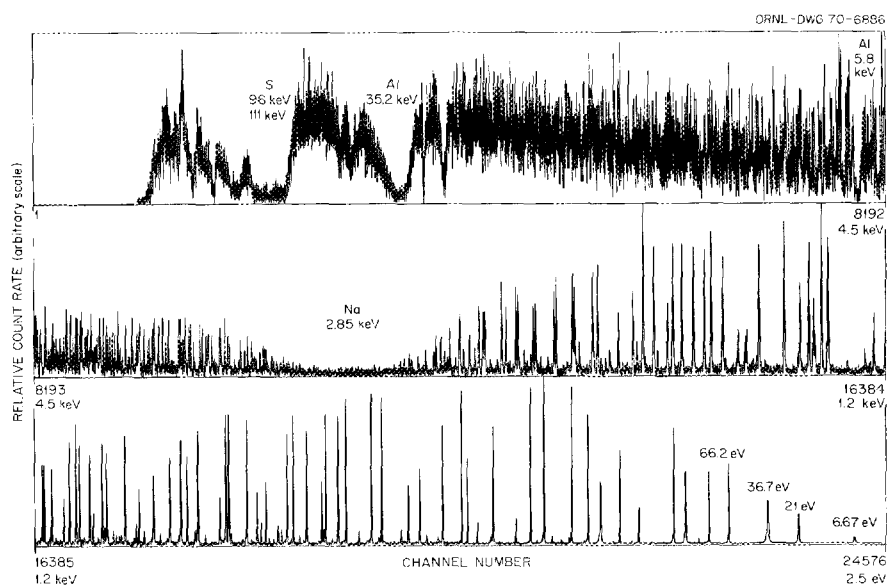


Fig. 1.3.2. Count Rate Observed with 25-mil ^{238}U Sample in ORELAST. Each of the three sections is individually normalized by an arbitrary scale factor. Resonance absorption filters were located in the neutron beam, and the filter notches are identified.

neutron spectrum, and hence the net count rates of the measurements with and without filters must be proportional.

Figure 1.3.5 shows the capture cross section (times $E^{1/2}$) determined from the 3-mil sample of ^{238}U . The curve has been provisionally normalized to a value of $10140 \text{ b}\cdot\text{eV}^{3/2}$ for the integral of $\sigma(E)E^{1/2}$: [where $\sigma(E)$ is the capture cross section] over the interval from

30 to 90 eV. The normalization value was obtained by using the resonance parameters given in Table 1.3.2 and computing the sample thickness effects with the Monte Carlo technique.

1.3.3 Conclusions

The previous discussion sketches the technique used in the analysis of the data. A thorough evaluation of

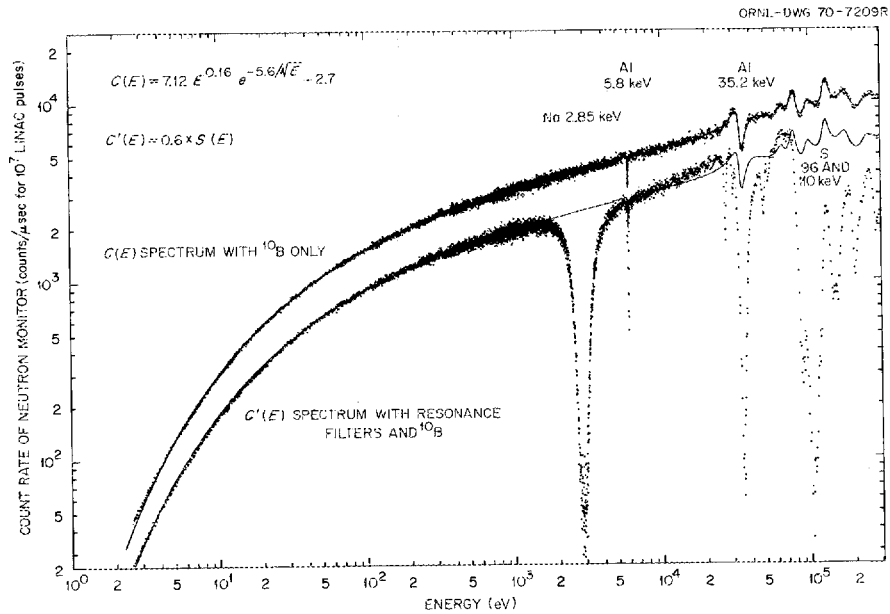


Fig. 1.3.3. Neutron Count Rates Observed with a BF_3 Fission Chamber, With and Without Resonance Absorption Filters. The solid lines represent analytical fits to the data.

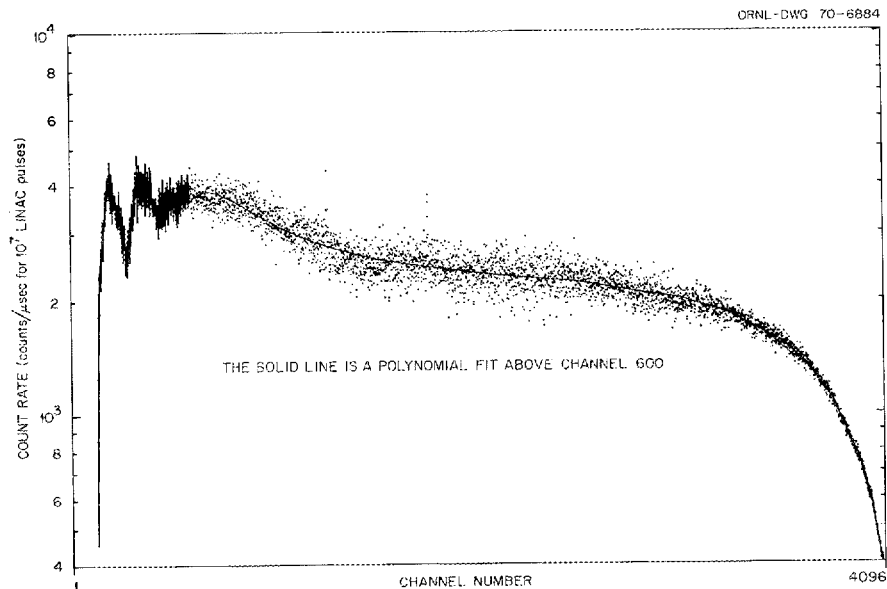


Fig. 1.3.4. Count Rate Observed in the ORELAST with a 3-mil Lead Sample. The solid line represents an analytical fit.

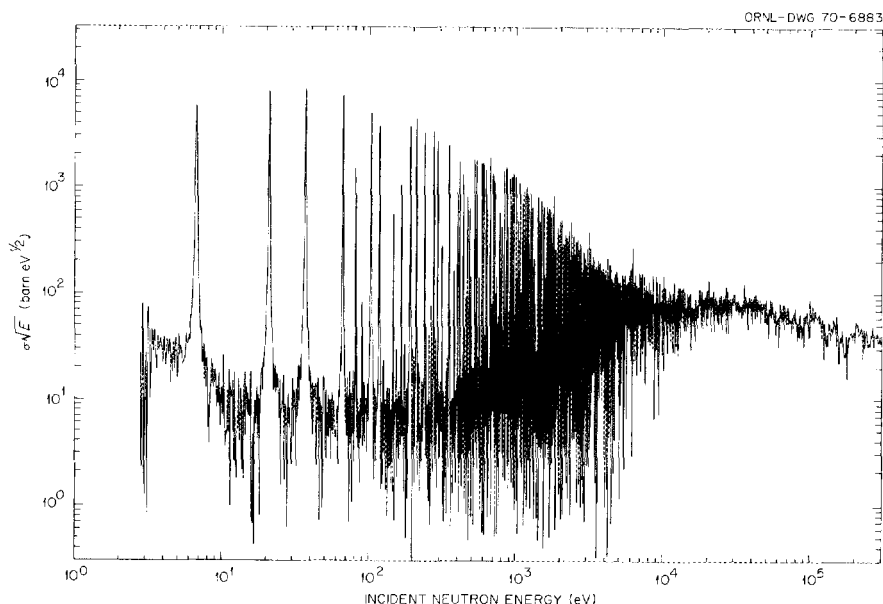


Fig. 1.3.5. Capture Cross Section of ^{238}U Obtained with a 3-mil Sample. The values shown are the cross section multiplied by $E^{1/2}$. The cross section has been normalized to $10140 \text{ b}\cdot\text{eV}^{3/2}$ between 30 and 90 eV.

Table 1.3.2. Parameters Used to Compute Preliminary Normalization^{a,b}

E_0 (eV)	Γ_n (mV)	Γ_γ (mV)
21.0	8.7	26.5
36.7	31	27.7
66.2	23.8	24.5
81.1	2	21.2
89.5	0.085	23.6
102.7	65.1	25.1

^aAll the levels are assumed to be s-wave levels.

^bFor a sample of 3.958×10^{-4} atoms/barn,

$$\int_{30 \text{ eV}}^{90 \text{ eV}} \sigma_{\text{eff}} E^{1/2} dE = 10140 \text{ b}\cdot\text{eV}^{3/2},$$

where σ_{eff} includes resonance self-shielding and multiple-scattering effects.

each step used in the data reduction and an estimate of the uncertainties involved will require a considerable amount of additional analysis. Further measurements will also be required to verify the normalization technique and to extend the measurement to higher energies.

Keeping in mind the preliminary nature of the present results, we have made several comparisons with some of the previous work in this area. Figure 1.3.6 shows the cross section, averaged over the intervals indicated by the histogram, compared with the results of Moxon¹⁴

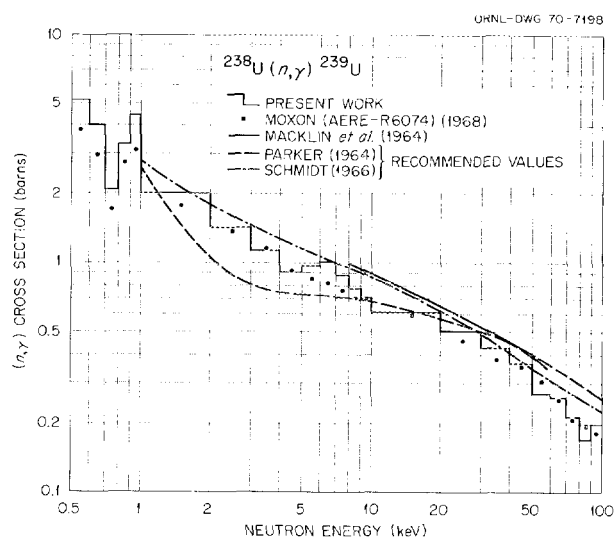


Fig. 1.3.6. Capture Cross Section of ^{238}U Averaged over the Intervals Shown. The points represent the values of Moxon. The recommended values of Parker and Schmidt are also shown, as are the results of Macklin.

and of Macklin,¹⁵ as well as with recommended values of Parker¹⁶ and Schmidt.¹⁷ The general agreement with Moxon's results is very good, especially in that the present data show the relatively fast decrease of the capture cross sections in the high-energy portion of the curve. The "hump" exhibited by the histogram around the 6-keV energy region may be associated with

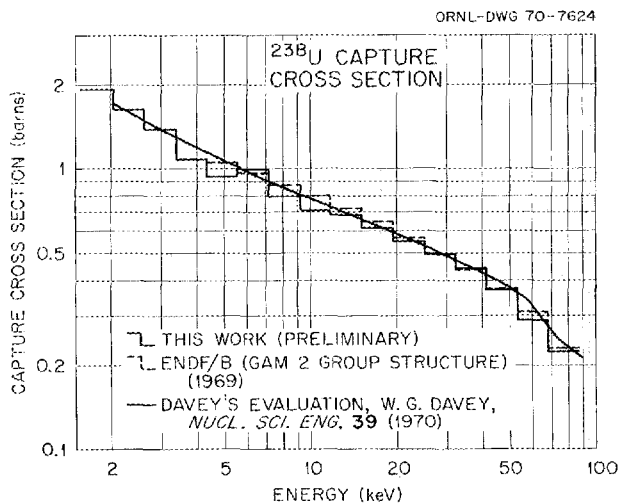


Fig. 1.3.7. Capture Cross Section of ^{238}U Averaged over the Intervals Shown, Compared with the Evaluation of Davey and with the ENDF/B Values as Interpreted with the GAM-2 Program.

uncertainties in eliminating the effect of a resonance in the capture cross section of aluminum. In Fig. 1.3.7 the solid line shows the present measurements averaged over the GAM-2 group structure and compared with a similar plot (broken lines) obtained from the ENDF/B files.^{2,18} The agreement is reasonably good and highly consistent with Davey's evaluation² shown in the figure as a smooth solid line.

As was mentioned previously, the present results are subject to much more careful and extensive revision and error analysis. Nonetheless, the results to date indicate that accurate data can be obtained from these measurements. Future work will be done to extend this work above 100 keV and to make the transmission and self-indication measurements needed to obtain accurate values of resonance parameters in the resolved range.

References

- ¹Instrumentation and Controls Division.
- ²Recent evaluations of the ^{238}U cross sections were performed by: W. G. Davey, *Nucl. Sci. Eng.* **39**, 337 (1970), and by T. Pitterle, "Evaluation of ^{238}U Neutron Cross Section for ENDF/B File," to be published as paper CN 26/83 in *Proc. IAEA Intern. Conf. on Nuclear Data for Reactors, Helsinki, Finland, June 15-19, 1970*.
- ³N. W. Glass *et al.*, *Neutron Cross Section Technology, Washington 1968*, Conf. 660303, vol. 1, p. 573.
- ⁴G. Rohr, H. Weigmann, and J. Winter, "Resonance Parameters from Neutron Radiative Capture in ^{238}U ,"

to be published as paper CN 26/17 in *Proceedings of IAEA International Conference on Nuclear Data for Reactors, Helsinki, Finland, June 15-19, 1970*.

⁵*Compilation of Requests for Nuclear Cross Section Measurements*, WASH-1144, requests 413, 414, 416, 419; *LMFBR Program Plan*, WASH-1109, vol. 9, *Physics*, pp. 9-53.

⁶E. G. Silver *et al.*, *Neutron Phys. Div. Ann. Progr. Rept. May 31, 1969*, ORNL-4433, p. 11.

⁷A. L. Boch *et al.*, *Neutron Phys. Div. Ann. Progr. Rept. May 31, 1969*, ORNL-4433, p. 9.

⁸The uranium chemistry was done under the direction of H. R. Gwinn, and the samples were rolled and prepared by W. B. Grisham; both are of the Isotopes Division.

⁹M. N. Greene, R. B. Perez, G. de Saussure and S. K. Penny, paper 1.9, this report.

¹⁰The BF_3 ionization chamber was designed and constructed by F. E. Gillespie, Instrumentation and Controls Division.

¹¹We are much indebted to N. Betz, J. W. Reynolds, and coworkers for developing the data acquisition programs on the SEL 810B computer.

¹²We gratefully acknowledge the contribution of J. H. Todd to the initial development of these electronics.

¹³For instance, G. de Saussure *et al.*, *Simultaneous Measurements of the Neutron Fission and Capture Cross Sections for ^{235}U for Incident Neutron Energies from 0.4 eV to 3 keV*, ORNL-TM-1804 (1967).

¹⁴M. C. Moxon, *The Neutron Capture Cross Section of ^{238}U in the Energy Region 0.5 to 100 keV*, AERE-R-6074, Harwell, England (1969).

¹⁵R. L. Macklin, P. J. Pasma, and J. H. Gibbons, private communication of unpublished data, 1964.

¹⁶K. Parker, *A Review of Evaluations of Neutron Cross Sections Available at UKEA*, AWRE 0-13/65 (November 1964).

¹⁷J. J. Schmidt, *Neutron Cross Sections for Fast Reactor Materials, Part 1, Evaluation*, KFK-120 (1966).

¹⁸We are grateful to D. J. Jenkins, ENDF/B-ORNL representative of the ENDF/B files and to R. Q. Wright of the Computing Technology Center for their kindness in providing us with the GAM-2 group structure averaged ^{238}U capture cross sections.

1.4 MEASUREMENT OF ETA AND THE FISSION AND TOTAL CROSS SECTIONS FOR ^{233}U BELOW 1 eV

L. W. Weston J. H. Todd¹

Measurements have been made at ORELA to determine relative values of the fission cross section and eta

and absolute values of the total cross section for ^{233}U in the neutron energy region from 0.02 to 1.0 eV. The fission cross section and eta and the total cross section were measured under as nearly the same conditions as possible and will be normalized by means of the total cross section.

The technique used at ORELA was quite different from that used for ^{233}U in the cooperative ORNL-RPI experiments.^{2,3} This additional data, covering part of the same neutron energy range, was taken to reduce or understand the uncertainties between the ORNL-RPI data and other published data. Even though this discrepancy was only a maximum of about 2%, the extreme sensitivity of the thermal breeder reactor to these parameters justified further study.

Eta, the number of fission neutrons produced per neutron absorbed, was measured by detecting the fission neutrons produced by placing a sample of known thickness in a known neutron flux. The fission neutron detectors were liquid scintillators with gamma-neutron discrimination. The flux was measured with a parallel-plate BF_3 counter which sampled the entire beam. Eta can be calculated from a knowledge of the fission rate, the cross sections, and the flux.

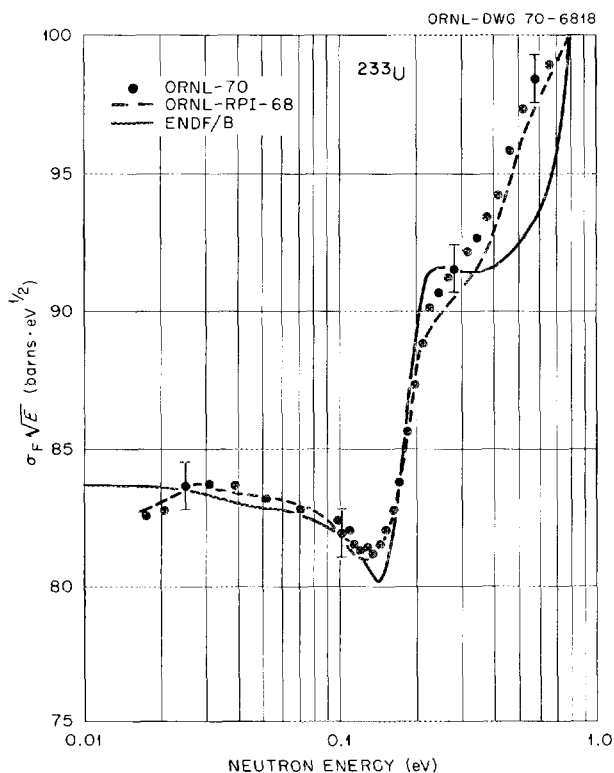


Fig. 1.4.1. The Fission Cross Section of ^{233}U Below 1-eV Neutron Energy.

The preliminary results of the fission cross-section measurement are shown in Fig. 1.4.1. The agreement with our previous ORNL-RPI measurements is better than 1%, which is quite acceptable considering the different conditions under which the measurements were made. The fission cross section in ENDF/B is shown for comparison. Our total cross-section measurement shows similar agreement with ENDF/B. The important feature of our measurements is that they form a consistent set of measurements made under as nearly the same conditions as possible.

The analysis of our data for eta is not complete at the present time. Due to the extreme accuracy required, corrections for scattering and instrumental effects must be carried out with great care. There are no surprising results indicated by very preliminary results.

Since the experimental measurements for this experiment are complete, the equipment is being modified for measurement of the capture and fission cross sections of ^{241}Pu at keV neutron energies.

References

- ¹Instrumentation and Controls Division.
- ²L. W. Weston *et al.*, *Nucl. Sci. Eng.* 34, 1 (1968).
- ³L. W. Weston *et al.*, *Neutron Fission and Capture Cross Section Measurements for ^{233}U in the Energy Region 0.02 to 1 eV*, ORNL-TM-2353 (February 1969).

1.5 ANALYTICAL DESCRIPTION OF THE NEUTRON CROSS SECTIONS OF ^{233}U BELOW 60 eV¹

G. de Saussure

The neutron fission and capture cross sections of ^{233}U below 60 eV were "least-squares fitted" with the Adler and Adler multilevel formalism. The physical interpretation of the resonance parameters is ambiguous, because such multilevel fits on ^{233}U are not unique. The main purpose of the analysis was to provide a simple analytical description of the ^{233}U cross sections for use in calculating reactor reaction rates and in data evaluation. The fission, capture, and total cross sections and the values of η obtained from the resonance parameters are compared with recent measurements of those quantities.

References

- ¹Abstract of ORNL-TM-2745 (November 1969).

**1.6 AUTOCORRELATION TECHNIQUE
FOR DETERMINING THE AVERAGE LEVEL
SPACING OF THE INTERMEDIATE
SUBTHRESHOLD STRUCTURE IN THE FISSION
CROSS SECTION OF ^{235}U AND ^{239}Pu ¹**

G. de Saussure R. B. Perez
M. N. Moore²

The interpretation given to the correlogram of the ^{235}U and ^{239}Pu fission cross sections is questioned as to its validity to estimate the average level displacement in the Strutinsky well appearing in the fission barrier for highly deformed nuclei.

References

¹ Abstract of *Phys. Letters* **31B**, 413 (1970).

² University of Arizona, Tucson.

**1.7 MULTILEVEL EFFECTS IN FISSILE
CROSS SECTIONS**

R. B. Perez G. de Saussure

The calculation of average cross sections and values of the average capture-to-fission ratio, α , in fissile nuclei is of general interest in the design of nuclear reactors. Due to the resonance interference effects, the reaction cross sections are not properly described by the superposition of single-level Breit-Wigner line shapes, and multilevel formulations^{1,2} have to be used. The average neutron reaction cross sections $\langle \sqrt{E} \sigma_{nx}(E) \rangle$ in the single-level (Breit-Wigner) or multilevel (Adler-Adler) formulations are given, respectively, by

$$\langle \sqrt{E} \sigma_{nx}(E) \rangle_{S-L} = \frac{\pi c}{\langle D \rangle} \langle G_k \rangle_{S-L}, \quad (1)$$

$$\langle \sqrt{E} \sigma_{nx}(E) \rangle_{M-L} = \frac{\pi c}{\langle D \rangle} \langle G_k \rangle_{M-L}, \quad (2)$$

where $c = 6.52 \times 10^5 \text{ b} \cdot \text{eV}^{1/2}$ and G_k is the symmetric part of the complex residue,

$$(G_k)_{S-L} = \frac{\Gamma_{kx} \Gamma_{kn}^{(0)}}{1/2 \Gamma_k}, \quad (3)$$

where

$\Gamma_{kn}^{(0)}$ = reduced neutron-level width,

Γ_{kx} = reaction-level width (x = fission or capture),

Γ_k = total-level width.

In the case of noninterfering resonances, the average indicated in Eq. 1 can be performed on the basis of the known distributions of the R -matrix parameters,³ yielding the well-known result

$$\langle \sqrt{E} \sigma_{nx}(E) \rangle_{S-L} = \frac{2\pi c \langle \Gamma_{kx} \rangle \langle \Gamma_{kn} \rangle}{\langle D \rangle \langle \Gamma_k \rangle} R_x, \quad (4)$$

where R_x is the statistical fluctuation factor. When multilevel interferences cannot be neglected, the situation is more complicated in view of the absence of analytical expressions for the statistical distribution of the Kapur-Peierls parameters. The technique utilized in this work makes use of the program SUPERPOLLA⁴ to obtain the statistical properties of the S -matrix parameters. In terms of the distributions obtained by the Monte Carlo technique via the SUPERPOLLA program, one can write the multilevel average cross section in a form similar to Eq. (4), that is, in terms of the corresponding single-level average cross section and an "interference factor," I_x :

$$\langle \sqrt{E} \sigma_{nx}(E) \rangle_{M-L} = \langle \sqrt{E} \sigma_{nx}(E) \rangle_{S-L} I_x. \quad (5)$$

Similarly one can write for the average α (capture-to-fission ratio),

$$\langle \alpha \rangle_{M-L} = \langle \alpha \rangle_{S-L} I_\alpha. \quad (6)$$

The variation of the three interference factors, I_F , I_C , and I_α , as defined above, has been studied for a set of interference conditions. In all cases studied the average neutron width, $\langle \Gamma_n^{(0)} \rangle$ and average level spacing, $\langle D \rangle$, were kept constant at the values of 0.1 MeV and 1.0 eV, respectively, these values being roughly representative of fissile nuclei. One hundred interfering levels were utilized in the calculations. Table 1.7.1 shows the changes experienced by the interference factors as a function of the average fission width $\langle \Gamma_{cf} \rangle$, assumed to be the same for each of four open fission channels. The average radiation width was kept constant at $\langle \Gamma_\gamma \rangle = 50$ MeV. The multilevel effect reduces the average fission cross section and increases the average capture cross section in respect to their single-level counterparts. In consequence I_α increases for growing degrees of interference.

Table 1.7.2 shows the behavior of the factors I_F , I_C , and I_α when the interference index $\langle \Gamma \rangle / \langle D \rangle$ is changed by increasing the averaged fission width in accordance with the relation

$$\langle \Gamma_f \rangle / \langle D \rangle = \frac{1}{2\pi} \sum_{n=1}^{\nu_F} P_n, \quad (7)$$

where the penetration factors, P_n , were taken as unity, and the number of open channels, ν_F , was varied from one to four. We then investigated a case in which the number of open fission channels was again varied between one and four. However, the average fission width in each channel was properly adjusted to keep the total average fission width, $\langle \Gamma_f \rangle$, constant. The results are shown in Table 1.7.3. All the interference factors tend toward the single-level limit when the number of open fission channels is increased. This behavior is understandable on the basis that as the number of fission channels is augmented, the possibility of destructive interference between them increases, leading to the above result.

Table 1.7.1. The Variation of the Interference Factors I_F , I_C , and I_α as a Function of the Average Fission Width

$\langle \Gamma_{cf} \rangle^a$ (eV)	I_F	I_C	I_α
0.0397	0.989	1.023	1.034
0.079	0.979	1.083	1.106
0.119	0.972	1.162	1.195
0.159	0.966	1.254	1.298
0.397	0.943	2.001	2.122

^aFour fission channels of equal average width, $\langle D \rangle = 1.0$ eV, $\Gamma_n^0 = 0.1$ MeV, and $\Gamma_\gamma = 50$ MeV.

Table 1.7.2. The Variation of the Interference Factors as a Function of the Number of Open Fission Channels

ν_F^a	I_F	I_C	I_α
1	0.93	1.075	1.15
2	0.945	1.15	1.22
3	0.96	1.20	1.26
4	0.97	1.23	1.27

^a $D = 1.0$ eV, $\Gamma_n^0 = 0.1$ MeV, and $\Gamma_\gamma = 50$ MeV.

Table 1.7.3. The Variation of the Interference Factors as a Function of the Number of Open Fission Channels with $\langle \Gamma_f \rangle$ Constant

ν_F^a	I_F	I_C	I_α
1	0.920	1.074	1.167
2	0.968	1.054	1.089
3	0.983	1.033	1.051
4	0.989	1.023	1.034

^a $\langle D \rangle = 1.0$ eV, $\langle \Gamma_n^0 \rangle = 0.1$ MeV, $\langle \Gamma_\gamma \rangle = 50$ MeV, and $\langle \Gamma_{cf} \rangle$ is adjusted to keep the average fission width constant.

In view of the fact that the previous results were obtained for 100 interfering levels, the question arises concerning the appropriateness of this number of levels to describe the multilevel effects. To answer this question we studied the variation of the fission and capture interference factors as a function of the level number between 1 and 100 levels which is the upper limit available in the present version of the program SUPERPOLLA. The results for I_F and I_C are exhibited in Figs. 1.7.1 and 1.7.2 respectively. In both instances, within the statistical uncertainties, the values of the interference factors reach an asymptotic behavior beyond $N = 80$ levels. In the case of the four fission channels calculations, the total average fission width was kept at the same value as the one used for the one-channel calculation.

The calculations reported here predict sizeable multilevel interference effects. When the resonance interference increases, the deviation from the single-level limit of the three interference factors also increases for a given number of open fission channels (Table 1.7.1). The contrary effect is observed when one increases the number of fission channels, keeping the total average fission width constant (Table 1.7.3), as a result of the

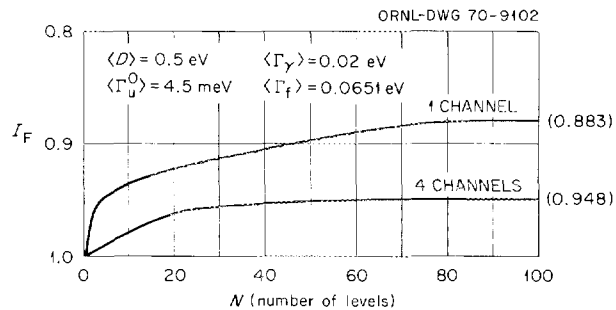


Fig. 1.7.1. The Interference Factor for Fission, I_F , vs the Number of Interfering Levels.

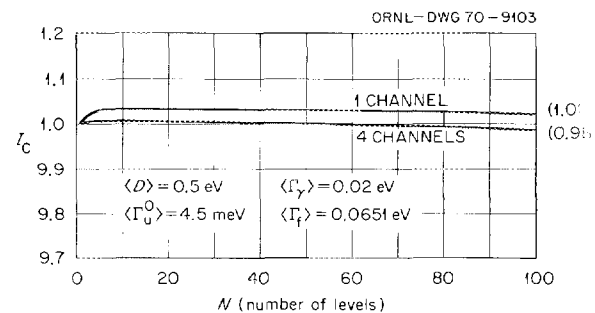


Fig. 1.7.2. The Interference Factor for Capture, I_C , vs the Number of Interfering Levels.

destructive interference effect mentioned previously. For the conditions corresponding to the results shown in Table 1.7.2, one establishes an intermediate situation with respect to the two previous instances, in which the effect of increasing the average fission width is partially compensated for by the destructive interference feature due to the opening of more fission channels. In view of these results, one concludes that the single-level approximation overestimates the average fission cross section and underestimates the average capture cross section. The value of $\langle \omega \rangle = \langle \sigma_c \rangle / \langle \sigma_f \rangle$ obtained from the single-level formalism may be too low by 20% or more, an effect which had already been noted by Lynn.⁵

References

¹P. L. Kapur and R. Peierls, *Proc. Roy. Soc. (London)* **A166**, 277 (1938).

²D. B. Adler and F. T. Adler, *Proc. Conf. on Breeding Economics and Safety in Large Fast Power Reactors*, ANL-6792, p. 695 (October 1963).

³C. E. Porter, *Statistical Theory of Spectra*, Academic, New York, 1965.

⁴See sect. 1.8 (this report).

⁵J. E. Lynn, *Nuclear Data For Reactors*, IAEA, Vienna, vol. II, p. 89 (1967).

1.8 SUPERPOLLA, A PROGRAM TO GENERATE THE STATISTICAL DISTRIBUTION OF THE S-MATRIX PARAMETERS

R. B. Perez G. de Saussure

In the last few years there has been increasing evidence of the importance of the role played by interference phenomena in the interpretation of the neutron cross sections of fissile nuclei.¹ In the Adler-Adler formalism, which is a form of the S -matrix or Kapur-Peierls² formalisms, the reaction cross section is parameterized in the form

$$\sqrt{E} \sigma_x(E) = \sum_k \frac{G_k^{(x)} v_k + (\mu_k - E) H_k^{(x)}}{(\mu_k - E)^2 + v_k^2}, \quad (1)$$

where x indicates the type of neutron reaction, $G_k^{(x)}$ and $H_k^{(x)}$ are the symmetric and asymmetric parts of the complex residue $R_k^{(x)} = G_k^{(x)} - iH_k^{(x)}$, and μ_k and v_k are the real and imaginary parts of the complex S -matrix poles $c_k = \mu_k - iv_k$. For vanishing level interference, the complex residues and poles become, in terms of the R -matrix parameters,

$$G_k^{(x)} = c(\Gamma_{nk}^{(0)} \Gamma_{kx}/v_k),$$

$$H_k^{(x)} = 0,$$

$$\mu_k = E_k,$$

$$v_k = 1/2 \Gamma_k, \quad (2)$$

where $c = 6.52 \cdot 10^5$ b·eV^{1/2}. In the general case, however, the S -matrix parameters are complicated functions of the R -matrix parameters. In order to introduce resonance interference effects in nuclear calculations,³ it becomes necessary to know the statistical distribution of the Kapur-Peierls residues and poles. Whereas the statistical features of the R -matrix parameters can be deduced from rather general properties of the nuclear Hamiltonian and its eigenfunctions,⁴ an equivalent theory for the S matrix is not available as yet. The usual approach to the problem is to invert the level matrix in order to construct the corresponding S matrix. This procedure is then repeated for each set of R -matrix parameters sampled from the corresponding distributions.⁵⁻⁷ Exact analytical expressions for the distribution functions have been derived by Hwang³ for the two-level case, and perturbative-type approximations to the many-level case have been obtained by Harris.⁸

The present work utilizes the previously developed POLLA program⁹ combined with Monte Carlo sub-routines allowing the generation and sampling of the appropriate distribution functions of the R -matrix parameters. For a specified set of average R -matrix resonance parameters, number of levels, and open fission channels, the program generates the distribution of the R -matrix and S -matrix parameters and obtains the corresponding averages and variances. In its present status this code package has the capability of handling 100 levels and up to 4 fission channels. Running times for an 80-level case are: 0.306, 0.451, 0.631, and 0.866 min for 1, 2, 3, and 4 fission channels respectively. Typically a problem involving a few fission channels and 100 levels takes on the order of 10 min to generate the number of samples necessary for statistical validity. The savings in computer time is due to the fact that the program avoids the time-consuming inversion of the level matrix by directly expanding the S matrix in partial fractions in the spirit of the Reich-Moore formalism.¹⁰ The program SUPERPOLLA was then utilized to study the effect of level interference in the statistical distribution of the resonance parameters. To this end we have performed calculations and compar-

isons between the 2- and 100-level cases for two different values of the interference index $\langle \Gamma \rangle / \langle D \rangle$.

The average R -matrix parameters utilized in the present calculations were $\langle D \rangle = 0.3$ eV (or 0.03 eV), $\langle \Gamma_n^{(0)} \rangle = 1.0$ MeV, $\langle \Gamma_\gamma \rangle = 0.3$ eV. The average fission width was varied to obtain the desired $\langle \Gamma \rangle / \langle D \rangle$ ratio.

Figure 1.8.1 shows the distribution of the level spacings, D^s , of the complex S -matrix poles. For a low value of the interference index ($\langle \Gamma \rangle / \langle D \rangle = 0.1$), both the 2- and 100-level calculations agree with the Wigner distribution, as was expected. For a high degree of interference the 2-level calculation exhibits a larger proportion of small-level displacements than predicted by the Wigner spacing distribution. However, the introduction of multilevel effects restores the Wigner law within the statistical fluctuations of the sampling procedure. The observed attenuation of the level repulsion effect seems to be typical only of the 2-level case, and it has been reported by Freeman and Garrison⁷ and also predicted analytically by Hwang.³ A comparison between Hwang's analytical results and our numerical calculations for the 2-level case is shown in Fig. 1.8.2. The statistical distribution of the imaginary part of the complex poles, ν_k , is shown in Fig. 1.8.3 for $\langle \Gamma \rangle / \langle D \rangle = 0.1$. Both the 2- and many-level cases agree with the expected χ^2 distribution for the four-channel case specified in this particular calculation. When one increases the ratio $\langle \Gamma \rangle / \langle D \rangle$ up to a value of 10, the majority of levels acquire a width, ν_k , around half the radiation width, Γ_γ , while a few of them show very large widths. The appearance of levels with large widths was also observed by Moldauer.⁵ This interesting fact requires more investigation, in particular concerning the

value of $\langle \Gamma \rangle / \langle D \rangle$ at which these large widths start appearing in the calculation.

The statistical distribution of the symmetric part, G_F , and asymmetric part, H_F , of the fission complex residues for the low-interference case ($\langle \Gamma \rangle / \langle D \rangle = 0.1$) is shown in Fig. 1.8.4. In this instance the interference between resonances is practically negligible, which

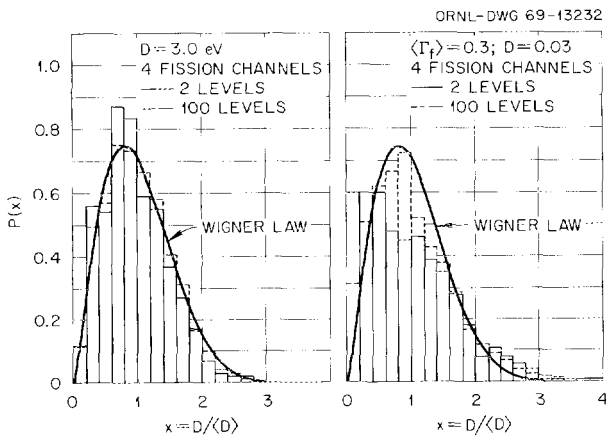


Fig. 1.8.1. The Statistical Distribution of the Level Spacing for the S -Matrix for 2 and 100 Levels: (a) $\langle \Gamma \rangle / \langle D \rangle = 0.1$; (b) $\langle \Gamma \rangle / \langle D \rangle = 10$.

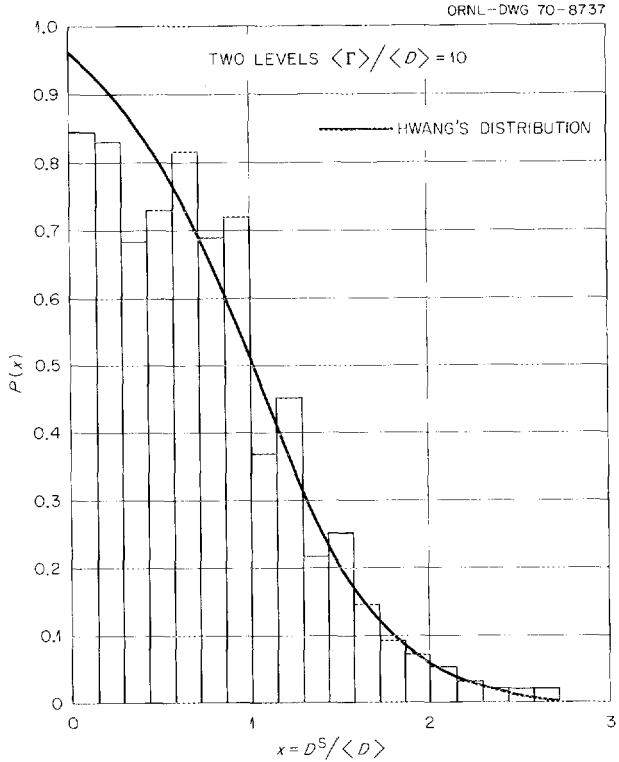


Fig. 1.8.2. Comparison Between Hwang's Analytical Results and SUPERPOLLA Results for 2 Levels; $\langle \Gamma \rangle / \langle D \rangle = 10$.

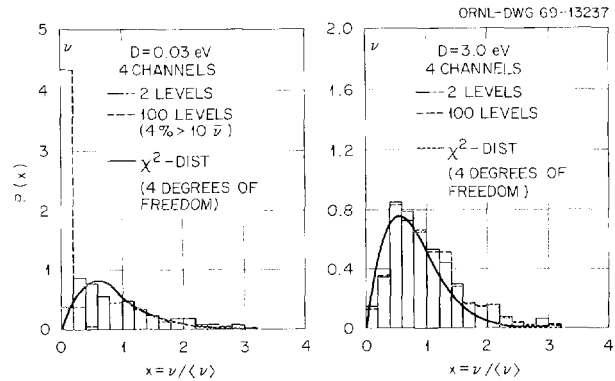


Fig. 1.8.3. The Statistical Distribution of the Imaginary Part of the Complex S -Matrix Poles for 2 and 100 Levels; $\langle \Gamma \rangle / \langle D \rangle = 0.1$.

explains the agreement between the 2- and many-level calculations. The results for the parameter G_F show the appearance of a large number of small negative values.¹¹ The corresponding distribution for H_F is symmetric, as it should be, in order to satisfy the sum rule

$$\sum_k H_{F,k} = 0.$$

As $\langle \Gamma \rangle / \langle D \rangle$ increases, the many-level calculation shows appreciable deviations from the behavior predicted by the 2-level case, the former exhibiting larger distribu-

tion widths (variances). This fact is illustrated in Fig. 1.8.5, which shows the distributions of the symmetric parts of the residues for fission and capture reactions, and in Fig. 1.8.6, which shows the associated asymmetric parts.

Finally, we have also studied the statistical distribution of the complex residues obtained from the fitting of the ^{235}U fission cross section by Derrien and de Saussure¹² and by Cramer.¹³ Cramer performed a Reich-Moore analysis and hence provided the results in terms of R -matrix parameters, which were transformed by the program POLLA⁹ into the corresponding Adler-Adler parameters. Figure 1.8.7 shows the distribution obtained for G_F and H_F from the experimental results mentioned previously. The values for $\langle G_F \rangle$ are in good agreement, as are the corresponding distributions in both sets of experimental data. Their general features are also consistent with the theoretical distribution functions discussed here. The main conclusion of this work is that for all cases but the one corresponding to a very low degree of resonance interference, the 2-level approximation does not describe satisfactorily the statistical distribution of the S -matrix parameters.

The SUPERPOLLA code package has been found to be highly flexible and very suitable to generate the statistical distributions of the S -matrix parameters. It will be used in the immediate future in the analysis of self-indication ratio experiments planned at varying temperatures and sample thicknesses, as well as in the

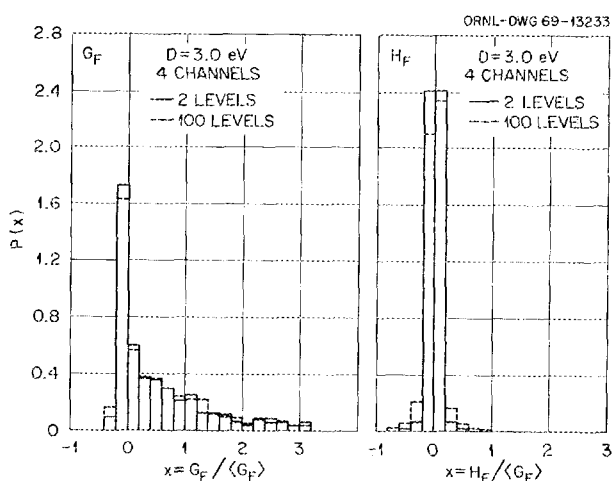


Fig. 1.8.4. The Statistical Distribution of the Complex S -Matrix Residues for Fission; $\langle \Gamma \rangle / \langle D \rangle = 0.1$. (a) The distribution function for the G_F parameter; (b) the distribution function for the H_F parameter.

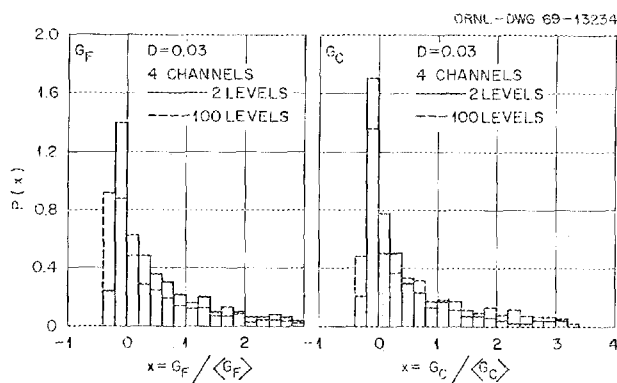


Fig. 1.8.5. The Statistical Distribution of the Symmetric Parts of the Complex S -Matrix Residues for Fission and Capture; $\langle \Gamma \rangle / \langle D \rangle = 10$. (a) The distribution function for the G_F parameter; (b) the distribution function for the G_C parameter.

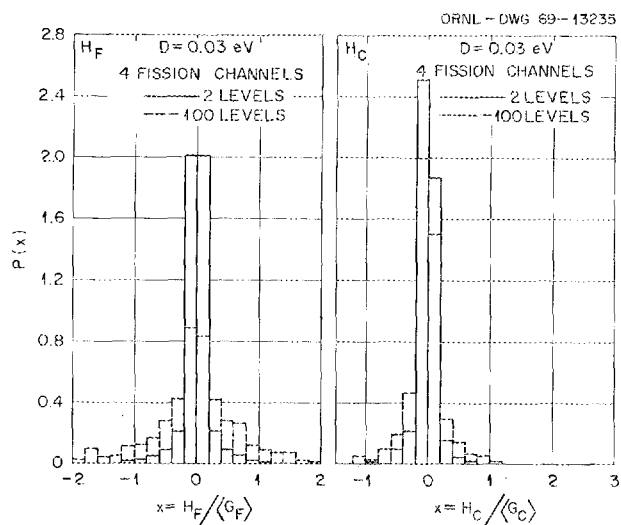


Fig. 1.8.6. The Statistical Distribution of the Asymmetric Parts of the Complex S -Matrix Residues for Fission and Capture; $\langle \Gamma \rangle / \langle D \rangle = 10$. (a) The distribution function for the H_F parameter; (b) the distribution function for the H_C parameter.

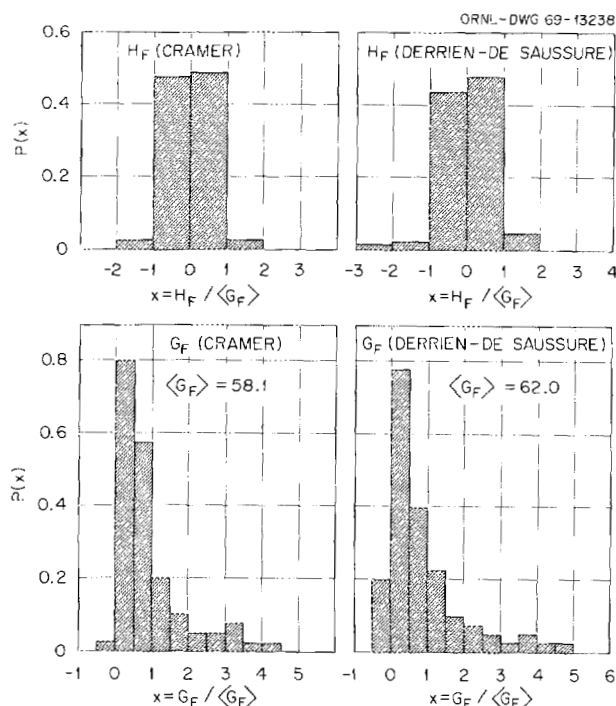


Fig. 1.8.7. The Distribution of the S -Matrix Residues for Fission Obtained from the Experimental Data of Derrien and de Saussure and of Cramer.

study of the statistical properties of cross sections in fissile materials.

References

- ¹D. B. Adler and F. T. Adler, *Proc. Conf. on Breeding Economics and Safety in Large Fast Power Reactors*, ANL-6792, p. 695 (October 1963).
- ²P. L. Kapur and R. Peierls, *Proc. Roy. Soc. (London)* **A166**, 277 (1938).
- ³R. N. Hwang, *Nucl. Sci. Eng.* **36**, 67 (1969).
- ⁴C. E. Porter, *Statistical Theory of Spectra*, Academic, New York, 1965.
- ⁵P. A. Moldauer, *Phys. Rev.* **135**, B642 (1964); *Interfering Response*, ANL-7467 (July 1968).
- ⁶F. T. Adler and D. B. Adler, *Conf. on Neutron Cross Section Technology, March 22-24, 1966, Washington, D.C.*, Conf-660303, book 2, p. 873 (1967).
- ⁷R. A. Freeman and J. D. Garrison, *Nucl. Phys.* **A124**, 577 (1969).
- ⁸D. R. Harris, *Perturbation Transformation of the Nuclear Cross Section Parameters Between Wigner-Eisenbud and Kapur-Peierls Formalisms; and the PERTA Program*, LA-4327 (November 1969).

⁹G. de Saussure and R. B. Perez, *POLLA, A Fortran Program to Convert R-Matrix-Type Multilevel Resonance Parameters for Fissile Nuclei into Equivalent Kapur-Peierls-Type Parameters*, ORNL-TM-2599 (June 1969).

¹⁰C. W. Reich and M. S. Moore, *Phys. Rev.* **112**, 203 (1958).

¹¹The cross section is, of course, always positive.

¹²H. Derrien and G. de Saussure, *Neutron Phys. Div. Ann. Progr. Rept. May 31, 1968*, ORNL-4280.

¹³J. D. Cramer, *The Multilevel Analysis of ^{235}U Fission Cross Sections*, LA-3917 (1968).

1.9 MSC, A PROGRAM TO EVALUATE MULTIPLE SCATTERING CORRECTIONS IN THICK SAMPLES

N. M. Greene¹ G. de Saussure
R. B. Perez S. K. Penny²

The interpretation of capture and fission cross-section measurements requires the evaluation of multiple scattering effects in the sample. After the early analytical approaches to this problem, developed by Dresner³ and Macklin,⁴ the most widely utilized technique has been based on the Monte Carlo method.^{5,6}

The specific problem that we wish to solve is that of extracting the resonance parameters from data obtained through the use of thick samples (several mean free paths). The required procedure involves iterative computational schemes in which one needs to calculate the derivative of the function pertinent to the problem. Because the Monte Carlo technique is not particularly suitable in this instance, in view of its inherent indeterministic nature and characteristically long running times, we have studied the performance of "deterministic" neutron transport codes from the view point of both accuracy and calculation time, which is at a premium when many iterations are needed to solve the problem at hand. The MSC code is built around a modified version of ANISN,⁷ a one-dimensional S_{11} multigroup transport program. ANISN solves the transport one-dimensional Boltzmann equation numerically by setting up a network of meshpoints in the energy, angle, and spatial coordinates. The scattering kernel is expanded in Legendre polynomials to any order of accuracy needed within reasonable computer memory capabilities and time. The other pieces of MSC are a code to evaluate cross sections at many points across a resonance and a code to calculate elastic scattering transfer matrices.

To facilitate the discussion that follows, we shall name the various cases studied in the form ${}^G S_n P_l^R$,

where the subindexes n and l indicate the number of mesh points in the angular coordinates and the order of truncation in the scattering kernel, respectively, and the superindexes G and R indicate the number of energy intervals taken (groups) and the number of space intervals defined along the thickness of the sample respectively. On the basis of the well-known relation

$$\int dE d\vec{\Omega} d\vec{r} \Sigma_x(E) \Phi(\vec{r}, \vec{\Omega}, E) \\ = \int dE \int d\vec{\Omega} \int d\vec{r} S(\vec{r}, \vec{\Omega}, E) \Phi^*(\vec{r}, \vec{\Omega}, E), \quad (1)$$

where

$\Sigma_x(E)$ = macroscopic cross section for a given neutron reaction,

$S(\vec{r}, \vec{\Omega}, E)$ = neutron source,

$\Phi(\vec{r}, \vec{\Omega}, E), \Phi^*(\vec{r}, \vec{\Omega}, E)$ = real and adjoint fluxes,

the total number of events is computed by the convolution of the neutron source and the adjoint flux. There are two reasons for the use of this procedure: (1) it eliminates the necessity for calculating the real flux for each neutron source energy, and (2) it takes advantage of the observed fact that the adjoint flux changes much more slowly with the angular and energy variables than does the real flux.⁸

In order to evaluate the performance of MSC, comparisons were made with a Monte Carlo code MULTSCA.⁹ The specific set of questions to be answered were related to the number of energy groups, angle mesh points, space intervals, and order of truncation in the scattering kernel necessary to obtain results of accuracy comparable with those yielded by the Monte Carlo technique. Besides these points we also wanted information on the effect of the finite radius of the sample, which is not accounted for in the one-dimensional ANISN code, and on the computing times required by the two techniques under study.

The following steps are involved in the MSC calculation:

- a. Compute the Doppler-broadened cross sections in the Breit-Wigner formalism or Adler-Adler¹⁰ formalism at a large number of points across a given resonance;
- b. With the scattering cross sections obtained in step a generate an elastic scattering transfer matrix such as required by the multigroup code ANISN;
- c. Perform a $^G S_n P_l^R$ transport calculation of the adjoint flux with the reaction cross section $\Sigma_x(E)$ used as a source in the adjoint Boltzmann equation;

- d. Compute the number of reaction events in accordance with Eq. (1).

The example considered in this work was the 6.67-eV capture resonance of ^{238}U . The sample had a radius of 3.81 cm and a thickness of 1.03 mfp, which are dimensions that correspond to actual experimental conditions. Typical timing (IBM 360/91) for the steps listed above is as follows: *a*, 0.3 sec; *b*, 94.0 sec; and *c* and *d* combined, 7.1 sec.

Several MSC calculations are shown in Table 1.9.1. Inspection of the results shows that case 11, corresponding to $(^{100}\text{S}_4\text{P}_1^5)$, compares very well with case 5 $(^{100}\text{S}_{48}\text{P}_3^5)$, the substantial differences occurring away from the resonance energy. This indicates that only a few angle mesh points together with linear anisotropic scattering are suitable for the calculation. The effect of the number of energy points across the resonance can be exhibited by the comparison of case 6 $(^{200}\text{S}_8\text{P}_3^5)$ and case 15 $(^{50}\text{S}_8\text{P}_3^5)$. For the particular points shown in Table 1.9.1, the agreement found is very good; however, the results around the peak of the resonance become marginal for the 50-group case. This suggests that one could use less than 100 groups with a denser energy mesh in the vicinity of the resonance peak and still obtain good results with a considerable saving in computer storage capability and running time. Cases 14 $(^{100}\text{S}_{16}\text{P}_3^5)$ and 12 $(^{100}\text{S}_{16}\text{P}_1^5)$ show that for all practical purposes a few spatial intervals will suffice. Further calculations have shown that, in fact, for sample thickness up to 15 mils as few as two space intervals yield accurate results.

Figure 1.9.1 displays a comparison between the MSC results and a Monte Carlo calculation by MULTSCA, which utilizes 100 energy bins and 10^4 neutron histories. The agreement for case 5 $(^{100}\text{S}_{48}\text{P}_3^5)$ is excellent. Case 11 $(^{100}\text{S}_4\text{P}_1^5)$, which is a much shorter calculation, also yields results which are accurate enough for our purposes. Both results indicate that indeed the finite size of the sample does not invalidate the MSC one-dimensional calculations.

The calculation time for each run shown in Table 1.9.1 does not include times for steps *a* and *b*. The time invested in the calculation of the Doppler-broadened cross section is a fraction of a second and does not add appreciably to the overall timing. The longest calculation by far is the one related to the elastic scattering transfer matrix; however, it need be calculated only once at the beginning of a set of iterations. Between successive iterations it is necessary only to scale the transfer matrix, which again takes about a fraction of a second. In the particular case at hand the Monte Carlo calculation run for 7.95 min is to be compared with

Table 1.9.1. MSC Calculations

Case	n of S_n	l of P_l	Spatial Intervals	Energy Spacing (eV)	Computer Time (min)	Response (Captures neutron ⁻¹ cm ⁻²)		
						5.195 eV	6.605 eV	7.505 eV
1	4	3	5	0.030	0.11	1.5188-4	3.6981-2	3.9399-4
2	8	3	5	0.030	0.11	1.4641-4	3.6952-2	3.8088-4
3	12	3	5	0.030	0.13	1.4523-4	3.6948-2	3.7838-4
4	32	3	5	0.030	0.29	1.4426-4	3.6945-2	3.7839-4
5	48	3	5	0.030	0.42	1.4443-4	3.6945-2	3.7916-4
6	8	3	5	0.015	0.21	1.4641-4	3.6946-2	3.8088-4
7	12	3	5	0.015	0.26	1.4523-4	3.6942-2	3.7839-4
8	32	3	5	0.015	0.52	1.4428-4	3.6940-2	3.7839-4
9	4	3	2	0.030	0.04	1.5188-4	3.7104-2	3.9398-4
10	4	3	10	0.030	0.13	1.5188-4	3.6961-2	3.9398-4
11	4	1	5	0.030	0.08	1.5189-4	3.6964-2	3.9404-4
12	16	1	5	0.030	0.18	1.4476-4	3.6928-2	3.7759-4
13	16	3	5	0.030	0.16	1.4475-4	3.6946-2	3.7751-4
14	16	3	25	0.030	0.68	1.4475-4	3.6918-2	3.7751-4
15	8	3	5	0.060	0.06	1.4643-4	3.70-2 ^a	3.82-4 ^a
16	12	3	5	0.060	0.07	1.4524-4	3.70-2 ^a	3.80-4 ^a
17	32	3	5	0.060	0.16	1.4426-4	3.70-2 ^a	3.80-4 ^a

^aThese points did not exist in the 0.060 spacing structure and are interpolated values.

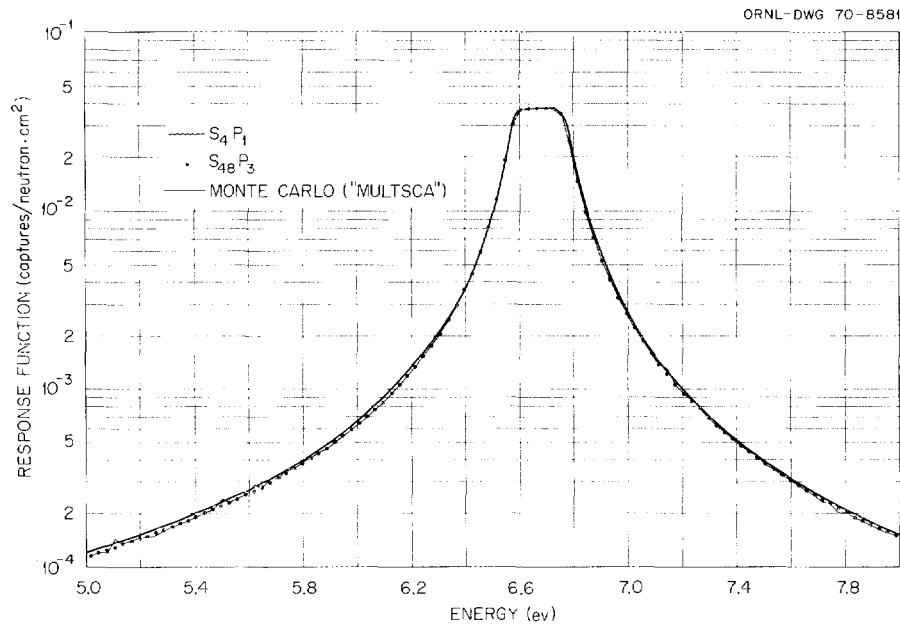


Fig. 1.9.1. Comparison Between the Monte Carlo Calculation and Various MSC Results.

0.42 min for case 5 ($^{100}S_{48}P_3^5$) and with only 0.08 min for case 11 ($^{100}S_4P_1^5$). In view of the above results, it seems then feasible to utilize deterministic codes for resonance parameter searches with thick-sample cross-section measurements used as input data.

Present work is concerned with combining steps *a* through *d* into a single callable code package to allow automating the resonance parameters adjustments.

References

- ¹Computing Technology Center, Union Carbide Corp., Oak Ridge, Tenn.
- ²Mathematics Division.
- ³L. Dresner, *Nucl. Instr. Methods* **16**, 176 (1962).
- ⁴R. L. Macklin, *Nucl. Instr. Methods* **26**, 213 (1964).
- ⁵F. H. Fröhner, *SESH - A Fortran IV Code for Calculated Self-Shielding Multiple Scattering Effect for*

Neutron Cross Section Data Interpretation in Unresolved Resonance Region, GA-8380 (Jan. 3, 1968).

⁶J. G. Sullivan and G. Warner, private communication, September 1968.

⁷W. W. Engle, *A Users Manual for ANISN, A One-Dimensional Discrete Ordinates Transport Code with Anisotropic Scattering*, K-1693 (1967).

⁸R. W. Brandon, J. C. Robinson, and C. W. Craven, *Nucl. Sci. Eng.* **39**, 151 (1970).

⁹G. de Saussure, *MULTSCA, A Monte Carlo Code to Evaluate Multiple Scattering Corrections*, unpublished (1969).

¹⁰D. B. Adler and F. T. Adler, *Proc. Conf. on Breeding Economics and Safety in Large Fast Power Reactors*, ANL-6792, p. 695 (October 1963).

1.10 DETERMINATION OF HETEROGENEOUS PARAMETERS BY THE NEUTRON WAVE TECHNIQUE¹

E. A. Bernard² R. B. Perez

The purpose of the present work is the study of some heterogeneous effects in reactor physics by the use of neutron wave propagation methods. In particular, we wanted to measure Galanin's constant,³ γ , by using a single fuel rod assembly as opposed to measurements which would demand the construction of expensive subcritical or critical assemblies. The experimental setup is extremely simple. It consists of a large body of heavy water with a fuel rod inserted centrally. The neutron source is located so as to generate essentially plane neutron waves propagating along the axial direction of the rod. With minor modifications the experimental procedure is the one described by Booth *et al.*⁴ The neutron pulses were followed both in the axial and the transverse directions and then analyzed into their Fourier components. Due to limitations imposed by the thermalizing tank,⁴ the highest meaningful wave frequency analyzed was around 350 cps.

The theoretical dispersion law was derived from the usual Fermi age-diffusion theory coupled with the methods of the small-source model.³ One obtains for the squared inverse complex relaxation length

$$\rho^2 = B_1^2 + \frac{1}{L_{th}^2} + \frac{i\omega}{D_0^{th}} - \gamma \left\{ \eta \rho e^{-(B_1^2 - \rho^2)\tau - i\omega l_s} - 1 \right\} W(r_0), \quad (1)$$

where the symbols have their customary meaning and $W(r_0)$ is a weight factor (cm^{-3}) which depends on the radial dimensions of the fuel rod and the moderator. Inspection of Eq. (1) immediately reveals that there are two frequencies, ω_M and ω_F , for the moderator alone and for the actual assembly at which the corresponding dispersion laws intersect. This fact provides, within the limitation of our model, the condition

$$\tan(2\alpha_F \xi_F \tau - \omega_F l_s) = (\omega_F - \omega_M) \left[\frac{1}{\gamma D_0^{th} W(r_0)} \right], \quad (2)$$

where α_F and ξ_F are, respectively, the real and imaginary parts of the system's dispersion law at the intersection. Equation (2) provides a new relation for the calculation of reactor physics parameters.

Table 1.10.1 compares the experimental and theoretical dispersion laws. Excellent agreement was found at low frequencies. As expected, the age-diffusion model breaks down at high frequencies where thermalization effects in the moderator play an important role. This is more dramatically indicated by the fact that the value of ω_F predicted by the theory was 310 cps as compared with the experimental value of 138 cps.

The value of the parameter γ was obtained by the best fit to the experimental dispersion law. The result was $\gamma = 0.25 \pm 0.02$, which is slightly below the value $\gamma = 0.32$ computed from diffusion theory.

The viability of the neutron wave technique to study heterogeneous effects has been shown. More experimentation should be performed, however, to study the interaction between fuel rods and its possible influence on the value of γ . This type of experimentation also does set a challenge for the development of more realistic theoretical models.

Table 1.10.1. Comparison of Experimental and Theoretical Dispersion Laws

Frequency (cps)	α_{th}	α_{exp}	ξ_{th}	ξ_{exp}
0	0.0385	0.038	0	0
50	0.042	0.042	0.0181	0.018
100	0.049	0.049	0.0311	0.031
150	0.056	0.056	0.0409	0.041
200	0.062	0.063	0.0491	0.048
250	0.068	0.070	0.0562	0.054
300	0.074	0.077	0.0625	0.059
350	0.079	0.080	0.0682	0.065

References

¹Paper presented at Meeting of American Nuclear Society, San Francisco, Calif., November 1969.

²Present address: Los Alamos Scientific Laboratory.

³A. D. Galanin, *Thermal Reactor Theory*, Pergamon, New York, 1960.

⁴R. S. Booth, R. G. Hartley, and R. B. Perez, *Nucl. Sci. Eng.* 28, 404 (1967).

1.11 A GENERAL FORMALISM FOR THE T MATRIX OF NUCLEAR REACTION THEORY

R. B. Perez A. J. Mockel¹

The purpose of this work is to show that the T matrix satisfies a general Ricatti-matrix equation as a function of any of the parameters relevant to the nuclear reaction process and to give for a wide class of problems its expression as a function of these parameters. To this end we start with an expression for the derivative of the R matrix obtained previously,² which is

$$\frac{d}{d\tau} \mathbf{R} = \mathbf{A}_0 + \mathbf{A}_1 \mathbf{R} + \mathbf{R} \mathbf{A}_1 + \mathbf{R} \mathbf{A}_2 \mathbf{R} + \mathbf{F}_0, \quad (1)$$

where the A matrices depend on the derivatives of the channel radii and boundary condition numbers with respect to the parameter τ , and

$$F_{cc'} = \int_S \int_{S'} dS dS' \eta_c \psi_c^* [\vec{r}(S)] \times \left\{ \int_V dV G[\vec{r}(S)|\vec{r}, \tau] \frac{d}{d\tau} [E(\tau) - V(\vec{r}, \tau)] G^+[\vec{r}|\vec{r}(S'), \tau] \right\} \times \eta_{c'} \psi_{c'} [\vec{r}(S')], \quad (2)$$

and

$$\eta_{c'} = \left(\frac{\hbar^2}{2M_c a_c} \right)^{1/2}, \quad (3)$$

where $G[\vec{r}(S)|\vec{r}, \tau]$ is the Green's function for the many-body Schrodinger equation, $\psi_c[\vec{r}(S)]$ is the channel function, and $V(\vec{r}, \tau)$ is the nuclear potential. Subsequently one takes the derivative of the following relationship between the \mathbf{T} and \mathbf{R} matrices:³

$$\mathbf{T} = -2\mathbf{I} - 2i\mathbf{P}^{-1/2} (\mathbf{L}^{-1} - \mathbf{R})^{-1} \mathbf{P}^{-1/2}, \quad (4)$$

$$\mathbf{L} = i\mathbf{P}, \quad (5)$$

where \mathbf{P} is the penetration factor diagonal matrix and we made the choice $\mathbf{S} = 0$ (valid for S -wave neutrons). Then after some algebra one finds the following Ricatti-matrix equation for the T matrix:

$$\frac{d}{d\tau} \mathbf{T} = \beta_0 + \beta_1 \mathbf{T} + \mathbf{T} \beta_1 + \mathbf{T} \beta_2 \mathbf{T}, \quad (6)$$

$$\beta_{0cc'} = 2i(P_c A_{0c} \delta_{cc'} + F_{cc'}), \quad (7)$$

$$\beta_{1cc'} = \left(\frac{1}{2} \frac{d}{d\tau} \ln P_c + A_{1c} + iP_c A_{0c} \right) \delta_{cc'} + iF_{cc'}, \quad (8)$$

$$\beta_{2cc'} = \left[\frac{1}{2} \frac{d}{d\tau} \ln P_c + \frac{i}{2} (P_c A_{0c} - P_c^{-1} A_{2c}) + A_{1c} \right] \delta_{cc'} + \frac{i}{2} F_{cc'}, \quad (9)$$

and

$$F_{cc'} = P_c^{1/2} F_{0cc'} P_c^{1/2}. \quad (10)$$

On the basis of the Reid⁴ and Redheffer⁵ method, the solution of Eq. (6) can be put in the form

$$\mathbf{T}(\tau) = \mathbf{T}(\tau_0) + \mathbf{Q}(\tau_1, \tau_0) \mathbf{Z}^{-1}(\tau_1, \tau_0) \quad (11)$$

(provided that the matrix \mathbf{Z} is nonsingular), where $\mathbf{Q}(\tau, \tau_2)$ and $\mathbf{Z}(\tau, \tau_0)$ are obtained from the solution of the differential system:

$$\frac{d}{d\tau} \mathbf{Z} = -\mathbf{C}_2 \mathbf{Z} - \mathbf{C}_3 \mathbf{Q} \quad (12)$$

and

$$\frac{d}{d\tau} \mathbf{Q} = \mathbf{C}_0 \mathbf{Z} + \mathbf{C}_1 \mathbf{Q}, \quad (13)$$

with

$$\mathbf{C}_0 = \beta_0 + \beta_1 \mathbf{T}(\tau_0) + \mathbf{T}(\tau_0) \beta_1 + \mathbf{T}(\tau_0) \beta_2 \mathbf{T}(\tau_0), \quad (14)$$

$$\mathbf{C}_1 = \beta_1 + \mathbf{T}(\tau_0) \beta_2, \quad (15)$$

$$\mathbf{C}_2 = \beta_1 + \beta_2 \mathbf{T}(\tau_0), \quad (16)$$

$$\mathbf{C}_3 = \beta_3, \quad (17)$$

$$\mathbf{Z}(\tau_0, \tau_0) = 0, \quad (18)$$

and

$$\mathbf{Q}(\tau_0, \tau_0) = \mathbf{I}. \quad (19)$$

In general, it might be more desirable to solve numerically Eq. (6) than the linear system, Eqs. (12) and (13). However, there are two cases of large physical interest which we have found to result into a closed form solution of Eq. (6) by the Reid-Redheffer method.

The first case appears when one identifies the parameter τ with the channel radius a_c and a square well potential, or with the boundary condition number B_c . Then the \mathbf{C} matrices are independent of the variable τ , so that one immediately obtains for the matrices \mathbf{Q} and \mathbf{Z} the expressions

$$\mathbf{Q}(\tau, \tau_0) = \frac{1}{2\pi i} \oint M^{-1}(s)(s\mathbf{I} + \mathbf{C}_2)\mathbf{C}^{-1} e^{s\tau} ds,$$

$$\mathbf{Z}(\tau, \tau_0) = \frac{1}{2\pi i} \oint \mathbf{C}_0^{-1}(s\mathbf{I} - \mathbf{C}_1) \times M^{-1}(s)\mathbf{C}_3(s\mathbf{I} - \mathbf{C}_1)^{-1} e^{s\tau} ds,$$

and

$$\mathbf{M} = [(s\mathbf{I} + \mathbf{C}_2)\mathbf{C}_0^{-1}(s\mathbf{I} - \mathbf{C}_1)\mathbf{C}_0 + \mathbf{C}_3\mathbf{C}_0],$$

which combined with Eq. (11) determine the T matrix. The second case in which a complete solution can be written is more general than the previous one. It arises whenever the parameter τ is neither the channel radius nor the boundary condition number. Then for any other of the parameters entering in the theory, such as the energy of the incident particle, the matrices \mathbf{C} can be written in the forms:

$$\mathbf{C}_0 = 2i \left[\mathbf{I} + \frac{1}{2} \mathbf{T}(\tau_0) \right] \mathbf{F}(\tau) \left[\mathbf{I} + \frac{1}{2} \mathbf{T}(\tau_0) \right],$$

$$\mathbf{C}_1 = i \left[\mathbf{I} + \frac{1}{2} \mathbf{T}(\tau_0) \right] \mathbf{F}(\tau),$$

$$\mathbf{C}_2 = i \mathbf{F}(\tau) \left[\mathbf{I} + \frac{1}{2} \mathbf{T}(\tau_0) \right],$$

and

$$\mathbf{C}_3 = \frac{i}{2} \mathbf{F}(\tau),$$

which allow the uncoupling of the differential system, Eqs. (12) and (13), yielding the following expression

for the T matrix:

$$\mathbf{T}(\tau) = \mathbf{T}(\tau_0) + \left\{ \mathbf{I} + \int_{\tau_0}^{\tau} d\tau' \left[\mathbf{I} + \frac{1}{2} \mathbf{T}(\tau_0) \right] \mathbf{F}(\tau') \right. \\ \left. \times \left[\mathbf{I} + \frac{1}{2} \mathbf{T}(\tau_0) \right] \right\} \left[\int_{\tau_0}^{\tau} d\tau' \mathbf{F}(\tau') \right]^{-1}$$

The present formalism affords a method of constructing the T matrix from its initial value up to any given value of the pertinent parameter. It is therefore expected to have ample applications in perturbation theory and in the utilization of nuclear structure calculation functions in reaction theory.

References

- ¹ University of Florida, Gainesville.
- ² A. J. Mockel and R. B. Perez, *Variation of the R-Matrix*, ORNL-TM-2816 (January 1970).
- ³ A. M. Lane and R. G. Thomas, *Rev. Mod. Phys.* **30**, 257 (1958).
- ⁴ W. T. Reid, *J. Math. Mech.* **8** (1959).
- ⁵ R. Redheffer, *J. Rational Mech. Anal.* **5** (1956).

1.12 THE ABSOLUTE SPECTRUM OF PHOTONS EMITTED IN COINCIDENCE WITH THERMAL-NEUTRON FISSION OF ^{235}U ¹

R. W. Peelle · F. C. Maienschein²

Data obtained earlier have been fully analyzed to yield the absolute energy spectrum of prompt photons emitted from the fission of ^{235}U by thermal neutrons. In the measurement, each of three types of NaI(Tl) scintillation spectrometers (single-crystal, Compton, and pair) was operated in coincidence with a fission chamber exposed to thermal neutrons from the Oak Ridge Graphite Reactor or the Bulk Shielding Reactor at the Oak Ridge National Laboratory. The effective coincidence resolving time was ≤ 69 nsec. Detailed and careful construction of the response functions of the spectrometer was based on their exposure to radioactive sources of known disintegration rates. These data were used to "unfold" the measured pulse-height spectra to give the absolute differential energy spectrum and uncertainty. The average number of photons per fission was 8.13 ± 0.35 , and the energy release per fission was 7.25 ± 0.26 MeV, both over the energy region from 10 keV to 10.5 MeV. Output spectra are given with an

effective resolution only slightly broader than the inherent energy resolution of the spectrometers except at energies above 5 MeV, where the raw pulse-height bins were made wider than the spectrometer resolution to reduce statistical uncertainties. Combinations of the data into four sets of coarser energy groups are also included to simplify use of these data in computations. The results obtained here are in approximate agreement with the measurement of Verbinski *et al.* in the energy region above 100 keV. From 1.5 to 4 MeV the calculation of Zommer *et al.* gives results which are surprisingly close to the measurements. The observed total energy release in photon emission per fission is predicted reasonably closely by the Thomas and Grover calculation, which takes into account the large angular momentum of the fission fragments.

References

¹ Analysis supported by the Los Alamos Scientific Laboratory; abstract of ORNL-4457 (April 1970).

² Joined by T. A. Love particularly for the experimental work, by R. O. Chester for characterization of the response functions, and by W. Zobel for the spectrum unscrambling.

1.13 OAK RIDGE ELECTRON LINEAR ACCELERATOR (ORELA)

N. A. Betz ¹	T. A. Lewis ⁴
A. L. Boch ²	F. C. Maienschein
J. A. Harvey ³	J. W. Reynolds ⁴
H. A. Todd ⁴	

The electron linear accelerator was accepted from the manufacturer, Varian Associates, on August 25, 1969. At the time of acceptance, the accelerator had met the following performance specifications: 140-MeV electron energy, 15-A peak electron current for pulses shorter than 24 nsec, 2.5- to 1000-nsec burst widths, repetition rates to 1000 pps, and 50-kW electron beam power for a pulse length of 26 nsec and 1000 pps. After acceptance the accelerator operated on a 24-hr-per-day, 5-day-per-week schedule until May 1, 1970 and since that date has operated on a 7-day-per-week schedule with occasional weeks scheduled for maintenance. From August 25, 1969, to June 1, 1970, 2223 hr of accelerator time were used by experimenters; a monthly breakdown is shown in Table 1.13.1. As is indicated in the table, the overall availability of the Linac has been 74%, which we consider to be excellent for the initial period of operation.

Since August 1969, as many as six experimenters have simultaneously used the Linac beam for neutron time-of-flight experiments, but the average number of experimenters has been about three. Table 1.13.2 shows the assignment of flight stations for specific experiments and gives references to other papers in this report and in the 1969 Physics Division Annual Progress Report, ORNL-4513, which describe these experiments. It is pertinent to note one result of general interest that was obtained in the experiments of Burgart *et al.*⁵ (see Sect. 2.37). A measurement of the fast-neutron energy spectrum from 0.8 to 18 MeV from the tantalum target was made at the 50-m shield test station with an NE-213 liquid scintillator. Results obtained both by the time-of-flight technique and by unfolding the pulse-height spectrum from the scintillator giving the neutron-energy spectrum are in excellent agreement. Furthermore, there is rather good agreement both in shape and magnitude with the calculations of Alsmiller, Gabriel, and Guthrie⁵ made prior to the measurements.

1.13.1 Linac Maintenance

The performance of the klystrons which are used as the main source for the 1300-Mc power has been very satisfactory. One klystron failed at 3005 high-voltage hours; three other klystrons have accumulated lifetimes of 2500 to 4000 high-voltage hours.

The key to the successful operation of ORELA as a short, intense pulsed-neutron source is the electron gun and the electronic circuit that drives it. The gun-grid drive pulse is generated by a hydrogen thyratron and is sharpened by a nonlinear circuit based on the use of ferrite-loaded delay lines. The heat-removal capacity, the degree of conservatism in component selection, and the ease of maintenance of the gun drive leave much to be desired. Limitations in the heat removal capacity of the gun-drive circuitry represent the most likely area of concern in attempting to improve the full power reliability of the machine. Thus we have initiated a program to replace this circuitry. The redesign is about one-third complete; the remaining design and construction are expected to require another ten months.

As recorded in last year's report⁶ electron guns have been operated with peak target currents as high as 18 A with a very satisfactory dark current. In order to increase the lifetime of the cathode, a different method of depositing the cathode surface was developed by the EIMAC Division of Varian Associates. This modified gun lasted 1600 hr, and peak target currents of 12 A were obtained. Efforts are being made to continue to improve the performance and lifetime of the electron guns.

Table 1.13.1. ORELA Operation for Period from August 25, 1969, to June 1, 1970

Date	Research Hours	Scheduled Maintenance Hours	Unscheduled Maintenance Hours	Availability (%)
8-25-69 to 9-30-69	272.2	32.0	14.8	94.8
10-1-69 to 10-31-69	216.4		307.6	41.3
11-1-69 to 11-30-69	243.5	48.0	14.5	94.3
12-1-69 to 12-31-69	315.0	40.0	24.3	93.0
1-2-70 to 1-31-70	273.9	32.0	28.9	90.5
2-2-70 to 2-28-70	292.5	32.0	114.9	71.8
3-2-70 to 3-26-70	167.0	32.0	218.4	43.3
3-30-70 to 5-1-70	176.5	227.0	13.1	93.1
5-1-70 to 6-1-70	265.6	100.0	51.0	83.9
Totals				
8-25-69 to 6-1-70	2222.6	543.0	787.5	73.8

Table 1.13.2 Experiments Performed at ORELA

Flight Path No.	Station	Date Available	Experiment(s)	Reference
1	80m	1-69	Total Neutron Cross Sections; Angular Distributions of Elastically Scattered MeV Neutrons	ORNL-4513, p. 62
1	200 m	8-70	Total Neutron Cross Sections	
2	Electron room	12-69	Fission Fragment Asymmetries from Aligned Fissile Nuclides; Cross Sections for Polarized Neutrons on Polarized Nuclei	ORNL-4513, p. 87 ORNL-4513, p. 106
3				
4	20 m	8-72	Auxiliary Experiments for Flight Path 6	
5	20 m	1-69	Preliminary Experiments for Flight Path 6; Measurements of η Near Thermal Energies	Paper 1.4
6	40 m	1-69	Neutron Cross-Section Measurements Using Scintillation Tank	Paper 1.2
6	150 m	12-70	As Above with Better Energy Resolution and Less Gamma Flash	
7	40 m	1-69	Neutron Capture Cross Sections for Nonfissile Materials in the keV Range	ORNL-4513, p. 33
8	20 m	3-71	Precision Neutron Cross-Section Measurements*	
9	30 m	10-69	Secondary Gamma-Ray Spectra for Shielding Studies	Paper 2.37
9	50 m	12-69	Secondary Gamma-Ray Spectra for Shielding Studies	
10				
11	Electron room	6-70	Gamma-Ray Spectra vs Energy of Neutron Capture	

*Being started on No. 5 at 20 m.

The operation of the thyratrons, CH-1191, 12 of which are used in the Linac, has been quite satisfactory. The average thyatron life is now several thousand hours.

Repeated breakdowns have occurred in the cables that carry the high-voltage pulse to the klystron. The sharply pulsed high-peak current has led to overheating of the cables provided with the Linac. At present, four cables of RG-19 in parallel are working satisfactorily. We are now attempting to obtain specially molded cables, complete with terminators, from the company that provides these for SLAC.

A spare-parts inventory-control program for the Linac has been put into operation on the computers of the phase I data-handling system. About 90% of the initially planned spare parts are now on hand.

1.13.2 Data-Handling System

The ORELA data-handling system consists of a series of computers for real-time data acquisition (phase I) and on-line analysis of the acquired data (phase II). The phase I system is based on two SEL 810B computers

that have attached, in addition to the standard peripherals, high-speed disks for the storage of experimental information. These semirandom-access, fixed-head disks can accept events at a rate of several thousand per second into either 300,000 or 700,000 channels.

The first experimental interface and software for the phase I data-handling system were in operation in June 1969, and data collection began in August 1969. A general-purpose monitor program ODAC, incorporating individualized "crunch" routines for sorting the time-of-flight data into channels, allows the use of the computers for a variety of experiments on a one-at-a-time basis. In particular, the phase I data-handling system has already been utilized in the experiments at flight paths Nos. 1(a), 6, 7, and 11, as shown in Table 1.13.2.

The next major step in the use of the phase I system is the extension of the monitor program to allow simultaneous use of each of the computers by more than one experimenter. The first steps in the extension have already been successfully tested. It should be fully implemented for multiple use of each computer by

ORNL DWG. 70-7588

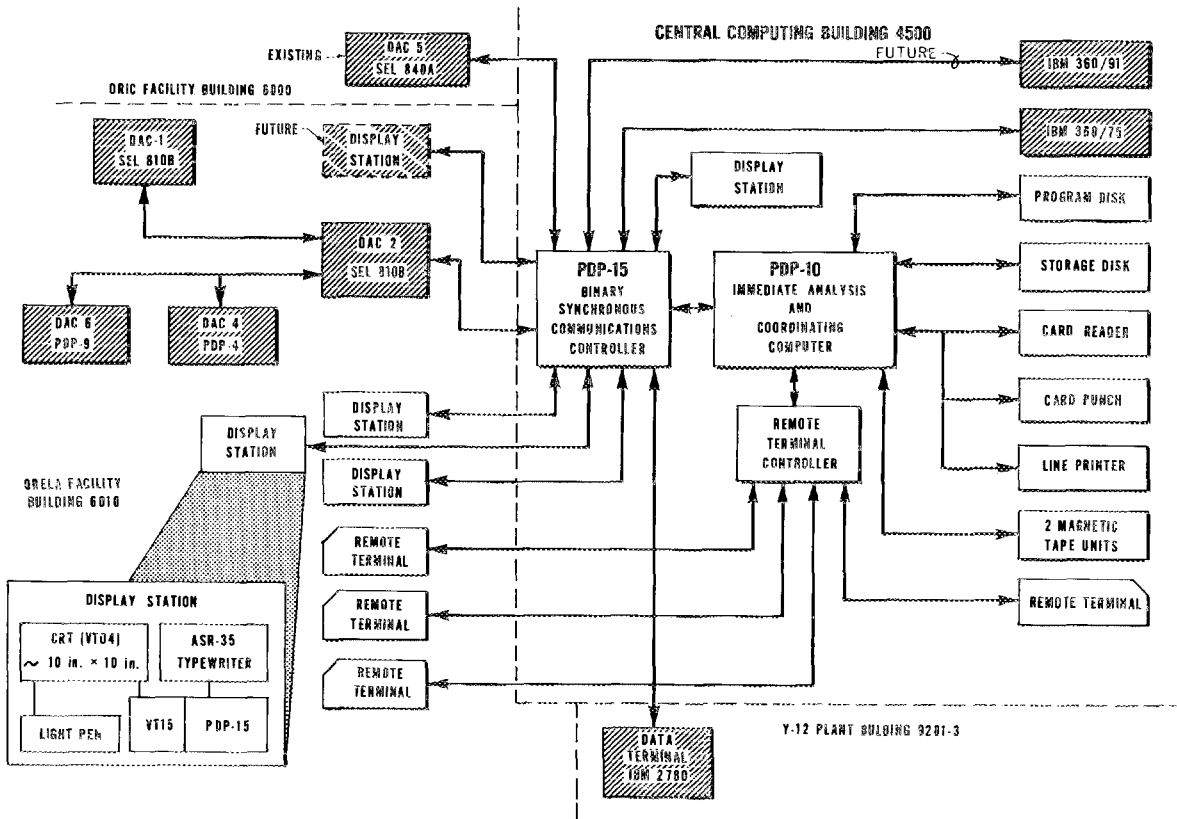


Fig. 1.13.1. ORELA Phase II Computer System.

about September 1970. A maximum of four experiments per computer is planned.

Considerable attention was given in the design and construction of the ORELA building to provide an isolated ground system for the experimental instrumentation with ground contact at a single point. In order to avoid multiple ground paths among experiments which are joined at the data-handling system, it is necessary to provide isolation between each experiment and the data-handling system. An isolation system has been designed, and tests are under way on a partial prototype. If the prototype is successful, an extension will be made to all experiments.

An extension of the phase I data-handling system to accept signals from an existing PDP-9 using an existing PDP-4 link has been designed for completion during the next year.

1.13.3 Immediate Analysis and Coordinating Computer (IACC)

The phase II system is a display-oriented time-sharing computer system⁷ having a response time of less than 5 sec to user requests through the display consoles. Its layout is shown in Fig. 1.13.1. This figure also shows connections to the phase I data-handling system and to other existing computers. The PDP-10, which provides the immediate-analysis capability, will also be used as the ORNL coordinating computer. In this capacity it will communicate with and stand between data-acquisition computers and remote batch-entry devices throughout the Laboratory and the large central computers, the IBM 360/75 and 360/91. A contract for the phase II data-handling system was signed on December 31, 1969; expected delivery of the system is December 1970, with acceptance to be completed by May 1, 1971. This system will be operated by the Mathematics Division. The preparation of the detailed specifications for the phase II system, which will cost approximately \$1.5 million, has required approximately two man-years of effort during the past year and two man-years previously.

References

- ¹ Mathematics Division.
- ² Director's Division.
- ³ Physics Division.
- ⁴ Instrumentation and Controls Division.
- ⁵ R. G. Alsmiller, Jr., T. A. Gabriel, and M. P. Guthrie, *Nucl. Sci. Eng.* **40**, 365 (1970).
- ⁶ A. L. Boch *et al.*, *Neutron Phys. Div. Ann. Progr. Rept. May 31, 1969*, ORNL-4433, p. 9.

⁷J. W. Reynolds, *Application Notes on the Immediate Analysis Display System for ORELA Data Acquisition and Handling*, ORNL-TM-2116 (January 1968).

1.14 PULSE-SHAPE MEASUREMENTS FOR THE OAK RIDGE ELECTRON LINEAR ACCELERATOR WITH GAMMA-RAY DETECTION TECHNIQUES¹

L. W. Weston J. H. Todd²

A study of the pulse-shape characteristics of the Oak Ridge Electron Linear Accelerator was carried out because the resolution of neutron cross-section and neutron spectra measurements is directly dependent upon this pulse shape. Gamma-ray detection with techniques commonly used in neutron time-of-flight experiments was used in the study because of the fidelity with which the pulse shape could be measured.

References

- ¹ Abstract of ORNL-TM-2833 (January 1970); also submitted for journal publication.
- ² Instrumentation and Controls Division.

1.15 FAST FISSION CHAMBER AMPLIFIER-DISCRIMINATOR SYSTEM¹

R. W. Ingle² F. E. Gillespie²
L. W. Weston

To measure the fission cross section of ²³³U as a function of neutron energy, instrumentation with fast-pulse rise time and short resolving-time characteristics is required. The efficient detection of fission-fragment pulses in the presence of a high-alpha background requires these characteristics. A fission detector with an electron collection time of 25 nsec and containing 1 g of ²³³U and an amplifier with a rise time of 7 nsec and an overall gain of 1000 were developed for this measurement. This system, detecting the fast-rising current pulse from a parallel-plate ionization chamber, is an integral part of the instrumentation used by a group at ORNL engaged in the measurement of the neutron fission and capture cross sections as a function of neutron energy. With this system the fission cross section of ²³³U was successfully measured over a neutron energy range from 0.4 to 2000 eV.

References

- ¹ Abstract of paper to be published in *Review of Scientific Instruments*.
- ² Instrumentation and Controls Division.

1.16 11-MeV PROTON INELASTIC SCATTERING FROM EVEN-EVEN MEDIUM-WEIGHT NUCLEI¹

C. M. Perey² J. K. Dickens
R. J. Silva³ F. G. Perey

The analysis of inelastic scattering of 11-MeV protons from quadrupole and octopole collective levels of 14 even-even nuclei between ⁴⁸Ti and ⁷⁶Ge is reported. The distorted-wave-Born approximation is used to calculate the cross sections using the collective model generalization of the optical model for inelastic scattering. The analysis is performed using both real and complex form factors for the model. A satisfactory description of all of the data is obtained when a contribution due to compound nucleus decay for most of the octopole levels and a few of the quadrupole levels is included.

References

¹ Abstract of article accepted for publication by *Physical Review*; also abstract of ORNL-TM-2861 (January 1970).

² Consultant to Neutron Physics Division.

³ Chemistry Division.

1.17 ISOBARIC SPIN DEPENDENCE IN PROTON TRANSFER REACTIONS¹

R. G. Couch² J. A. Biggerstaff³
F. G. Perey K. K. Seth⁴

Results of an experimental investigation of ⁵⁴Fe(*d,n*)⁵⁵Co reactions are presented, and spectroscopic strengths for both *T*< and *T*> states are derived. It is concluded that within the limits of experimental and analytical uncertainties there is no discrepancy between the spectroscopic factors for *T*> analog states as derived from the (*d,n*) and (³He,*d*) reactions.

References

¹ Abstract of *Phys. Letts.*, **29B**, No. 10 (Aug. 18, 1969).

² Present address: Kellogg Radiation Laboratory, California Institute of Technology, Pasadena.

³ Physics Division.

⁴ Present address: Northwestern University, Evanston, Ill.

1.18 MEASUREMENTS OF (*d,n*) REACTIONS ON ⁵⁸Ni, ⁶⁰Ni, ⁶²Ni, AND ⁶⁴Ni AT 5 AND 10 MeV¹

A. L. Marusak²

Absolute differential cross sections for ⁵⁸Ni(*d,n*)⁵⁹Cu, ⁶⁰Ni(*d,n*)⁶¹Cu, ⁶²Ni(*d,n*)⁶³Cu, and ⁶⁴Ni(*d,n*)⁶⁵Cu at 5 and 10 MeV were measured by time-of-flight techniques in order to obtain energy levels, *l* values, and spectroscopic strengths for the odd-*A* copper isotopes and to compare these results with those obtained from the (³He,*d*) and (*α,t*) proton stripping reactions.

Pulsed deuteron beams with pulses of 1 nsec FWHM and currents of 1 to 2 μA were obtained from the Oak Ridge National Laboratory 5.5-MV Van de Graaff and the Tandem Van de Graaff accelerators. Neutrons were detected in 2-in.-thick liquid scintillators optically coupled to phototubes. Gamma rays were discriminated against to reduce background, and the deuteron beam was monitored by measuring elastically scattered deuterons with a silicon surface-barrier detector. Measurements were made at angles ranging from 15 to 120 deg with flight paths varying from 7 to 34 m. Flight times for ground-state neutrons from ⁵⁸Ni(*d,n*)⁵⁹Cu were measured with a resolution of about 2 nsec.

All data were accumulated in a PDP-7 computer. Peak areas and centroids were extracted by means of a light pen which interacted with the PDP-7 by detecting light from an oscilloscope display. Absolute efficiency of the neutron detectors was calculated with a Monte Carlo computer program.

Angular distributions were compared with predictions of DWBA theory using optical model potentials of the Woods-Saxon form, taking into account nonlocality, spin-orbit terms, and finite-range effects in the (*p,n*) interaction. Optical model parameters were obtained from elastic scattering of deuterons on ⁶⁰Ni. Angular distributions predicted by DWBA analysis agreed well with the 10-MeV data but poorly with the 5-MeV data.

Spectroscopic strengths were obtained for 14 levels in ⁵⁹Cu, 19 levels in ⁶¹Cu, 10 levels in ⁶³Cu, and 9 levels in ⁶⁵Cu. Agreement with spectroscopic strengths obtained from (³He,*d*) measurements was good.

Relative spectroscopic strengths of the first few low-lying levels in the odd-*A* copper isotopes are in marked disagreement with those predicted by the simple excited-core model but in fair agreement with predictions of more extended models.

References

¹ Abstract of ORNL-TM-2472 (February 1970).

²Present address: University of California, Los Alamos Scientific Laboratory, P. O. Box 1663, Los Alamos, N.M. 87544.

1.19 SPECTROSCOPY OF $^{65,67,69}\text{Ga}$ BY (d,n) REACTION¹

R. G. Couch² F. G. Perey
J. A. Biggerstaff³ S. Raman⁴
K. K. Seth⁵

The $^{64,66,68}\text{Zn}(d,n)^{65,67,69}\text{Ga}$ reactions have been studied by the neutron time-of-flight method. Absolute differential cross sections have been measured and have been analyzed in terms of the distorted-wave Born approximation. Spin and parity assignments for several levels are proposed on the basis of l values and transition strengths. The experimental results for $^{67,69}\text{Ga}$ are compared with existing theoretical calculations. Only limited agreement is found.

References

¹Abstract of paper accepted for publication in the *Physical Review*; also abstract in ORNL-4513 (June 1970).

²Present address: Kellogg Radiation Laboratory, California Institute of Technology, Pasadena.

³Physics Division.

⁴Nuclear Data Project.

⁵Present address: Northwestern University, Evanston, Ill.

1.20 FINITE-SAMPLE CORRECTIONS TO NEUTRON SCATTERING DATA¹

W. E. Kinney

The correction of neutron-scattering data for finite-sample effects in solid cylindrical samples up to 0.5 total mean free path in radius with height-to-diameter ratios of from 1 to 3 is described. Neutron attenuation is well approximated by assuming the sample to be a disk with the neutrons incident edge-on in a parallel beam. Angular spread is corrected by a factor obtained by numerical integration of the single-scattering integral. Multiple scattering is corrected by a combination of Monte Carlo results and traditional analytic methods, the energy change in inelastic scattering being included explicitly in the formulation. The effect of anisotropic scattering is shown to amount to a few percent at most and to lie within the errors introduced by the assumptions. The Monte Carlo calculations and the validity of the assumptions are considered in an appendix.

Reference

¹Abstract of *Nucl. Instr. Methods* 77, 141–58 (1970).

1.21 NEUTRON ELASTIC- AND INELASTIC-SCATTERING CROSS SECTIONS FOR SODIUM IN THE RANGE OF 5.4 TO 8.5 MeV¹

F. G. Perey W. E. Kinney

We present numerical values for neutron elastic- and inelastic-scattering cross sections for sodium for incident energies from 5.4 to 8.5 MeV. In this energy region there exists only one previous measurement, at 7 MeV, for the inelastic scattering to the first excited state. This datum point is consistent with our results. Two ENDF/B evaluations for sodium are compared with our data. Both evaluations are in fairly good agreement with the integrated elastic cross sections but give poorer agreement for the differential elastic cross sections. For the inelastic-scattering cross sections, one of the evaluations does not go above 5 MeV and the other, although it reproduces the cross section for the first excited state fairly well, fails to reproduce the decrease in the inelastic cross sections as a function of energy for the other levels.

Reference

¹Abstract of ORNL-4518 (June 1970).

1.22 CALCIUM NEUTRON ELASTIC- AND INELASTIC-SCATTERING CROSS SECTIONS FROM 4.0 TO 8.5 MeV¹

F. G. Perey W. E. Kinney

Numerical values are given for neutron elastic- and inelastic-scattering cross sections from calcium in the range of 4.0 to 8.5 MeV. A brief description of the experimental and data-reducing techniques is presented to assist in the evaluation of the data. Elastic angular distributions at two energies are in very good agreement with previous data. There does not exist any previous measurement of inelastic scattering with which to compare our data. The data are compared with the present ENDF/B evaluation. Very good agreement is found for elastic scattering. For inelastic scattering the shapes of the angular distributions are in fair agreement, but there are some serious discrepancies in the magnitudes of the cross sections.

Reference

¹ Abstract of ORNL-4519 (April 1970).

1.23 SULFUR NEUTRON ELASTIC- AND INELASTIC-SCATTERING CROSS SECTIONS FROM 4.0 TO 8.5 MeV¹

F. G. Perey W. E. Kinney

Numerical values are given for neutron elastic- and inelastic-scattering cross sections from sulfur in the range of 4.0 to 8.5 MeV. A brief description of the experimental and data-reducing techniques is presented to assist in the evaluation of the data. Our data are in general agreement with other data in this energy region.

Reference

¹ Abstract of ORNL-4539 (June 1970).

1.24 NEUTRON ELASTIC- AND INELASTIC-SCATTERING CROSS SECTIONS FOR COBALT IN THE ENERGY RANGE 4.19 TO 8.56 MeV¹

W. E. Kinney F. G. Perey

We present numerical values of neutron elastic - and inelastic-scattering cross sections for natural cobalt, ⁵⁹Co, in the incident neutron energy range from 4.19 to 8.56 MeV. Our results are in reasonable agreement with the results of others. Because of the high level density of cobalt, we list data at all energies of measurement as angle-averaged continuum spectra which show structure previously seen in iron and ⁶⁰Ni. There exists no evaluation with which to compare our data. The data partially fulfill a priority II request to NCSAG.

Reference

¹ Abstract of ORNL-4549 (June 1970).

1.25 NEUTRON ELASTIC- AND INELASTIC-SCATTERING CROSS SECTIONS FOR MAGNESIUM IN THE ENERGY RANGE 4.19 TO 8.56 MeV¹

W. E. Kinney F. G. Perey

We present numerical values for neutron elastic-scattering cross sections for natural magnesium and

cross sections per atom of natural magnesium for inelastic scattering to levels in ²⁴Mg for incident neutron energies from 4.19 to 8.56 MeV. Our data are in good agreement with the results of others. We find that ENDF/B-evaluated magnesium angular distributions are in fair agreement with our data. The ENDF/B total elastic-scattering cross section agrees well with the experiment below 5 MeV, but at higher energies it is generally higher than the data, the difference being as much as 40%. The ENDF/B total inelastic-scattering cross sections are in good agreement with the experimental data.

Reference

¹ Abstract of ORNL-4550 (June 1970).

1.26 CARBON NEUTRON ELASTIC- AND INELASTIC-SCATTERING CROSS SECTIONS FROM 4.5 TO 8.5 MeV¹

F. G. Perey W. E. Kinney

Numerical values are given for neutron elastic- and inelastic-scattering cross sections from carbon in the energy range 4.5 to 8.5 MeV. A brief description of the experimental and data-reducing techniques is presented to assist in the evaluation of the data. A comparison was made with other data in this energy region, and fairly good agreement was found, particularly with previous time-of-flight data. Our data were also compared with the predictions obtained from the current ENDF/B file of "evaluated" cross sections for carbon. The ENDF/B file was found to reproduce very poorly the data for both elastic and inelastic cross sections. This is not too surprising in view of the rapid changes in the shapes of the cross sections and the paucity of data previously available in this energy region.

Reference

¹ Abstract of ORNL-4441 (December 1969).

1.27 ⁶⁰Ni NEUTRON ELASTIC- AND INELASTIC-SCATTERING CROSS SECTIONS FROM 6.5 TO 8.5 MeV¹

F. G. Perey C. O. Le Rigoleur²
W. E. Kinney

Numerical values are given for neutron elastic- and inelastic-scattering cross sections from ⁶⁰Ni at five

energies from 6.5 to 8.5 MeV. A brief description of the experimental and data-reducing techniques is presented to assist in the evaluation of the data. Angular distributions are given for elastic scattering and inelastic scattering to the low-lying excited states. Above 3-MeV excitation in the residual nucleus, our experimental energy resolution is inadequate to resolve the inelastic scattering to individual levels. This continuum portion of the inelastic spectrum presents much structure which is very similar at all the energies. Angular distributions were extracted for the five lowest peaks in this continuum which are at about 3.2-, 3.7-, 4.1-, 4.4-, and 4.6-MeV excitation.

References

¹ Abstract of ORNL-4523 (April 1970).

² Present address: C.E.N., Cadarache (13), St. Paul lez Durance, France.

1.28 NEUTRON ELASTIC- AND INELASTIC-SCATTERING CROSS SECTIONS FOR SILICON IN THE ENERGY RANGE 4.19 TO 8.56 MeV¹

W. E. Kinney F. G. Perey

We present numerical values for neutron elastic-scattering cross sections for natural silicon and cross sections per atom of natural silicon for inelastic scattering to levels in ²⁸Si for incident neutron energies from 4.19 to 8.56 MeV. Our data are in reasonable agreement with the results of others. The ENDF/B-evaluated silicon cross sections are, with few exceptions, in good agreement with experimental data.

Reference

¹ Abstract of ORNL-4517 (June 1970).

1.29 NEUTRON ELASTIC- AND INELASTIC-SCATTERING CROSS SECTIONS FOR ⁵⁶Fe IN THE ENERGY RANGE 4.19 TO 8.56 MeV¹

W. E. Kinney F. G. Perey

We present numerical values of neutron elastic- and inelastic-scattering cross sections to levels in ⁵⁶Fe per atom of natural iron for incident neutron energies from 4.19 to 8.56 MeV. Our results compare favorably with the results of others. We also compare three sets of evaluated iron cross sections with experimental data and find that the total scattering cross sections are in

fair agreement with the experimental data, but the differential elastic-scattering cross sections are not a good representation of the data beyond the first minimum.

Reference

¹ Abstract of ORNL-4515 (June 1970).

1.30 A MONOENERGETIC 6130-keV GAMMA-RAY SOURCE FOR DETECTOR CALIBRATION^{1,2}

J. K. Dickens R. D. Baybarz³

A monoenergetic 6130-keV gamma-ray source based upon the reaction ¹³C(α, n)¹⁶O has been fabricated using ²⁴⁴Cm as the alpha source.

References

¹ Abstract of paper accepted for publication in *Nuclear Instruments and Methods*; also abstract of ORNL-TM-2958.

² This work funded by the Defense Atomic Support Agency under Subtask No. RRP-2068.

³ Chemical Technology Division.

1.31 COMPARISON OF A METHOD FOR MEASURING ($n, x\gamma$) CROSS SECTIONS USING A PULSED VAN DE GRAAFF ACCELERATOR WITH A METHOD USING AN ELECTRON LINAC^{1,2}

J. K. Dickens F. G. Perey

Operating results for a system to measure ($n, x\gamma$) cross sections for E_n between 4 and 11 MeV using a pulsed Van de Graaff are presented.

References

¹ Abstract of paper accepted for publication in *Nuclear Instruments and Methods*.

² This work partially funded by the Defense Atomic Support Agency under Subtask No. RRP-2068.

1.32 THE ¹⁴N($n, x\gamma$) REACTION FOR $8.5 \leq E_n \leq 11$ MeV^{1,2}

J. K. Dickens F. G. Perey

Differential cross sections are given for the production of discrete-energy gamma rays by neutron interaction with nitrogen for E_n between 8.5 and 11 MeV. The

data supplement similar results for $E_n \leq 8.6$ MeV previously reported in ref. 3. The experimental apparatus, techniques, and difficulties are essentially the same as those previously reported.

References

¹ Abstract of *Nucl. Sci. Eng.* **40**, (1970); also abstract of ORNL-TM-2778 (November 1969).

² This work funded by the Defense Atomic Support Agency under Subtask No. RRP-2068.

³ J. K. Dickens and F. G. Perey, *Nucl. Sci. Eng.* **36**, 280 (1969).

1.33 THE $^{16}\text{O}(n,x\gamma)$ REACTION FOR $6.7 \leq E_n \leq 11$ MeV^{1,2}

J. K. Dickens F. G. Perey

We have obtained gamma-ray spectra for the reactions $^{16}\text{O}(n,n'\gamma)^{16}\text{O}$ and $^{16}\text{O}(n,\alpha\gamma)^{13}\text{C}$ for incident mean neutron energies (E_n) between 6.7 and 11.0 MeV. The gamma rays were detected using a 30-cm³ coaxial Ge(Li) detector placed at 55 and 90 deg with respect to the incident neutron direction. Time-of-flight electronics was used with the gamma-ray detector to discriminate against unwanted pulses due to neutrons and background gamma radiation. Two samples of 75 to 31 g of BeO in the form of right circular cylinders were used. The incident neutron beam was produced by bombarding a deuterium-filled gas cell with a pulsed deuteron beam of appropriate energy; for $E_n \leq 8.5$ MeV the deuteron beam was obtained from the ORNL 6-MV Van de Graaff, and for $E_n \geq 8.6$ MeV it was obtained from the ORNL Tandem Van de Graaff. These data have been reduced to differential cross sections for production of gamma rays from ^{16}O . The cross sections have been compared, where possible, with previously measured values with reasonable agreement. However, there are several important differences, and these are discussed. Summing the partial cross sections yields values for the total nonelastic cross section which are in good agreement with values for the nonelastic cross section obtained from the difference between the total cross section and the total elastic cross section.

References

¹ Abstract of *Nucl. Sci. Eng.* **40**, 283 (1970); also abstract of ORNL-TM-2770 (November 1969).

² This work partially funded by Defense Atomic Support Agency under Subtask No. PC068.

1.34 $^{28-30}\text{Si}(n,x\gamma)$ REACTIONS FOR $5.3 \leq E_n \leq 9.0$ MeV^{1,2}

J. K. Dickens

Interactions of neutrons with silicon have been studied by measuring gamma-ray-production cross sections. For incident mean neutron energies $E_n = 5.35, 5.85, 6.4, 6.9, 7.45, 7.95, 8.5,$ and 9.0 MeV, spectra were obtained for a natural silicon sample. The gamma rays were detected using a coaxial Ge(Li) detector of 30 cm³ active volume. Data were obtained for gamma-ray scattering angles of 55 and 90 deg for all E_n , 35 deg for $E_n = 7.45$ and 8.5 MeV, and 75 deg for $E_n = 6.4$ and 7.45 MeV. Time of flight was used with the detector to discriminate against pulses due to neutrons and background radiation. Data were also obtained at $E_n = 5.9$ MeV and $\theta_\gamma = 55$ deg for a sample of $^{29}\text{SiO}_2$ enriched to 95% in ^{29}Si and for a similarly enriched sample of $^{30}\text{SiO}_2$. These data have been studied to obtain absolute cross sections for production of gamma rays for the incident neutron energies quoted above. The cross sections have been compared, where possible, with previously measured values with fair agreement.

The spectra were studied for gamma rays which could be associated with deexcitation of nuclear levels having unknown decay modes. For ^{29}Si , gamma rays were found having energies appropriate for decay of levels at excitation energies $E_x = 4.736, 4.836, 4.893,$ and 5.249 MeV. For ^{30}Si gamma rays were found for decay of levels at excitation energies $E_x \geq 4.826$ MeV. The spin of the 4.826-MeV state in ^{30}Si is reasonably limited to 2, 3, or 4. No previously unknown transitions were found for ^{28}Si or ^{25}Mg ; for ^{28}Al the evidence suggests that the 1.624-MeV level is a doublet of 3-keV separation.

References

¹ Abstract of article accepted for publication by the *Physical Review*; also abstract of ORNL-TM-2883 (February 1970).

² This work partially funded by the Defense Atomic Support Agency under Subtask No. RRP-3068.

1.35 THE $\text{Fe}(n,x\gamma)$ REACTION FOR $5.35 \leq E_n \leq 9.0$ MeV¹

J. K. Dickens F. G. Perey

As part of a continuing program² to obtain production cross sections for gamma rays produced by the interaction of neutrons with nuclei, we have measured differential cross sections for the reaction $\text{Fe}(n,x\gamma)$ for

nine bombarding neutron energies between 5.35 and 9.0 MeV.

The $D(d,n)^3\text{He}$ reaction was used for the neutron source. Pulsed deuteron beams of ~ 1 -nsec width, obtained from the ORNL 5.5-MV and Tandem Van de Graaff accelerators, struck a gas cell through which D_2 gas was circulated. The emerging neutrons interacted with a 30-g iron sample placed 8 to 10 cm from the target and were monitored by a scintillation-photomultiplier neutron detector. Gamma rays from the sample were detected with a 30-cm^3 Ge(Li) detector placed 75 to 90 cm from the sample. Fast-timing discrimination was used to designate a detected gamma ray as "prompt" or "background." Details of the experimental arrangement, which uses a PDP-7 computer for on-line data accumulation as well as off-line data reduction, may be found in the papers cited in ref. 2.

Several parameters had to be determined before absolute values of $d\sigma/d\omega$ could be obtained; these included the efficiency of the germanium detector, attenuation of gamma rays in the samples, effects due to finite sizes of the neutron source and due to sample neutron attenuation and multiple scattering, and the efficiency of the monitor system. Details of the determination of most of these parameters are given in the previous reports;² facets specific to the present report are discussed briefly.

The major uncertainties associated with reduction of the iron data were (a) the very large number of gamma rays observed (more than 100 peaks in a spectrum, including escape peaks, due to 60 or more different gamma rays), and (b) the fact that deexcitation modes for levels in ^{56}Fe with $E_x \geq 4.9$ MeV are not known. The large number of gamma rays resulted in a substantial underlying Compton distribution; peaks related to differential cross sections of < 0.5 mb/sr could not be extracted with any reliability. The lack of knowledge of the decay modes of the highly excited states resulted in uncertainties in assignment of many observed gamma rays and, in addition, resulted in much uncertainty about the relationship between energies of observed peaks and the energies of the gamma rays producing these peaks. That is, an observed peak could have been a full-energy peak due to a gamma ray having $E_\gamma = E_{\text{observed}}$, or it could have been a double-escape peak due to a gamma ray with $E_\gamma = E_{\text{observed}} + 1.022$ MeV, or a combination of these. This problem was particularly acute for peaks having small areas where neither energy E_γ could be associated with a known transition in ^{56}Fe ; it contributed to the uncertainty in cross-section evaluation even in some cases where one

of the energies E_γ could be associated with a known transition.

Because of these difficulties it was decided to concentrate on reducing the data for the well-known transitions whose cross sections were large enough to report with reasonable confidence. These differential cross sections are collected in Table 1.35.1. The uncertainties assigned to the cross-section data are as follows: 10% for $d\sigma/d\omega > 20$ mb/sr, 15% for $20 \geq d\sigma/d\omega \geq 2$ mb/sr and 20% for $d\sigma/d\omega < 2$ mb/sr. Our data are compared with previously published gamma-ray cross-section data³ and with curves computed using compound-nucleus formalism,⁴ the comparisons are shown in Figs. 1.35.1 and 1.35.2 for the 0.846-MeV transition from the first excited state in ^{56}Fe and the

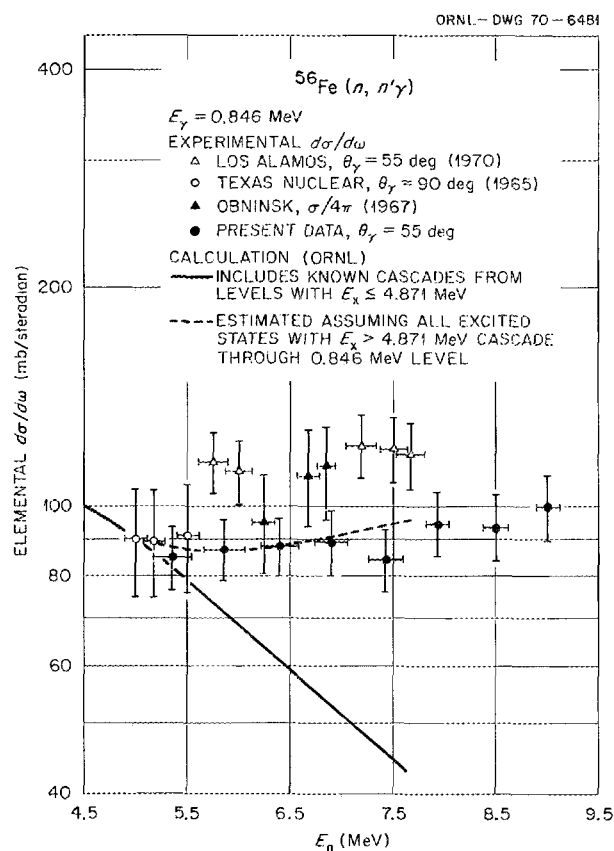


Fig. 1.35.1. Elemental Differential Cross Sections for Gamma-Ray Production Due to Neutron Excitation of the 0.846-MeV First Excited State in ^{56}Fe . The present data, for a gamma-ray scattering angle of 55 deg, are compared with previously published data and with cross sections calculated using compound-nucleus formation combined with direct-interaction excitation.

Table 1.35.1. Elemental Differential Cross Sections for Gamma-Ray Production Due to Neutron Interactions with Iron^a

E_γ (keV)	Level (keV)	Cross Section (mb/sr) for E_n of –															
		5.35 ± 0.20		5.85 ± 0.02		6.40 ± 0.20		6.90 ± 0.15		7.45 ± 0.15		7.95 ± 0.10		8.50 ± 0.10		9.0 ± 0.1	
		MeV		MeV		MeV		MeV		MeV		MeV		MeV		MeV	
		55°	90°	55°	90°	55°	90°	55°	90°	55°	90°	55°	90°	55°	90°	55°	90°
⁵⁶ Fe Isotope																	
846	846	85.0	81.7	86.6	83.2	88.0	82.0	89.2	84.2	84.6	77.5	94.6	84.2	93.4	85.1	101.0	88.8
1038	3123	5.7	5.7	5.6	5.6	6.5	6.1	6.5	6.4	6.3	5.8	7.0	5.3	7.9	6.4	7.4	7.3
1168	3826	2.1	2.2	2.2	1.9	2.5	2.1	1.6	1.8	1.9	1.8	2.6	1.8	2.2	1.9	1.8	2.0
1175	4298																
1238	2085	23.9	22.6	27.0	23.5	28.9	24.5	30.0	25.3	29.6	27.5	33.2	27.2	34.5	31.1	40.0	33.7
1771	3857	2.2	3.2	2.4	3.3	2.4	2.4	2.6	3.1	1.9	2.2	2.0	2.0	2.3	2.3	2.4	1.8
1811	2658	9.3	10.6	11.2	9.6	9.9	8.9	11.0	9.5	9.6	8.2	9.6	8.1	9.2	8.5	9.6	9.0
2035	4120	1.4	1.9	2.8	2.1	2.4	2.3	1.6	1.7	2.2	2.5	2.0	1.4	2.8	2.2	2.6	2.4
2113	2960	5.5	5.9	5.1	5.2	5.4	4.9	5.2	4.7	4.2	4.2	4.3	3.7	4.1	3.7	4.3	4.4
2274	3123	3.3	3.4	2.4	2.9	2.1	2.6	2.2	2.6	2.5	2.8	2.3	2.0	1.7	1.6	2.4	1.8
2523 ^b	3370	5.3	4.5	5.0	3.8	3.5	3.4	3.6	2.0	1.8	1.7	1.6	1.4	2.4	2.2	2.1	1.8
2599 ^c	3445 ^c	3.7	5.8	5.3	5.2	5.6	6.3	6.0	6.7	5.8	6.0	5.5	5.8	5.8	6.0	5.1	5.7
2759	3604	3.2	3.1	3.2	2.6	2.6	2.1	2.4	1.7	1.7	1.7	1.7	1.5	1.9	1.4	1.0	1.1
3202	4049	2.4	1.9	2.7	1.5	1.6	1.8	2.3	1.8	1.6	1.4	1.9	1.7	2.2	1.8	2.1	1.4
3445	3445	2.5	3.5	2.3	3.0	2.4	2.8	1.9	2.0	1.6	2.0	2.2	2.4	1.8	1.6	2.8	1.4
3451	4298																
3548 ^b	4395	2.0	2.2	2.9	2.6	2.2	2.5	1.7	1.9	1.5	2.2	1.1	1.5	2.0	1.4	2.8	1.9
3598 ^d	3598 ^d	2.6	3.3	2.9	2.6	2.4	2.5	2.4	1.9	1.8	1.6	1.5	1.4	1.6	1.2	1.2	1.4
⁵⁴ Fe Isotope																	
1130	2538	1.3	1.1	1.0	1.0	1.2	1.2	1.1	1.3	1.6	1.3	2.1	1.5	1.6	1.3	1.4	1.3
1408	1408	3.8	4.2	3.7	3.0	4.1	3.3	4.4	3.5	3.7	3.3	3.3	2.8	4.2	3.7	4.4	3.5

^aNot corrected for relative abundances of the isotopes.

^b2523- and 3548-keV lines each appear to be doublet.

^cThese data include contributions from 2599- and 2604-keV transitions from 3445- and 3450-keV levels.

^dThese data include contributions from 3598- and 3604-keV ground-state transitions.

1.238-MeV transition from the second excited state. The solid lines represent the calculations which include the known or probable contributions for gamma transitions from levels in ⁵⁶Fe up to 4.87-MeV excitation. As is seen for $E_n > 5.5$ MeV, the calculations predict too little cross section for both transitions shown. We conjecture that nearly all of the levels in ⁵⁶Fe with $E_x > 4.87$ MeV decay through the first excited state. This conjecture is supported quite well by the nearly complete lack of gamma rays in our raw spectra which can be associated with ground-state transitions from highly excited states. The dashed curve in Fig. 1.35.1 shows the predicted excitation function for the 0.846-MeV gamma ray if the conjecture were completely valid.

It is evident, however, that a bigger detector with more efficiency for high-energy gamma rays and better resolution as well as a better understanding of the ⁵⁶Fe nucleus will be required before we can reliably obtain more complete results on this element.

References

¹This work partially funded by the Defense Atomic Support Agency under Subtask No. RRP-3068.

²J. K. Dickens and F. G. Perey, *Nucl. Sci. Eng.* **36**, 280 (1969); J. K. Dickens and F. G. Perey, *Nucl. Sci. Eng.* **40**, 283 and 346 (1970); J. K. Dickens and F. G. Perey, *Nuclear Instruments and Methods* (to be published); J. K. Dickens, the *Physical Review* (to be published).

³R. W. Benjamin, P. S. Buchanan, and J. L. Morgan, *Nucl. Phys.* **79**, 241 (1966); W. E. Tucker, *Phys. Rev.* **140**, B1541 (1965); D. L. Broder *et al.*, *Izv. Akad. Nauk. SSSR, Ser. Fiz* **31**, 327 (1968) (Translation, *Bull. Acad. Sci. USSR, Phys. Ser.*, **31**(2), 311 (1968)); D. M. Drake *et al.*, *Nucl. Sci. Eng.* **40**, 294 (1970).

⁴W. E. Kinney and F. G. Perey, *Calculated ⁵⁶Fe Neutron Scattering and Gamma-Ray Production Cross Sections from 1.0 to 7.6 MeV*, ORNL-4249 (1968); W. E. Kinney and F. G. Perey, *Nucl. Sci. Eng.* **40**, 396 (1970).

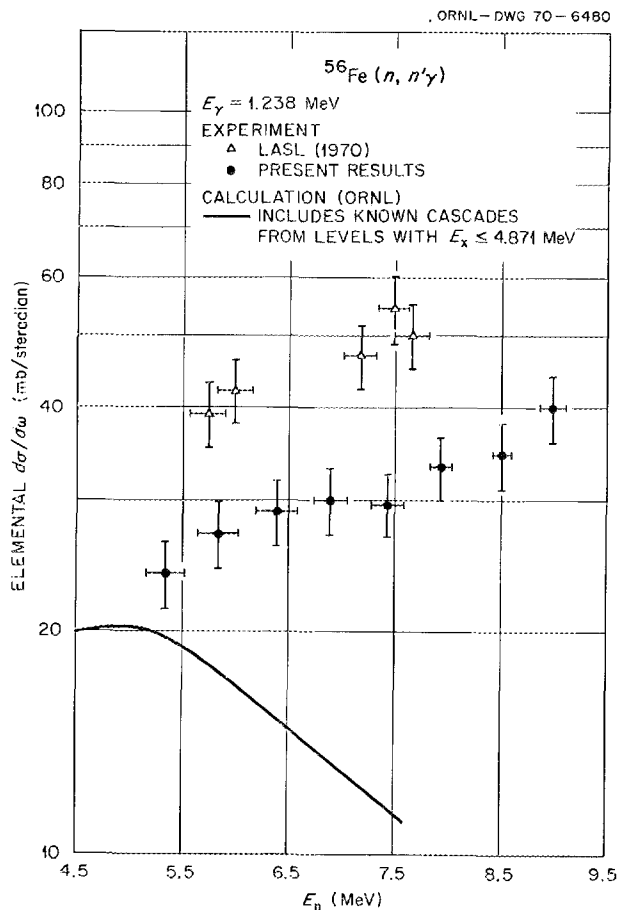


Fig. 1.35.2. Elemental Differential Cross Sections for Gamma-Ray Production Due to Neutron Excitation of the 2.084-MeV Second Excited State in ^{56}Fe Compared with Previously Published Data and with Cross Sections Calculated Using Compound Nucleus Formation. The difference between the data and the calculated curve suggests that levels with $E_x > 4.871$ MeV deexcite through the 2.084-MeV level.

1.36 CALCULATED ^{56}Fe NEUTRON ELASTIC AND INELASTIC SCATTERING AND GAMMA-RAY PRODUCTION CROSS SECTIONS FROM 1.0 TO 7.6 MeV^{1,2}

W. E. Kinney F. G. Perey

Measurements of neutron elastic and inelastic scattering from ^{56}Fe have been analyzed theoretically. The shape-elastic scattering cross sections, calculated with an optical-model potential using energy-independent parameters, added to the compound-elastic contribution obtained from a Hauser-Feshbach calculation including width fluctuation connections agree reasonably well with the data from 4 to 7.6 MeV. Inelastic scattering cross sections from the Hauser-Feshbach

calculation agree well with the data from 1 to 7.6 MeV. From the known branching ratios for the decay of the levels of ^{56}Fe , calculated gamma-ray production cross sections are in reasonable agreement with the data. It is suggested that such calculations form the basis for consistent sets of (n,n') and $(n,n'\gamma)$ cross sections for shielding calculations.

References

- ¹ Abstract of *Nucl. Sci. Eng.* **40**, 396-406 (1970).
- ² This work partially funded by the Defense Atomic Support Agency under Subtask No. RRP-3068.

1.37 A REEVALUATION OF NATURAL IRON NEUTRON AND GAMMA-RAY PRODUCTION CROSS SECTIONS, ENDF/B MATERIAL 1124^{1,2}

S. K. Penny³ W. E. Kinney

Recent data and good agreement among calculated and experimental cross sections prompted the reevaluation of natural iron neutron and gamma-ray production cross sections with the aim of improving angular distributions, extending inelastic excitation functions, and putting the evaluated cross sections in the ENDF/B format. Calculations are described and are shown to be in good agreement with experiment. Below 2 MeV, neutron elastic scattering cross sections and cross sections for inelastic scattering to levels in ^{56}Fe are obtained by fitting experimental results. Above 2 MeV, neutron elastic scattering cross sections and cross sections for inelastic scattering to levels in ^{56}Fe up to an excitation energy of 4.116 MeV are obtained from calculations. Cross sections for inelastic scattering to the continuum are obtained from fits to experimental results. The total cross sections are those of Irving and Straker from 330 keV to 15 MeV and those of U.K. DFN91 from 10^{-5} eV to 330 keV. The (n,p) and (n,γ) cross sections were taken from U.K. DFN64, while the $(n,2n)$ cross sections are those of ENDF/B material 1108. The (n,γ) cross sections were taken from U.K. DFN91. The gamma-ray production cross sections were calculated from the evaluated (n,n') and (n,γ) cross sections, together with known and assumed branching ratios. The evaluated cross sections are presented in graphical form.

References

- ¹ Research sponsored by the Defense Atomic Support Agency under Union Carbide Corporation's contract with the U.S. Atomic Energy Commission.
- ² Abstract of ORNL-TM-3100 (to be published).
- ³ Mathematics Division.

2. Reactor and Weapons Radiation Shielding

2.0 INTRODUCTION

C. E. Clifford

The objectives of the ORNL shielding program, which is largely supported by the Space Electric Power Office (SEPO) project, the Defense Atomic Support Agency (DASA), and the Division of Reactor Development and Technology for the LMFBR, are the development of basic methods for solving radiation transport problems, the testing of these methods by comparison with experimental results, and the development of data and techniques that engineers can use with a high degree of confidence in designing shields to meet their requirements. Further, the intent is to provide design techniques that are general in nature so that shields can be optimized not only with respect to weight, as required for the SEPO program, but also with respect to cost, radiation heating, radiation damage, or any other requirement or constraint that may be imposed by the design engineers.

The experimental effort in support of the program has been expanded to include the use of a shielding facility added to ORELA during the past year (see Sect. 1.13). State-of-the-art instrumentation has been assembled for neutron spectral measurements utilizing an NE-213 detector by time-of-flight and pulse-height unfolding techniques, and a gamma-ray spectrometer using an NaI single-crystal detector is under development. The facility will be used for time-dependent radiation transport studies and for experimental evaluations of cross-section data of interest to DASA. It will also be used for measurements of cross sections for secondary gamma-ray production in materials of interest to the Space Shielding Program (for SEPO) and for calibration of instrumentation to be used both at ORELA and at the Tower Shielding Facility.

During the past year a large part of the Monte Carlo work has been concerned with the debugging and documentation of the MORSE code, which is a multi-group neutron and gamma-ray transport code. Because of its high degree of flexibility and the many options available within the code, the programming and check-out tasks were extensive and time consuming. The use of many test problems having solutions obtained

through the discrete ordinates methods expedited the debugging process, however. Collision analysis routines have been developed for use with MORSE which eliminate much of the drudgery formerly required for processing collision tapes generated by O5R. These analysis routines (SAMBO) are a further development of the in-core analysis-utilized subroutines in the O6R-ACTIFK code package and thus can be used with O6R as well as with other random-walk generating codes.

The intercomparison of the discrete ordinates and Monte Carlo results has also been beneficial in the development of the discrete ordinates methods. This has been particularly true in the evaluation of the time-dependent code ANISN-T1, since little or no experimental data exist which are suitable for use in such an evaluation. Monte Carlo transport results of the spectra transmitted through thick iron spheres have also been useful in evaluating the selection of the group structure for multigroup cross-section sets for iron. Cross-section sets having up to 300 fine groups whose width and energy are tailored to fit the iron total cross sections were found to be necessary in order to match the Monte Carlo results. Efforts are continuing to collapse the 300-group set to a 40- or 80-group set with the appropriate weighting required to predict accurately integral quantities such as total flux or dose. The effort here has not been completely successful, and factors of approximately 2 are observed from results of the fine- and coarse-group calculations.

In addition to the MORSE work, the Monte Carlo program has continued to develop a priori biasing in the selection of directions after collisions. A technique has been documented (see Sect. 2.7) which greatly simplifies the mechanics of calculating and utilizing the altered distributions from which selections are made. This technique has been incorporated into the O6R system of codes and is designated as O6R-D.

Application of the advanced calculational techniques requires continued improvement in the basic cross-section data needed as input. A sizeable effort has been maintained in both the measurement and calculation of the cross-section data for neutron-induced gamma rays. Experiments have been conducted at the TSF which are

used to evaluate the adequacy of existing information for the gamma rays produced in shielding materials, including lead, uranium, and tungsten, and the materials found in soils and concrete. These data, and also experimental data from Gulf General Atomic for tungsten and uranium, have been utilized to compare newly evaluated cross-section sets for use in the shielding library. Nuclear model theory continues to be studied as a useful tool for evaluating existing cross-section information and hopefully for extrapolating the data in a systematic way.

As part of the DASA program, a number of practical problems have been studied in order to continue to develop the detailed description of the nuclear environment in which the military must operate. Time-dependent data have been developed for the transport of neutrons and secondary gamma rays in an air-over-ground geometry for a number of neutron sources. Included are data of heating in the ground as well as energy and angular time-dependent spectra for many points within the atmosphere.

2.1 THE MORSE CODE --- A MULTIGROUP NEUTRON AND GAMMA-RAY MONTE CARLO TRANSPORT CODE¹

E. A. Straker V. R. Cain
P. N. Stevens² D. C. Irving

The MORSE code is a multipurpose neutron and gamma-ray transport Monte Carlo code. Through the use of multigroup cross sections, the solution of neutron, gamma-ray, or coupled neutron--gamma-ray problems may be obtained in either the forward or adjoint mode. Time dependence for both shielding and criticality problems is provided. General three-dimensional geometry, as well as specialized one-dimensional geometry descriptions, may be used with an albedo option available at any material surface.

Standard multigroup cross sections such as those used in discrete ordinates codes may be used as input; either ANISN or DTF-IV cross-section formats are acceptable. Anisotropic scattering is treated for each group-to-group transfer by utilizing a generalized Gaussian quadrature technique. The modular form of the code with built-in analysis capability for all types of estimators makes it possible to solve a complete neutron--gamma-ray problem as one job and without the use of tapes.

A detailed discussion of the relationship between forward and adjoint flux and collision densities, as well as a detailed description of the treatment of the angle

of scattering, is given in the appendices. Logical flow charts for each subroutine add to the understanding of the code.

References

¹ Abstract of ORNL-CF-70-2-31 (Feb. 18, 1970); to be reissued as ORNL-4585.

² University of Tennessee, Knoxville.

2.2 SAMBO, A COLLISION ANALYSIS PACKAGE FOR MONTE CARLO CODES¹

V. R. Cain

SAMBO² is a package of computer routines which handles most of the drudgery associated with analysis of collisions in a Monte Carlo code. It was written for use with the MORSE multigroup Monte Carlo code³ but should be readily adaptable to incorporation into other random-walk generating codes. An arbitrary number of detectors, energy-dependent response functions, energy bins, time bins, and angle bins are allowed, with virtually no numerical limitations other than the available core storage. Analysis is divided into (1) uncollided and total response (fluence⁴ integrated over each response function at each detector), (2) fluence vs energy and detector, (3) time-dependent response (time-dependent fluence integrated over each response at each detector), (4) fluence vs time, energy, and detector, and (5) fluence vs angle, energy, and detector. Each quantity in the above arrays is output, along with an associated fractional standard deviation.

References

¹ Abstract of ORNL report to be published.

² Stochastic Analysis Machine for Bookkeeping, if the reader insists on an acronym; the derivation was actually inspired by Samuel Finley Breese Morse's first and third names.

³ See Sect. 2.1.

⁴ Current, collision density, or any other fluence-like quantity may be substituted for fluence at each detector. For example, if current and fluence at a plane are desired, two separate detectors would be used.

2.3 A REVIEW OF SOME RECENT MULTIDIMENSIONAL DISCRETE ORDINATES SHIELDING CALCULATIONS^{1,2}

F. R. Mynatt³

Radiation transport calculations which are time dependent and involve only one space dimension are now

relatively commonplace. The several "exact" methods which are available — moments method, spherical harmonics, characteristic integration, integral methods, discrete ordinates, and Monte Carlo — differ widely in capability and state of development. However, with modern computers it is relatively easy to perform highly accurate one-dimensional calculations.

For problems requiring transport calculations with two space dimensions or time-dependent problems in one or two space dimensions, the present capability is much less. The only "exact" methods which have been widely developed for these problems are discrete ordinates and Monte Carlo. Although all numerical methods give approximations to a true solution, the term "exact" is used to describe a method in which the approximations are continuously adjustable to give a solution as close to the true answer as desired.

In recent years the two-dimensional discrete ordinates method has been generalized sufficiently to qualify as an "exact" method. This development effort plus the significant advances in computer capabilities and the concurrent improvement of cross-section data and processing codes has provided the means to solve some rather difficult neutron and gamma-ray transport problems.

Some of the specific problems which have been solved illustrate the increasing utility of the method. The problem of a monodirectional beam source incident on large slabs of lead and polyethylene demonstrated the effect of the anisotropic scattering treatment using Legendre expansions up to P_8 .⁴ Earlier calculations illustrated the accuracy of low-order (P_2, P_3) scattering approximations for predicting fast-neutron dose in water and the effect of positive difference methods on mesh stability.⁵ The effect of convergence acceleration in the inner iterations has been demonstrated in calculations of intermediate-energy neutrons in lead⁶ and by special test problems.⁷ Flux anomalies in problems having a point source in air over a ground interface, which were due to the ray effect, were resolved by the use of an analytic first-collision source.⁸ A related difficulty was encountered in attempting to calculate the effect of streaming in a large-radius annular slit in a missile silo cover shield.⁹ This problem was solved by using a biased high-order quadrature which could accurately represent the streaming paths in the slit. In the calculation of a long, thin ($L/D \sim 50$) unit cell with an implicit white boundary condition, the traditional mesh sweep is not suitable for converging the boundary condition. However, an alternate mesh sweep which iterates to first converge the boundary condition for each polar angle level and axial interval is successful in obtaining convergence within ten inner iterations.

Much progress has been made, and the two-dimensional discrete ordinates method is now being routinely applied to real design problems rather than to test cases. However, most of the difficulties associated with anisotropic scattering, convergence acceleration and criteria, quadrature, and stability and accuracy of the difference equations have been reduced to acceptable levels rather than completely resolved.

References

¹Summary of paper presented at the American Nuclear Society Meeting, San Francisco, Calif., Nov. 30–Dec. 4, 1969.

²This work supported by the Defense Atomic Support Agency under Union Carbide Corporation's contract with the U.S. Atomic Energy Commission.

³Computing Technology Center, Union Carbide Corp., Oak Ridge, Tenn.

⁴F. R. Mynatt *et al.*, "Angle-Dependent Spectra Emergent from Slab Shields — Comparison of Two-Dimensional Discrete Ordinates Calculations with Experiment," *Trans. Am. Nucl. Soc.* **11**, 195 (1968).

⁵F. R. Mynatt *et al.*, "On the Application of Discrete Ordinates Transport Theory to Deep-Penetration Fast Neutron Dose Calculations in Water," *Trans. Am. Nucl. Soc.* **9**, 366 (1966).

⁶F. R. Mynatt *et al.*, *Development of Two-Dimensional Discrete Ordinates Transport Theory for Radiation Shield*, CTC-INF-952 (1969).

⁷E. M. Gelbard and L. A. Hageman, "The Synthetic Method as Applied to the S_n Equations," *Nucl. Sci. Eng.* **37**, 288 (1969).

⁸E. A. Straker and F. R. Mynatt, *Calculations of the Effect of the Air-Ground Interface on the Transport of Fission Neutrons Through the Atmosphere*, ORNL-TM-1819 (1968).

⁹F. R. Mynatt, "The Use of Two-Dimensional Discrete Ordinates Calculations to Evaluate Streaming Effects in Annular Ducts," *Trans. Am. Nucl. Soc.* **12**, 370 (1969).

2.4 A STUDY OF THE OVERLAP CONDITIONS AND RESULTING ACCURACY OBTAINED IN SEQUENTIAL DISCRETE ORDINATES TRANSPORT CALCULATIONS FOR A POINT SOURCE IN A 5000-m RADIUS SPHERE OF AIR^{1,2}

J. V. Pace³ F. R. Mynatt³

In order to perform a DOT calculation for an air-over-ground geometry for a range up to 5000 m, it is necessary to run the problem as several overlapping

segments, a procedure called bootstrapping. In order to determine the necessary conditions for the overlap, a study was performed in which the one-dimensional problem of a point 14-MeV source in a 5000-m-radius sphere of air was calculated with a single ANISN run and was then calculated with a sequence of ANISN runs arbitrarily limited to 60 space intervals. It was determined that with vacuum boundary conditions on the subproblems, a large overlap of approximately 300 m was required for 1% accuracy. With a properly determined albedo boundary condition, the overlap for comparable accuracy was reduced to approximately 30 m.

References

¹This work funded by the Defense Atomic Support Agency under Union Carbide Corporation's contract with the U.S. Atomic Energy Commission.

²Abstract of CTC-40 (to be published).

³Computing Technology Center, Union Carbide Corp., Oak Ridge, Tenn.

2.5 O6R-ACTIFK, MONTE CARLO NEUTRON TRANSPORT CODE¹

C. L. Thompson² E. A. Straker

A preliminary version of O6R has been written for the IBM 360 to permit simultaneous neutron transport and analysis. This report serves as a modification of the reports on O5R and ACTIFK.

References

¹Abstract of ORNL-CF-69-8-36 (Aug. 20, 1969).

²Mathematics Division.

2.6 O6R-D, A DISCRETE SCATTERING VERSION OF O6R WITH IMPORTANCE SAMPLING OF THE ANGLE OF SCATTER^{1,2}

C. E. Burgart

Discrete angle scattering, angular importance sampling, and angular-dependent path length stretching have been incorporated into O6R, a Monte Carlo neutron transport code. This report contains a description of the modifications and additions to O6R and NUSECT, the cross-section preparation code. A brief description of the methods of importance sampling is given here in the context of O6R-D. An example of a method of preparation of importance sampling parameters is also presented.

References

¹Research partially funded by the Defense Atomic Support Agency under Union Carbide Corporation's contract with the U.S. Atomic Energy Commission.

²Abstract of ORNL-TM-3031 (to be published).

2.7 A GENERAL METHOD OF IMPORTANCE SAMPLING THE ANGLE OF SCATTERING IN MONTE CARLO CALCULATIONS¹⁻⁴

C. E. Burgart P. N. Stevens⁵

The application of the Monte Carlo method to the solution of deep-penetration radiation transport problems requires the use of "importance sampling." A systematic approach to obtaining an importance function is to calculate the solution of the inhomogeneous adjoint transport equation (using the Monte Carlo estimator of the answer of interest as the source term) and to use this adjoint flux (or value function) as the importance function. The adjoint flux is calculated for simplified geometries using one-dimensional discrete ordinates methods.

In three-dimensional deep-penetration Monte Carlo calculations, the alteration of both the transport and the collision kernel is desirable. The exponential transform is quite useful for altering the transport kernel. However, selection from the altered collision kernel is much more difficult. The approach taken here is to introduce an angular grid with 30 discrete directions fixed in the laboratory coordinate system, along which particles are required to travel. After determining appropriate scattering probabilities and values of the importance function for each of the discrete directions, the selection of the outgoing direction and, hence, energy from the resulting discrete distribution is easily performed.

The effects of the discrete angular grid and the capability of angular-biased Monte Carlo have been investigated for neutron transport by comparison with standard Monte Carlo and discrete ordinates calculations, experiment, and exact analytic solutions for several configurations. In all cases the discrete grid alone (no angular biasing) was observed to have no significant effect on the results. Monte Carlo calculations were performed utilizing the exponential transform, nonleakage, source energy biasing, Russian roulette, and splitting plus the angular biasing. The results of these calculations illustrate the general usefulness of this discrete grid approach to angular biasing in several ways. First, meaningful results were obtained with angular biasing at much greater distances from the

source than were practically possible with the earlier biasing techniques. The answers, variances, and computer times were all on the same order or better than those obtained with the earlier biasing techniques. Finally, this method utilizing the discrete grid to incorporate angular biasing requires very little human interaction once the adjoint configuration is selected.

References

¹ Research partially funded by the Defense Atomic Support Agency under Union Carbide Corporation's contract with the U.S. Atomic Energy Commission.

² Abstract of ORNL-TM-2890 (Mar. 3, 1970).

³ Accepted for publication in *Nuclear Science and Engineering*.

⁴ Doctoral dissertation submitted by Calvin E. Burgart to the University of Tennessee, Dept. of Nuclear Engineering.

⁵ University of Tennessee, Knoxville.

2.8 TREATMENT OF ${}^6\text{Li}(n,dn)\alpha$, ${}^7\text{Li}(n,tn)\alpha$ REACTIONS IN O6R RANDOM WALK AND ANALYSIS¹

C. E. Burgart

Subroutines treating ${}^6\text{Li}(n,dn)\alpha$ and ${}^7\text{Li}(n,tn)\alpha$ reactions for use in O6R random walk and analysis for point detectors have been written. These subroutines utilize ENDF/B cross-section information except for energies near the threshold. All cross-section data and angular distributions are included in a block data subroutine.

Reference

¹ Abstract of ORNL-CF-70-4-32 (Apr. 23, 1970).

2.9 THE ADJOINT BOLTZMANN EQUATION AND ITS SIMULATION BY MONTE CARLO^{1,2}

D. C. Irving

The Boltzmann equation for neutron transport is discussed in both integrodifferential and integral form. The "value" or "importance" equation is derived and shown to be equivalent, in the integral form, to the adjoint of the collision density. However, the value is also equivalent to the adjoint of the flux when the adjoint operation is carried out on the integrodifferential equations. Possible ways of simulating both the forward and the adjoint equation by Monte Carlo are discussed. Because the value equation is a "flux-like" equation, direct simulation of it proves to be

unwieldy. Instead a "collision density" for adjoint particles, equal to the value or adjoint flux times the total cross section, is introduced. The equation for this adjoint collision density may be simulated by the same routines as were used for the forward calculation, and only the cross sections need to be changed. The extension of this to problems involving multiplying media is also included.

References

¹ Research partially funded by the Defense Atomic Support Agency under Subtask No. PE074-01.

² Abstract of ORNL-TM-2879 (May 18, 1970).

2.10 PLOTTER, A GENERAL-PURPOSE PLOTTING ROUTINE^{1,2}

D. C. Irving H. S. Moran

The INTRIGUE Calcomp plotting package has been modified to make the height of the plot variable. This variable-height plotting package has been incorporated in a general-purpose routine, PLOTTER, controlled by input cards. This obviates the need for the user to write a main routine to call the INTRIGUE package.

References

¹ Research partially funded by the Defense Atomic Support Agency under Subtask No. PE074-01.

² Abstract of ORNL-TM-2873 (May 22, 1970).

2.11 PICTURE: AN AID IN DEBUGGING GEOM INPUT DATA^{1,2}

D. C. Irving G. W. Morrison³

Program PICTURE was written to provide aid in preparing correct input data for the general-geometry routine GEOM. PICTURE provides a printed view of arbitrary two-dimensional slices through the geometry. By inspection of these "pictures" one may determine if the geometry specified by the input cards is indeed the desired geometry. Input specifications for PICTURE, sample problem input, and program listings are all contained in this report.

References

¹ Research partially funded by the Defense Atomic Support Agency under Subtask No. PE074-01.

² Abstract of ORNL-TM-2892 (May 14, 1970).

³ Computing Technology Center, Union Carbide Corp., Oak Ridge, Tenn.

2.12 NEUTRON-ENERGY-DEPENDENT CAPTURE GAMMA-RAY YIELDS IN ^{238}U ^{1,2}

R. S. Booth F. J. Muckenthaler
K. J. Yost J. E. White
S. K. Penny

In earlier papers^{3,4} we have described methods for calculating neutron-capture and inelastic-scattering gamma-ray yields to be used in the preparation of gamma-ray production cross sections. In the present paper we present the results of a series of such calculations in the form of neutron-energy-dependent capture gamma-ray yields for ^{238}U in conjunction with a description of a relatively simple experimental technique for validating the calculated yields. The measurements were performed at the Tower Shielding Facility at ORNL, and many aspects of the experiment have been reported by Maerker and Muckenthaler.⁵ In this paper we compare theoretical predictions and measurements of gamma-ray spectra from thermal-neutron and intermediate-energy neutron interactions with ^{238}U .

References

- ¹To be submitted for journal publication.
- ²Abstract of ORNL-TM-3059 (to be published).
- ³K. J. Yost, "A Method for the Calculation of Neutron-Capture Gamma-Ray Spectra," *Nucl. Sci. Eng.* **32**, 62 (1968).
- ⁴K. J. Yost, P. H. Pitkanen, and C. Y. Fu, "The Calculation of Gamma-Ray Transition Probabilities in Odd-A Nuclei," *Nucl. Sci. Eng.* **39**, 379 (1970).
- ⁵R. E. Maerker and F. J. Muckenthaler, *Gamma-Ray Spectra Arising from Thermal Neutron Capture in Elements Found in Soils, Concretes and Structural Materials*, ORNL-4382 (August 1969).

2.13 THE TOTAL GAMMA-RAY ENERGY SPECTRUM ABOVE 1 MeV FROM NEUTRON INTERACTIONS IN ^{235}U AND ^{238}U ¹

R. S. Booth F. J. Muckenthaler

The work discussed in this report is a ramification of an experimental program designed to determine the gamma-ray energy spectrum resulting from neutron interactions with elements found in reactors and shields. These measurements were made at the Tower Shielding Facility (TSF) at ORNL, and many aspects of the experiment have been reported by Maerker and Muckenthaler.² The emphasis of this report shall be upon the analysis of ^{235}U and ^{238}U data. Some

general results derived from less accurate data taken for ^{233}U and ^{239}Pu will also be discussed.

Correlation analysis is used to remove background from the ^{235}U and ^{238}U data. We prove that the measured background for the experiment represented only part -- sometimes a very small part -- of the total background. The final analysis of these data is accomplished through an iterative technique where the intensities of known backgrounds, both measured and derived, are determined with correlation analysis.

The derived gamma-ray spectra are compared on an absolute basis with other measurements and with theoretical predictions.

References

- ¹Abstract of ORNL-TM-3060 (to be published).
- ²R. E. Maerker and F. J. Muckenthaler, *Gamma-Ray Spectra Arising from Thermal-Neutron Capture in Elements Found in Soils, Concretes, and Structural Materials*, ORNL-4382 (August 1969).

2.14 A COMPARISON OF FOLDING AND UNFOLDING TECHNIQUES FOR DETERMINING THE GAMMA SPECTRUM FROM THERMAL-NEUTRON CAPTURE IN ALUMINUM¹⁻³

R. S. Booth

The gamma-ray spectrum above 1 MeV resulting from thermal-neutron capture in aluminum is determined by both a folding and an unfolding analysis of data taken at the Tower Shielding Facility. This results in a comparison of the relative merits of the two analysis techniques and demonstrates the accuracy that can be obtained in unfolding a complex spectrum. It is concluded that the accuracy of the final photon spectrum is not governed by the technique employed to unfold the measured counts.

References

- ¹Research partially funded by the Defense Atomic Support Agency under Subtask No. PE037.
- ²Abstract of ORNL-TM-2898 (Mar. 5, 1970).
- ³Abstract of paper submitted for journal publication.

2.15 ANALYSIS OF PROPORTIONAL COUNTER PULSE-HEIGHT SPECTRA

R. M. Freestone, Jr.

Three hydrogen-filled proportional counters, constructed according to the design of Benjamin *et al.*,¹ are

being used at the Tower Shielding Facility in order to measure spectra of neutrons having energies in the kilovolt range. These counters are spherical, with a radius of 2.36 cm, and are filled with hydrogen to pressures of 1, 3, and 10 atm respectively. The basis for the counter design is the premise that, for a counter of a given diameter and filling pressure, there exists a limited energy range which can be observed without distortion due to either gamma-ray events or wall effect.

The pulse-height spectra resulting from measurements with these counters are unfolded to produce neutron energy spectra by an IBM 360 program, SPEC4, which is essentially identical with the SPEC4 program of Benjamin and Kemshall.² We have made some small modifications, adding provision for background subtraction and a normalization step required because our method of obtaining an estimate of the high-energy (>1 MeV) portion differs from that of Benjamin.

Briefly, SPEC4 computes and subtracts from the input spectrum the contribution due to neutrons having energies greater than the energy range of interest, then unfolds the differential of the pulse-height curve using an internally computed differential response matrix, a device intended to eliminate spurious oscillations in the result. Residual wall effects are taken into account by employing the analytic equations derived by Snidow and Warren.³

Results obtained to date from the counters and the unfolding code have been of mixed quality. The counters were operated in beams of monoenergetic neutrons produced by the ORNL 3-MeV Van de Graaff during October 1969, and the unfolded results were reasonably satisfactory. Peaks were found at or very close to the proper energies, and all but a negligibly small fraction of the counts were concentrated in the peak.

On the other hand, it is reasonable to expect that if an unknown continuous spectrum is examined by each of the counters in turn, the unfolded results will agree, within statistics, in the energy regions where the results overlap. We have had a great deal of difficulty in consistently realizing this expectation. From the evidence of very, very many test unfoldings of the same spectrum in which input parameters were arbitrarily varied, the difficulties seem to be related to inaccuracies in calibration values and in determining true analyzer linearity zero. The unfolding procedure seems to be inordinately sensitive to both of these quantities.

However, present evidence indicates that varying these quantities within the limits of reasonable experimental error (assumed to be ± 1 to 2% in calibration, ± 1

to $1\frac{1}{2}$ channels in analyzer zero) can usually force agreement between the three counters in their overlap regions. Arriving at the proper combination of variations, however, can be a tedious procedure.

References

¹P. W. Benjamin *et al.*, *Nucl. Instr. Methods* **59**, 77–85 (1968).

²P. W. Benjamin and C. D. Kemshall, *The Analysis of Recoil Proton Spectra*, AWRE Report No. 0-7/67 (1967).

³N. L. Snidow and H. D. Warren, *Nucl. Instr. Methods* **51**, 109–16 (1967).

2.16 THE CALCULATION OF GAMMA-RAY TRANSITION PROBABILITIES IN ODD-A NUCLEI¹

K. J. Yost P. H. Pitkanen
C. Y. Fu

Gamma-ray transition probabilities intended for use in the preparation of gamma-ray production cross sections have been calculated for four odd-*A* nuclei and compared with experiment. Wave functions used in the calculation of *M1* and *E2* transition matrix elements were generated with a deformed shell (Nilsson) model code which allows for asymmetric quadrupole deformations. Inverse moments of inertia and deformations were treated as adjustable parameters. The collective gyromagnetic ratio was assumed to be a constant for all levels. The results suggest in the context of the simplified model an angular momentum dependence of the nuclear deformation.

Reference

¹ Abstract of *Nucl. Sci. Eng.* **39**, 379–86 (1970).

2.17 A UNIFIED MODEL OF DEFORMED ODD-ODD NUCLEI FOR NUCLEAR DATA GENERATION AND ANALYSIS¹⁻⁴

C. Y. Fu K. J. Yost

A unified model of deformed odd-odd nuclei has been formulated as an aid in nuclear data generation and evaluation. The model employs products of single-particle Nilsson wave functions as basis functions. The coupling of angular momenta of the odd nucleons is assumed to obey the Gallagher-Moszkowski coupling rules. The matrix elements of the proton-neutron residual interaction potential are evaluated with the use

of oscillator brackets. The validity of the model has been established by computing and comparing with experimental data nuclear energy levels and/or gamma-ray transition probabilities for ^{23}Na , ^{28}Al , ^{166}Ho , ^{182}Ta , and ^{238}Np . The calculated results compare quite well with experiment. Special attention has been given to the establishment of an efficient computational method.

References

- ¹ Abstract of ORNL-TM-2832 (Jan. 20, 1970).
- ² To be published in *Nuclear Science and Engineering*, August 1970.
- ³ Abstract of paper to be presented at American Nuclear Society Annual Meeting, Los Angeles, Calif., June 29, 1970.
- ⁴ Abstract of doctoral dissertation submitted by C. Y. Fu to the University of Tennessee, Department of Nuclear Engineering.

2.18 THE APPLICATION OF EXTENDED R-MATRIX THEORY TO ELASTIC SCATTERING OF NEUTRONS BY ^{12}C

K. J. Yost P. H. Pitkanen

The present method for cross-section generation and analysis has two primary ingredients: (a) the core-quasi-particle coupling or bootstrap model for describing intermediate and highly excited states of the nucleus,³ and (b) the extended *R*-matrix theory of nuclear reactions.⁴ One motivation for the mating of (a) and (b) is to produce a method for resonance cross-section analysis which is practical from the computational standpoint. Some preliminary results for elastic scattering in ^{12}C are presented.

Let X^n represent a nuclear structure wave function, which can be expressed as

$$X^n = \sum_k a_k^n \chi^k, \quad (1)$$

where the χ^k 's are a harmonic oscillator basis function and the a_k^n 's are determined by a bootstrap model calculation. Further, let Ψ be the wave function of the target nucleus-incident neutron system. If r_0 is the nuclear radius, then

$$\Psi = \sum_\alpha \Phi_\alpha U_\alpha(r_\alpha), \quad r \gg r_0, \quad (2)$$

where α denotes a reaction channel, Φ_α contains nonradial components of Ψ , and r_α is the separation

distance between the incident/exit particle and the target/residual nucleus. An alternative representation is

$$\Psi = \sum_n C^n X^n, \quad 0 \leq r < \infty. \quad (3)$$

Since the X^n 's do not satisfy the appropriate boundary conditions at infinity, the C^n 's are optimized over the range $0 \leq r \leq a$, and Eq. 2 is used for $r > a$. Invoking Green's theorem,⁴ the representation in Eq. 3 is, in practice, required to be valid in the range $r_0 \leq r \leq a$.

Figures 2.18.1 and 2.18.2 show comparisons between measured⁵ and calculated resonances in the elastic scattering cross section in ^{12}C . The sharp resonance of Fig. 2.18.1 is the result of a $5/2^+$ state at 7.02 MeV in ^{13}C . The smoother resonance is due to a $1/2^-$ state at 9.19 MeV. The bootstrap model wave functions used in the extended *R*-matrix calculations were generated by achieving a best fit between measured and calculated energies for the first six levels in ^{13}C . For each resonance the ^{13}C energies calculated with the bootstrap model were adjusted to coincide with the corresponding ^{12}C resonance energies.

Six channel radii were chosen for the calculation of the elastic scattering cross sections. The same channel radii were used in a preliminary calculation of the inelastic scattering cross sections for ^{12}C . Results indicated the need for an additional parameter giving a

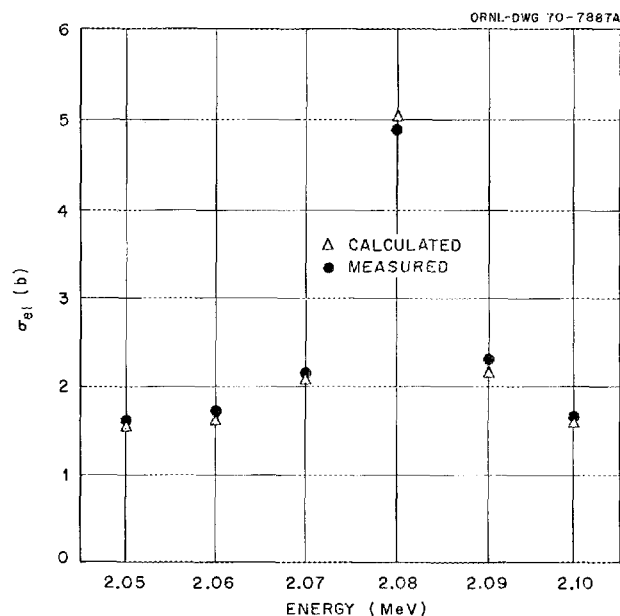


Fig. 2.18.1. The 2.08-MeV Elastic Scattering Resonance in ^{12}C .

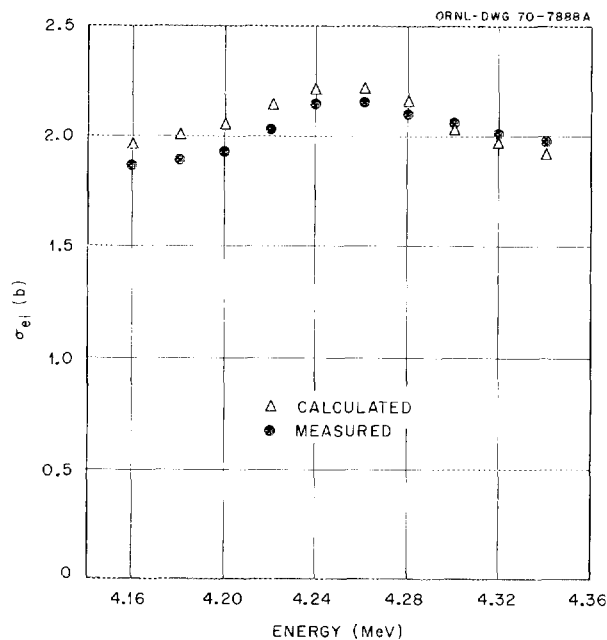


Fig. 2.18.2. The 4.25-MeV Elastic Scattering Resonance in ^{12}C .

background contribution to the R -matrix elements representing states not predicted by the bootstrap calculation. This problem is currently under investigation.

References

- ¹Paper to be presented at Meeting of American Nuclear Society, Washington, D.C., Nov. 15–19, 1970.
- ²Reactor Division.
- ³K. Kumar and K. J. Yost, *Bull. Am. Phys. Soc.* **15**, No. 4 (April 1970).
- ⁴I. Garside and W. Tobocman, *Phys. Rev.* **173**, 1047 (1968).
- ⁵J. R. Stehn *et al.*, *Neutron Cross Sections*, Vol. I, $Z = 1$ to 20, BNL-325, 2d ed., suppl. No. 2 (1964).

2.19 NEUTRON ENERGY-DEPENDENT CAPTURE GAMMA-RAY YIELDS FOR ^{181}Ta ^{1,2}

K. J. Yost J. E. White
C. Y. Fu

In the ^{181}Ta capture gamma-ray yield calculation there are two possible s -wave ($\ell = 0$) neutron capture state spins, 3^+ and 4^+ . The data of Wasson *et al.*³ were used to establish average intensities for 35 primary transitions for 3^+ and 4^+ resonance capture respectively. Measured energy levels in ^{182}Ta were used in the range $0 \leq E \leq 0.174$ MeV.⁴ A nuclear model⁵ appropriate to odd-odd nuclei was used to generate energy levels in the range $0.174 \leq E \leq 1.01$ MeV. ^{182}Ta level density parameters were determined by comparing a calculated thermal-neutron capture gamma-ray pulse-height distribution with a corresponding measurement at the Tower Shielding Facility. This set of parameters was then used in the calculation of gamma-ray yields for neutron energies up to 1 MeV.

The capture gamma-ray yields for ^{181}Ta given in Table 2.19.1 compared well with an integral measurement performed at the ORNL Tower Shielding Facility.

References

- ¹Portion of paper presented at American Nuclear Society Annual Meeting, Los Angeles, Calif., June 30, 1970.
- ²Summary of paper to be published as an ORNL-TM report and submitted for journal publication.
- ³O. A. Wasson, R. E. Chrien, M. A. Love, R. M. Bhat, and M. Beer, *Nucl. Phys.* **A132**, 161 (1969).
- ⁴L. V. Groshev *et al.*, "Compendium of Thermal-Neutron Capture Gamma-Ray Measurements, Part 3, $Z = 68$ to $Z = 94$ (Er to Pu)," *Nucl. Data Tables* **A5**, 328 (1969).
- ⁵C. Y. Fu and K. J. Yost, "A Unified Model of Odd-Odd Nuclei for Nuclear Data Generation and Analysis," to be published in *Nuclear Science and Engineering*.

Table 2.19.1. ^{181}Ta Capture Gamma-Ray Yields

E_γ (MeV)	Gamma-Ray Yield (photons/capture $\times 100$) for E_n of ^a																													
	Thermal	3.06 eV	3.93 eV	5.04 eV	6.48 eV	8.32 eV	10.7 eV	13.7 eV	17.6 eV	22.6 eV	29.0 eV	37.3 eV	47.8 eV	61.4 eV	78.9 eV	101.3 eV	130.1 eV	167.0 eV	214.5 eV	275.4 eV	353.6 eV	2.61(3) ^b eV	3.36(3) eV	5.25(4) eV	1.11(5) eV	3.02(5) eV	4.98(5) eV	6.72(5) eV	9.07(5) eV	
1.0-1.25	35.1	32.4	32.2	32.2	32.2	32.5	32.9	32.9	32.9	32.1	32.8	31.5	31.9	32.6	32.1	32.8	32.1	32.7	32.2	32.2	32.4	32.3	32.1	42.4	36.1	30.9	30.3	29.6	29.0	
1.25-1.5	32.8	31.2	31.1	31.1	31.1	31.1	31.1	31.1	31.1	31.0	30.4	30.8	31.2	31.0	31.0	31.0	31.0	31.0	31.0	31.0	31.0	31.0	31.0	31.0	36.5	33.0	30.2	30.1	29.9	29.8
1.5-1.75	29.8	28.9	28.9	28.9	28.9	28.7	28.5	28.5	28.5	28.8	28.5	28.3	28.6	28.8	28.8	28.5	28.8	28.5	28.7	28.7	28.7	28.7	28.8	31.2	29.6	28.5	28.9	29.1	29.2	
1.75-2.0	26.4	26.1	26.1	26.1	26.0	25.8	25.5	25.5	25.5	26.0	25.5	25.5	25.8	25.8	26.0	25.6	26.0	25.6	25.9	25.9	25.8	25.8	26.0	26.6	26.1	26.1	26.8	27.3	27.7	
2.0-2.25	22.8	22.8	22.8	22.8	22.8	22.6	22.3	22.3	22.3	22.7	22.3	22.3	22.6	22.6	22.7	22.3	22.7	22.4	22.7	22.7	22.5	22.6	22.7	22.4	22.6	23.2	24.0	24.7	25.4	
2.25-2.5	19.2	19.4	19.4	19.4	19.4	19.2	19.0	19.0	19.0	19.4	19.0	19.0	19.2	19.2	19.4	19.0	19.4	19.0	19.3	19.3	19.2	19.2	19.4	18.6	19.1	20.0	20.9	21.8	22.5	
2.5-2.75	15.8	16.1	16.1	16.1	16.1	15.9	15.7	15.8	15.7	16.1	15.8	15.8	16.0	15.9	16.1	15.8	16.1	15.8	16.0	16.0	15.9	16.0	16.1	15.2	15.8	16.7	17.7	18.6	19.4	
2.75-3.0	12.7	13.0	13.0	13.0	13.0	12.9	12.8	12.8	12.8	13.0	12.8	12.8	12.9	12.9	13.0	12.8	13.0	12.8	13.0	13.0	12.9	13.0	13.0	12.3	12.8	13.7	14.6	15.5	16.3	
3.0-3.25	10.1	10.3	10.4	10.4	10.3	10.3	10.2	10.2	10.2	10.4	10.2	10.2	10.3	10.2	10.4	10.2	10.4	10.2	10.3	10.3	10.3	10.3	10.4	9.8	10.2	11.0	11.8	12.6	13.4	
3.25-3.5	7.9	8.1	8.1	8.1	8.1	8.1	8.0	8.0	8.0	8.1	8.0	8.0	8.1	8.0	8.1	8.0	8.1	8.0	8.1	8.1	8.1	8.1	8.1	7.7	8.0	8.6	9.3	10.0	9.8	
3.5-3.75	6.1	6.3	6.3	6.3	6.3	6.3	6.3	6.3	6.3	6.3	6.3	6.2	6.3	6.2	6.3	6.3	6.3	6.3	6.3	6.3	6.3	6.3	6.3	6.1	6.3	6.7	7.2	7.8	7.2	
3.75-4.0	4.8	4.9	4.9	4.9	4.9	4.9	4.9	4.9	4.9	4.9	4.9	4.9	4.8	4.9	4.8	4.9	4.9	4.9	4.9	4.9	4.9	4.9	4.9	4.8	4.9	5.2	5.6	6.0	5.6	
4.0-4.25	3.8	3.8	3.8	3.8	3.8	3.9	3.9	3.9	3.9	3.8	3.9	3.8	3.8	3.8	3.8	3.8	3.9	3.8	3.8	3.8	3.8	3.9	3.8	3.8	3.8	4.0	4.2	4.6	4.2	
4.25-4.5	3.0	3.0	3.0	3.0	3.0	3.1	3.1	3.1	3.1	3.0	3.1	3.0	3.0	3.0	3.0	3.1	3.0	3.1	3.0	3.1	3.0	3.1	3.0	3.1	3.0	3.1	3.3	3.5	3.2	
4.5-4.75	2.4	2.4	2.4	2.4	2.4	2.5	2.6	2.6	2.6	2.4	2.5	2.4	2.4	2.4	2.4	2.4	2.5	2.4	2.5	2.4	2.4	2.5	2.4	2.5	2.5	2.4	2.5	2.6	2.4	
4.75-5.0	1.9	2.0	2.0	1.9	2.0	2.0	2.1	2.1	2.1	1.9	2.1	1.9	1.9	2.0	1.9	2.1	2.0	2.1	2.0	2.0	2.0	2.0	2.0	2.0	2.0	1.9	2.0	2.0	1.8	
5.0-5.25	1.7	2.2	2.2	2.2	2.2	2.4	2.8	2.8	2.8	1.3	2.7	2.1	3.1	1.4	1.2	2.6	1.3	2.4	1.5	1.5	1.9	1.8	1.3	1.1	1.4	1.5	1.6	1.6	1.4	
5.25-5.5	0.95	1.7	1.8	1.8	1.8	1.6	1.4	1.4	1.4	1.8	1.4	1.7	2.2	1.8	1.8	1.5	1.8	1.5	1.7	1.7	1.6	1.7	1.8	0.7	1.8	2.5	0.97	1.3	1.1	
5.5-5.75	0.49	0.56	0.55	0.55	0.56	0.61	0.69	0.68	0.69	0.79	0.69	0.63	0.58	0.99	0.8	0.7	0.8	0.71	0.8	0.8	0.75	0.74	0.8	0.33	1.5	1.9	2.4	1.2	0.86	
5.75-6.0	1.6	1.7	1.7	1.7	1.7	1.6	1.4	1.4	1.4	2.0	1.4	1.9	0.96	2.3	2.0	1.5	2.0	1.5	1.9	1.9	1.8	1.8	2.0	0.48	0.4	0.85	1.4	1.5	1.1	
6.0-6.25	0.62	0.23	0.15	0.14	0.18	0.36	0.55	0.55	0.55	0.8	0.56	2.0	0.39	0.38	0.8	0.58	0.8	0.6	0.8	0.75	0.7	0.75	0.8	0.17	1.2	1.1	0.39	1.0	0.84	
6.25-6.5																										1.2			0.36	0.5
6.5-6.75																													0.93	0.25
6.75-7.0																														0.57

^a E_n = upper limit of neutron energy interval.

^bRead: 2.61×10^3

2.20 A BOOTSTRAP METHOD FOR THE CALCULATION OF HIGH-LYING NUCLEAR LEVELS AND ELECTROMAGNETIC MOMENTS (I). THEORY¹

K. Kumar

The high-lying (about 4–8 MeV) nuclear levels, into which a neutron may be captured via compound nucleus formation, are of some interest from the point of view of the calculation of neutron cross sections.² Although much progress has been made during recent years,³ the calculation of such states has remained a challenging problem.

The method outlined below is not a revolutionary new one. It is an attempt to combine the good and essential features of several well-known models in the simplest possible, yet nontrivial, manner.

The basic idea in this method is that given the states of a nucleus A , those of the nucleus $A + 1$ ($A - 1$) can be obtained by coupling a particle (hole) to the core (known nucleus). This idea has been employed extensively⁴⁻⁶ for the calculation of the low-lying and intermediate levels of odd- A nuclei. We attempt to extend this idea to higher energy levels and also to improve the description of the intermediate levels.

The method under study consists of two parts, the first being the core-quasiparticle coupling treatment of odd- A nuclei. As in the core-excitation model of de-Shalit,⁴ the core levels and electromagnetic moments are taken from experiment. The core may be spherical, transitional, deformed, or noncollective. As in the unified model of Bohr and Mottelson,⁵ the core-nucleon interaction is derived from the deformation-dependent expansion of the average nuclear potential. This interaction is cast in such a form that all multipoles and static moments (for which core information is available) can be included with the use of a single strength parameter. As in the quasi-random-phase approximation of Kisslinger and Sorensen,⁶ the pairing theory and the quasiparticle technique are employed to describe the odd nucleon. This allows for the inclusion of both particle and hole states in the same calculation, a better treatment of the Pauli principle, and a more realistic treatment of nuclear level densities and electromagnetic moments (compared with methods⁴⁻⁵ not including pairing effects). Numerical results for ^{13}C and ^{209}Pb are described elsewhere.⁷

The second part of the study is the bootstrap method of generating higher-lying levels of even- A and odd- A nuclei. This procedure is intended to compensate for the insufficiency of the core information needed for the first part. The 1,3,... quasiparticle states of odd- A nuclei

and the 2,4,... quasiparticle states of even- A nuclei are generated by starting from the zero quasiparticle (collective) states of an even-even nucleus and coupling a single quasiparticle at a time. The coupling mechanism is the same as that discussed above, but the roles of the core and final nucleus are interchanged after each cycle. Since the quasiparticle energy varies typically from 1 to 5 MeV, each successive addition takes us to higher energies. The number of core states and hence the final matrix size does increase after each cycle. This part of the program is incomplete as yet, but we hope to report numerical results in the near future.

Nuclear structure wavefunctions of ^{13}C obtained via core-quasiparticle coupling have been combined with extended R -matrix theory in order to calculate the elastic ($n, ^{12}\text{C}$) scattering. Comparison with experiment is discussed elsewhere.⁸

References

¹ Summary of paper submitted for publication in *Nuclear Physics*.

² K. J. Yost, *Nucl. Sci. Eng.* **32**, 62 (1968).

³ K. J. Yost, P. H. Pitkanen, and C. Y. Fu, *Nucl. Sci. Eng.* **36**, 189 (1969) and **39**, 379 (1970); N. C. Francis *et al.*, *Phys. Rev.* **176**, 1213 (1968); J. E. Purcell, *Phys. Rev.* **185**, 1279 (1969).

⁴ A. de-Shalit, *Phys. Rev.* **122**, 1530 (1961).

⁵ A. Bohr and B. R. Mottelson, *Kgl. Danske Videnskab. Selskab. Mat. Fys. Medd.* **27**, No. 16 (1953); lectures at Copenhagen.

⁶ L. S. Kisslinger and R. A. Sorensen, *Rev. Mod. Phys.* **35**, 853 (1963).

⁷ See Sect. 2.21.

⁸ See Sect. 2.18.

2.21 A BOOTSTRAP METHOD FOR THE CALCULATION OF HIGH-LYING NUCLEAR LEVELS AND ELECTROMAGNETIC MOMENTS (II). APPLICATION TO ^{13}C AND ^{209}Pb ^{1,2}

K. Kumar K. J. Yost
C. Y. Fu

In a previous paper³ the theory and the relevant references are given.

We report here some initial results for ^{13}C and ^{209}Pb . Energy levels and wave functions of these nuclei are calculated by coupling a neutron to an even-even core (^{12}C or ^{208}Pb). The core-particle interaction is a scalar product of core moments and particle moments. The core moments, related to certain gamma-ray transition strengths, and energy levels are taken from

experiment. The particle moments are obtained from the quasi-particle model which combines shell effects and pairing effects. The single-particle energies and the core-quasiparticle coupling strength are the parameters (five for ^{13}C , eight for ^{209}Pb) of the calculation. Using a single coupling strength parameter, we have included $\lambda = 2,3$ multipoles for ^{13}C and $\lambda = 2,3,4,5$ for ^{209}Pb .

Figure 2.21.1 shows the comparison of theoretical and experimental levels of ^{13}C . Although the agreement is quite encouraging, the calculation in its present form is not adequate for levels above 8 MeV. This is evidenced by the comparison with the experimental electromagnetic moments in Table 2.21.1. The first row of Table 2.21.1 compares the ground state magnetic moment. Note that no additional parameter has been

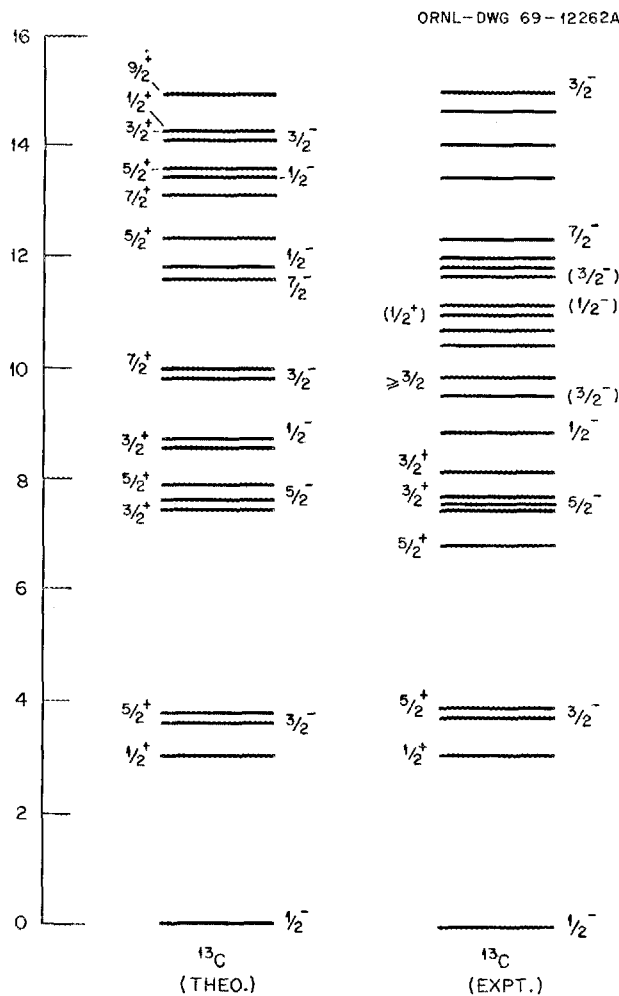


Fig. 2.21.1. Comparison of Theoretical and Experimental Energy Levels for ^{13}C . The experimental levels are taken from Fleming *et al.*, *Phys. Rev.* **166**, 1012 (1968).

used. The rest of the table compares the transition widths. Again, there is no additional parameter for the magnetic transitions. However, an effective charge of one unit has been used (as in previous calculations⁴) for the electric transitions. The discrepancy in the last row of the table arises from the fact that in this initial calculation only the $N = 0,1,2$ oscillator shells have been included. Calculations including also the higher shells are in progress.

Figure 2.21.2 gives some details of our calculation for ^{209}Pb . The single-particle energies given in column SPL have been obtained by fitting the experimental levels. The quasiparticle energies in column QPL have been obtained by solving the pairing equations. Note that even the "hole" state $p_{1/2}$ is allowed and appears in the final spectrum of ^{209}Pb at an excitation energy of only 2.2 MeV. The pairing theory is particularly useful for describing such states. The column CALC gives, in addition to the energy levels, the calculated spectroscopic factors (X100). These values lie within the range of the experimental values⁵ (not given here for the sake

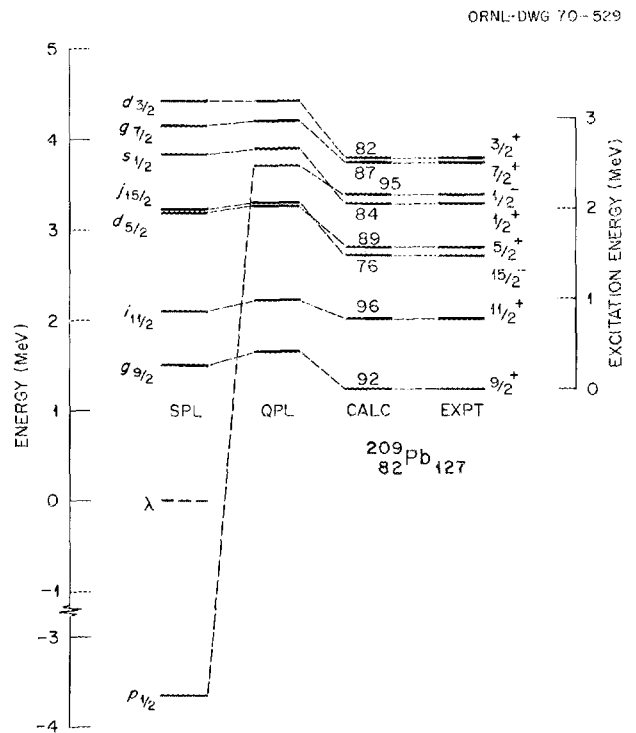


Fig. 2.21.2. Comparison of Theoretical and Experimental Energy Levels for ^{209}Pb . The experimental levels are taken from Bjerregaard *et al.*, *Nucl. Phys.* **A113**, 484 (1968). The calculated spectroscopic factor percentages are also given. SPL and QPL stand for single-particle levels and quasi-particle levels.

Table 2.21.1. Comparison of Theoretical and Experimental Magnetic Moments and Radiative Transition Widths

Initial		Final		Type	Radiative Transition Width (eV)	
Energy	J^π	Energy	J^π		Theoretical	Experimental
0.0	$1/2^-$	0.0	$1/2^-$	M.M.	0.758	0.7024 ^a
3.085	$1/2^+$	0.0	$1/2^-$	E1	1.31	>2.60 E-2 ^b
3.680	$3/2^-$	0.0	$1/2^-$	M1	3.26 E-1	3.58 ± 0.45 E-1 ^c
		0.0	$1/2^+$	E2	3.76 E-3	3.61 ± 0.39 E-3 ^c
		3.085	$1/2^-$	E1	2.19 E-4	>1.83 E-4 ^b
3.850	$5/2^+$	0.0	$1/2^-$	M2	9.82 E-5	5.87 ± 2.05 E-5 ^b
		0.0	$1/2^-$	E3	1.69 E-7	7.90 ± 4.70 E-7 ^b
		3.085	$1/2^+$	E2	9.67 E-7	8.40 ± 3.24 E-7 ^b
		3.680	$3/2^-$	E1	1.99 E-5	3.30 ± 1.17 E-5 ^b
6.85	$5/2^+$	0.0	$1/2^-$	M2	13.5 E-5	6.9 ± 3.6 E-5 ^c
7.54	$5/2^-$	0.0	$1/2^-$	E2	1.73 E-1	1.15 ± 0.06 E-5 ^c
8.86	$1/2^-$	0.0	$1/2^-$	M1	4.79 E-2	3.36 ± 0.46 ^c

^aMagnetic moment in nuclear magnetons, tabulated by G. H. Fuller and V. W. Cohen, *Nucl. Data Tables A5*, 433 (1969).

^bS. J. Skorka, J. Hertel and T. W. Retz-Schmidt, *Nucl. Data A2*, 347 (1966).

^cG. Wittwer, H. G. Clerc and G. A. Beer, *Phys. Letters 30B*, 634 (1969).

of brevity). Attempts are in progress to extend the ^{209}Pb calculation to higher energies.

The model is presently being used⁶ in the generation of neutron elastic and inelastic scattering cross sections in ^{12}C , ^{56}Fe , ^{207}Pb , and ^{208}Pb and inelastic and capture gamma-ray yields in the same nuclei. This choice of nuclei is dictated by cross-section requirements for SNAP shield design and weapons effect analysis.

References

¹Research partially funded by the Defense Atomic Support Agency under Union Carbide Corporation's contract with the U.S. Atomic Energy Commission.

²Summary of paper to be published as an ORNL-TM report and submitted for journal publication.

³See Sect. 2.20.

⁴L. S. Kisslinger and R. A. Sorensen, *Rev. Mod. Phys.* **35**, 853 (1963).

⁵G. Igo *et al.*, *Phys. Rev.* **177**, 1831 (1969), and references quoted there.

⁶See Sect. 2.18.

2.22 COLLECTIVE TREATMENT OF THE PAIRING HAMILTONIAN (I). FORMULATION OF THE MODEL¹

D. R. Bès² R. P. J. Perazzo²
R. A. Broglia² K. Kumar

We develop a treatment of the pairing force problem in terms of two collective variables: the intrinsic

deformation α and the gage angle φ . The comparison between the results obtained by solving the corresponding quantum mechanical Hamiltonian and those obtained by an exact diagonalization shows the adequacy of the present approach.

References

¹Abstract of the paper published in *Nucl. Phys.* **A134**, 1 (1970).

²University of Minnesota, Minneapolis.

2.23 THE PROLATE-OBLATE DIFFERENCE AND ITS EFFECT ON ENERGY LEVELS AND QUADRUPOLE MOMENTS¹

K. Kumar²

The existence of a rotational spectrum means not only that the nucleus has a permanently deformed shape, but also that it has a strong preference for prolate over oblate shapes (or vice versa, depending on the sign of the quadrupole moment). Moreover, nuclei considered previously to be spherical and good vibrators are found to have large static quadrupole moments.^{3,4} It has been suggested⁵ that such quadrupole moments can be attributed to the prolate-oblate difference (POD) caused by the cubic term in deformation. Even in a nucleus whose equilibrium shape is spherical, the cubic term can lead to a "rotational" value (denoted in what follows by Q_R) for the static quadrupole moment Q_{2+} . The POD is directly responsible^{5,6} for the splitting of 2^+_γ and 4^+ states.

We take a closer look at the numerical results⁷ for the W, Os, and Pt region and obtain simple, semiquantitative relations among POD, $E_{2\gamma^+} - E_{4^+}$, and Q_{2^+}/Q_R .

A convenient measure of POD is V_{PO} , the energy difference between the oblate, prolate minima of the potential energy of deformation (V_{PO} is defined here to be positive for prolate nuclei). The calculated and observed⁸ splittings of $2\gamma^+, 4^+$ levels are plotted against the calculated V_{PO} in Fig. 2.23.1. The straight line

corresponds to the relation

$$S = E_{2\gamma^+} - E_{4^+} \approx \frac{1}{2} V_{PO}$$

$$(-0.6 < V_{PO} < 1.5 \text{ MeV}). \quad (1)$$

This straight line passes through the origin in accordance with the Wilts-Jean rule⁶ that the $2\gamma^+, 4^+$ levels in a

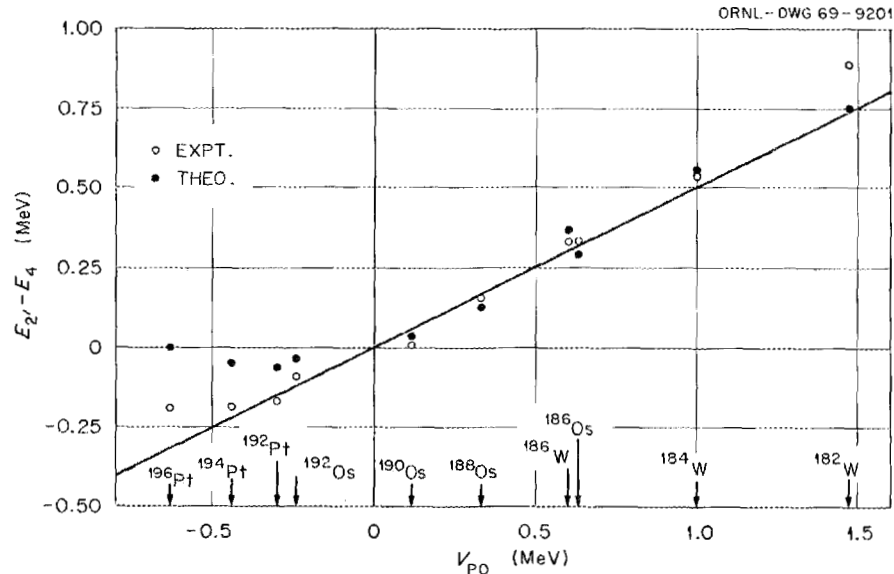


Fig. 2.23.1. The $2\gamma^+, 4^+$ Level Splitting and the Prolate-Oblate Difference. The straight line has been drawn for convenience, but it certainly does not give the correct behavior at large $|V_{PO}|$.

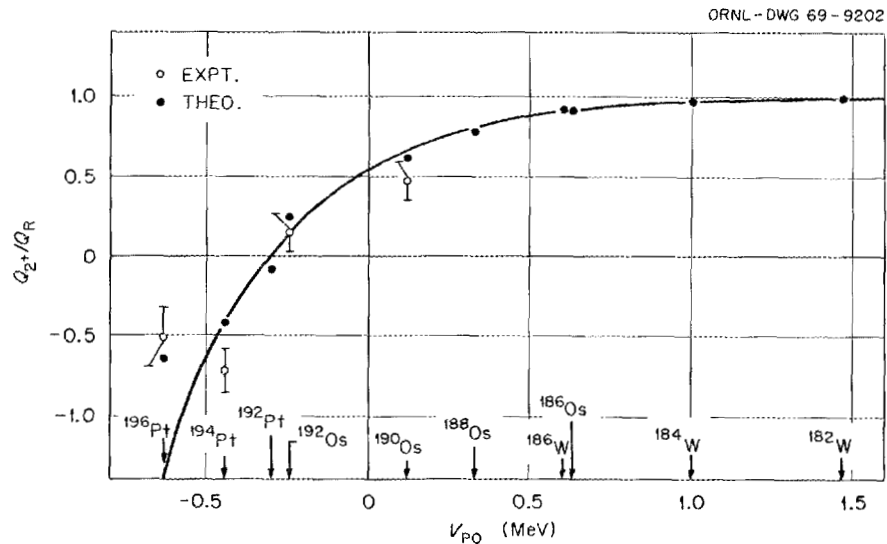


Fig. 2.23.2. The Quadrupole Moment Ratio and the Prolate-Oblate Difference. The smooth curve has been drawn for convenience, but it certainly does not give the correct behavior of $V_{PO} \ll 0$.

γ -independent potential well are degenerate (no matter how large or small the magnitude of β_{\min} may be!). However, the change of sign of S in Fig. 2.23.1 is a direct consequence of the β - γ dependence of the mass parameters.

The calculated and observed values of Q_{2+}/Q_R are plotted against V_{PO} in Fig. 2.23.2. The smooth curve corresponds to the relation

$$Q_{2+}/Q_R = 1 - 0.45 \exp(-2.6 V_{PO})$$

$$(-0.6 < V_{PO} < 1.5 \text{ MeV}). \quad (2)$$

The net quadrupole moment is nonzero even when V_{PO} equals zero! The reason is that the mass parameters favor prolate shapes and hence increase the domain of "prolate" type quadrupole moments.

These semiquantitative relations predict correctly the trends of Q_{2+}/Q_R for ^{24}Mg , ^{56}Fe , ^{110}Cd , and ^{152}Sm . However, for precise predictions or fits, detailed numerical calculations of the type discussed previously,^{5,7} are needed.

References

- ¹Based on paper published in *Phys. Rev. C1*, 369 (1970).
- ²Initial stages of this work were completed while the author was at the Niels Bohr Institute, Copenhagen.
- ³J. de Boer and J. Eichler, *Advances in Nuclear Physics*, vol. 1, ed. by M. Baranger and E. Vogt, Plenum, New York, 1968.
- ⁴J. X. Saladin *et al.*, *Phys. Rev. Letters* **20**, 1298 (1968); also see *Phys. Rev. C1*, 1573 (1970).
- ⁵K. Kumar, *Nuclear Structure: Dubna Symposium*, International Atomic Energy Agency, Vienna, 1968.
- ⁶L. Wilts and M. Jean, *Phys. Rev.* **102**, 788 (1956).
- ⁷K. Kumar and M. Baranger, *Nucl. Phys.* **A122**, 273 (1968); also see *Phys. Rev. Letters* **17**, 1146 (1966).
- ⁸C. M. Lederer, J. M. Hollander, and I. Perlman, *Tables of Isotopes*, 6th ed., Wiley, New York, 1967.

2.24 UKE -- A COMPUTER PROGRAM FOR TRANSLATING NEUTRON CROSS-SECTION DATA FROM THE UKAEA NUCLEAR DATA LIBRARY TO THE EVALUATED NUCLEAR DATA FILE FORMAT¹

R. Q. Wright² S. N. Cramer² D. C. Irving³

A computer program, UKE, has been written to translate neutron cross sections on computer tape from the United Kingdom Atomic Energy Authority Nuclear

Data Library to the Evaluated Nuclear Data File, ENDF/B. The code will translate UK library smooth cross-section data, secondary angular distributions, and secondary energy distributions to the ENDF/B format. No resonance parameters, thermal scattering data, or photon data are considered, however. The secondary angular distributions are translated as differential scattering probabilities only, and no Legendre expansion coefficients are given.

General information is presented concerning the format of the two libraries along with a detailed description of the translation from the UK secondary energy distribution laws to those of ENDF/B. Programming details and a user's guide are also presented.

References

- ¹Abstract of ORNL-TM-2880 (March 1970).
- ²Computing Technology Center, Union Carbide Corp., Oak Ridge, Tenn.
- ³Present address: 816 Legare Road, Aiken, S.C. 29801.

2.25 REACTOR RADIATION SHIELDING PROGRAM AT THE TOWER SHIELDING FACILITY

C. E. Clifford K. M. Henry
F. J. Muckenthaler J. L. Hull
L. B. Holland

A Tower Shielding Facility experimental program was continued to generate accurate data for use in evaluating the current calculational techniques used for radiation transport problems. Evaluations of the techniques can best be realized through a comparison of the measured and calculated neutron and gamma-ray energy spectra. Such spectra have been measured in the SEPO program, which has consisted of a study of lithium hydride and heavy metal shields utilizing a SNAP U-ZrH reactor as a source, and in an experimental program being performed in support of the LMFBR project.

The LMFBR effort is mainly concerned with (1) the evaluation and development of calculational techniques for predicting the fluence of neutrons penetrating a sodium and stainless steel shield protecting the reactor grid plate,¹ (2) the penetration of neutrons through a solid iron shield covering the top of the reactor tank, and (3) the prediction of the neutron-spectra arriving at the bottom surface of the iron shield. The prediction of the penetration of neutrons through the iron shield has top priority in the FFTF design support program. The problem is complicated by the fact that there are many penetrations through the top shield which are filled

with plugs that must have clearance gaps surrounding them.

In order to provide data against which the techniques can be checked, measurements have been taken of the neutron spectra transmitted through iron shields up to 36 in. thick. The spectra were determined for the energy region from 50 keV to 1.5 MeV using the hydrogen-filled proportional counters of the spherical type and the techniques originally developed by Benjamin *et al.*² These results have been used primarily to evaluate a number of different iron cross-section point data sets and to develop suitable multigroup cross-section sets.³ The LMFBR program has occupied approximately one-third of the effort at the TSF during this reporting period. However, it is anticipated that the future program will be expanded to utilize one-half to three-fourths of the effort at the TSF.

The major effort in the SNAP program during this fiscal year has been concerned with the measurement of gamma-ray spectra transmitted by shields of single materials and also of shields which were laminates of heavy metals and lithium hydride. In these experiments, slabs of material were placed directly beneath the SNAP reactor and gamma-ray spectral measurements were made with a 5-in. NaI single-crystal spectrometer placed at a distance of approximately 28 ft from the slab. Gamma-ray spectral measurements were completed for a slab of lithium hydride 12 in. thick, slabs of lead from 1½ to 6 in. thick, slabs of ²³⁸U from 1½ to 4½ in. thick, and tungsten powder in thicknesses up to the equivalent of 6 in. of natural tungsten.

For the laminated configurations, the following slab arrangements were used: (1) 3, 4, and 6 in. of lead, adjacent to the reactor, each followed by 6 in. of lithium hydride; (2) 6 in. of lithium hydride followed by 1½ in. of lead; (3) 6 in. of lithium hydride followed by 1½ and 4½ in. of ²³⁸U; (4) three layers of uranium and three layers of lithium hydride; and (5) a configuration simulating a specific shield design and containing 4 in. of lead followed by 26 in. of lithium hydride, 1 in. of uranium, and 6 in. of lithium hydride.

Considerable effort was required during the course of these experiments to minimize the background so that the spectral measurements could be obtained through the thicker shields. Because of difficulty in predicting the measured gamma-ray spectra transmitted by the shields described above, additional measurements were made of the gamma-ray spectra produced from thin samples in a good geometry configuration.⁴ Samples of lead, tantalum, ²³⁸U, and Hastelloy were used. Gamma-ray spectra emerging from thick samples in good geometry were also measured for polyethylene

and laminations of lead, uranium, and hevimet with lithium hydride, as well as for various thicknesses of lead and uranium. Analysis of these data is still in progress. However, preliminary results indicate that large discrepancies still exist between predicted and measured values of gamma rays emerging from thick lead or uranium shields.

References

- ¹ See Sect. 2.26.
- ² P. W. Benjamin *et al.*, *Nucl. Instr. Methods* **59**, 77--85 (1968).
- ³ See Sect. 2.27.
- ⁴ See Sects. 2.30 and 2.31.

2.26 LMFBR SHIELDING DEVELOPMENT PROGRAM — INTERIM REPORT: PRELIMINARY EVALUATION OF TECHNIQUES FOR PREDICTING THE SPECTRA OF NEUTRONS TRANSMITTED BY GRID PLATE SHIELDS¹

C. E. Clifford F. R. Mynatt²
H. C. Claiborne

This is an interim progress report on the status of the LMFBR shielding program in progress at Oak Ridge National Laboratory. The effort is mainly concerned with the evaluation and development of calculational techniques for predicting the fluence of neutrons that penetrate a sodium and stainless steel shield to reach the grid plate beneath the FFTF core. Experimental determinations of the spectra of neutrons transmitted through up to 24-in.-thick shields of pure sodium in iron pins plus sodium and of pure iron are compared with two-dimensional discrete ordinates calculations and, in some cases, with Monte Carlo calculations of these spectra. Also presented are the results of a series of one-dimensional ANISN calculations made to evaluate the effect of material choice in an early FFTF configuration. On the basis of the studies completed to date, a number of conclusions are presented outlining the current situation regarding shielding design calculations of this nature.

References

- ¹ Abstract of ORNL-TM-2896 (to be published).
- ² Computing Technology Center, Union Carbide Corp., Oak Ridge, Tenn.

2.27 NEUTRON TRANSPORT IN IRON^{1,2}

F. R. Mynatt³ E. A. Straker
 F. J. Muckenthaler R. Q. Wright³
 M. L. Gritzner³ L. R. Williams³
 R. M. Freestone, Jr.

The study of neutron transport in iron which is reported in this paper is a mixture of several efforts. A purely calculational part of the program is the study of the effects due to different cross-section sets (evaluations) and the use of multigroup cross sections. This is done by comparing several Monte Carlo and discrete ordinates calculations for a point fission source in a 1.5-m-radius sphere of iron. Cross-section sets used include O5R, ENDF-B, and new evaluations by ORNL⁴ and Westinghouse.⁵ The multigroup calculations were performed using a large number of groups (~300) selected to best fit the important valleys of the total cross section.

Discrete ordinates calculations have been performed for comparison with two integral experiments. The first of these was performed at the ORNL Tower Shielding Facility. Transmitted neutron spectra in the energy region from 50 keV to 15 MeV have been measured for 8-, 16-, and 24-in.-thick iron cylinders which are 20 in. in diameter and for several thicknesses of large iron slabs. In order to test the effects of heterogeneous iron-sodium shields, experiments and two-dimensional calculations have been performed for a 0.591-in.-pitch square array of 881 iron pins, 0.375 in. in diameter, which were immersed in sodium. Explicit Monte Carlo and approximate two-dimensional discrete ordinates calculations were compared with the experiment. Calculations have also been performed for comparison with angle-dependent neutron spectra measured for a spherical iron assembly by Cerbone.⁶ The hollow sphere has a maximum iron thickness of 13.41 in.

References

¹Summary of paper presented at the American Nuclear Society Meeting, Los Angeles, Calif., June 29–July 2, 1970.

²Work funded by the Defense Atomic Support Agency under Union Carbide Corporation's contract with the U.S. Atomic Energy Commission.

³Computing Technology Center, Union Carbide Corp., Oak Ridge, Tenn.

⁴D. C. Irving and E. A. Straker, "Evaluation of the Total Cross Section of Iron," *Trans. Am. Nucl. Soc.* 12(2), 924 (1969).

⁵N. Azziz and J. W. Connelley, *Iron Cross-Section Evaluation*, WCAP 7281 (to be published).

⁶R. J. Cerbone, *Measurement of Neutron Penetration Standards, Vol. 1, Angular Neutron and Gamma-Ray Spectrum Measurements in a Bulk Iron Assembly*, GA-9149 (Mar. 27, 1969).

2.28 COMPARISONS OF MONTE CARLO CALCULATIONS WITH MEASUREMENTS OF NEUTRON LEAKAGE FROM THE TSF-SNAP REACTOR¹

V. R. Cain

The TSF-SNAP reactor is being used at ORNL as a realistic source for investigations of the light-weight shields required for space power systems. As part of this program, experimental and analytical determinations have been made of the energy and angular distribution of neutrons leaving an area roughly equal to 10% of the reactor lower surface. The agreement between experiment and Monte Carlo calculations was found to be quite good when the reactor was described in sufficient detail in the calculations.

Reference

¹Abstract of paper to be published as a Technical Note in *Nuclear Science and Engineering*.

2.29 THE IMPORTANCE DISTRIBUTION OF NEUTRON REACTIONS RELATIVE TO THEIR CONTRIBUTION TO THE SECONDARY GAMMA-RAY DOSE TRANSMITTED BY TUNGSTEN AND LAMINATED LITHIUM HYDRIDE AND TUNGSTEN SHIELDS¹

J. V. Pace² F. R. Mynatt²

The determination of the importance, as a function of neutron reaction type, energy of reacting neutron, and position in the shield, for the events which produce secondary gamma rays that contribute to the exit gamma-ray dose is of interest in determining what cross sections and features of the transport process need to be improved. For one-dimensional shields of tungsten and laminated lithium hydride and tungsten, the ANISN code has been used to determine the gamma-ray importance function for an exit gamma-ray dose response and the neutron flux distribution for an incident leakage spectrum for the TSF-SNAP reactor. Convolution of these distributions with selected secondary gamma-ray production data displays the origin of the

secondary gamma-ray dose as it is distributed in space and neutron energy.

References

- ¹Abstract of CTC-41 (to be published).
²Computing Technology Center, Union Carbide Corp., Oak Ridge, Tenn.

2.30 GAMMA-RAY SPECTRA ARISING FROM FAST-NEUTRON INTERACTIONS IN ELEMENTS FOUND IN SOILS, CONCRETES, AND STRUCTURAL MATERIALS^{1,2}

R. E. Maerker F. J. Muckenthaler

Experimental data are presented for the production of secondary gamma rays arising from the interaction of a fission-like spectrum of fast neutrons with oxygen, carbon, iron, aluminum, copper, zinc, titanium, nickel, silicon, calcium, potassium, sodium, barium, sulfur, and a stainless steel. Measurements of the gamma-ray spectra for these elements were made at the Tower Shielding Facility with a carefully calibrated 5- by 5-in. NaI(Tl) detector. These data are useful in evaluating the accuracy of (n, γ) cross-section sets. The data are differential in the gamma-ray energy from 1 MeV to approximately 6.5 MeV and are expressed as values of 4π times the average differential gamma-ray production cross section at 90 deg to the incident neutron beam for all neutrons in the beam lying above 1 MeV. These results are estimated to have an accuracy of $\pm 30\%$ and to include the contribution from both discrete and continuum gamma rays. Comparisons of these data with results obtained by averaging previously published differential cross sections over the incident spectrum indicate that considerable differences exist between the values obtained at the Tower Shielding Facility and the earlier data. Very approximate experimental data are presented for gamma rays arising from resonance capture of neutrons from a $1/E$ energy spectrum in the energy range 10–200 keV.

References

- ¹Research funded by the Defense Atomic Support Agency under Union Carbide Corporation's contract with the U.S. Atomic Energy Commission under Subtask No. RRP-A2-11.037.
²Abstract of ORNL-4475 (April 1970) and of paper submitted to *Nuclear Science and Engineering*.

2.31 GAMMA-RAY SPECTRA ARISING FROM THERMAL-NEUTRON CAPTURE IN ELEMENTS FOUND IN SOILS, CONCRETES, AND STRUCTURAL MATERIALS¹

R. E. Maerker F. J. Muckenthaler

Gamma-ray spectra arising from the capture of thermal neutrons have been measured for several naturally occurring elements of interest to the shielding community. The spectral intensities in units of photons per 100 captures are presented as sums over 0.5-MeV intervals. These results have an estimated accuracy of $\pm 15\%$ and include the contributions from both discrete and continuum gamma rays. The present results do not go below 1 MeV, but when the relatively small contributions from energies less than 1 MeV are added to them, binding energy checks averaging within $\pm 5\%$ are obtained.

Reference

- ¹Abstract of Technical Note to be published in *Nuclear Engineering and Design*.

2.32 GAMMA-RAY SPECTRA ARISING FROM FAST-NEUTRON INTERACTIONS IN IRON, ALUMINUM, COPPER, ZINC, AND TITANIUM^{1,2}

R. E. Maerker F. J. Muckenthaler

An extensive study of secondary gamma-ray production cross sections has now been completed at the Tower Shielding Facility; we report here the first series of results for fast-neutron interactions.

Thin slabs of the materials of the order of 5-ft square and varying in thickness between $\frac{1}{4}$ and $\frac{1}{16}$ in. were placed in a collimated beam emanating from the TSR-II. The slabs were oriented at an angle of 45° to the incident beam, and a collimated 5- by 5-in. NaI(Tl) crystal was placed at 90° to the beam. For the results presented here, the crystal response due to a known spectrum of fast neutrons (see Table 2.32.1) was measured by placing a ~ 2 -cm-thick boron filter over the reactor collimator. Small corrections to the response from gamma rays arising from capture of incident thermal neutrons which leaked through the reactor shield were made, as were approximate corrections from gamma rays above ~ 6 MeV arising from resonance capture of incident neutrons in the energy range 10 to 200 keV which leaked through the boron filter.

From knowledge of the absolute neutron spectrum above 1 MeV incident on the slab samples and the unfolded absolute spectral intensities of the gamma rays, production cross sections were determined as $4\pi d\bar{\sigma}/d\Omega$ (90°), where $d\bar{\sigma}/d\Omega$ (90°) is the production cross section in millibarns per steradian at 90° to the neutron beam averaged over the neutron spectrum above 1 MeV.

The uniqueness of these results lies in the determination of any continuum contribution to the spectra in addition to the discrete contribution. They are intended primarily to serve as integral checks on production cross-section sets obtained by other means which are differential in the neutron energy.

Table 2.32.1. Relative Number of Neutrons Incident on the Slab Samples as a Function of Neutron Energy

Neutron Energy (MeV)	Number	Neutron Energy (MeV)	Number
1-1.5	0.174	5.5-6	0.026
1.5-2	0.163	6-6.5	0.021
2-2.5	0.169	6.5-7	0.015
2.5-3	0.118	7-7.5	0.011
3-3.5	0.079	7.5-8	0.008
3.5-4	0.063	8-9	0.009
4-4.5	0.056	9-10	0.005
4.5-5	0.045	10-12	0.003
5-5.5	0.034	12-14	0.001

Table 2.32.2. Values of $4\pi d\bar{\sigma}/d\Omega$ (90°) in Millibarns from Fast-Neutron Interactions in Iron, Aluminum, Copper, Zinc, and Titanium

Gamma-Ray Energy (MeV)	Iron ^a	Aluminum	Copper	Zinc	Titanium
1-1.5	278	181	~1090 ^b	909	688 ^c
1.5-2	110	36	256	195	116
2-2.5	101	103	127	113	97
2.5-3	74	26	87	59	48
3-3.5	44	42	45	41	22
3.5-4	33	8.8	35	27	20
4-4.5	8.7	5.8	24	16	9.5
4.5-5	5.6	6.9	13.5	<13.3	5.1
5-5.5	3.8	4.9	9.1	<6.4	<4.4
5.5-6	2.4	2.0	<5.9	<5.6	<2.8
6-6.5	<2.1	<1.7	<6.2		<2.4

^aFor $E_\gamma = 0.85$ MeV, $4\pi d\bar{\sigma}/d\Omega$ (90°) ~ 600 mb.

^b0.98-1.50 MeV.

^c0.99-1.50 MeV.

Table 2.32.2 presents the results for iron, aluminum, copper, zinc, and titanium. The overall accuracy of the values is estimated to be $\pm 30\%$ for each gamma-ray interval.

References

¹Research funded by the Defense Atomic Support Agency under Union Carbide Corporation's contract with the U.S. Atomic Energy Commission.

²Summary of paper presented at the American Nuclear Society Meeting, Los Angeles, Calif., June 29-July 2, 1970.

2.33 THE POPOP4 LIBRARY OF SECONDARY GAMMA-RAY DATA^{1,2}

W. E. Ford III³

The data-set titles and literature sources of the data in the initial distribution of the POPOP4 library are listed. This library is a compendium of secondary gamma-ray data for the various neutron-induced reactions and is available on magnetic tape from the Radiation Shielding Information Center. The data are in a format for use with the POPOP4 system of codes in the preparation of multigroup cross sections for coupled neutron-gamma transport calculations. Input and output from sample cases using data from the library with the POPOP4 system of codes is shown.

References

¹Abstract of USAEC Report CTC-42 (to be published).

²Research partially sponsored by the Defense Atomic Support Agency under Union Carbide Corporation's contract with the U.S. Atomic Energy Commission.

³Computing Technology Center, Union Carbide Corp., Oak Ridge, Tenn.

2.34 THE USE AND "TESTING" OF Al, Fe, Ni, Cu, AND Pb SECONDARY GAMMA-RAY PRODUCTION DATA SETS FROM THE POPOP4 LIBRARY^{1,2}

W. E. Ford III³ D. H. Wallace³

Aluminum, iron, nickel, copper, and lead secondary gamma-ray yield data sets for gamma rays resulting from neutron capture and inelastic scattering reactions were evaluated by comparing calculated secondary gamma-ray pulse-height spectra with spectra measured at the Tower Shielding Facility. The calculated spectra

were obtained by using a discrete ordinates transport code to calculate the secondary gamma-ray angular flux resulting from the exposure of slabs of the materials of interest to bare, cadmium-filtered, boron-filtered, and "thermal" neutron beams from the TSR-II reactor and by then folding the angular flux into pulse-height spectra.

The FORTRAN-IV codes LINFOLD, A Sample Simple Coupling Code, and POPOP4 Library Tape Maker are described. LINFOLD folds the calculated intensity of photons striking an NaI(Tl) detector into secondary gamma-ray pulse-height spectra and compares calculated and measured spectra. A Sample Simple Coupling Code couples P_N neutron cross-section sets, P_N gamma-ray cross-section sets, and POPOP4 P_O secondary gamma-ray-production cross sections into P_N coupled cross sections for use with ANISN, DOT, MORSE, etc., transport codes. POPOP4 Library Tape Maker makes or updates a binary library tape of yield data sets for use with POPOP4. The latter code also makes or updates a BCD formatted library tape of yield data sets.

References

¹ Abstract of USAEC Report CTC-20.

² Research partially sponsored by the Defense Atomic Support Agency under Union Carbide Corporation's contract with the U.S. Atomic Energy Commission.

³ Computing Technology Center, Union Carbide Corp., Oak Ridge, Tenn.

2.35 SIMULTANEOUS FAST-NEUTRON SPECTRAL MEASUREMENTS BY TIME-OF-FLIGHT AND PULSE-HEIGHT UNFOLDING TECHNIQUES^{1,2}

E. A. Straker T. A. Love
C. E. Burgart R. M. Freestone, Jr.

As a first step in neutron measurements conducted at the ORELA Shielding Facility, neutron spectra were measured simultaneously by both time-of-flight (TOF) and unfolding pulse-height spectra (UPHS) techniques to provide an internal check on the experimental system and to provide an additional check on the UPHS technique that has previously been employed^{3,4} at the Tower Shielding Facility. Fast-neutron spectra are usually measured by TOF techniques if the source is

time dependent and by UPHS techniques if a steady-state radiation field is used. Linear accelerators have the unique ability of providing short pulses of neutrons with a wide spectrum of energies. This ability makes possible the collection of two-parameter data⁵ (time and pulse height) and the simultaneous collection of pulse-height and time-of-flight spectra.

The radiation source for the ORELA Shielding Facility consists of a 140-MeV electron linear accelerator capable of producing up to 15 A of electron current per pulse, 1000 pulses/sec, and pulse widths of 2.3 nsec to 1 μ sec. Neutrons produced in a water-cooled tantalum converter are observed at 165 deg to the electron beam. Two shielding rooms at 30 and 50 m provide space for neutron and gamma-ray measurements.

For these measurements, several materials were placed in good geometry at 9 m from the electron target along the collimated flight path, and the nominal 2- by 2-in. NE-213 was placed at 48.5 m. An RCA-8575 photo-multiplier tube with a linear signal derived from dynode 9 and a fast-timing signal from the anode were used. Gamma-ray discrimination was provided by using cross-over timing pulse-shape discrimination techniques with double front edge timing between fast signal and pulse crossover. A built-in fiducial time was obtained from gamma flash events in the detector, but these events were generally not stored. Pulse-pileup rejection techniques were used to eliminate dead-time corrections. The data were sorted by software programs in the on-line PDP-9 computer so as to store pulse-height distributions regardless of time and time-of-flight distributions integrated over pulse height. The dynamic range of the NE-213 in neutron energy was 45.

Spectra transmitted by 3.5 in. of depleted uranium, 8 in. of water + 3.5 in. of ^{238}U , and 8 in. of carbon + 3.5 in. of ^{238}U were measured. Figure 2.35.1 shows results obtained for the C- ^{238}U sample. The agreement between the TOF results (solid line) and the UPHS results obtained with FERDOR⁶ (vertical bars) is excellent, with differences being due to the poorer resolution inherent in the UPHS techniques. This is further illustrated by other higher-resolution TOF data not shown. Comparisons with calculations must therefore take into account the resolution inherent in the particular measurement.

These results clearly illustrate that there is internal consistency in the two neutron spectroscopy techniques and further validates the results of previous measurements that depended on unfolding pulse-height spectra.

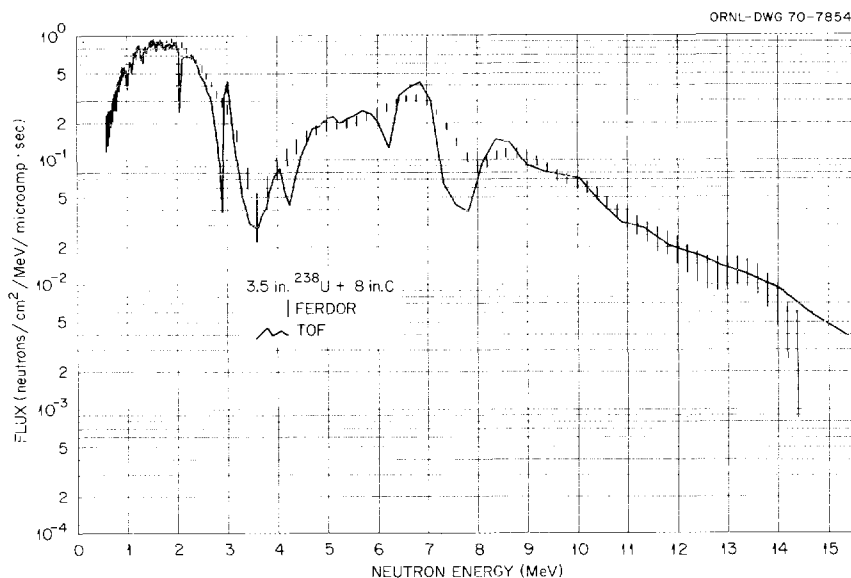


Fig. 2.35.1. Comparison of Time-of-Flight and Unfolded Pulse-Height Spectra for the Neutron Spectrum Transmitted Through 3.5 in. of ^{238}U and 8 in. of Carbon.

References

¹Research funded by the Defense Atomic Support Agency under Union Carbide Corporation's contract with the U.S. Atomic Energy Commission.

²Abstract of paper to be presented at American Nuclear Society Annual Meeting in Washington, D.C., November 1970.

³L. Harris, Jr., and H. Kendrick, *Trans. Am. Nucl. Soc.* 12, 959 (1969).

⁴C. E. Clifford *et al.*, *Nucl. Sci. Eng.* 27, 299 (1967).

⁵E. A. Straker, *Nucl. Sci. Eng.* 34, 114 (1968).

⁶W. R. Burrus, *Utilization of A Priori Information in the Statistical Interpretation of Measured Distributions*, ORNL-3743 (1964).

2.36 MEASUREMENT OF TIME-DEPENDENT GAMMA-RAY SPECTRA FROM POLYETHYLENE¹

C. E. Burgart R. M. Freestone, Jr.
T. A. Love E. A. Straker

A measurement of the time-dependent secondary gamma rays from polyethylene due to a Linac neutron source has been made to provide a benchmark-type experiment to test time-dependent transport codes. There has been an increased interest in the past few years in determining the time-dependent behavior of

the radiation fields from weapons. Several time-dependent transport codes have been written for calculating such fields; however, there are few experiments that may be used to validate the codes. Although the time-dependent solution by Monte Carlo techniques is straightforward, discrete ordinates calculations of the time-dependent neutron and secondary gamma-ray fields are more difficult due to coupling effects in the space-time mesh. A preliminary set of measurements has been made at the ORELA Shielding Facility to provide data useful in testing time-dependent transport codes.

The Linac neutron source is produced by 140-MeV electrons incident on a water-cooled tantalum target. For this experiment the neutrons were collimated down a flight path 165 deg to the electron beam. ^{10}B and ^{238}U filters ($3/4$ and $3 1/2$ in., respectively) placed in the flight path 9 in. from the target filtered out low-energy neutrons and target-produced gamma rays. A 6-in.-thick polyethylene slab was positioned in the flight path 48.5 m from the target and at an angle of 45 deg from the nearly parallel beam of neutrons. The gamma-ray detector, a 5- by 5-in. NaI crystal mounted in a lead and lithiated paraffin shield, was placed 43 in. from the polyethylene at an angle of approximately 135 deg from the neutron beam. The anode signal was used to determine the time of flight, and a linear signal taken from dynode 10 was used to determine the pulse height. These two-parameter data were stored in an

on-line PDP-9 computer. The gamma flash from the Linac provided a time fiducial but was not intense enough to require the photomultiplier tube. A pulse pileup circuit was used to eliminate bias due to system dead time.

The preliminary data clearly illustrate the 4.43-MeV gamma ray from neutron inelastic scattering in carbon at early times ($t \lesssim 1.2 \mu\text{sec}$), with the 2.22-MeV hydrogen capture gamma ray appearing at later times. Figure 2.36.1 shows the time-dependent count rate integrated over pulse height; the structure due to the inelastic cross section is clearly visible. At longer times, $>2.5 \mu\text{sec}$, the hydrogen capture gamma rays dominate.

Figure 2.36.2 shows pulse-height distributions for the time intervals marked in Fig. 2.36.1. Besides the carbon inelastic and hydrogen capture gamma rays, there is a prominent 6.9-MeV gamma ray in the background. The time dependence of the 4.43-MeV carbon inelastic gamma ray is due almost entirely to the time dependence of the source and thus may provide a test of the time-dependent source and wave propagation capabilities of the codes. The buildup and decay of the low-energy neutron capture gamma ray in hydrogen is due entirely to the high-energy neutrons incident on the shield and thus can provide a check of time-dependent particle transport capabilities.

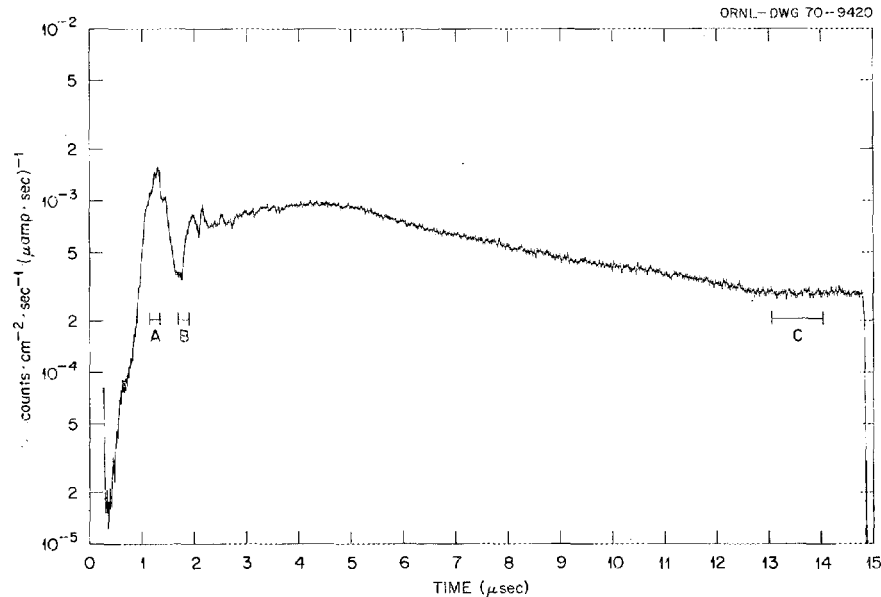


Fig. 2.36.1. Investigation of Time-Dependent Secondary Gamma-Ray Production in Polyethylene: Gamma-Ray Count Rate vs Time After Linac Pulse.

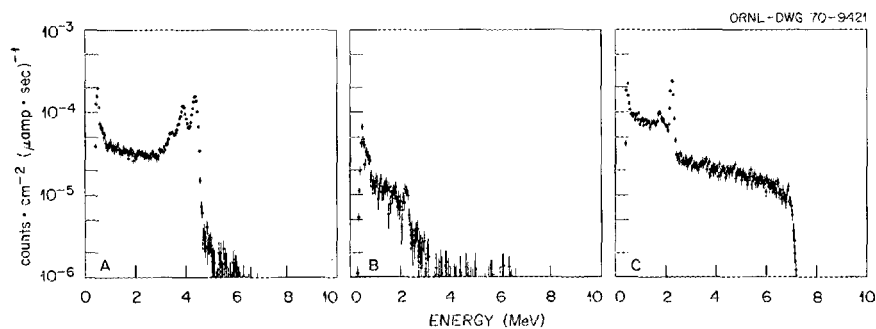


Fig. 2.36.2. Gamma-Ray Pulse-Height Distributions for the Time Intervals Shown in Fig. 2.36.1.

Reference

¹Research sponsored by the Defense Atomic Support Agency under Union Carbide Corporation's contract with the U.S. Atomic Energy Commission.

2.37 THE ENERGY SPECTRUM OF PHOTONEUTRONS PRODUCED BY 140-MeV ELECTRONS INCIDENT ON TANTALUM^{1,2}

C. E. Burgart T. A. Love
E. A. Straker R. M. Freestone, Jr.

The neutron energy spectrum produced by 140-MeV electrons incident on tantalum has been measured by time of flight in the 0.7- to 20-MeV energy range. This energy spectrum normalized per incident electron is in excellent agreement with previous calculations.

References

¹Research sponsored by the Defense Atomic Support Agency under Union Carbide Corporation's contract with the U.S. Atomic Energy Commission.

²Abstract of ORNL-TM-3022 (to be published) and paper submitted for journal publication as a Technical Note.

2.38 TIME-DEPENDENT COUPLED NEUTRON-GAMMA CALCULATIONS IN POLYETHYLENE^{1,2}

C. E. Burgart W. W. Engle, Jr.³

Preliminary calculations have been made of the time-dependent neutron and secondary gamma-ray spectra emerging from a polyethylene slab due to a time-dependent incident neutron source. The configuration consisted of a monodirectional neutron beam originating 50 m from the slab and having a pulse width of 24 nsec. This beam impinged normally on a 6-in. slab of polyethylene. Neutron and gamma-ray time-dependent energy spectra returning from the surface of the slab toward the source were calculated. The source energy spectrum was that calculated by Alsmiller *et al.*⁴ for 150-MeV electrons impinging on 20 radiation lengths of tantalum. This configuration is similar to a proposed experiment at the ORELA Shielding Facility.

These time-dependent coupled neutron-gamma calculations were performed using MORSE and ANISN-T1. MORSE is a multigroup Monte Carlo code,⁵ while ANISN-T1 is a time-dependent one-dimensional discrete ordinates code.⁶ Each of these codes is capable of solving the coupled time-dependent problem in a single pass on the computer with no tapes. These

calculations utilized cross sections from GAM-II and MUG with 21 neutron groups and 18 gamma-ray groups.

In the MORSE calculation, estimation of the energy spectra at the front face was performed following each real collision utilizing the SAMBO analysis package.⁷ Source energy biasing and nonleakage were utilized. In the ANISN-T1 calculation a time-dependent boundary source was used to describe the time and energy dependence of the neutrons entering the slab. This calculation was performed with fine time steps for both neutrons and secondary gamma rays. The neutron velocities in both calculations corresponded to the mean energy of each group, except for the thermal group, which was assigned a velocity of 2200 m/sec.

Agreement between MORSE and ANISN-T1 was excellent for all times and energies. Shown in Figure 2.38.1 are the time distributions of two gamma energy

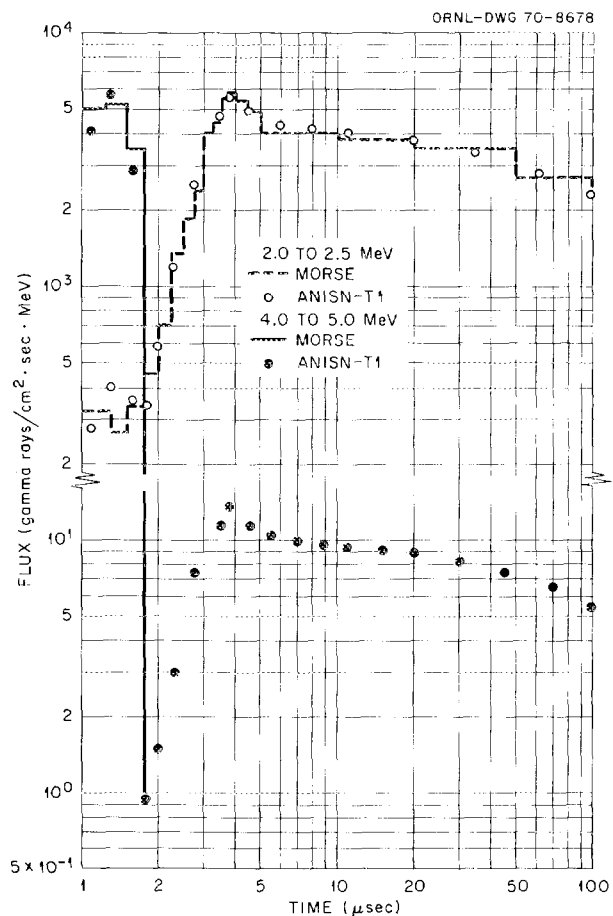


Fig. 2.38.1. Time Dependence of Gamma-Ray Flux Emerging from Polyethylene in the Energy Groups 2.0 to 2.5 and 4.0 to 5.0 MeV.

groups, 4 to 5 and 2 to 2.5 MeV. Due to the large distance from the source to the slab, the time separation between the carbon inelastic gammas (4.43 MeV) and the hydrogen (2.22 MeV) and carbon (4.95 MeV) capture gammas may be easily observed. The intensity of the carbon inelastic gammas and the hydrogen capture gamma is of the same order of magnitude.

These calculations have proved to be useful as an intercomparison of the codes and as an aid in designing the experiment. Following the experiment they will be useful in evaluating the cross sections and the ability of these codes to perform time-dependent coupled neutron-gamma-ray calculations.

References

¹Research funded by the Defense Atomic Support Agency under Union Carbide Corporation's contract with the U.S. Atomic Energy Commission.

²To be presented at American Nuclear Society Annual Meeting, Washington, D.C., November 1970.

³Computing Technology Center, Union Carbide Corp., Oak Ridge, Tenn.

⁴R. G. Alsmiller, Jr., T. A. Gabriel, and M. P. Guthrie, *Nucl. Sci. Eng.* **40**, 365--74 (1970).

⁵See Sect. 2.1.

⁶W. W. Engle, Jr., and F. R. Mynatt, *Trans. Am. Nucl. Soc.* **12**, 400 (1969).

⁷See Sect. 2.2.

2.39 ON-LINE DATA-ACQUISITION AND TREATMENT PROGRAMS FOR A PDP-9 COMPUTER

R. M. Freestone, Jr. C. E. Burgart

A computer-based data acquisition system located at the Tower Shielding Facility (TSF) was described in a previous report.¹ The equipment described is now at the ORELA Facility, where it is being used in time- and energy-dependent shielding experiments. This new application of the PDP-9 computer² necessitated the development of a fresh set of programs tailored to fit the specific needs of the current experiments.

The intent underlying the program development has been to minimize the amount of core required for program storage and to maximize the amount available for data storage. Operating programs are restricted to the lower half of memory, leaving 4096 18-bit words in the upper half for data storage. All programs are written in assembly language. Minimum-length I/O handlers were written to serve all programs and peripherals.

Presently in use during data taking are routines to accept pulse-height data from the analog-to-digital converters, sort it, store it as pulse-height or time-of-flight spectra, present it as a continuously updated oscilloscope display³ having a variety of x and y scale factors, including a semilog option, and output compiled results in typed, punched paper tape or magnetic tape (DECtape) modes. Soon to be added is a multiplexer connection which will allow data from the PDP-9 to be transmitted to the peripherals, including disk storage and IBM-compatible magnetic tape, of the main ORELA data system.

Programs which are not in continuous demand during an experimental run are stored on DECtape and recalled to core as required by simple keyboard commands. One of these is LSTSQ, a routine which computes a linear least-squares fit over any scope-displayed, light-pen-designated⁴ region of interest. It is used during calibration of an organic scintillator neutron spectrometer, and not only ensures accuracy but cuts the time required to obtain a calibration value by a factor of at least 10 over previous hand-plot, hand-fit methods.

References

¹R. M. Freestone, Jr., and K. M. Henry, *Neutron Phys. Div. Ann. Progr. Rept. May 31, 1969*, ORNL-4433, pp. 38--39.

²PDP-9 stands for Programmed Data Processor No. 9, a product of Digital Equipment Corp. (DEC), Maynard, Mass.

³The display routine was adapted from a PDP-4 routine originally written by L. W. Weston.

⁴A light pen is a rather simple arrangement consisting of a glass-fiber-optics light pipe, a photomultiplier, and associated circuitry. When the pen is positioned over an illuminated point on the oscilloscope screen, a flag is set in the computer. The flag can be sensed by the program in progress and appropriate action taken.

2.40 DESIGN CONSIDERATIONS FOR AN ORELA TARGET USING TANTALUM FOLLOWED BY BERYLLIUM^{1,2}

R. S. Booth

Presented here are the nuclear calculations associated with the design of a neutron source composed of tantalum followed by beryllium for the Oak Ridge Electron Linear Accelerator (ORELA). Electrons incident on the tantalum converter produce a narrow beam of intense photons which then generate neutrons in the

beryllium. The primary considerations associated with this analysis are the size of the beryllium block and the distance between the beryllium block and the tantalum converter. Monte Carlo calculations of the neutron interactions in the beryllium are used to predict the expected neutron intensity at two flight stations as a function of position in the source plane and time of arrival (energy) of the neutron flux. The time spread, caused by migration in the beryllium, of a mono-energetic neutron pulse is calculated for the same flight stations. The final predicted neutron intensity is compared with a measured neutron intensity from a target system similar to the one designed here.

References

¹Research funded by the Defense Atomic Support Agency under Subtask No. PE075-01.

²Abstract of ORNL-TM-2925 (Mar. 31, 1970).

2.41 A TANTALUM-BERYLLIUM TARGET FOR ORELA

J. Lewin

On the basis of Booth's calculations,¹ a tantalum-beryllium target was designed and fabricated. Figure 2.41.1 shows a plan view of the assembly and its location in the ORELA target room. It is anticipated that the target will be operable up to a beam power of 50 kW for an unfocused (quadrupoles off) beam. The beryllium will reach a temperature of about 800°F at its hottest point and will be cooled by radiation to the target room walls as well as by conduction to a water-cooled base plate. The assembly is retractable so as to be fully interchangeable in the target position with the present tantalum assembly. Installation in the target room is planned for July 1970.

Reference

¹See Sect. 2.40.

2.42 TIME-DEPENDENT NEUTRON AND SECONDARY GAMMA-RAY TRANSPORT IN INFINITE AIR AND IN AIR OVER GROUND^{1,2}

E. A. Straker

The general description of the radiation field was determined for several neutron source energies in infinite air and in an air-over-ground geometry for

source heights of 50 and 1125 ft. The effect on dose of source height and detector height and the effect of the ground on energy, angular, and time dependence are discussed for both fission and 12.2- to 15-MeV neutron sources. The satisfactory agreement of calculations with experimental results from operations BREN and HENRE and the agreement between Monte Carlo and discrete ordinates results lend confidence to the cross sections used and the computational techniques.

References

¹Research funded by the Defense Atomic Support Agency under Subtask No. PBO50.

²Abstract of ORNL-TM-2781 (May 7, 1970) and of paper submitted for journal publication.

2.43 NEUTRON AND SECONDARY GAMMA-RAY INDUCED HEAT IN THE GROUND DUE TO POINT 12.2-TO-15-MeV AND FISSION SOURCES AT AN ALTITUDE OF 50 ft^{1,2}

E. A. Straker M. B. Emmett³

M. L. Gritzner⁴

The energy deposited in ground due to neutrons and the secondary gamma rays has been determined as a function of range, ground depth, and time from instantaneous point source neutrons for a fission spectrum and for a 12.2-to-15-MeV energy band. In all cases the source was at a height of 50 ft above the air-ground interface. Discrete ordinates and Monte Carlo calculations illustrated that there is a significant effect on the energy deposited due to source energy distribution, but little effect due to ground composition. The importance of gamma rays produced by low-energy neutrons was found to be small for the 12.2-to-15-MeV source, but large for the fission source.

References

¹Research funded by the Defense Atomic Support Agency under Union Carbide Corporation's contract with the U.S. Atomic Energy Commission.

²Abstract of ORNL-TM-3003 (to be published) and of paper to be submitted for journal publication.

³Mathematics Division.

⁴Computing Technology Center, Union Carbide Corp., Oak Ridge, Tenn.

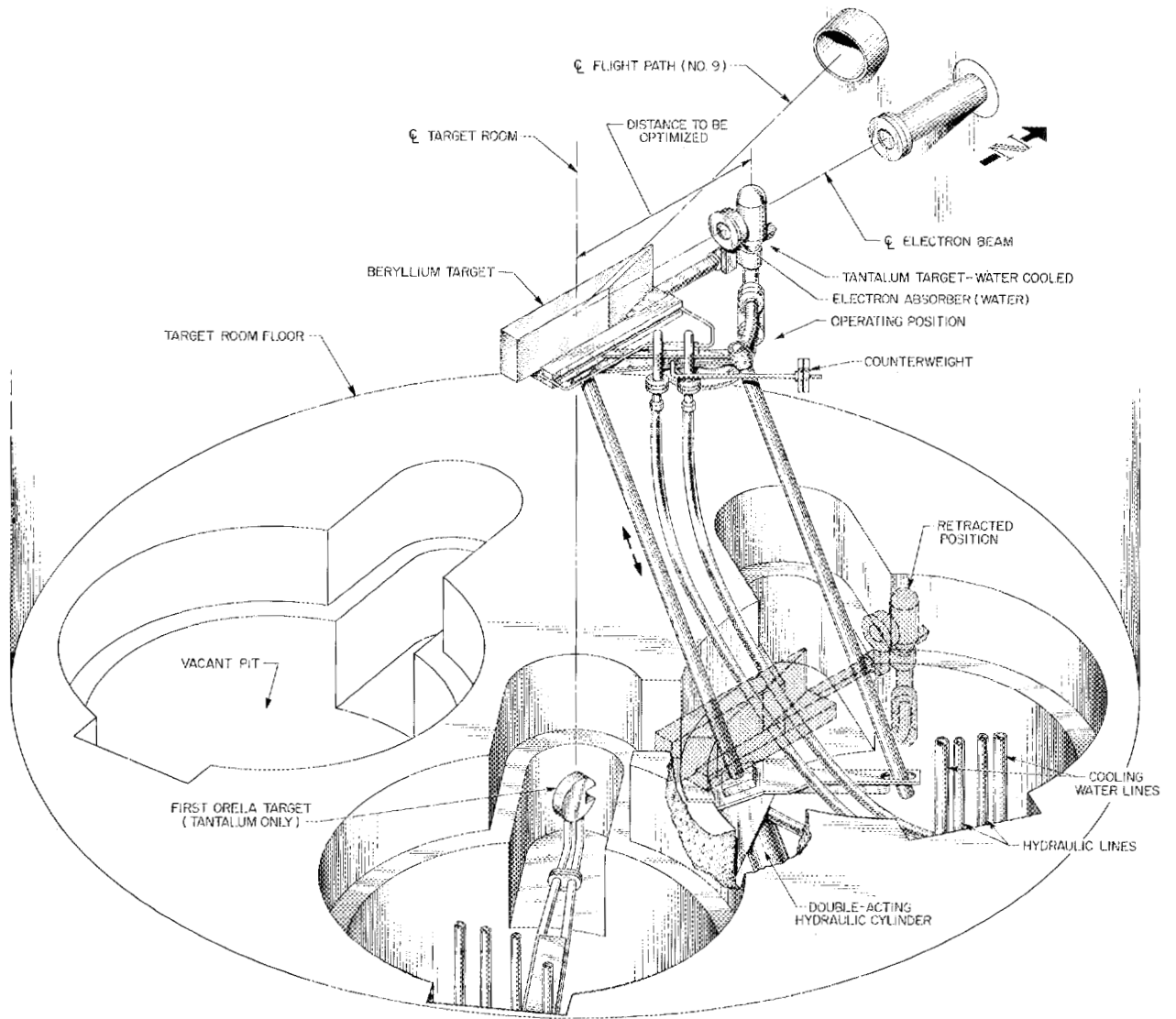


Fig. 2.41.1. Tantalum-Beryllium Target Installation in ORELA Target Room.

2.44 GROUND HEATING DUE TO A POINT SOURCE OF 12.2-TO-15-MeV NEUTRONS AT AN ALTITUDE OF 50 ft¹⁻³

E. A. Straker M. B. Emmett⁴
C. L. Thompson⁴

The heat deposited in the ground as a function of range, ground depth, and time due to the neutrons and their secondary gamma rays from a 12.2-to-15-MeV neutron source has been determined. The source was situated at an altitude of 50 ft above the ground in air of uniform density (1.10 g/liter). Both Monte Carlo and discrete ordinates methods were used to transport the neutrons and gamma rays through the atmosphere and into the ground. The importance of low-energy neutrons and the secondary gamma rays to the total heat deposited is shown.

References

- ¹Research funded by the Defense Atomic Support Agency under Subtask No. PB050.
²Abstract of ORNL-TM-2587 (Aug. 19, 1969).
³*Trans. Am. Nucl. Soc.* **12**(2), 954 (1969).
⁴Mathematics Division.

2.45 SENSITIVITY OF SECONDARY GAMMA-RAY DOSE TO ANGULAR DISTRIBUTION OF GAMMA RAYS FROM NEUTRON INELASTIC SCATTERING^{1,2}

E. A. Straker

It is well known that the gamma rays produced by the inelastic scattering of high-energy neutrons are not always emitted isotropically. There is also experimental evidence that the angular distribution sometimes peaks in both the forward and backward directions (measured with respect to the neutron direction). However, the current practice in solving transport problems is to assume isotropic emission of these gamma rays, and in order to obtain some idea of the sensitivity of transport results to this assumption, the secondary gamma-ray dose due to a 12.2-to-15-MeV neutron source in infinite homogeneous air was calculated for three assumptions for the angle of emission of the gamma rays. First, the gamma rays were assumed to be isotropic; second, they were assumed to be emitted in the straight-ahead direction, that is, in the direction of the neutron; and third, they were assumed to be emitted straight backward, that is, 180 deg from the neutron direction. The secondary gamma-ray dose as a

function of range was determined for these cases. (Note: The contribution to the secondary dose by capture gamma rays is very small at these source energies.)

References

- ¹Research sponsored by the Defense Atomic Support Agency under Union Carbide Corporation's contract with the U.S. Atomic Energy Commission.
²Abstract of Technical Note, *Nucl. Sci. Eng.* **41**, (1), 147 (July 1970).

2.46 STATUS OF NEUTRON TRANSPORT IN THE ATMOSPHERE^{1,2}

E. A. Straker

Attempts have been made since the mid-1940's to determine the radiation fields from nuclear weapons. Earlier attempts were experimental in nature, with the efforts in the last few years being mostly calculational. A review of the progress that has been made in the past few years, the information that is currently available, and approaches to solving the problem of determining the detailed radiation field description is given.

References

- ¹Research supported by the Defense Atomic Support Agency under Union Carbide Corporation's contract with the U.S. Atomic Energy Commission.
²Abstract of paper presented at the American Nuclear Society Annual Meeting, Los Angeles, Calif., June 1970; also to be published as an ORNL-TM report.

2.47 A FORTRAN-360 SUBROUTINE PACKAGE FOR PRODUCING PRINTED LINEAR, SEMILOGARITHMIC, OR LOGARITHMIC GRAPHS¹

C. L. Thompson²

A FORTRAN-360 subroutine package has been written to produce printed linear, semilog, or log-log plots similar to those produced on the CALCOMP Digital Incremental Plotters by the subroutine package INTRIGUE.

References

- ¹Abstract of ORNL-TM-3079 (to be published).
²Mathematics Division.

2.48 DOSE RATES IN A SLAB PHANTOM FROM MONOENERGETIC GAMMA RAYS^{1,2}

H. C. Claiborne D. K. Trubey

Gamma-ray flux-to-dose-rate conversion factors obtained with a philosophy consistent with that used for neutrons have not been generally available. To eliminate this inconsistency and develop more realistic gamma-ray conversion factors, gamma-ray dose-rate distributions were determined in a slab phantom.

Calculations were made with the discrete ordinates code ANISN and by the Monte Carlo code OGRE. Agreement between calculations and the available experimental results was excellent. Based on these results, a recommended curve was prepared for use when low-level exposure is the consideration.

References

¹ Research partially funded by the Defense Atomic Support Agency under Union Carbide Corporation's contract with the U.S. Atomic Energy Commission.

² Abstract of *Nucl. Appl. Tech.* 8, 450 (May 1970).

2.49 PROJECT SAFEGUARD

H. C. Claiborne

Under Interagency Agreement No. 48-185-69, assistance in engineering shield design has been given to the U.S. Army Corps of Engineers for the Safeguard project. This assistance included shielding calculations for various enemy threats and consultation with the design personnel. Several informal reports have been made on the results. However, since the work is classified, no results are given here.

2.50 THE CALCULATION OF NEUTRON-INDUCED PHYSICAL DOSES IN HUMAN TISSUES^{1,2}

J. J. Ritts³ M. Solomito
P. N. Stevens⁴

The purpose of this investigation was to calculate improved multicollision neutron fluence-to-dose conversion factors by solving the combined neutron and gamma-ray transport problems in phantom models designed to represent human beings. Also, new neutron fluence-to-kerma factors and improved secondary gamma-ray yields were to be determined for the elements composing the slabs.

The neutron and gamma-ray cross-section data used in the calculation came primarily from ENDF/B and the OGRE Library respectively.

The computer code ANISN was employed in solution of the transport equation.

The neutron fluence-to-kerma factors calculated herein agree very well with previous work. The results are presented for the eleven most common elements in the standard man.

Multicollision neutron fluence-to-dose conversion factors were calculated for neutron sources, either beams or isotropic fluxes of energies from 15 MeV to thermal incident on a 30-cm slab with infinite or finite transverse dimensions. The curves representing the total of the neutron and gamma-ray energy deposition were found to range from approximately 6% to a factor of 2 lower than those previously reported. This effect is attributed primarily to the treatment of secondary gamma rays and becomes more pronounced with increasing depth. Results are presented for 38 different combinations of source and geometry and for the maximums as a function of the source energy for each set of calculations.

References

¹ Research partially funded by the Defense Atomic Support Agency under Subtask No. PE074-01.

² Abstract of ORNL-TM-2991 (May 22, 1970) and of a thesis presented to the University of Tennessee by J. J. Ritts in partial fulfillment of the requirements for the Degree of Master of Science.

³ Present address: Westinghouse Advanced Reactor Division, Waltz Mill Site, Madison, Pa. 15663.

⁴ University of Tennessee, Knoxville.

2.51 DIFFERENTIAL NEUTRON AND SECONDARY GAMMA-RAY ALBEDOS FOR STEEL-COVERED CONCRETE SLABS: VOLS. I-VI^{1,2}

M. B. Wells³ J. D. Marshall³

Calculations were performed with the two-dimensional S_n procedure DOT to determine the distribution in energy and angle of the neutrons and secondary gamma rays reflected from steel-covered concrete slabs for 27 incident neutron energy intervals ranging from 14.918 MeV to 2.53×10^{-8} MeV and for 5 incident directions. The doubly differential neutron current albedo was computed for 30 emergent directions and for each of the 27 energy intervals lying between and including the incident energy interval and 2.53×10^{-8} MeV.

The secondary gamma-ray doubly differential current albedo was computed for the same parameters as those

used to define the neutron albedo, except that 13 energy intervals between 10.0 and 0.01 MeV were used to define the reflected secondary gamma-ray energy distribution.

The neutron and secondary gamma-ray doubly differential current albedos were converted to number albedos, differential current- and flux-dose albedos, and current- and flux-dose albedos. These data are compared with albedo data reported by other investigators for iron slabs and concrete slabs.

References

¹ Research sponsored by the Defense Atomic Support Agency and performed under subcontract 3109 for the Oak Ridge National Laboratory, operated by Union Carbide Corp. under contract with the U.S. Atomic Energy Commission.

² Abstract of RRA-T97-I-VI (July 10, 1969).

³ Radiation Research Associates, Inc., Fort Worth, Tex.

2.52 ANALYSIS OF INITIAL RADIATION PROTECTION ABOARD SHIP^{1,2}

R. L. French³ J. M. Newell³

A system of machine codes has been developed to calculate the protection against initial radiation from nuclear weapons that may be afforded at various positions aboard ship. The codes transform and regroup arbitrary free-field neutron and gamma-ray angle and energy distributions into a fixed set of incident angle and energy groups for each of the major exterior surfaces of the ship. Transmission matrices for iron slabs, which represent the hull, exposed decks, and superstructure of the ship, are then folded with these distributions. The transmitted radiation (including secondary gamma rays produced in the slabs) is treated as a "virtual" source in calculating subsequent penetration to the detector. Attenuation by the ship's internal structure is represented by a modified "mush" model. This model gives the proper mass thickness along the line of sight between individual differential areas of the virtual source and the detector. Uncollided radiation traveling directly from the virtual source to the detector is treated precisely by this approach. Radiation scattered to the detector by materials off the line of sight, including backscatter from material beyond the detector, is approximated by that scattered from the mush. Secondary gamma radiation produced in the interior of the ship is treated in a like manner.

References

¹ Research sponsored by the Defense Atomic Support Agency and performed under subcontract for the Oak Ridge National Laboratory, operated by Union Carbide Corp. under contract with the U.S. Atomic Energy Commission.

² Abstract of RRA-M91 (June 13, 1969) and of *Trans. Am. Nucl. Soc.* 12, (1), 366 (1969).

³ Radiation Research Associates, Inc., Fort Worth, Tex.

2.53 PREDICTION OF NUCLEAR WEAPON NEUTRON RADIATION ENVIRONMENTS^{1,2}

R. L. French³ L. G. Mooney³

Techniques were developed for applying the results of Straker's recent discrete ordinates calculations⁴ of neutron transport in an air-over-ground geometry to predict the neutron radiation environment produced by the detonation of nuclear weapons. Straker's results include the spatial, energy, and angle distributions of neutrons at the air-ground interface from source neutrons in each of nine source energy bands emitted from a point isotropic source 50 ft above the ground. The source energy bands cover the range from 0.0033–0.111 to 12.2–15.0 MeV. The energy spectrum of the leakage neutrons from a particular weapon may be integrated over corresponding energy bands to obtain source intensities which are then multiplied by the transport data for corresponding bands and summed over source energy. The results thus obtained are for Straker's original air density of 1.1×10^{-3} g/cm³, but they may be scaled to other air densities by use of mass equivalent ranges. A satisfactory adjustment to source heights other than the 50-ft height used in the original calculations may be made with the "first-last collision method" if the source-detector separation is as much as two or three mean free paths (~1000 ft). When folded with leakage spectra for numerous test devices and adjusted to the proper air density and burst height, Straker's data give neutron dose spatial distributions generally within 25% of those measured in field tests.

References

¹ Research sponsored by the Defense Atomic Support Agency and performed under subcontract for the Oak Ridge National Laboratory, operated by Union Carbide Corp. under contract with the U.S. Atomic Energy Commission.

² Abstract of RRA-M92 (Nov. 26, 1969) and of *Trans. Am. Nucl. Soc.* 12 (2), 954 (1969).

³ Radiation Research Associates, Inc., Fort Worth, Tex.

⁴ E. A. Straker, *Time-Dependent Neutron and Secondary Gamma-Ray Transport in an Air-Ground Geometry. Vol. II. Tabulated Data*, ORNL-4289, vol. II (September 1968).

2.54 CALCULATIONS OF WEAPON RADIATION DOSES IN SINGLE-COMPARTMENT ABOVE-GROUND CONCRETE STRUCTURES^{1,2}

L. G. Mooney³

Calculations were performed to determine energy and angle distributions of the fission-product gamma-ray, air-ground secondary gamma-ray, and neutron fluences incident on structures resulting from the detonation of a representative intermediate-yield thermonuclear weapon 100 m above the ground. These energy and angle distributions were used as input data to the ANISN discrete ordinates code to calculate the penetration of the radiation through various thicknesses of type O-HW1 concrete. The production and transport of concrete capture gamma rays were calculated in tandem with the neutron transport. The penetration results were used to calculate the various radiation components at the center of a simple concrete blockhouse. The inside lengths and widths of the structure varied from 10 to 50 ft, and the inside height was fixed at 10 ft. Wall and roof thicknesses varied from 6 to 60 in. The results of the calculations were expressed as structure protection coefficients (dose at the receiver per unit free-field dose). The neutron dose was found to contribute the highest fraction of the total dose for wall and roof thicknesses up to 12 in. For thicknesses of 18 in. and more, the air-ground secondary gamma rays and concrete capture gamma rays were found to dominate, becoming increasingly more important with increasing thickness. The relative magnitude of each component did not vary significantly with structure size; however, all components were found to decrease with an increase in structure size for a given wall and roof thickness.

References

¹ Research sponsored by the Defense Atomic Support Agency and performed under subcontract for the Oak Ridge National Laboratory, operated by Union Carbide Corp. under contract with U.S. Atomic Energy Commission.

² Abstract of RRA-M93 (Nov. 26, 1969) and of *Trans. Am. Nucl. Soc.* 12 (2), 962 (1969).

³ Radiation Research Associates, Inc., Fort Worth, Tex.

2.55 ANALYSIS OF INITIAL RADIATION PROTECTION ABOARD THE CVA-66^{1,2}

R. L. French³ J. M. Newell³
L. G. Mooney³ N. M. Schaeffer³

The ship shielding codes were applied to an analysis of the CVA-66. This system of machine codes was developed to calculate the protection against initial radiation from nuclear weapons at various positions aboard ship. The codes transformed and regrouped representative free-field neutron and gamma-ray angle and energy distributions into a fixed set of incident angle and energy groups for each of the major exterior surfaces of the ship. Transmission matrices for iron slabs, which represent the hull, exposed decks, and superstructure of the ship, were then folded with these distributions. The transmitted radiation (including secondary gamma rays produced in the slabs) was treated as a "virtual" source in calculating subsequent penetration to several detector positions. Attenuation by the ship's internal structure was represented by a modified "mush" model.

Neutron and gamma-ray attenuations for representative positions below deck are given, as well as dose by radiation component for a range of weapon yields and overpressures.

References

¹ Work sponsored by the Defense Atomic Support Agency and performed under subcontract 3094 for the Oak Ridge National Laboratory, operated by Union Carbide Corp. under contract with the U.S. Atomic Energy Commission.

² Abstract of RRA-T707 (Apr. 15, 1970); preliminary draft.

³ Radiation Research Associates, Inc., Fort Worth, Tex.

2.56 SYSTEM OF SHIP SHIELDING CODES^{1,2}

J. M. Newell³ R. Kimmell³
R. L. French³ J. K. Warkentin³

A system of three machine codes has been developed to calculate the protection against initial radiation from nuclear weapons that may be afforded aboard ship. The codes were written in FORTRAN and are operational

on the IBM 360 model 75 and 91 computer systems at ORNL. One of the codes, called the Source Code, regroups and transforms arbitrary input free-field neutron and gamma-ray energy and angle distributions into a fixed set of incident energy and angle groups. The code then folds the incident distributions with energy- and angle-dependent transmission matrices for iron slabs of several thicknesses. The transmitted radiation (including secondary gamma rays produced in the slabs) is recorded on tape and is treated as a "virtual source" in calculating subsequent penetration to the detector. The Geometry Code, which is applied independently of the Source Code, analyzes an array of rectangular compartments which approximates the structure of the ship in the same manner used in the Ship Vulnerability Model. All outer surfaces of the ship are identified and divided into differential areas. The code then traces a line of sight from each dA to the detector and records on tape the cumulative thickness of iron along the line of sight between the dA and the detector. The Integration Code accepts the Source and Geometry Code output tapes, interpolates the Source Code output to obtain the radiation transmitted through each dA , then applies a modified mush model to obtain the attenuation along individual lines of sight. The modified mush model approximates radiation scattered to the detector by material off the line of sight and includes secondary gamma rays produced in the ship's interior.

References

¹Work sponsored by the Defense Atomic Support Agency and performed under subcontract 3094 for the Oak Ridge National Laboratory, operated by Union Carbide Corp. under contract with the U.S. Atomic Energy Commission.

²Abstract of RRA-T706 (June 30, 1970) (to be published).

³Radiation Research Associates, Inc., Fort Worth, Tex.

2.57 WEAPONS RADIATION SHIELDING HANDBOOK: STATUS REPORT

L. S. Abbott, H. C. Claiborne,
and C. E. Clifford, Editors

The recent publication of Chap. 2 of the *Weapons Radiation Shielding Handbook* (DASA-1892-5) in-

creases the number of published chapters to five. Titled "Basic Concepts of Radiation Shielding Analysis" and authored by P. N. Stevens and H. C. Claiborne, the chapter discusses quantities that are used to describe radiation fields, radiation interactions, and responses to radiation. It also discusses in some detail the processes whereby neutrons and gamma rays are produced, as well as the processes whereby these radiations interact with materials. The chapter is a necessary prerequisite to the understanding of radiation transport calculations by the sophisticated methods described in Chaps. 3-6.

The first shield engineering chapter of the Handbook has also been completed and is awaiting approval by the Defense Atomic Support Agency. To be issued as Chap. 7, it is titled "Engineering Method for Designing Initial Radiation Shields for Blast-Hardened Underground Structures" and is authored by L. G. Mooney, M. B. Wells, and H. C. Claiborne.

The current Handbook effort is centered on revising and enlarging one of the basic chapters, Chap. 3, "Methods for Calculating Neutron and Gamma-Ray Attenuation," and on editing the second engineering chapter, Chap. 8, "Engineering Method for Designing Initial Radiation Shields for Above-Ground Structures." In addition, preparation of a new chapter, which will be issued as Chap. 9 and titled "Methods for Calculating Neutron and Gamma-Ray Dose Rates in Structures," has been begun. Chapter 9 will be based on data currently being generated in the ORNL-DASA program and elsewhere and will be aimed at providing techniques for predicting dose rates in missile silos and other types of shelters. An index of all the published chapters is also under way. The form of the index will be such that it can be easily updated and reissued with each new chapter or chapter revision.

The status of a chapter on an engineering method for designing fallout radiation shelters is at present uncertain. If the chapter is published it will rely heavily on a method already available and will be integrated in the Handbook only so that all aspects of the radiation shielding problems will have been covered. As such, it would probably be published as the tenth and final chapter of the Handbook. The only other remaining chapter is Chap. 1, which is to be an introductory chapter that cannot be prepared until all other chapters of the Handbook become fixed.

3. Radiation Shielding Information Center

3.1 RECENT DEVELOPMENTS IN RSIC OPERATIONS¹

D. K. Trubey Betty F. Maskewitz
R. W. Roussin

The Radiation Shielding Information Center continues to serve the technical community engaged in radiation shielding research and development.² This community represents a wide variety of interests, as indicated by the fact that RSIC is supported by three agencies: the Atomic Energy Commission, the National Aeronautics and Space Administration, and the Defense Atomic Support Agency. The people served by RSIC generally have interests in parallel with or are doing work for one of those agencies.

The Center's operations have continued to develop in the area of data collecting, checkout, and distribution. This activity may be regarded as consisting of three parts: (1) acquisition of differential cross sections in ENDF/B format and data checkout in collaboration with the Brookhaven National Laboratory National Neutron Cross Section Center (NNCSC) and the Cross Section Evaluation Working Group (CSEWG) Shielding Subcommittee, (2) acquisition, packaging, and distribution of fine-group cross sections and other shielding data, and (3) collaboration with the Benchmark Problems Group of the American Nuclear Society Shielding Standards Subcommittee in the acquisition and publishing of shielding benchmark problems. All of these activities are described in more detail below.

3.1.1 Data Libraries

Data libraries on magnetic tape or in other form continue to be packaged, maintained, and distributed in a manner analogous to computer code distribution. Each data set carries a Data Library Collection (DLC) number and is packaged as a unit. The package includes a suitable handling program, which is sent with each DLC data set for editing and/or otherwise manipulating the data, and documentation, which includes an RSIC-prepared abstract. Additions to and revisions of the data libraries are announced in the RSIC Newsletter.

Both cross-section data, especially energy group cross sections, and voluminous results of calculations of radiation environment are typical examples of data in the collection. Maintaining and distributing data libraries separately from the codes which use the data as input has proved to be an efficient mode of operation. Thus a code package does not have to be revised each time new data are available. Also, as data formats become standardized, each library is likely to be used by at least several codes.

A summary of the DLC data sets is given in Table 3.1.1.

A total of 234 separate shipments of these data sets were made in the year's operations.

3.1.2 Code Center Operations

The year completed has witnessed a consolidation and stabilization of the RSIC Code Center functions in implementing the technical institute concept.^{3,4} The integration of the Radiation Shielding Information Center into the many functions and programs of the parent organization, the Neutron Physics Division, can be clearly seen in the computer codes operations. This year has also seen increased cooperation between RSIC and the general shielding community, and feedback into the Center is substantial.⁵

Table 3.1.2 shows the percentage distribution of RSIC Code Center services. Since, to a large extent, the universities and private firms are doing their research and development under contract, with government funds, it is estimated that about 85% of RSIC services are for government-related work. The 15% spinoff reflects the guiding principle of the funding agencies of "permitting and encouraging the dissemination of scientific and technical information so as to provide that free interchange of ideas and criticism which is essential to scientific progress."^{6,7}

A manpower level of about six is devoted to the codes part of RSIC operations.

Statistics compiled over 12 months of RSIC Code Center operations show a 26% increase in the total number of letters of request received and a 35%

Table 3.1.1. Summary of RSIC-DLC Data Sets

Data Library Designation	Contributor	Form	Data Type/Computer Code/Comment
DLC-1/LEP	ORNL-N	16 mm Microfilm Magnetic tape Machine listings	Bertini low-energy intranuclear cascade results. Output from ANALYSIS Codes I and II and from EVAP (ORNL-3433).
DLC-2/99G	ORNL-N	Magnetic tape	99-group, $\leq P_8$ expansion, neutron cross sections for input to ANISN/DOT/DTF-IV/MORSE. Produced from ENDF/B Category I, Version I, data by SUPERTOG (1969). Energy range 14.92 MeV to 0.414 eV.
DLC-4/HPIC	ORNL-N	Magnetic tape	Gamma-ray photoelectric and pair-production data in OGRE format (ORNL-3805). Data same as in DLC-7.
DLC-5/HALLMARK	ORNL-N	Magnetic tape	Output from DOT, O5R-ACTIFK, and OGRE. Straker's time-dependent air-over-ground results for point isotropic sources. Handling routines also combine results for arbitrary source neutron energy spectrum. Sources: Neutron energy range 15 MeV to 3.3 keV. Results include neutron and secondary gamma-ray fluxes (ORNL-4289, vol. II).
DLC-7/HPIC	LRL	Magnetic tape	Livermore gamma-ray interaction data in ENDF/B format. Elements $Z = 1-83, 86, 90, 92, 94$. Energy range: 1 keV to 100 MeV (UCRL-50400, vol. VI; UCRL-50174 Sect. II, May 1969).
DLC-8A/BP-3	ORNL-N	Cards	22-group, P_5 expansion, cross sections for air in the ANISN/DOT/MORSE format. Data used by Straker for Benchmark Problem No. 3, neutron spectrum from point sources in infinite air (ORNL-RSIC-25). Energy range: 15 MeV to thermal.
DLC-9/FARS	ORNL-N, CTC	Magnetic tape	104-group neutron, 18-group gamma-ray, P_8 expansion, coupled cross sections for H, C, N, O, Mg, Al, Si, Ca, and Fe. Data format for ANISN/DOT/DTF-IV/MORSE. Compiled by F. Schmidt for concrete calculations (ORNL-RSIC-26). Energy range: neutron, 15 MeV to thermal; gamma ray, 10--0.02 MeV.
DLC-10/AVKER	ORNL-N	Magnetic tape	Data library of neutron fluence-to-kerma factors for many elements. The retrieval program will compute energy group values for any composition for use with group fluence to calculate dose or heating (ORNL-TM-2558). Energy range: 19.2 MeV to 0.023 eV.
DLC-11/RITTS	ORNL-R, ORNL-N, CTC	Magnetic tape	100-group neutron, 21-group gamma-ray, P_3 expansion, coupled cross sections for H, C, O, N, Na, Mg, P, S, Cl, K, and Ca. The 100-group neutron set is also provided. Also, 121 group coupled, P_3 , macroscopic data for standard man, skin, bone, tissue, brain, lung, red marrow, and muscle. Data format ANISN/DOT/MORSE. Energy range: neutron, 15 MeV to thermal; gamma-ray, 14 to 0.01 MeV (ORNL-TM-2991).
DLC-12/POPLIB	CTC, ORNL-N	Magnetic tape	A compendium of neutron-induced secondary gamma-ray yield and production cross-section data. Data library for PSR-11/POPOP4 code. Original library has 139 data sets (CTC-INF-1004).
DLC-13/GARLIB	LRC	Magnetic tape	32-group resonance region neutron capture and scattering cross sections for moderated tungsten and uranium slabs. Produced by the GAROL code. Group fluxes calculated by GAROL are also included for further collapsing of the group structure. Energy range: 1.234 keV to 0.414 eV (NASA TM X-1909).

Library contributors:

CTC	Computing Technology Center, Union Carbide Corp., Oak Ridge, Tenn.
NASA-LE	NASA Lewis Research Center, Cleveland, O.
ORNL-N	Oak Ridge National Laboratory, Neutron Physics Div., Oak Ridge, Tenn.
ORNL-R	Oak Ridge National Laboratory, Reactor Div., Oak Ridge, Tenn.
LRL	Lawrence Radiation Laboratory, Livermore, Calif.

Table 3.1.2. Percentage Distribution of RSIC Code Center Services

Organization	Percent
USAEC ^a	27.5
DASA ^a	20.9
NASA ^a	18.5
Other Govt.	0.8
Universities	11.0
Private firms	10.1
Foreign	11.2

^aAgencies or their contractors.

increase in the number of codes packaged over that of the previous year. Other statistics are as follows:

Improvements Made to the Computer Code Collection:

1. 34 additional codes were packaged.
2. 24 code packages in the collection were updated, several of which included major modifications and extensions to the program.
3. 11 new hardware versions of existing code packages were fed back into RSIC by installations where conversions were made.
4. 10 data library sets were collected and packaged; improvements were made to the documentation in each of the data sets.

Services to the Shielding Community by the Code Center:

1. 1200 letters of request were logged into the Center — over 100/month, resulting in more than 2900 separate actions required to satisfy the requests.
2. 628 separate code packages were shipped, including full documentation.
3. 113 abstracts of code packages or computer lists of programs were mailed.
4. 37 requests for updated material were filled.
5. 317 requests were handled in which staff members spent considerable time in trouble-shooting specific codes as a requester was learning how to use the codes, including advice concerning his input preparation.
6. 192 requests were handled in which time was spent in assisting the requester to solve his problems — general advice and counsel.
7. 182 requests were handled in which assistance was given in the selection of the computer code to

fit the requester's problem, his computer, and his capabilities.

8. 307 separate miscellaneous service requests were filled.

The work of the RSIC Code Center got under way in mid-1963 with only a few shielding codes, written in assembly language for the IBM 704. Annual growth may be seen in Fig. 3.1.1 and in Table 3.1.3, which show the number of requests filled in each category per working day, averaged over each year.

Currently (June 1970), 142 shielding code package numbers have been assigned. A survey shows that users have added to the existing packages new and different versions, bringing the count of distinct code packages to 216. The 22 peripheral shielding code packages available at the beginning of the year have been increased by 5 additional versions.

Abstracts of computer code packages were written and published as additions to ORNL-RSIC-13.⁸ As codes are packaged, additional abstracts will be issued.

Literature describing computer codes is reviewed as a routine RSIC function. The literature of interest is indexed, and an abstract is written. Currently, information has been retained for 1215 separate documents written to describe computer codes.

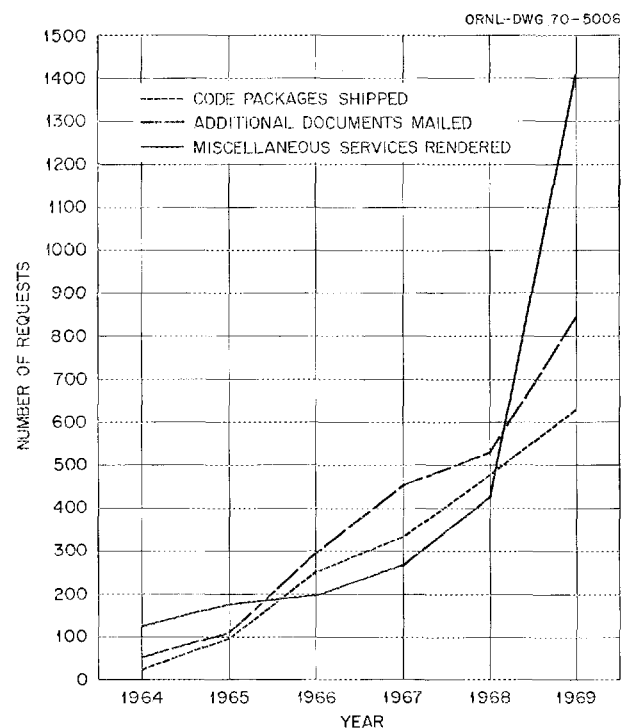


Fig. 3.1.1. Chart, by Year, of Number of Requests Filled by RSIC Code Center, 1964-1969.

Table 3.1.3. Annual Growth of RSIC Code Center Services

Average Number of Requests per Workday	Year					
	1964	1965	1966	1967	1968	1969
Code packages shipped	0.08	0.20	0.38	0.96	1.26	2.5
Answers to specific inquiries about codes	0.10	0.25	0.42	1.14	1.74	3.3
Miscellaneous services performed in connection with shielding calculations	0.49	0.55	0.70	0.74	1.03	4.8
Sum of requests handled on an average day	0.67	1.0	1.5	2.84	4.03	10.6

3.1.3 RSIC Foreign Visits

In implementation of the USAEC-ENEA (OECD) Exchange Agreement, an RSIC staff member spent three weeks in 1969 at Ispra (Varese), Italy, conferring with the European Nuclear Energy Agency Computer Programme Library (ENEA CPL) staff and with visiting members of the European shielding community. New sources of shielding information were discovered, impetus was given to the flow of European shielding literature into RSIC, and several new computer codes were placed in the RSIC collection. Firsthand study of procedures at the ENEA CPL was of value in connection with the work involved with the RSIC codes depository.

A visit to the European Organization for Nuclear Research (CERN) computer Codes Library cemented the tentative efforts in effect to cooperate in information exchange. RSIC has been placed on direct distribution of information about codes placed in the CERN library, and requests for computer codes of interest to the U.S. shielding community will be honored.

Travel in the USSR was undertaken to make contact with Soviet shielding scientists to investigate the possibility of information exchange. Visits were made to the Joint Institute for Nuclear Research (JINR), Dubna, Moscow Region, and to the Physics and Power Engineering Institute (PPEI), Obninsk, Kaluga Region. There was evidence of considerable shielding research and development at PPEI and interest shown in a cooperative sharing of information. Several books and technical reports of interest to the shielding community have been sent to RSIC as a result of the visit.

3.1.4 Cooperative Efforts

In furtherance of the effective use of computers in the nuclear industry, an RSIC staff member served as general chairman of the biennial topical meeting of the

Mathematics and Computation Division of the American Nuclear Society (ANS) in 1969 and published the proceedings.⁹ RSIC is also represented on Subcommittee 10 of the ANS Standards Committee, charged with promoting standards and guidelines¹⁰ in documentation and programming to facilitate exchange of computer codes.

3.1.5 Shielding Subcommittee, Cross-Section Evaluation Working Group (CSEWG)

RSIC works in close collaboration with the National Neutron Cross Section Center (NNCSC) at Brookhaven National Laboratory and the Shielding Subcommittee of the Cross Section Evaluation Working Group (CSEWG). D. K. Trubey of the RSIC staff is chairman of the subcommittee. The Center's role in this activity is to assist in the acquisition, checkout, and review of "shielding" cross sections in ENDF/B format which will ultimately be placed in the ENDF/B file. In this context, "shielding" cross sections are evaluations performed in the shielding community which are likely to have an emphasis on gamma-ray production cross sections, gamma-ray interaction cross sections, and neutron cross sections in the energy range of interest for shielding with detailed energy and angular distribution resolution.

In order to organize the acquisition, computerized checking, and Phase I testing¹¹ of shielding data on hand and expected in FY 1971, a multilaboratory task force within the Shielding Subcommittee was appointed (Task Force 1) with D. J. Dudziak, Los Alamos Scientific Laboratory, as chairman. The task force met at Los Alamos May 12-13, and a number of actions were taken, including the following:

1. the photon interaction data for elements $Z = 1-83$, 86, 90, 92, and 94, energy 1 keV to 100 MeV, available at RSIC as DLC-7C (Table 3.1.1) are

considered to have passed Phase I review and should be made available as part of ENDF/B Version II.

2. RSIC will extend the NNCSC codes CHECKER and PLOTFB to be able to check and plot gamma-ray production data (files 12--16) in the new format.
3. RSIC will receive new data, run CHECKER, and otherwise check and, in some cases, revise data before forwarding to NNCSC.
4. NNCSC will prepare packets for individuals to perform Phase I reviews of the data. The packets will include review forms, graphics, listings, output from CHECKER, and physics-checking codes. The data will be available as part of the ENDF/A file until accepted for ENDF/B.

Task Force 2, R. E. Maerker of Neutron Physics Division, Chairman, has also been initiated to plan and implement Phase II testing which involves the comparison of transport calculational results based on the data with integral measurements.

In connection with the ENDF data handling, RSIC participates in the ORNL CSEWG work and the central ORNL data library management in cooperation with several other groups.

As a means of acquiring evaluated data in the UKAEA Nuclear Data Library, the computer code UKE (PSR-15) was developed to translate data in UK format to ENDF/B format.

3.1.6 Seminar-Workshops on Group Cross-Section Preparation and Two-Dimensional Discrete Ordinates Calculations

A dual-topic seminar-workshop was held at Oak Ridge Sept. 30--Oct. 3 under sponsorship of Neutron Physics and Reactor Divisions. The topics were: (1) two-dimensional discrete ordinates calculations, with special emphasis on the DOT-II code (CCC-89), and (2) multigroup cross-section preparation -- theory, techniques, and computer codes.

There were 124 participants (88 from outside Oak Ridge) from 57 separate organizations. There were eight papers on discrete ordinates calculations and 24 papers on multigroup cross-section preparation and application. Half-day workshops were held to teach input preparation for DOT-II and XSDRN and an informal question-answer session followed.

The proceedings were issued as ORNL-RSIC-27 (see below).

3.1.7 RSIC Newsletter

As of May 31 the newsletter was being sent to 1100 subscribers, most of whom are individual shielding

specialists. This number is about the same as last year, with additions replacing withdrawals. The subscribers were required to indicate that they wished to continue, and many revisions of the list resulted from this.

Several issues of the newsletter have been used to transmit and publicize recently available basic data of great interest. These were *thermal-neutron capture and fission gamma-ray spectra*. Other uses of the newsletter have been to publicize conferences and short courses of interest, to announce computer codes and data libraries newly available from RSIC, to announce changes in codes or data, to outline RSIC policies, to announce personnel changes of address, and to publish the RSIC literature accessions.

3.1.8 General Information Services

The Center provides a variety of information services, such as personal conferences regarding shielding problems, computer searches of bibliographic material, computer-produced abstracts, microfiche copies of difficult-to-obtain reports, and inquiries regarding RSIC services or reports. During the year ending May 31, 1034 requests were processed in addition to those requests connected with computer codes.

The reprogramming of the computerized information retrieval system was essentially completed, and the new system was placed in operation on the IBM 360 computer at the Union Carbide Corp. Computing Technology Center. Taking advantage of modern hardware and software, the new system is faster, more powerful, and easier to operate. The speed results principally from the use of the large fast-memory, disk, and data cell storage compared with the use of multiple tapes with the previous system on the IBM 7090. The increase in power is manifested in the flexible Boolean logic available in search and sorting and in the availability of a multiple citation search capability. The ease of operation is due to the system's correction routines and the single data file format.

The program is now being extended to use magnetic tape typewriter input which will largely eliminate the use of punched cards as the primary data input.

References

¹Work partially supported by National Aeronautics and Space Administration under NASA Order W-12792 and by Defense Atomic Support Agency under DASA Task No. PE055.

²D. K. Trubey, "The Radiation Shielding Information Center -- A Technical Information Service for Nuclear Engineers," *Nucl. Eng. Des.* 9, 392--407 (1969).

³*Proceedings of the Forum of Federally Supported Information Analysis Centers*, Nov. 7–8, 1967, PF 177051.

⁴*Science, Government and Information*, a report of the President's Science Advisory Committee, The White House, Jan. 10, 1963.

⁵B. F. Maskewitz, D. K. Trubey, H. E. Comolander, H. R. Hendrickson, I. J. Brown, R. W. Roussin, V. A. Jacobs, C. M. Anthony, J. Gurney, M. W. Landay, and A. B. Gustin, *The Information Analysis Center Concept as Developed by the Radiation Shielding Information Center*, ORNL-TM-2973 (Apr. 28, 1970).

⁶United States Atomic Energy Act of 1954.

⁷National Aeronautics and Space Act of 1958.

⁸Betty F. Maskewitz, *Abstracts of Digital Computer Code Packages Assembled by the Radiation Shielding Information Center*, ORNL-RSIC-13 (revised 1969).

⁹Betty F. Maskewitz, R. Ehrlich (KAPL), and D. R. Vondy (ORNL Reactor Division), *Proc. Conf. on the Effective Use of Computers in the Nuclear Industry*, Knoxville, Tenn., Apr. 21–23, 1969, CONF-690401 (1969).

¹⁰*A Code of Good Practices for the Documentation of Digital Computer Programs*, Standard ANS-STD.2-1967, Subcommittee 10, American Nuclear Society Standards Committee (December 1967).

¹¹Phase I testing is the computerized and manual checking for obvious errors of data as it exists on tape.

3.2 THE RADIATION SHIELDING INFORMATION CENTER – A TECHNICAL INFORMATION SERVICE FOR NUCLEAR ENGINEERS¹

D. K. Trubey

The Radiation Shielding Information Center (RSIC) at Oak Ridge National Laboratory is a technical institute serving the international scientific community. It serves those engaged in research and development for the design of shields that provide protection from biological and physical damage due to penetrating, ionizing radiation.

The Center is sponsored by the United States Atomic Energy Commission (USAEC) under contract with the Union Carbide Corp. and is also supported by the National Aeronautics and Space Administration (NASA) and the Defense Atomic Support Agency (DASA). In serving the interests of these agencies, RSIC is concerned with the shielding of radiation from nuclear reactors, nuclear weapons, radioisotopes, accelerators, and radiation present in space.

Reference

¹Abstract of *Nucl. Eng. Design* **9**, 392–95 (1969).

3.3 COMPUTER CODES FOR SHIELDING CALCULATIONS – 1969^{1,2}

D. K. Trubey Betty F. Maskewitz

An extensive library of computer codes useful for radiation transport or shielding calculations is available from the Radiation Shielding Information Center at Oak Ridge National Laboratory. In addition to the point kernel, Monte Carlo, and discrete ordinates codes used for neutron and gamma-ray transport calculations, the collection includes cross-section libraries and codes for processing cross sections, calculating fission product inventories, proton penetration of spacecraft, and electron-photon transport, and analyzing neutron activation detector data to determine spectra. A list of the most current codes is given, and essential information for each is included.

References

¹Abstract of *Nucl. Eng. Design* **10**, 505–17 (1969).

²Work partially funded by the National Aeronautics and Space Administration and the Defense Atomic Support Agency.

3.4 THE INFORMATION ANALYSIS CENTER CONCEPT AS DEVELOPED BY THE RADIATION SHIELDING INFORMATION CENTER IN ITS COMPUTER CODES ACTIVITIES^{1,2}

B. F. Maskewitz	R. W. Roussin
D. K. Trubey	V. A. Jacobs
H. E. Comolander	C. M. Anthony
H. R. Hendrickson	J. Gurney
I. J. Brown	M. W. Landay

A. B. Gustin

In implementing the information analysis center concept of acquiring, analyzing, and synthesizing a body of information, the Radiation Shielding Information Center (RSIC) packages and distributes computer codes. These codes, used for calculating radiation transport, solving related problems, or processing needed data, are used by scientists and engineers in research or shield design work for government and industry. A description is given of the objectives, scope, recent accomplishments, and auxiliary activities of the RSIC Computer Codes Center. A brief summary of the available codes is also given (see Table 3.4.1).

Table 3.4.1. Computer Code Packages Available from RSIC

CCC No./ Code Name	Contributor ^a	Computer ^b	Radiation Type	Method	Geometry	Ref. ^c	Comments
CCC-116/TRECO	NASA-G	(A) IBM 360/75 (B) CDC 6600	p,e	Numerical integr.	3-dimens.	1,2	Integrates earth radiation belt flux along satellite orbits.
CCC-117/BETA	ART	IBM 7090	e,Brems.	Monte Carlo	Complex	3	Uses importance sampling throughout.
CCC-118/SIGMA	MD-A	IBM 7090	p,e	Kernel integr.	Complex	4	Computes space radiation dose inside space vehicle; uses CCC-70/CHARGE data.
CCC-119/ELBA	NASA-MSFC	IBM 7090	e,Brems.	dE/dx	Slab	5	Computes electron and Bremsstrahlung dose behind aluminum slab.
CCC-120/ SPACETRAN	ORNL-N	IBM 360/75	n, γ	Numerical integr.	3-dimens.	6	Computes dose at detector points due to leakage from cylindrical surface.
CCC-121/SABINE	EURATOM	IBM 360/75	n,sec- γ	Spinney	1-dimens.	7	Particular attention paid to energy transfer in removal source.
CCC-122/RAD 2	GGA	IBM 7090	fp	Numerical		8	Computes fission product activity distributions, decay chain any length. Designed for gas-cooled reactor problems.
CCC-123/XSDRN	CTC,ORNL-N	IBM 360/75	n	Discrete ordinates	1-dimens.	9	Designed to flux-weight cross sections; has extensive data library.
CCC-124/KDLIBE	GE-N	GE 635	n, γ	Kernel integr., Spinney	Complex	10-12	Incorporates CCC-48/QAD, NRN-like code, and others into system.
CCC-125/RSAC	PPC	IBM 7044	γ	Kernel integr.	Infinite cloud	13	Computes dose from release of fission products to atmosphere.
CCC-126/ASOP	CTC	IBM 360/75	n, γ	Discrete ordinates	1-dimens.	14	Designed to optimize shields using CCC-82/ANISN.
CCC-127/MORSE	ORNL-N	(A) CDC 1604 (B) IBM 360/75	n, γ	Multigroup Monte Carlo	Complex	15	Uses same cross-section format CCC-82/ANISN.
CCC-128/06R	ORNL-N	(A) CDC 1604 (B) IBM 360/75	n	Monte Carlo	Complex	16-18	Revised version of CCC-17/OSR.
CCC-129/ TWO TRAN	GGA,LASL	(A) CDC 6600 (B) IBM 360/75	n, γ	Discrete ordinates	2-dimens.	19,20	Coarse-mesh and Chebyshev convergence accelerations, general anisotropic scattering, positive spatial difference scheme.
CCC-130/DIF665	SL	CDC 6600	x, γ	Discrete ordinates	1-dimens.	21	Special version of CCC-42/DIF-IV for x-ray transport.

^aCode contributors: ART, ART Research Corp., Los Angeles, Calif.; CTC, Computing Technology Center, Union Carbide Corp., Oak Ridge, Tenn.; EURATOM, EURATOM Joint Nuclear Research Center, Ispra (Varese), Italy; GE-N, General Electric Co., Nuclear Systems Programs, Cincinnati, O.; GGA, Gulf General Atomic, San Diego, Calif.; LASL, Los Alamos Scientific Lab., Los Alamos, N.M.; MD-A, McDonnell Douglas Astronautics Co., Western Div., Huntington Beach, Calif.; NASA-G, NASA Goddard Space Flight Center, Greenbelt, Md.; NASA-MSFC, NASA Geo. C. Marshall Space Flight Center, Huntsville, Ala.; ORNL-N, Oak Ridge National Lab., Neutron Physics Div., Oak Ridge, Tenn.; PPC, Phillips Petroleum Co., Atomic Energy Div., Idaho Falls, Idaho; and SL, Sandia Laboratories, Albuquerque, N.M.

^bComputer for which versions are available.

^cReferences: (1) NASA SP-3024 (1966), (2) NSSDC 68-02 (1968), (3) AFWL-FR-68-111 (1968), (4) DAC-60878 (1967), (5) NASA SP-169, p. 529 (1968), (6) ORNL-TM-2592 (1969), (7) EUR 3636.e (1967) and Addendum (1969), (8) GAMD-6519 (1965), (9) ORNL-TM-2500 (1969), (10) GESP-226 (1969), (11) GEMP-456 (1966), (12) GEMP-599 (1968), (13) IDO-17151 (1966), (14) CTC-INF-941 (1969), (15) ORNL-CF 70-2-31 (1970), (16) ORNL-CF 69-8-36 (1969), (17) ORNL-3622 (1965), (18) ORNL-3856 (1966), (19) GA-8747 (1968), (20) LA-4058 (1969), and (21) SC-RR-69-739 (1969).

References

¹Work partially funded by the National Aeronautics and Space Administration and by the Defense Atomic Support Agency.

²Abstract of ORNL-TM-2973 (Apr. 28, 1970); paper presented at Semiannual USAEC Computer Conference, Washington, D.C., Apr. 30–May 1, 1970.

3.5 THE 1969 RSIC COMPUTER-BASED INFORMATION RETRIEVAL SYSTEM IN BRIEF^{1,2}

J. G. Jones³ D. K. Trubey
J. Gurney

The computer-based information retrieval system used by the Radiation Shielding Information Center (RSIC) since 1963 has been reprogrammed to take

advantage of modern computer hardware and software. The logic of the new system is similar to the old one but has additional retrieval power and flexibility. The new system is much easier to maintain, update, and operate.

A brief description of the system is given to aid those using it and to inform those who might use it for their own information files (see Fig. 3.5.1). A detailed system description will be published by the Computing Technology Center, Union Carbide Corp.

References

¹Work partially funded by the Defense Atomic Support Agency under Subtask PE055 and the National Aeronautics and Space Administration under Order W-12792.

²Abstract of ORNL-TM-2719 (Nov. 14, 1969).

ORNL-DWG 70-9944

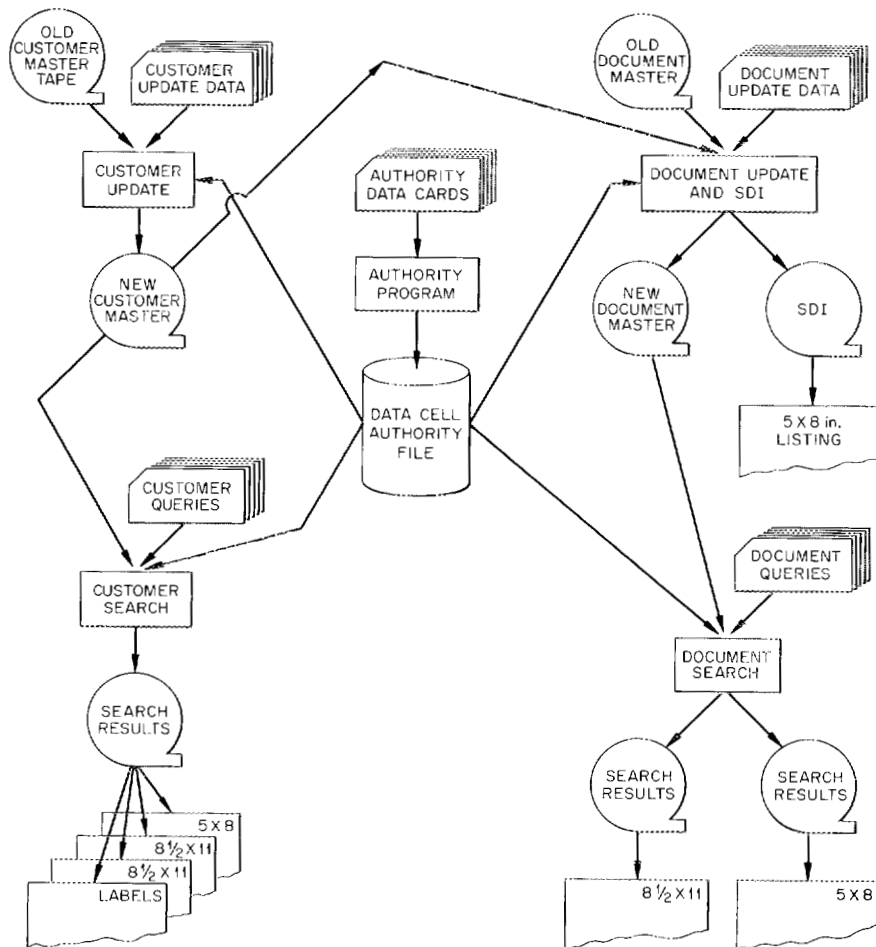


Fig. 3.5.1. RSIC Information Retrieval System Schematic.

³Computing Technology Center, Union Carbide Corp., Oak Ridge, Tenn.

3.6 ABSTRACTS OF DIGITAL COMPUTER CODE PACKAGES ASSEMBLED BY THE RADIATION SHIELDING INFORMATION CENTER¹

Betty F. Maskewitz

Volume II of the Abstracts was updated in July 1969. Abstracts for computer code packages CCC-88 through CCC-115 were added.

Reference

¹Work partially funded by the Defense Atomic Support Agency and the National Aeronautics and Space Administration; report issued as ORNL-RSIC-13.

3.7 SHIELDING BENCHMARK PROBLEMS^{1,2}

A. E. Profio, Editor³

The Benchmark Problems Group of the American Nuclear Society Shielding Standards Subcommittee (ANS-6) has selected several benchmark problems for testing computational methods of radiation transport. Problems are described and solution data are presented. It is anticipated that publication of these problems will serve to focus attention so that careful work will produce solutions which are representative of the state of the art. The problems will also serve to specify standard configurations so that meaningful comparisons can be made between different calculational methods and between experimental and calculational results.

Supplement 1 provides an additional solution to a problem issued previously (neutron spectrum in graphite) and presents a new problem (nucleon-meson cascade in iron).

References

¹Work partially funded by the Defense Atomic Support Agency and the National Aeronautics and Space Administration.

²Abstract of ORNL-RSIC-25 (ANS-SD-9) (June 1969), suppl. 1 (1970).

³University of California, Santa Barbara.

3.8 THE ATTENUATION PROPERTIES OF CONCRETE FOR SHIELDING OF NEUTRONS OF ENERGY LESS THAN 15 MeV^{1,2}

F. A. R. Schmidt³

A review of the literature concerning the attenuation properties of concrete for shielding neutrons of energies up to 14 MeV has been made, and calculations of neutron transmission, including the secondary gamma rays, were carried out.

In connection with the literature review, analytical formulas were developed which are based on neutron removal-diffusion theory and gamma-ray buildup fac-

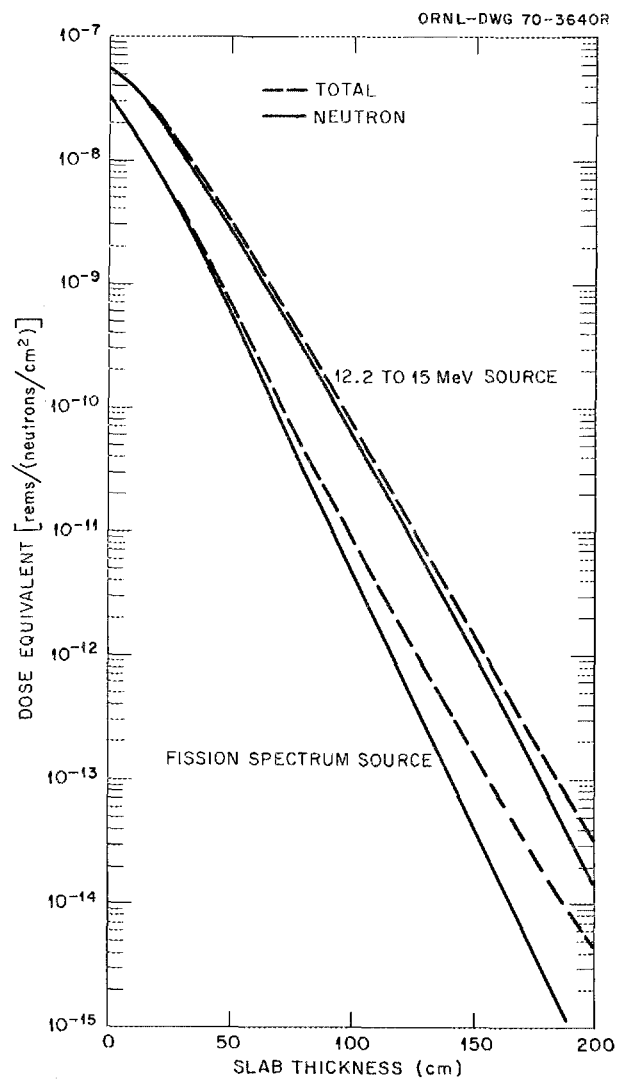


Fig. 3.8.1. Total and Neutron Dose Equivalent (rems) as a Function of Concrete Slab Thickness for 12.2- to 15-MeV and Fission Neutron Sources at Nearly Normal Incidence.

tors. They provide a reasonable tool to compare shielding properties of different concretes.

In view of the unsatisfactory state of available attenuation data, especially the lack of secondary gamma-ray results, calculations were performed by the discrete ordinates method, and results are presented for various slab thicknesses, incident energies, and angles. The results show the great importance of the secondary gamma rays for large thicknesses (see typical curves in Fig. 3.8.1).

In the course of the work extensive cross sections and other data were compiled. The cross-section data are available on computer tape from the Radiation Shielding Information Center. The other data are given in the tables of the report.

References

¹Work partially funded by the Defense Atomic Support Agency under Subtask No. PE055.

²Abstract of ORNL-RSIC-26 (June 1970).

³Present address: Institut für Kernenergetik, Stuttgart, Germany.

3.9 A REVIEW OF MULTIGROUP NUCLEAR CROSS-SECTION PREPARATION – THEORY, TECHNIQUES, AND COMPUTER CODES^{1,2}

D. K. Trubey and Jane Gurney, Compilers

Summaries are presented of papers given at a seminar-workshop titled "Multigroup Cross Section Preparation – Theory, Techniques, and Computer Codes" held at Oak Ridge, Tenn., Oct. 1–3, 1969. The papers, in their review of the state of the art, show that great progress has been made recently in coping with what is the most important problem in radiation transport – cross sections.

The papers describe the large number of computer codes, techniques, and data files now available for cross-section preparation for use in transport codes.

The recently developed codes SUPERTO³, XSDRN,⁴ and DOT-II⁵ have been placed with the Radiation Shielding Information Center for routine dissemination.

References

¹Work partially funded by Defense Atomic Support Agency under Subtask No. PE055.

²Abstract of ORNL-RSIC-27 (January 1970).

³R. Q. Wright, J. L. Lucius, N. M. Greene, and C. W. Craven, Jr., *SUPERTO: A Program to Generate Fine*

Group Constants and P_n Scattering Matrices from ENDF/B, ORNL-TM-2679 (September 1969).

⁴N. M. Greene and C. W. Craven, Jr., *XSDRN: A Discrete Ordinates Spectral Averaging Code*, ORNL-TM-2500 (July 1969).

⁵F. R. Mynatt, F. J. Muckenthaler, and P. N. Stevens, *Development of Two-Dimensional Discrete Ordinates Transport Theory for Radiation Shielding*, CTC-INF-952 (Aug. 11, 1969).

3.10 COMPARISONS OF THE RESULTS OBTAINED WITH SEVERAL ELECTRON-PENETRATION CODES^{1,2}

W. Wayne Scott³

Comparisons of the results obtained for several similar hypothetical problems using electron-penetration codes available from the Radiation Shielding Information Center are presented. These codes are designed to determine the tissue surface dose as a function of shield thickness. Transmitted electron spectra from those codes which provide such spectra are also compared. Significant differences between the results given by the various codes are found. (Typical results are shown in Fig. 3.10.1.)

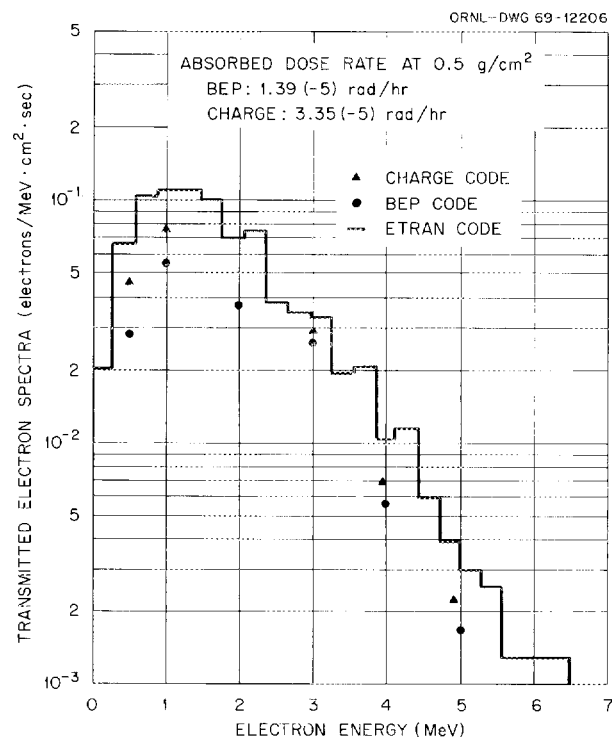


Fig. 3.10.1. Transmitted Electron Spectra Behind a Semi-infinite Slab of Aluminum of Thickness 0.5 g/cm².

References

¹Work funded by the National Aeronautics and Space Administration under Order W-12792(10).

²Abstract of ORNL-RSIC-28 (March 1970).

³Present address: Graduate student at Ohio State University, Columbus.

3.11 KERNEL METHODS FOR RADIATION SHIELDING CALCULATIONS^{1,2}

D. K. Trubey

A review is given of the development and use of kernel methods in solving problems of radiation shield design and radiation transport. Two classes of kernels are identified: empirical and computational. An analysis of the various techniques is made, and examples are given. The relevant computer codes in the collection of the Radiation Shielding Information Center are listed and briefly described.

It is concluded that kernel methods are valuable for quick estimates, hand calculations, checks of transport computer code results, and engineering parameter studies. However, the method can give underestimates for situations which the applied kernel cannot treat properly.

References

¹Work partially funded by the Defense Atomic Support Agency, Subtask No. PE055, and the National Aeronautics and Space Administration, Order W-12792.

²Abstract of paper presented at Special Session on Multidimensional Shielding Calculations, American Nuclear Society Winter Meeting, 1969 [*Trans. Am. Nucl. Soc.* 12(2), 943 (Dec. 1969), and to be published in ANS-SD report and in *Nuclear Engineering and Design*].

3.12 ADJOINT S_N CALCULATIONS OF COUPLED NEUTRON, GAMMA-RAY TRANSPORT THROUGH CONCRETE SLABS^{1,2}

R. W. Roussin F. A. R. Schmidt³

The use of the discrete ordinates computer code ANISN⁴ to obtain solutions to the adjoint Boltzmann equation is discussed. These solutions allow the calculation of transmission factors which give the tissue dose equivalent from particles transmitted through a concrete slab due to an incident source particle in a given energy-angle bin. A coupled set of multigroup (22

neutron, 18 gamma-ray) cross sections allowed the consideration of primary neutron, secondary gamma-ray, and primary gamma-ray transport in a single ANISN calculation. Tables of transmission factors are presented which allow the calculation of dose equivalent transmission through concrete slabs from 15 to 200 cm thick for any arbitrary neutron or gamma-ray source energy and angular distribution. The use of these factors is illustrated, and comparisons are made with other calculations. (A typical example of the results is given in Fig. 3.12.1)

References

¹Work partially funded by the Defense Atomic Support Agency.

²Abstract of paper to be presented at the American Nuclear Society June 1970 meeting; paper also submitted to *Nuclear Engineering and Design*.

³Present address: Institut für Kernenergetik, Universität Stuttgart, Germany.

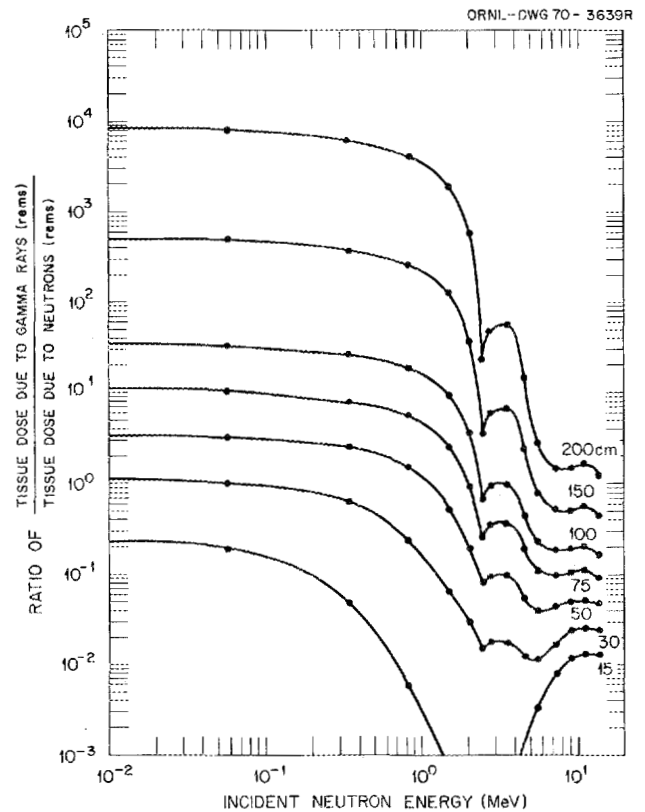


Fig. 3.12.1. Ratio of Tissue Dose Due to Secondary Gamma Rays to Tissue Dose Due to Neutrons as a Function of Incident Neutron Energy for Various Concrete Slab Thicknesses and Nearly Normal Incidence.

⁴W. W. Engle, Jr., *A Users Manual for ANISN – A One-Dimensional Discrete Ordinates Transport Code with Anisotropic Scattering*, K-1693 (March 1967).

3.13 GAMMA-RAY BUILDUP FACTOR COEFFICIENTS FOR CONCRETE AND OTHER MATERIALS^{1,2}

D. K. Trubey

Coefficients for the Berger formula gamma-ray buildup factor are given for ordinary, magnetite, and barytes concrete, air, sand, wood, and lithium hydride. The original data can be reproduced using these coefficients with an error for source energies greater than 2 MeV to generally less than about 5%. Errors for energies 0.5 to 2 MeV may be of the order of 20%. (Typical results are shown in Fig. 3.13.1, in which the data points are from Chilton.³)

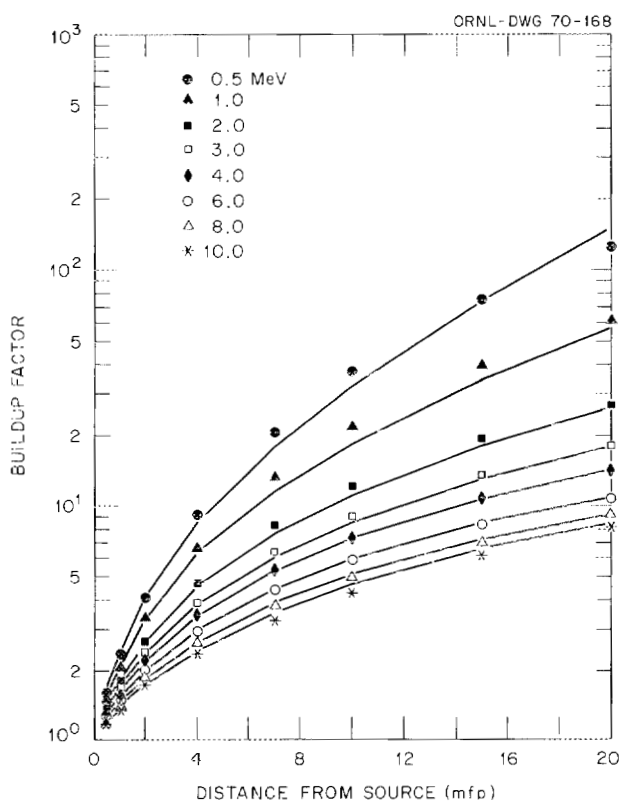


Fig. 3.13.1. Exposure Buildup Factors for Ordinary Concrete. Solid lines, Berger Formula; data points, Chilton.

References

¹Work partially funded by the Defense Atomic Support Agency, Subtask No. PE055.

²Abstract of Technical Note submitted to *Nuclear Applications and Technology*.

³A. B. Chilton, *Nucl. Eng. Design* 6, 205 (1967).

3.14 UKE – A COMPUTER PROGRAM FOR TRANSLATING NEUTRON CROSS-SECTION DATA FROM THE UKAEA NUCLEAR DATA LIBRARY TO THE EVALUATED NUCLEAR DATA FILE FORMAT^{1,2}

R. Q. Wright³ S. N. Cramer³
D. C. Irving⁴

A computer program, UKE, has been written to translate neutron cross sections on computer tape from the United Kingdom Atomic Energy Authority Nuclear Data Library to the Evaluated Nuclear Data File, ENDF/B. The code will translate UK library smooth cross-section data, secondary angular distributions, and secondary energy distributions to the ENDF/B format. No resonance parameters, thermal scattering data, or photon data are considered, however. The secondary angular distributions are translated as differential scattering probabilities only, and no Legendre expansion coefficients are given.

General information is presented concerning the format of the two libraries, along with a detailed description of the translation from the UK secondary energy distribution laws to those of ENDF/B. Programming details and a user's guide are also presented.

References

¹Work partially funded by Defense Atomic Support Agency under Subtask No. PE055.

²Abstract of ORNL-TM-2880 (ENDF-134) (March 1970).

³Computing Technology Center, Union Carbide Corp., Oak Ridge, Tenn.

⁴Present address: Savannah River Laboratory, Aiken, S.C.

3.15 OGRE CROSS-SECTION PACKAGE FOR USING PHOTON INTERACTION DATA IN ENDF/B FORMAT¹

D. K. Trubey J. R. Stockton²

A new version of the OGRE Monte Carlo computer code system for gamma-ray transport³ makes use of

ENDF/B formatted photon interaction data (File 23). These data may be either BCD or binary, and they eliminate the use of the OGRE-format BCD and binary master tapes and the master tape handling program (MASTAPE).

The new subroutines, which replace the original GENSIG routine, are available from the Radiation Shielding Information Center as part of CCC-46E/OGRE, together with current data packaged as DLC-7.

References

¹Abstract of ORNL-TM-2757 (Oct. 27, 1969).

²Present address: Tennecomp, Inc., Oak Ridge, Tenn.

³S. K. Penny, D. K. Trubey, and M. B. Emmett, *OGRE, A Monte Carlo System for Gamma-Ray Transport Studies, Including an Example (OGRE-P1) for Transmission Through Laminated Slabs*, ORNL-3805 (April 1966).

3.16 OGRE MASTAPE -- PHOTON INTERACTION CROSS-SECTION LIBRARY AND DATA HANDLING CODE¹

D. K. Trubey H. E. Francis

The OGRE master cross-section data handling code MASTAPE has been revised to utilize a BCD data tape, as well as card input, to produce a master binary tape for use by the photon transport code OGRE.² The code and library of photoelectric and pair-production cross sections are distributed by the Radiation Shielding Information Center as DLC-4.

References

¹Abstract of ORNL-TM-3046 (formerly ORNL-CF-69-7-60) (July 30, 1969).

²S. K. Penny, D. K. Trubey, and M. B. Emmett, *OGRE, A Monte Carlo System for Gamma-Ray Transport Studies, Including an Example (OGRE-P1) for Transmission Through Laminated Slabs*, ORNL-3805 (April 1966).

3.17 USING ANISN TO REDUCE THE DLC-2 100-GROUP CROSS-SECTION DATA TO A SMALLER NUMBER OF GROUPS¹

R. W. Roussin

The use of several options, available in the discrete ordinates code ANISN,² for collapsing a "many-group"

set is discussed. The many-group set considered in the DLC-2 100-group set generated from ENDF/B cross-section data by the program SUPERTO³.

References

¹Abstract of ORNL-TM-3049 (formerly ORNL-CF-69-5-20) (May 7, 1969).

²W. W. Engle, Jr., *A Users Manual for ANISN -- A One-Dimensional Discrete Ordinates Code with Anisotropic Scattering*, K-1693 (March 1967).

³R. Q. Wright, J. L. Lucius, N. M. Greene, and C. W. Craven, Jr., *SUPERTO: A Program to Generate Fine Group Constants and P_n Scattering Matrices from ENDF/B*, ORNL-TM-2679 (September 1969).

3.18 JRMACRO: A PROGRAM FOR CONVERTING MICROSCOPIC MULTIGROUP, P_n EXPANSION CROSS-SECTION DATA INTO CORRESPONDING MACROSCOPIC DATA FOR MIXTURES OR COMPOUNDS¹

J. J. Ritts² R. W. Roussin
I. J. Brown

JRMACRO is used to read microscopic, multigroup, P_n expansion cross-section data, to "mix" this data to produce macroscopic cross-section data as needed, and to write on computer tape the resulting set in a suitable output format. The cross-section data considered here is of the general type used by particle transport computer codes such as DTF-IV,³ ANISN,⁴ DOT,⁵ and MORSE.⁶

JRMACRO accepts input cross sections by means of cards, tape written in card image format, and unformatted tape (binary), or a combination of the above. Formatted input (cards or card image tape) is first read and stored on a tape or disk before any mixing of cross-section data is performed.

The output cross-section data may be in the form of a card image tape, an unformatted tape, or both.

Sample problems illustrating the use of JRMACRO are discussed.

References

¹Abstract of ORNL-TM-3052 (formerly ORNL-CF-70-3-6) (Mar. 6, 1970).

²Present address: Westinghouse Electric Corp., Waltz Mill Site, Madison, Pa.

³B. G. Carlson, W. J. Worlton, W. Guber, and M. Shapiro, *DTF Users Manual*, UNC-Phys/Math-3321, vol. 1 (Nov. 1963), vol. 2 (May 1964).

⁴W. W. Engle, Jr., *A Users Manual for ANISN – A One-Dimensional Discrete Ordinates Transport Code with Anisotropic Scattering*, K-1693 (March 1967).

⁵F. R. Mynatt, F. J. Muckenthaler, and P. N. Stevens, *Development of Two-Dimensional Discrete Ordinates Transport Theory for Radiation Shielding*, CTC-INF-952 (Aug. 11, 1969).

⁶E. A. Straker, P. N. Stevens, D. C. Irving, and V. R. Cain, *The MORSE Code – A Multigroup Neutron and Gamma-Ray Monte Carlo Transport Code*, ORNL-4585 (formerly ORNL-CF-70-2-31) (Feb. 18, 1970).

3.19 CALCULATED DATA FOR INCLUSION IN THE SPACE SHIELDING HANDBOOK¹

R. T. Santoro F. S. Alsmiller
H. C. Claiborne R. G. Alsmiller, Jr.

Calculations are being carried out to estimate the absorbed dose and dose equivalent inside space vehicles bombarded by solar-flare protons and Van Allen belt protons. The results of the calculations are to be included in a space shielding handbook for use by aerospace engineers.

The calculational model being used at the present time is that of a spherical shell spacecraft having a 30-cm-diam tissue ball at the geometric center to simulate an astronaut. In Fig. 3.19.1 the absorbed dose from primary and secondary particles is shown as a function of depth in the tissue ball when a solar-flare proton spectrum, which is assumed to be exponential in rigidity² ($P_0 = 100$ MV), is incident on a spherical shell spacecraft of aluminum of thickness 35 g/cm^2 . The

incident flare spectra is normalized to 10^9 protons/cm² with energy >30 MeV. The results shown in the figure were obtained from the nucleon-meson transport code NMTC.³ Primary protons are defined to be those protons that do not undergo any nuclear reaction in the shield or in the tissue, and secondary particles are defined to be all particles that arise from nuclear interactions, that is, from protons and neutrons, from positively, negatively, and neutrally charged pions, and from mu-mesons, photons, electrons, and positrons.

Calculations carried out with the nucleon-meson transport code NMTC, such as those shown in Fig. 3.19.1, are very time consuming, and even for the relatively thick shield considered in Fig. 3.19.1, the contribution of the secondary particles to the dose is not large. Therefore a large amount of the shielding data that will be included in the handbook will be obtained by neglecting all secondary-particle production.

Figure 3.19.2 gives the absorbed dose from primary protons only at the center of a spherical shell shield as a function of shield thickness when Van Allen belt proton spectra are incident. The incident spectra used to obtain the results given in Fig. 3.19.2 were generated with the code TRECO⁴ and are characteristic of circular orbits with inclinations of 30, 60, and 90 deg at a height of 240 nautical miles. The results in Fig. 3.19.2 represent the absorbed dose in a point tissue ball at the center of the shield and were obtained using the code that treats primary-proton transport only. Work is in progress to extend this primary-proton transport code to include the tissue ball at the center of the spherical shell shield.

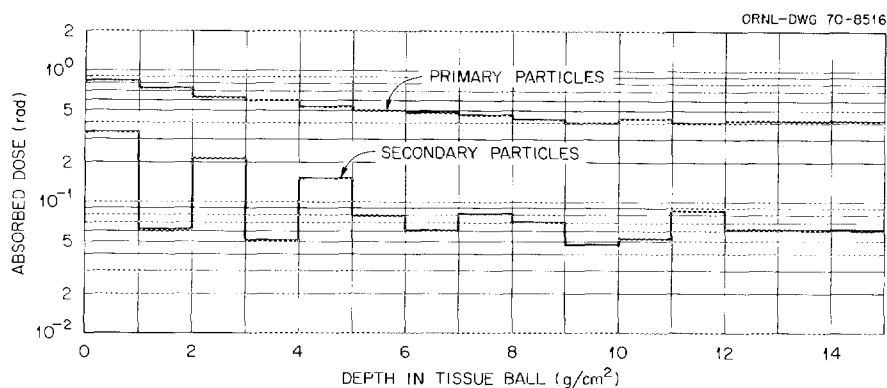


Fig. 3.19.1. The Absorbed Dose from Primary and Secondary Particles When a Solar-Flare Spectrum with Characteristic Rigidity of 100 MV Is Incident on a 35 g/cm^2 -Thick Spherical Shell Shield of Aluminum.

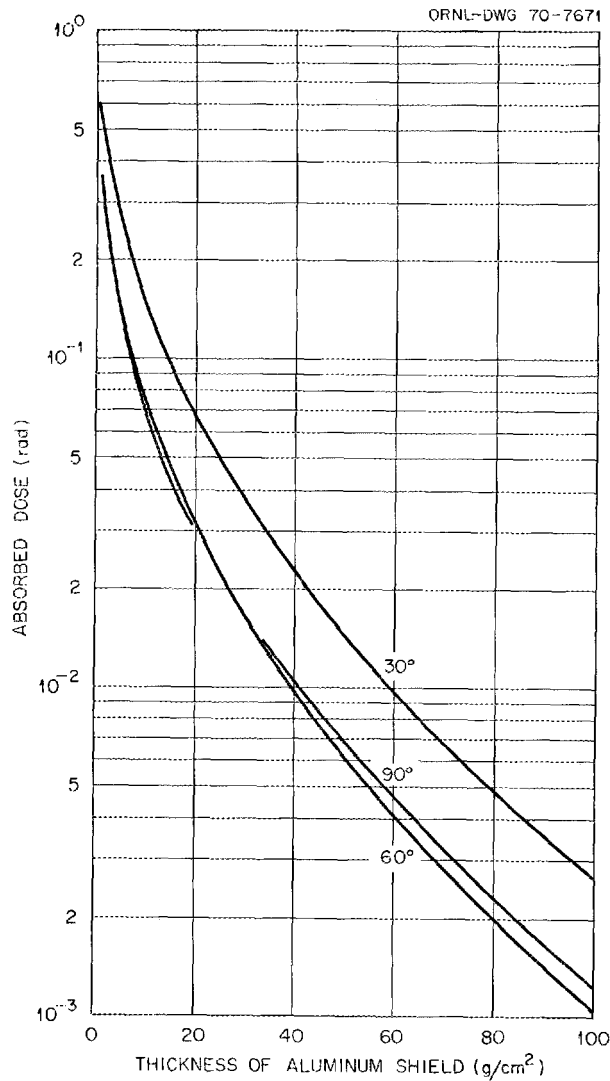


Fig. 3.19.2. The Absorbed Dose as a Function of Aluminum Shield Thickness for Incident Van Allen Belt Proton Spectra at an Altitude of 240 Nautical Miles for Orbit Inclinations of 30, 60, and 90 deg.

References

- ¹Work funded by the National Aeronautics and Space Administration under Order H-38280A.
- ²R. G. Alsmiller, Jr., *Nucl. Sci. Eng.* **27**, 158 (1967).
- ³W. A. Coleman and R. G. Alsmiller, Jr., *Nucl. Sci. Eng.* **34**, 104 (1968); see also W. A. Coleman, *Thermal-Neutron Flux Generation by High-Energy Protons*, ORNL-TM-2206 (July 1968).
- ⁴Data Users' Note, *TRECO and Orbital Integration Computer Program for Trapped Radiation*, NSSDC 68-02, National Space Science Data Center, NASA, Goddard Space Flight Center (January 1968).

4. Theoretical Studies for Medium- and High-Energy Radiation Shielding

4.0 INTRODUCTION

R. G. Alsmiller, Jr.

Theoretical studies of medium- and high-energy radiation transport are pursued on a continuing basis. The main purpose of the program is to provide basic data and to study transport methods that are applicable to the shielding of manned space vehicles and high-energy accelerators, but during the past year a part of the program has also been directed at space physics applications of the transport methods developed. While many of the problems involved in the shielding of manned spacecraft are quite different from those involved in shielding high-energy accelerators, the two disciplines have a sufficient area of overlap that it is efficient for them to be considered under the same general program. An excellent example of the overlap between interests of the National Aeronautics and Space Administration and the U.S. Atomic Energy Commission is provided by the calculations of the radioactive residual nuclei produced in matter by a high-energy nucleon-meson cascade. The ability of the nucleon-meson transport code, developed as part of this program, to predict with some reliability the production of these nuclei has been used extensively in the design of the shielding around the multi-GeV accelerator under construction at the National Accelerator Laboratory and has been used to estimate the radioactive nuclei induced in the moon by solar-flare and cosmic-ray bombardment.

One of the fundamental difficulties in the study of medium- and high-energy nucleon transport has always been the lack of information concerning particle production from nucleon-nucleus and pion-nucleus collisions; therefore a substantial portion of the program is devoted to the calculation of such particle-production cross sections. Because of the very large amount of data required, a reliance on experimental information is not practical, but efforts are continually made to obtain experimental verification of the theoretical cross sections by comparing them with available experimental data. Using these theoretical cross sections, transport

methods are studied, and the best available transport methods are used to provide design data as required by those space and accelerator shielding groups engaged in designing particular shields.

The transport of low-energy (of the order of a few MeV) electrons through matter is important in the shielding of manned space vehicles that are orbited through the Van Allen electron belt. Studies of low-energy electron transport by means of Monte Carlo techniques are available, but because of the poor statistical accuracy which can be obtained, a nonstatistical method of calculation is needed. To fill this need, studies have been undertaken during the past year to adapt the method of discrete ordinates, which has been used extensively in the low-energy neutron shielding program, to the transport of low-energy electrons.

4.1 CALCULATION OF NUCLEAR REACTIONS FOR INCIDENT NUCLEONS AND π -MESONS IN THE ENERGY RANGE 30 TO 2700 MeV^{1,2}

H. W. Bertini

The two-step intranuclear-cascade evaporation approach is used in the calculation of nuclear reactions for incident nucleons and π -mesons in the energy range where the production of π -mesons is important. The model of the target nuclei includes the effects of the diffuse nuclear boundary, the motion of the bound nucleons, and the exclusion principle. The calculated inelastic cross sections, particle multiplicities, energy spectra, angular distributions, and radiochemical cross sections are compared with experiment, and reasonable agreement is found, in general, over broad incident-particle energy ranges and target mass values. Even though the agreement found in the present set of comparisons is very encouraging, additional comparisons must be made to clearly delineate the areas in which the model may or may not reproduce experimental results.

References

¹Work partially funded by the National Aeronautics and Space Administration under Order H-38280A.

²Abstract of invited paper presented at the Second International Conference on Accelerator Dosimetry and Experience, Stanford Linear Accelerator Center, Nov. 3-5, 1969; to be published in the Proceedings.

4.2 RESULTS FROM MEDIUM- AND HIGH-ENERGY INTRANUCLEAR-CASCADE CALCULATION¹

H. W. Bertini M. P. Guthrie

The low-energy intranuclear-cascade calculation² has been extended to medium and high energies, and data from a series of nuclear reactions in these regions will be available shortly. The reactions calculated are incident neutrons and protons at 500, 1000, 1500, 2000, 2500, and 3000 MeV and incident π^+ and π^- mesons at 500, 1000, 1500, 2000, and 2500 MeV on ^{16}O , ^{27}Al , ^{65}Cu , ^{100}Ru , and ^{207}Pb .

The available data include total nonelastic cross sections, radiochemical cross sections, energy spectra, angular distributions, and multiplicities of emitted particles. The data are generated by a consolidated version of the analysis codes described in detail elsewhere³ and have been put on microfiche, which will be distributed by the Radiation Shielding Information Center.

A paper that illustrates comparisons of the results from an earlier version of the code with experimental data involving incident nucleons and emitted cascade nucleons has been published.⁴ It was felt that the deficiencies in the earlier version would not greatly affect those particular reactions. A paper comparing the results from the final version of the code with pertinent experimental data is in preparation. The data to be distributed were generated using the final version.

References

¹Work partially funded by the National Aeronautics and Space Administration under Order H-38280A.

²H. W. Bertini, *Phys. Rev.* **131**, 1801 (1963).

³H. W. Bertini, *Description of Printed Output from Intranuclear Cascade Calculation*, ORNL-3433 (1963).

⁴H. W. Bertini, *Phys. Rev.* **188**, 1711 (1969).

4.3 THE MASKING EFFECT OF MULTIPLE SCATTERING ON THE DETERMINATION OF THE TWO-NUCLEON CORRELATION FROM π^- -ABSORPTION EXPERIMENTS^{1,2}

H. W. Bertini

The absorption reactions of π^- -mesons by complex nuclei have been calculated assuming that the absorptions take place by two-nucleon pairs within the nucleus. The life histories of each nucleon of the absorbing pair and of all particles involved in subsequent collisions within the nucleus are followed using the method of intranuclear cascades. The effects of the exclusion principle, the diffuse nuclear surface, the motion of the bound nucleons, and the nuclear potentials for both pions and nucleons are taken into account in the nuclear model. The results indicate that the ratio of escaping $n-n$ to $n-p$ pairs is considerably different from the ratio of $n-p$ to $p-p$ pairs that initially absorb the π^- . This distortion is introduced by the nucleons that are knocked out when the initial absorbing pair scatters internally and by the nucleons that are knocked out when all the other nucleons involved in subsequent collisions scatter. It is suggested that the ratio of nucleon pairs that absorb the pion can be ascertained accurately if experiments are performed that detect only those nucleons that absorb the pion and escape the nucleus without subsequently colliding.

References

¹Work partially funded by the National Aeronautics and Space Administration under Order H-38280A.

²Abstract of ORNL-TM-2561 (July 25, 1969) and *Phys. Letters* **30B**(5), 300 (1969).

4.4 ABSORPTION, CHARGE-EXCHANGE, AND DOUBLE-CHARGE-EXCHANGE REACTIONS OF π -MESONS WITH COMPLEX NUCLEI: COMPARISON OF THEORETICAL PREDICTIONS WITH EXPERIMENTAL RESULTS^{1,2}

H. W. Bertini

The two-step intranuclear-cascade evaporation model is used in the calculation of nucleon spectra, particle multiplicities, and radiochemical cross sections following stopped π^- absorptions by complex nuclei. The nucleon spectra and particle multiplicities from the pion absorption by light elements are, in general, predicted quite well. The theoretical particle yields from the heavy elements are overestimated, and the

particle spectra are too soft. These discrepancies are attributed to an insufficient number of pion absorptions near the edge of the nucleus for the heavy elements in the theoretical model. The magnitudes of the theoretical radiochemical cross sections from slow π^- absorption by iodine are in fair agreement with those from experiments, but the peak in the cross-section distribution vs isotope mass for some of the isotopes appears at lower mass values than the measured ones. This discrepancy is consistent with those above. The model does well in predicting the charge-exchange cross section but does poorly in estimating the double-charge-exchange cross section for pions with energies below 200 MeV. These cross sections represent about 1% or less of the total interaction cross section, and the theoretical model does not accurately reproduce such events in general.

References

¹Work partially funded by the National Aeronautics and Space Administration under Order H-38280A.

²Abstract of ORNL-TM-2699 (July 14, 1969) and *Phys. Rev.* **1**(2), 423 (1970).

4.5 AN EXTRAPOLATION METHOD FOR PREDICTING NUCLEON AND PION DIFFERENTIAL PRODUCTION CROSS SECTIONS FROM HIGH-ENERGY (>3 GeV) NUCLEON-NUCLEUS COLLISIONS^{1,2}

T. A. Gabriel R. G. Alsmiller, Jr.
M. P. Guthrie

An extrapolation procedure which relates the differential cross sections for nucleon and pion production from nucleon-nucleus collisions at energies >3 GeV to the differential cross sections for nucleon and pion production from 3-GeV nucleon-nucleus collisions is described. Calculated results for 3-GeV nucleon-nucleus collisions obtained from the intranuclear-cascade model of nuclear reactions are used in conjunction with the extrapolation procedure to obtain differential cross sections which may be compared with the experimental data from high-energy (12.5 to 70 GeV) collisions. In some instances the agreement between the calculated and the experimental data is very good, but this is not always the case.

References

¹Work partially funded by the National Aeronautics and Space Administration under Order H-38280A.

²Abstract of ORNL-4542 (May 1970).

4.6 CALCULATION OF THE NEUTRON SPECTRA FROM PROTON-NUCLEUS NONELASTIC COLLISIONS IN THE ENERGY RANGE 15-18 MeV AND COMPARISON WITH EXPERIMENT^{1,2}

R. G. Alsmiller, Jr. O. W. Hermann³

The energy distribution of neutrons from proton-nucleus nonelastic collisions for 18-MeV protons on ¹⁴N, ²⁷Al, ⁵⁶Fe, ¹⁸¹Ta, and ²⁰⁸Pb and for 15-MeV protons on ²⁷Al and ²⁰⁸Pb has been calculated with the intranuclear-cascade evaporation model of nuclear reactions and with the evaporation model of nuclear reactions. Comparisons between the calculated neutron spectra and experimental data are presented, and it is shown that neither model is entirely reliable in the energy region considered, but that the intranuclear-cascade evaporation model is the more reliable of the two.

References

¹Work partially funded by the National Aeronautics and Space Administration under Order H-38280A.

²Abstract of ORNL-TM-2752 (Sept. 15, 1969) and *Nucl. Sci. Eng.* **40**, 254 (1970).

³Computing Technology Center, Union Carbide Corp., Oak Ridge, Tenn.

4.7 CALCULATION OF THE PHOTON-PRODUCTION SPECTRUM FROM PROTON-NUCLEUS COLLISIONS IN THE ENERGY RANGE 15 TO 150 MeV AND COMPARISON WITH EXPERIMENT^{1,2}

Y. Shima³ R. G. Alsmiller, Jr.

Calculations of the differential photon-production cross sections from proton-nucleus collisions in the energy range 15 to 150 MeV have been carried out and compared with experimental measurements on ¹²C, ¹⁶O, ²⁷Al, and ⁵⁶Fe. The calculations are based on the intranuclear-cascade evaporation model of nuclear reactions and simple assumptions about the deexcitation of excited nuclei. The calculated total photon-production cross sections are within roughly a factor of 2 of the experimental values, but the calculated photon spectra are not in good agreement with the experimental spectra.

References

¹Work partially funded by the National Aeronautics and Space Administration under Order H-38280A.

²Abstract of ORNL-TM-2908 (Nov. 20, 1969); submitted for journal publication.

³Present address: Soreq Nuclear Research Center, Yavne, Israel.

4.8 ELECTROMAGNETIC- AND NUCLEAR-CASCADE CALCULATIONS AND THEIR APPLICATION IN SHIELDING AND DOSIMETRY^{1,2}

R. G. Alsmiller, Jr.

Some of the more recent studies conducted at the Oak Ridge National Laboratory in the areas of high-energy shielding and dosimetry are reviewed. The subjects considered are electron-photon cascades, photonucleon and photopion production, nucleon-meson cascades, and muon transport.

Calculated results on the dose in tissue from electrons in the energy range 0.1 to 20 GeV and from photons in the energy range 0.01 to 20 GeV are presented, and the calculated dose as a function of depth for 5.2-GeV electrons normally incident on a tissue slab is compared with experimental dose-vs-depth results.

An essential element in calculating the shielding requirements of electron accelerators is the determination of the energy and angular distributions of nucleons and pions from high-energy photon-nucleus nonelastic collisions. A model for calculating these distributions is briefly described, and calculated results are presented and compared with experimental results for photons in the energy range 50 to 350 MeV.

Nucleon-meson cascade calculations carried out using Monte Carlo techniques are described. In particular, the determination of the radioactive residual nuclei induced in matter by a high-energy nucleon-meson cascade is discussed, and comparisons between experimental and calculated data for 1- and 3-GeV protons incident on a very thick iron target are given. Calculated results on the energy deposition in tissue for 525-MeV neutrons are also presented and compared with experimental data.

The use of Monte Carlo methods to study the properties of nucleon cascades is often unsatisfactory because of the poor statistical accuracy which can be achieved in deep-penetration problems. To avoid these statistical difficulties, the applicability of the method of discrete ordinates to the study of nucleon cascades has been considered. Results obtained using the method of discrete ordinates are presented and compared with similar results obtained using Monte Carlo methods.

In the shielding of high-energy electron accelerators, it is often necessary to consider the transport of very high-energy muons through matter. Muon-transport calculations are discussed, and calculated results obtained with several approximations are presented and compared with experimental data on the transport of photomuons produced by 18-GeV electrons in a thick copper target through a thick iron shield.

References

¹Work partially funded by the National Aeronautics and Space Administration under Order H-38280A.

²Abstract of ORNL-TM-2722 (Aug. 15, 1969) and of invited paper presented at the Second International Conference on Accelerator Dosimetry and Experience, Stanford Linear Accelerator Center, Nov. 3-5, 1969; to be published in the Proceedings.

4.9 ELECTRON TRANSPORT WITH THE METHOD OF DISCRETE ORDINATES¹

D. E. Bartine² F. R. Mynatt²
R. G. Alsmiller, Jr. W. W. Engle, Jr.²
J. Barish²

The transport of low-energy (of the order of a few MeV) electrons through matter is important in the shielding of manned space vehicles that orbit through the Van Allen electron belt. A code that treats this transport by means of Monte Carlo methods is available,³ but because of the poor statistical accuracy which can be obtained, a nonstatistical method of calculation is needed. To fill this need, the method of discrete ordinates has been adapted to the transport of low-energy electrons.

In principle, the discrete ordinates code ANISN⁴ may be used to transport electrons by the simple expedient of introducing into the code the differential cross sections for electron-nucleus elastic collisions, electron-nucleus bremsstrahlung-producing collisions, and electron-electron collisions. In practice, however, these cross sections are quite different from those which occur in neutron transport where the method of discrete ordinates has been used extensively, and it is not clear to what extent the method may be used successfully to transport electrons. In the Monte Carlo treatment of electron transport, the individual electronic collisions are not considered, but rather the theories of multiple Coulomb scattering and continuous slowing down are used to group together large number of collisions.³

In the work reported here, the individual electronic collisions are treated except that those electron-electron collisions which result in very small energy transfers (of the order of the average ionization potential of the atom) are treated using the continuous slowing-down theory. The differential cross sections for electron-nucleus elastic collisions and electron-nucleus bremsstrahlung production are taken from standard sources.^{5,6} The differential cross section given by Moller^{5,7} is used to describe electron-electron collisions which result in large energy transfers, and the usual stopping-power formula⁸ with the energy loss due to large energy transfers subtracted out is used to treat electron-electron collisions which result in small energy transfers.

In Fig. 4.9.1 the transmitted electron spectrum given by the discrete ordinates code ANISN is compared with the experimental transmitted spectrum⁹ from 1-MeV electrons normally incident on an 0.11-g/cm²-thick aluminum slab. The calculated results are in excellent agreement with the experimental data for energies below about 0.85 MeV and are in approximate agreement for the larger transmitted energies. The applicability of the method to thicker shields and higher energies remains to be tested.

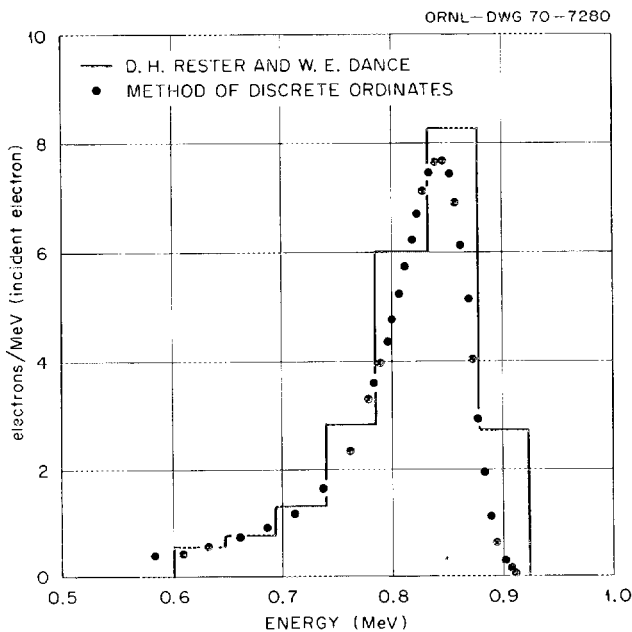


Fig. 4.9.1. Transmitted Electron Spectrum for 1-MeV Electrons Normally Incident on an 0.11-g/cm²-Thick Aluminum Slab.

References

- ¹Work funded by the National Aeronautics and Space Administration under Order H-38280A.
- ²Computing Technology Center, Union Carbide Corp. Oak Ridge, Tenn.
- ³M. J. Berger and S. M. Seltzer, *ETRAN, Monte Carlo Code System for Electron and Photon Transport Through Extended Media*, NBS-9836 (1968), NBS-9837 (1968).
- ⁴W. W. Engle, Jr., *A Users Manual for ANISN, a One-Dimensional Discrete Ordinates Transport Code with Anisotropic Scattering*, K-1693, Computing Technology Center, Union Carbide Corp., Oak Ridge, Tenn. (1967).
- ⁵C. D. Zerby and F. S. Keller, *Nucl. Sci. Eng.* **27**, 190 (1967).
- ⁶H. W. Koch and J. W. Motz, *Rev. Mod. Phys.* **31**, 920 (1959).
- ⁷C. Moller, *Ann. Physik* **14**, 531 (1932).
- ⁸M. J. Berger and S. M. Seltzer, *Tables of Energy Losses and Ranges of Electrons and Positrons*, NASA-SP-3012 (1964).
- ⁹D. H. Rester and W. E. Dance, *Investigation of Electron Interactions with Matter*, L.T.V. Report No. 0-71000/6R-18 (1966).

4.10 THE LATERAL SPREAD OF HIGH-ENERGY (≤ 400 -MeV) NEUTRON BEAMS AND EARTHSHINE¹

R. G. Alsmiller, Jr. M. L. Gritzner²
 F. R. Mynatt² J. V. Pace²
 J. Barish²

Calculated results obtained with the method of discrete ordinates are presented for the cases of zero-width beams of 100- and 400-MeV neutrons normally incident along the axis of a cylindrical shield of silicon dioxide with 5% water by weight. The results include the omnidirectional neutron flux per unit energy as a function of depth and radius in the shield and the neutron and photon dose equivalents as a function of depth and radius in the shield.

In the vicinity of well-shielded target areas of high-energy accelerators, the neutrons and photons which diffuse through the ground under the shield, "earthshine," often pose a radiation hazard. Calculated results of the earthshine in a specific geometry are presented and discussed.

References

¹Abstract of ORNL-TM-3025 (in press); to be submitted for journal publication.

²Computing Technology Center, Union Carbide Corp., Oak Ridge, Tenn.

4.11 PHOTON LEAKAGE FROM THE MOON DUE TO SOLAR-FLARE BOMBARDMENT^{1,2}

T. W. Armstrong R. G. Alsmiller, Jr.
H. S. Moran

By measuring the photon spectrum from the moon using a lunar orbiting satellite, the average lunar soil composition over large areas can be inferred.³ The lunar photon albedo arises from both galactic cosmic-ray (GCR) and solar cosmic-ray (SCR) bombardment, and knowledge of the contribution of each will aid in interpreting the measured spectrum. The photons from SCR bombardment are comprised of a prompt component, which exists only during bombardment, and a delayed component, which arises from the decay of radionuclides produced during bombardment. In the present work the time-dependent photon leakage from the moon due to the decay of radionuclides induced by SCR bombardment is calculated.

The calculations were carried out using Monte Carlo methods to determine the development of the nucleon-meson cascade, the radionuclide production, and the photon transport.^{4,5} The lunar composition as determined from the Apollo 11 flight was used.⁶

Figure 4.11.1 shows the photon leakage flux during a solar cycle due to radionuclide decay. The incident proton flux was assumed to be isotropic, and all flare spectra were taken to be exponential in rigidity. The flare intensities and characteristic rigidities used are based on the data for solar cycle 19 (1954 through 1964).⁷ Radionuclide production by previous solar cycles was taken into account by using the flare data for cycle 19 for all previous cycles.

Accurate estimates of the photon leakage due to GCR bombardment for the same composition as used here are not available. However, very approximate calculations for the basaltic-type composition give a prompt photon leakage flux approximately 100 times higher than the maximum flux given in Fig. 4.11.1 for the SCR contribution.⁸ Calculations to determine more accurately the photon leakage due to GCR bombardment are in progress.

Calculated results for the prompt photon-leakage spectra, the time-dependent photon-leakage spectra, the

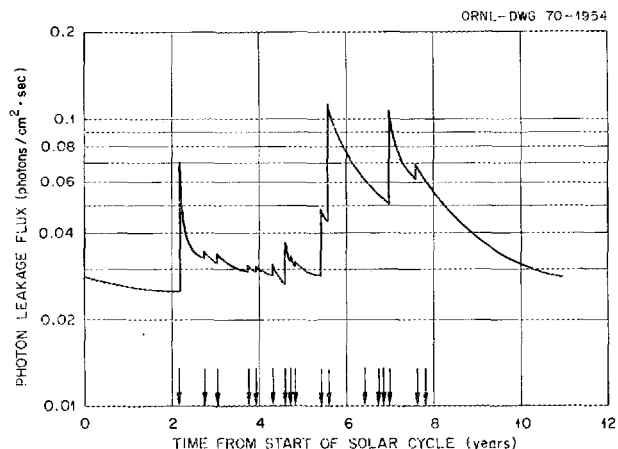


Fig. 4.11.1. Photon Leakage Flux from the Moon Arising from SCR Bombardment During Solar Cycle 19. The times at which flares occurred are indicated by arrows.

neutron-leakage spectra, the spatial distribution of produced radionuclides, and the spatial distribution of the absorbed dose and dose equivalent from SRC bombardment have also been obtained.

References

¹Work funded by the National Aeronautics and Space Administration under Order T-85613.

²Summary of paper to be presented at the American Nuclear Society Meeting, Los Angeles, Calif., June 28–July 2, 1970, and to be published in the ANS Transactions.

³Paul Gorenstein and Herbert Gursky, *Characteristic Gamma and X Radiation in the Planetary System*, ASE-2262, American Science and Engineering, Cambridge, Mass. (August 1969).

⁴W. A. Coleman and R. G. Alsmiller, Jr., *Nucl. Sci. Eng.* 34, 104 (1968).

⁵S. K. Penny, D. K. Trubey, and M. B. Emmett, *OGRE, a Monte Carlo System for Gamma-Ray Transport Studies, Including an Example (OGRE-P1) for Transmission Through Laminated Slabs*, ORNL-3805 (1966).

⁶The Lunar Sample Preliminary Examination Team, *Science* 165, No. 3899, 1211 (1969).

⁷C. E. Fichtel *et al.*, *Solar Proton Manual*, Frank B. McDonald, ed., NASA TR R-169 (1963).

⁸T. W. Armstrong and R. G. Alsmiller, Jr., *Astronautica Acta* 14, 143 (1969).

4.12 THE ABSORBED DOSE AND DOSE EQUIVALENT FROM NEUTRONS IN THE ENERGY RANGE 60 TO 3000 MeV AND PROTONS IN THE ENERGY RANGE 400 TO 3000 MeV^{1,2}

R. G. Alsmiller, Jr. T. W. Armstrong
W. A. Coleman³

Nucleon-meson cascade calculations have been carried out for monoenergetic neutrons (60 to 3000 MeV) and protons (400 to 3000 MeV) normally incident on a semiinfinite slab of tissue 30 cm thick, and the absorbed dose and dose equivalent as a function of depth in the tissue are presented. The calculated absorbed doses from 180- and 525-MeV incident neutrons and 660- and 730-MeV protons are compared with experimental data. For 525-MeV incident neutrons, the experimental and calculated absorbed doses are in good agreement, but this is not the case with the other comparisons.

References

¹Work partially funded by the National Aeronautics and Space Administration under Order H-38280A.

²Abstract of ORNL-TM-2924 (Mar. 20, 1970); submitted for journal publication.

³Work done while at the U.S. Army Nuclear Defense Laboratory, Edgewood Arsenal, Md. Present address: Science Applications, Inc., La Jolla, Calif.

4.13 THE ABSORBED DOSE AND DOSE EQUIVALENT FROM NEGATIVELY AND POSITIVELY CHARGED PIONS IN THE ENERGY RANGE 10 TO 2000 MeV¹

R. G. Alsmüller, Jr. T. W. Armstrong
B. L. Bishop

The nucleon-meson transport code NMTC has been used to calculate the absorbed doses and dose equivalents as a function of depth when broad beams of negatively charged and positively charged pions are normally incident on a 30-cm-thick slab of tissue. The method of calculation is the same as that used previously for incident neutrons and protons² except that the present results include an approximate transport calculation for the electrons and positrons that arise from muon decay. The energy deposition data for electrons were obtained from the electron-photon cascade code written by Zerby and Moran.^{3,4}

In Fig. 4.13.1 the absorbed dose and dose equivalent from 84-MeV negatively and positively charged pions

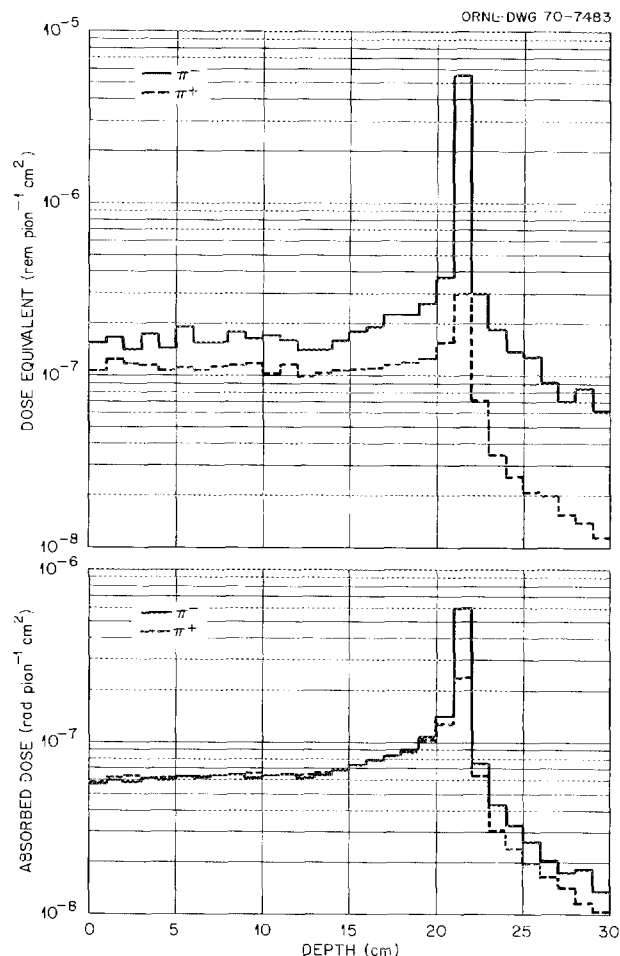


Fig. 4.13.1. The Absorbed Dose and Dose Equivalent vs Depth for 84-MeV Negatively and Positively Charged Pions Normally Incident on a 30-cm-Thick Slab of Tissue.

are shown as a function of depth. The large peak in the results for negatively charged pions arises from the low-energy particles produced when these pions are captured at the end of their range. This peak is very pronounced in the dose equivalent results because many of the particles produced by negative pion capture are heavily ionizing particles and thus have a large quality factor.⁵ The peak in the results for positively charged pions arises from the decay products produced when these pions decay at the end of their range.

Calculated results for incident pion energies of 10, 150, 500, 1000, and 2000 MeV have also been obtained.

References

¹Work partially funded by the National Aeronautics and Space Administration under Order H-38280A.

²R. G. Alsmiller, Jr., T. W. Armstrong, and W. A. Coleman, *The Absorbed Dose and Dose Equivalent from Neutrons in the Energy Range 60 to 3000 MeV and Protons in the Energy Range 400 to 3000 MeV*, ORNL-TM-2924 (197); submitted for journal publication.

³C. D. Zerby and H. S. Moran, *Studies of the Longitudinal Development of High-Energy Electron-Photon Cascade Showers in Copper*, ORNL-3329 (1962).

⁴C. D. Zerby and H. S. Moran, *A Monte Carlo Calculation of the Three-Dimensional Development of High-Energy Electron-Photon Cascade Showers*, ORNL-TM-422 (1962).

⁵M. P. Guthrie, R. G. Alsmiller, Jr., and H. W. Bertini, *Nucl. Instr. Methods* **66**, 29 (1968).

4.14 CALCULATION OF THE RADIATION HAZARD AT SUPERSONIC AIRCRAFT ALTITUDES PRODUCED BY AN ENERGETIC SOLAR FLARE – II.^{1,2}

T. W. Armstrong H. S. Moran

Calculations have been carried out to estimate the absorbed-dose and dose-equivalent rates at various depths in the atmosphere produced by an energetic solar flare – the flare of Feb. 23, 1956. The dose rates were determined both by computing flux spectra in air only and applying flux-to-dose conversion factors and by computing the dose rates in tissue for an air-tissue-air arrangement. The two methods of calculation are in reasonable agreement when the flux-to-dose factors are applied to the forward-flux spectra, but the calculations indicate that previous results obtained using omnidirectional-flux spectra overestimate the dose rates. Also, the effect of the fuel carried by a supersonic aircraft on the dose received by the passengers in the event of a solar flare has been considered and found not to be substantial.

References

¹Work partially funded by the National Aeronautics and Space Administration under Order H-38280A.

²Abstract of ORNL-TM-2844 (Dec. 31, 1969); to be published in *Nuclear Science and Engineering*.

4.15 CALCULATION OF THE RADIONUCLIDE PRODUCTION IN TISSUE BY SOLAR-FLARE BOMBARDMENT^{1,2}

T. W. Armstrong K. C. Chandler³

An accurate estimate of the dose received by astronauts in the event of solar-flare exposure is of prime importance. Preliminary investigations⁴ indicate that post-flight measurement of photons from the decay of radionuclides induced in the astronaut's body may be capable of providing a sensitive estimate of the whole-body dose received. To further investigate this method of dosimetry, calculations have been carried out to determine the dose, induced radioactivity, and time-dependent photon-leakage spectrum due to solar-flare bombardment of tissue.

The particle-transport calculations were carried out using Monte Carlo methods.⁵⁻⁷ The calculations have been performed for an isotropic flux of flare protons incident on one side of an infinite slab of tissue (whole-body composition) 30 cm in thickness. Incident protons with energies between 30 and 3000 MeV were considered, and the proton spectrum was taken to be exponential in rigidity. The time dependence of the flare spectrum was not taken into account; that is, all of the protons were assumed to be incident at the same time. From the proton and neutron flux spectra in the tissue and available experimental^{8,9} and calculated^{10,11} radionuclide production cross sections, the spatial distribution of those radionuclides with significant production was obtained. Photons from radionuclide decay were then transported to obtain the energy spectrum of those photons escaping from the face of the slab on which the protons are incident. The absorbed dose and dose equivalent in the tissue from both primary protons and all secondary particles, neutrons, protons, charged pions, photons from neutral pions, muons, electrons and positrons from muon decay, photons, and heavy nuclei, were also computed.

Figure 4.15.1 shows the photon leakage spectrum at various times after a flare. These spectra were obtained for a flare with a characteristic rigidity of 100 MV and an omnidirectional integral fluence of 1 proton/cm² above 30 MeV. The energy of the photons emitted by various radionuclides is indicated in Fig. 4.15.1. For times ≥ 10 hr, the most prominent line is due to ¹¹C ($E_\gamma = 0.51$ MeV), whereas for longer times the ⁷Be ($E_\gamma = 0.48$ MeV) line is strongest. Calculated results for the absorbed dose, dose equivalent, and the photon leakage spectra for other flare spectra have also been obtained.

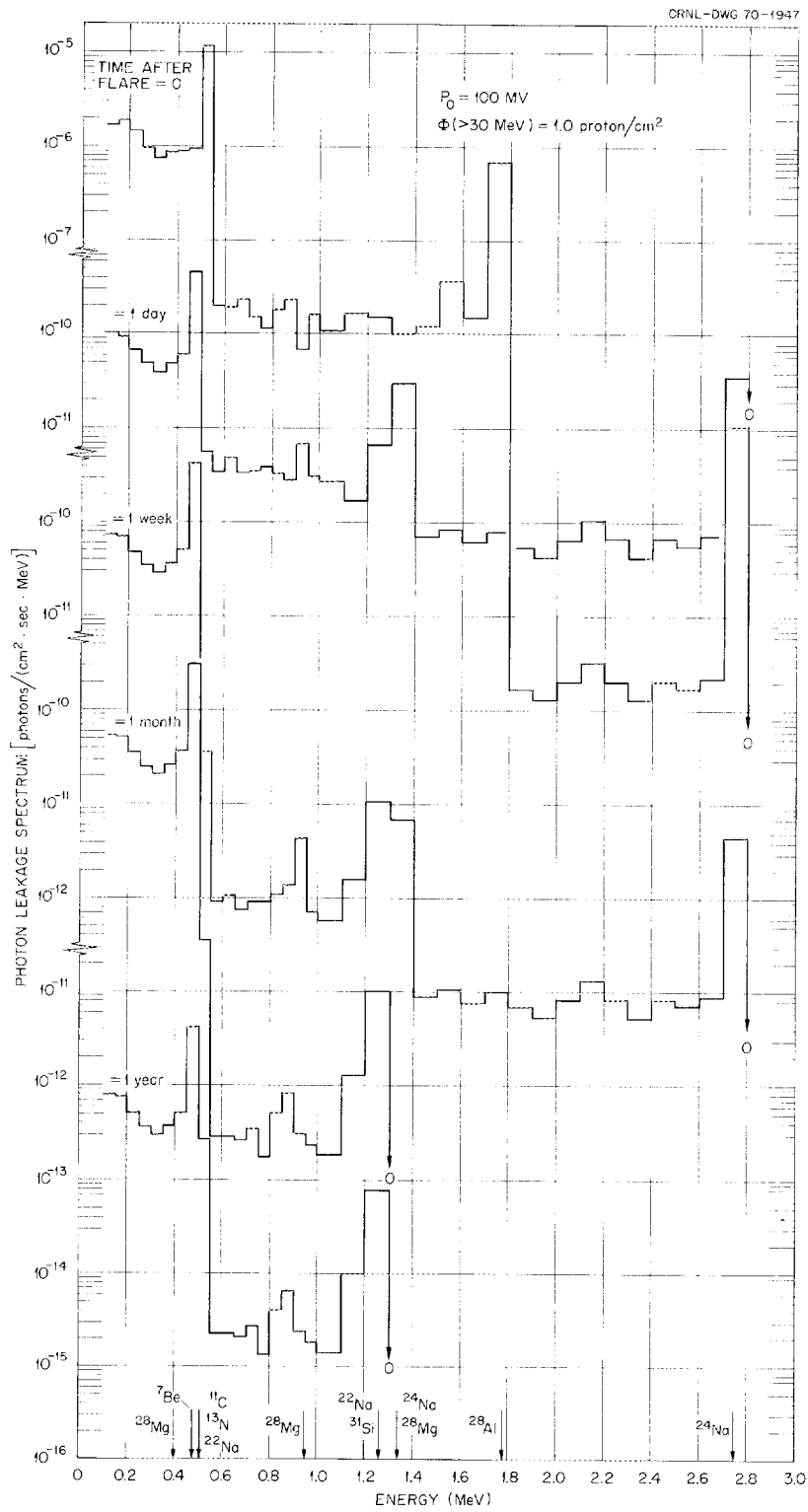


Fig. 4.15.1. Photon Leakage Spectrum at Various Times After a Solar Flare.

References

¹Work partially funded by the National Aeronautics and Space Administration under Orders H-38280A and L-12,186.

²Summary of paper to be presented at the American Nuclear Society Meeting, Los Angeles, Calif., June 28--July 2, 1970, and to be published in the ANS Transactions.

³Mathematics Division.

⁴R. L. Brodzinski, N. A. Wogman, and R. W. Perkins, *Trans. Am. Nucl. Soc.* **12**, 394 (1969).

⁵W. A. Coleman and R. G. Alsmiller, Jr., *Nucl. Sci. Eng.* **34**, 104 (1968); see also W. A. Coleman, *Thermal-Neutron Flux Generation by High-Energy Protons*, ORNL-TM-2206 (1968).

⁶D. C. Irving, R. M. Freestone, Jr., and F. B. K. Kam, *ORNL-3622*, A General-Purpose Monte Carlo Neutron Transport Code, ORNL-3622 (1965).

⁷S. K. Penny, D. K. Trubey, and M. B. Emmett, *OGRE, A Monte Carlo System for Gamma-Ray Transport Studies, Including an Example (OGRE-PI) for Transmission Through Laminated Slabs*, ORNL-3805 (1966).

⁸R. Bernas and E. Gradsztajn, *Ann. Phys.* **44**, 426 (1967).

⁹H. W. Bertini, *Phys. Rev.* **171**, 1261 (1968); see also H. W. Bertini, *Comparison of Calculated Radiochemical Cross Sections with Experimental Results for Incident Protons and π^- Mesons in the 50- to 400-MeV Region: Effect of Varying a Few Nuclear Parameters in the Calculations*, ORNL-4105 (1968).

¹⁰H. W. Bertini, H. E. Francis, and M. P. Guthrie, *Instructions for the Operation of Codes Associated with the Low-Energy Intranuclear-Cascade Calculation*, ORNL-3844 (1966).

¹¹S. G. Rudstam, *Z. Naturforsch.* **21a**, 1027 (1966).

4.16 CALCULATION OF THE NUCLEON-MESON CASCADE INDUCED IN IRON BY 19.2 GeV/c PROTONS AND COMPARISON WITH EXPERIMENT¹

T. W. Armstrong B. L. Bishop

The nucleon-meson transport code NMT,² which is restricted to energies $\gtrsim 3$ GeV, has been extended to

higher energies by using an extrapolation method³ to obtain the description of nonelastic collision products $\gtrsim 3$ GeV. This extrapolation method uses the differential cross sections for the production of nucleons and pions from 3-GeV nucleon-nucleus collisions and 2.5-GeV pion-nucleus collisions as predicted by the intranuclear-cascade evaporation model, together with energy, angle, and multiplicity scaling relations which are consistent with the sparse experimental data available for high-energy interactions, to estimate the particle production at the higher energies.

To test the validity of this new high-energy nucleon-meson transport code (HENMT), the cascade induced by a zero-width beam of 19.2-GeV/c protons incident normally on a half-space of iron has been calculated, and comparisons have been made with the experimental data obtained by Citron *et al.*⁴ for this same configuration. Comparison of the calculated and measured longitudinal development of the cascade in terms of the laterally integrated star density and track intensity is shown in Fig. 4.16.1. The calculated star density refers to nuclear interactions produced by all particles with energies >200 MeV, and the calculated track intensity consists of tracks produced by charged pions >80 MeV and protons >500 MeV. Both the calculated and measured star densities have been normalized to unity at zero depth. The agreement between calculation and experiment is reasonably good at small depths ($\gtrsim 1000$ g/cm²), but the calculation overestimates both the star density and track intensity at the larger depths.

References

¹Work partially funded by the National Aeronautics and Space Administration under Order H-38280A.

²W. A. Coleman and R. G. Alsmiller, Jr., *Nucl. Sci. Eng.* **34**, 104 (1968).

³T. A. Gabriel, R. G. Alsmiller, Jr., and M. P. Guthrie, *An Extrapolation Method for Predicting Nucleon and Pion Differential Production Cross Sections from High-Energy (>3 GeV) Nucleon-Nucleus Collisions*, ORNL-4542 (1970).

⁴A. Citron, L. Hoffman, C. Passow, W. R. Nelson, and M. Whitehead, *Nucl. Instr. Methods* **32**, 48 (1965).

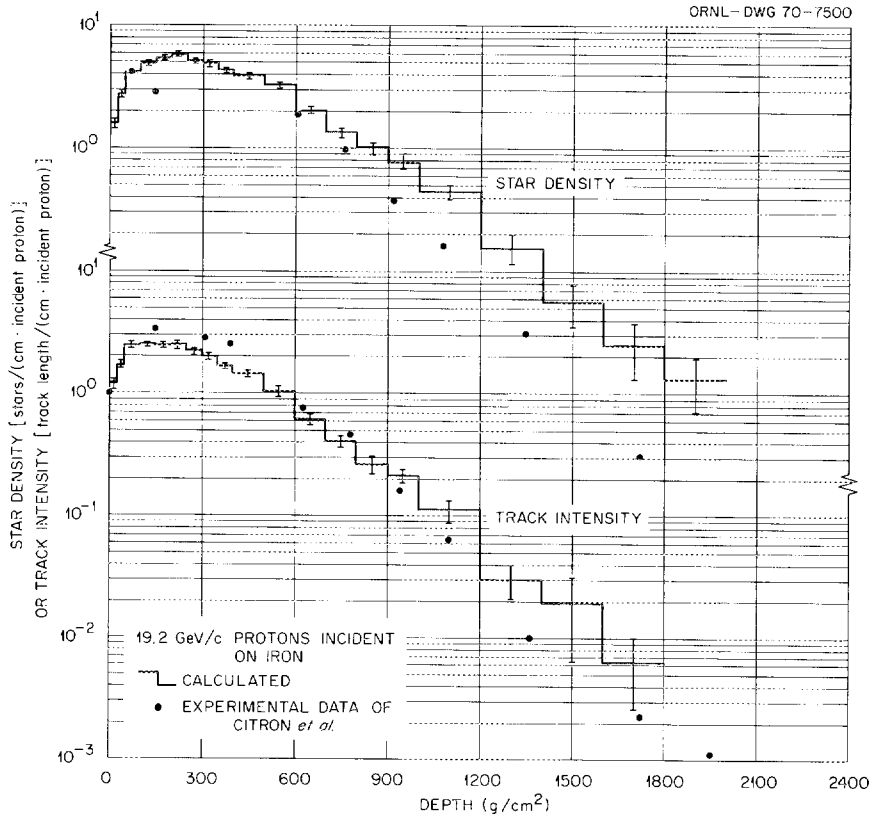


Fig. 4.16.1. Star Density and Track Intensity vs Depth. The error bars represent statistical errors of one standard deviation.

4.17 AN APPROXIMATE DENSITY-EFFECT CORRECTION FOR THE IONIZATION LOSS OF CHARGED PARTICLES^{1,2}

T. W. Armstrong R. G. Alsmiller, Jr.

An approximate density-effect correction for determining the stopping power and range of high-energy charged particles is discussed and evaluated. For a variety of materials and all particle energies, using the approximate density-effect correction, which can be easily computed for both elements and compounds, overestimates the stopping power by $\approx 6\%$ and underestimates the range by $\approx 4\%$. This error should be acceptable in many practical problems that involve materials for which the correct density effect has not been evaluated.

References

¹ Work partially funded by the National Aeronautics and Space Administration under Order H-38280A.

² Abstract of ORNL-TM-2868 (Jan. 12, 1970); to be published in *Nuclear Instruments and Methods*.

4.18 CALCULATIONS EVALUATING SEVERAL METHODS FOR REDUCING THE RESIDUAL PHOTON DOSE RATE AROUND HIGH-ENERGY PROTON ACCELERATORS¹

T. W. Armstrong J. Barish²

Calculations have been carried out to evaluate several methods for reducing the residual photon dose rate inside an accelerator tunnel due to the activation of the concrete tunnel walls by thermal neutrons from a 3-GeV proton beam located on the axis of an iron cylinder. The reduction of the thermal-neutron production of ^{24}Na in the concrete, obtained by placing cadmium and boron at the surface of the concrete and by adding boron to the concrete, is calculated. The photon dose due to the activation of the concrete is combined with the results from a previous calculation for the dose contributed by the iron to obtain the total photon dose rate inside the tunnel. The calculations were carried out by Monte Carlo methods.

References

¹ Abstract of ORNL-TM-2768 (Nov. 10, 1969) and *Nucl. Sci. Eng.* **40**, 128 (1970).

²Computing Technology Center, Union Carbide Corp., Oak Ridge, Tenn.

4.19 CALCULATED ACTIVATION OF COPPER AND IRON BY 3-GeV PROTONS¹

T. W. Armstrong J. Barish²

An estimate of the residual photon dose rate and the neutron leakage induced in an accelerator magnet by a beam of 3-GeV protons is computed. The magnet is approximated as an infinite cylinder of copper surrounded by a layer of iron, with the proton beam located on the cylinder axis. Monte Carlo methods are used to determine the development of the nucleon-meson cascade, the residual nuclei production, and the photon transport.

References

¹Abstract of ORNL-TM-2902 (Feb. 16, 1970); paper also to be published in *Nuclear Science and Engineering*.

²Computing Technology Center, Union Carbide Corp., Oak Ridge, Tenn.

4.20 CALCULATION OF THE LONG-LIVED INDUCED ACTIVITY IN SOIL PRODUCED BY 200-MeV PROTONS¹

T. A. Gabriel

Calculations have been carried out to obtain the time and spatial dependence of the long-lived induced activity in soil produced by 200-MeV protons incident on a small cylinder of graphite buried in soil. Only radioactive nuclei with half lives greater than or equal to that of ⁷Be (0.147 year) were considered. Monte Carlo methods were applied to determine the induced neutron flux which was combined with both calculated and experimental radiochemical cross sections to determine the rate of residual-nuclei production. Through the use of the results of the calculations, a procedure has been established whereby the approximate contribution of each target nucleus to the production of a particular radioactive nucleus can be obtained. The results of the calculations are also used to approximate the long-lived induced activity in soil when the small cylinder of graphite is embedded first in another material, such as iron, which is in turn surrounded by soil.

Reference

¹Abstract of ORNL-TM-2848 (Jan. 23, 1970); paper also to be published in *Nuclear Applications and Technology*.

4.21 CALCULATION OF THE LONG-LIVED INDUCED ACTIVITY IN THE SOIL AROUND HIGH-ENERGY ACCELERATOR TARGET AREAS¹

T. A. Gabriel R. G. Alsmiller, Jr.

Nucleon-meson cascade calculations have been carried out and estimates of the induced activity in the soil surrounding high-energy accelerator target areas have been obtained. Results on the contribution to the induced activity from various residual nuclei are presented for a specific irradiation time and as a function of time after beam shutdown for a 3-GeV and a 200-GeV proton accelerator. Because of the lack of particle production data at very high energies, the calculated results for the 200-GeV incident proton beam are much more approximate than those for the 3-GeV incident proton beam.

Reference

¹Abstract of ORNL-TM-3033 (in press); paper also submitted for journal publication.

4.22 HIGH-ENERGY (<18 GeV) MUON TRANSPORT CALCULATIONS AND COMPARISON WITH EXPERIMENT -- II.¹

R. G. Alsmiller, Jr. J. Barish²

Calculations of the transport of high-energy photo-muons through a very thick iron shield have been carried out. The results presented differ from those given previously in that the angular distribution of the photons which produce the photomuons is included in the calculations. It is shown that the effect of this angular distribution is small and does not account for the previously reported discrepancy between calculated and experimental results.

References

¹Abstract of ORNL-TM-2669 (July 21, 1969) and *Nucl. Instr. Meth. Letters* 75, 344 (1969).

²Computing Technology Center, Union Carbide Corp., Oak Ridge, Tenn.

4.23 CALCULATION OF THE ENERGY DEPOSITED IN THICK TARGETS BY HIGH-ENERGY (1 GeV) ELECTRON-PHOTON CASCADES AND COMPARISON WITH EXPERIMENT – II.¹

R. G. Alsmiller, Jr. H. S. Moran

Electron-photon cascade calculations have been carried out for a zero-width beam of 1-GeV electrons normally incident on semiinfinite slabs of water and aluminum. The calculated results presented here differ from those given in a previous paper in that the density-effect correction to the stopping power of matter for electrons has been taken into account. The calculated results are compared with experimental data, and it is shown that the agreement between calculated and experimental energy-deposition data is improved considerably when the density-effect correction is included in the calculations.

Reference

¹ Abstract of ORNL-TM-2843 (Jan. 15, 1970) and *Nucl. Sci. Eng.* **40**, 483 (1970).

4.24 PHOTONUCLEON AND PHOTOPION PRODUCTION FROM HIGH-ENERGY (50 TO 400 MeV) ELECTRONS IN THICK COPPER TARGETS¹

T. A. Gabriel R. G. Alsmiller, Jr.

Electron-photon cascade calculations have been carried out for high-energy electrons incident on a thick (infinite) copper target. The photon track length per unit energy from these calculations has been used in conjunction with a recently developed model of photon-nucleon and photopion production from photon-nucleus collisions to calculate the energy and angular distributions of high-energy photonucleons and photopions produced when electrons in the energy range 50 to 400 MeV are incident on a thick copper target.

Reference

¹ Abstract of ORNL-4443 (August 1969); paper also partially published in *Nucl. Phys.* **B14**, 303 (1969).

4.25 ANALYTIC REPRESENTATION OF PHOTONUCLEON AND PHOTOPION DIFFERENTIAL YIELDS RESULTING FROM HIGH-ENERGY ELECTRONS ($50 \leq E_0 \leq 400$ MeV) INCIDENT ON AN INFINITE COPPER TARGET¹

T. A. Gabriel

Analytic fits of the Monte Carlo calculated differential photoparticle yields when electrons of energy 50, 100, 200, 300, and 400 MeV are incident on an infinite copper target have been obtained by the method of linear least squares. For all of the above-mentioned electron energies, analytic expressions are given for the photoproton, photoneutron, and photopion differential yields in the target in the laboratory angular intervals defined by the incident electrons of 0–30, 30–60, 60–90, 90–120, 120–180, and 0–180 deg.

Reference

¹ Abstract of ORNL-4442 (August 1969).

4.26 THE ENERGY DISTRIBUTION OF PHOTONEUTRONS PRODUCED BY 150-MeV ELECTRONS IN THICK BERYLLIUM AND TANTALUM TARGETS¹

R. G. Alsmiller, Jr. T. A. Gabriel
M. P. Guthrie

Electron-photon cascade calculations and photoneutron-production calculations have been carried out for 150-MeV electrons on thick targets of beryllium and tantalum. The calculated neutron production spectra cover the energy range 0.01 MeV to approximately 100 MeV. Results on the photoproton production spectra are also given.

Reference

¹ Abstract of ORNL-TM-2751 (Sept. 11, 1969) and *Nucl. Sci. Eng.* **40**, 365 (1970).

5. Medium-Energy Nucleon Spectroscopic Studies

5.0 INTRODUCTION

R. W. Peelle

Scintillation neutron spectrometers based on observation of proton recoils in liquid organic scintillants have been successfully applied in the MeV region for a variety of purposes even though the necessary data analysis is quite complicated. The potential of such spectrometers for dependable operation in remote locations seems to have been demonstrated by our successful observation last year of the pulse-height spectrum induced by neutrons at the top of the atmosphere. Inferences about this "albedo" source of protons for the Van Allen belt might be drawn from knowledge of the spectrum of neutrons of several tens of MeV leaking from the atmosphere, but long flights or satellite observations will apparently be required to obtain adequate intensity for energies above 15 to 20 MeV.

Our extensive experiments to determine charged-particle spectra arising from 30- to 60-MeV protons on a series of nuclides have led to publication of tabular data for most of the cases studied, and this documentation work is continuing as a part-time activity. Final cross sections must yet be documented for the rather complete studies on targets of carbon and oxygen. The cross sections behave in an orderly manner incompletely represented, even in the continuum, by the intranuclear cascade model. We shall be challenged to elucidate this orderliness in a fully satisfactory manner with the resources at hand.

Difficult experiments are now under way to determine the companion outgoing neutron spectra from (p, xn) reactions from 40- and 60-MeV protons on a few targets. In this region of incident energy below 100 MeV, where space radiations are intense, the validity of the intranuclear cascade model has been only weakly tested for neutron production. (Though experimental tests on neutron production for higher incident energies are inconclusive or imprecise, the general validity of the model is much more sure at 500 MeV than at 50 MeV.)

Helium nuclei are present in solar flares with intensity comparable with that of the protons, though they are less able to penetrate through the skins of the space-

craft. Some data are now being analyzed giving the charged-particle cross sections induced by incident 58-MeV alpha particles, so that comparisons will be made of outgoing proton cross sections with estimates being prepared in the theoretical group. Unfortunately, the experimental program may be terminated before a critical test can be made of the corresponding spectra of neutrons from (α, xn) reactions.

5.1 MEASUREMENT OF NEUTRON SPECTRA IN THE ENERGY RANGE 2 TO 60 MeV IN THE UPPER ATMOSPHERE

W. Zobel J. T. Delorenzo¹
T. A. Love C. O. McNew¹

In the last annual report we described an engineering test flight to measure neutrons in the upper atmosphere. As a result of the experience gained in that flight, certain modifications were deemed advisable in the equipment.

The drift in the cross-over timing, which led to the abortion of the engineering test flight, was remedied by changing the delay lines in the linear amplifier to a different type with better temperature characteristics. To further ensure that we could perform pulse-shape discrimination even if other unforeseen factors caused drift in the cross-over point, we decided to telemeter the digitized linear pulse-height signal and the corresponding digitized output of the time-to-amplitude converter, which was used to determine the cross-over discrimination point, as a coupled pair. This enables us to impose the pulse-shape discrimination criteria during the analysis and vary them if required.

We had thought that the heat buildup in the electronic equipment could be cured by removing the equipment from the insulated box in which it was housed during the first flight. Tests at ORNL in an environmental chamber in which the equipment could be subjected to the reduced pressure and lowered temperature to be encountered at float altitude showed that inadequate heat transfer due to lowered convection cooling resulted in "hot spots" in the equipment with

resulting drift in the output. We therefore decided to retain the pressurized equipment box for the second flight but to rearrange the interior configuration, reducing the insulation surrounding it and making provision for cooling it by passing Freon through tubes soldered to four of its sides. This last change was made only shortly before the equipment was shipped to the launch site, and no provision was included to monitor the cooling system. We therefore do not know if, or when, it turned on during flight. The temperature in the box stayed between 32 and 52°C. A white cloth cover was draped over the top of the gondola during the flight to reduce the heat load from the sun.

The other major change was the removal of the detector from the gondola, hence from the mass that was located thereon. The $\frac{1}{8}$ -in.-thick stainless steel pressure can of the first flight was replaced by a $\frac{1}{16}$ -in.-thick aluminum can to reduce the mass surrounding the detector. Foam insulation was retained

around the can, since the detector must be kept above 15°C. The assembly, which now also included the high-voltage power supplies for the photomultipliers and the preamplifier, was lowered after launch from the gondola by a distance of ~ 90 ft. Since it was impractical to attempt to hoist it in again prior to landing, an exterior can of 16-gage sheet steel surrounded the foam insulation to take the impact expected on landing.

The flight was launched on June 17, 1969 at 0627 hours CDT from the NCAR launch site at Palestine, Texas.² The lowering of the detector was accomplished successfully shortly after launch. The system ascended at an average rate of 849 ft/min to a float altitude of 104,400 ft. The flight was terminated after floating at altitude for 9 hr and 24 min. The gondola was parachuted safely to the ground 2 miles southeast of Bronte, Texas. The equipment was recovered un-

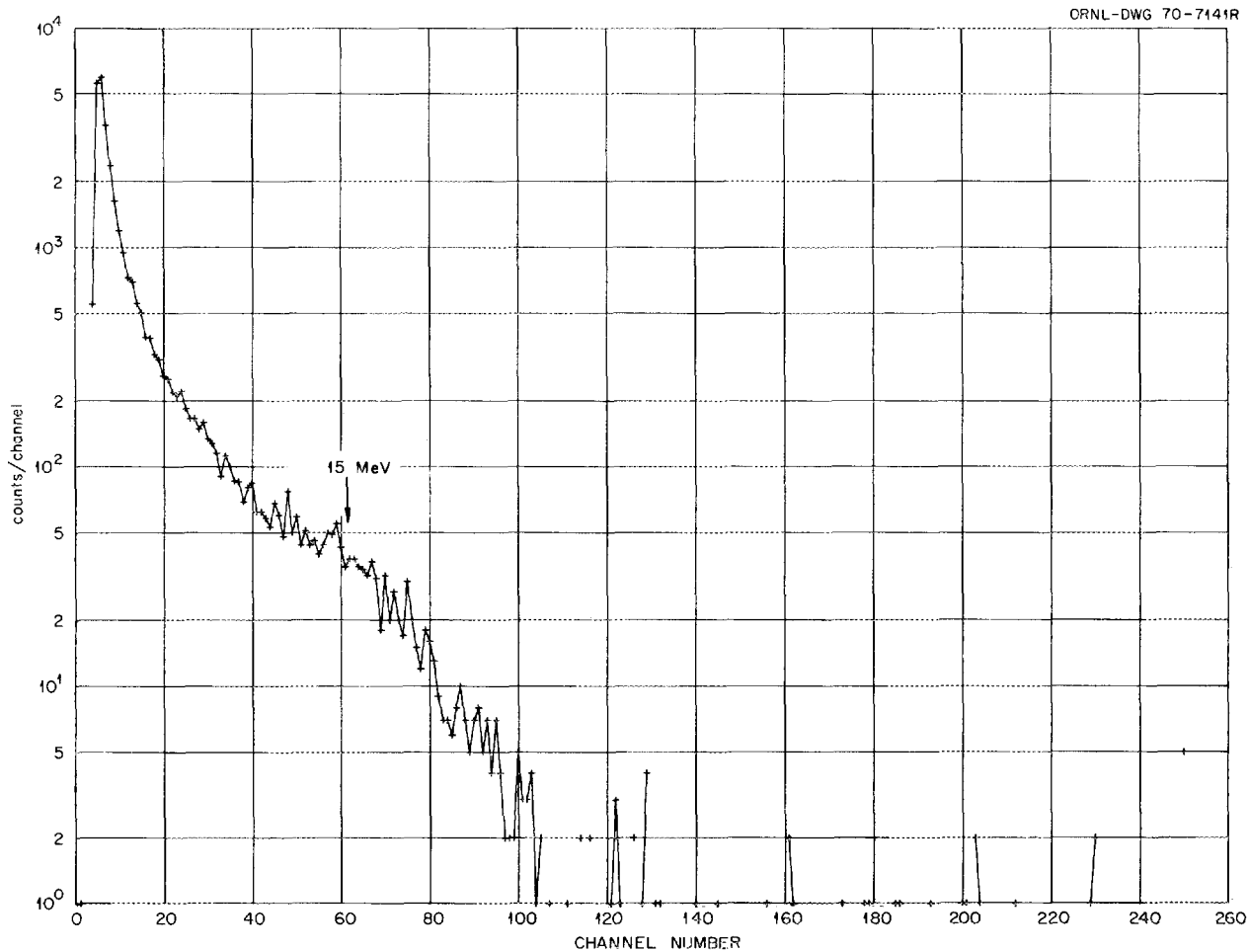


Fig. 5.1.1. Cumulative Neutron Spectrum from Balloon Flight 17, June 1969.

harmed, and after being returned to ORNL it functioned normally.

The telemetered data taken during the flight were recorded on magnetic tape in real time and were also accumulated on a TMC multichannel analyzer for monitoring purposes. The magnetic tapes from the recorder are not compatible with computers, so that some way must be devised to transform the data so that they can be analyzed. To this end, equipment was designed, built, and tested which enables us to convert the data to computer-compatible form using the division's PDP-8 computer. Suitable programs for this computer were written and debugged to accomplish this task and are currently being extended to increase their usefulness. Conversion of the data is expected to take place in the near future.

The data stored in the multichannel analyzer, while not including all the available data, were combined into

cumulative pulse-height spectra separated into neutron and gamma-ray events by using an on-board hardware-set flag. These pulse-height spectra are shown in Figs. 5.1.1 and 5.1.2 respectively. It is apparent from Fig. 5.1.1 that there are some events due to high-energy neutrons (channel 230 corresponds approximately to recoil protons of 60 MeV); it is also obvious that the time during which data were taken was quite insufficient to acquire good statistics for high-energy events.

It does not appear feasible at this time to obtain data from balloon flights lasting weeks or months. Since we are interested largely in the neutron spectrum above the atmosphere, it seems more practical to endeavor to make such measurements with equipment carried aboard a satellite. We have therefore submitted a proposal to NASA to fly a neutron spectrometer, similar to the one used in the balloon flights, aboard a proposed High Energy Astronomy Observatory. In the

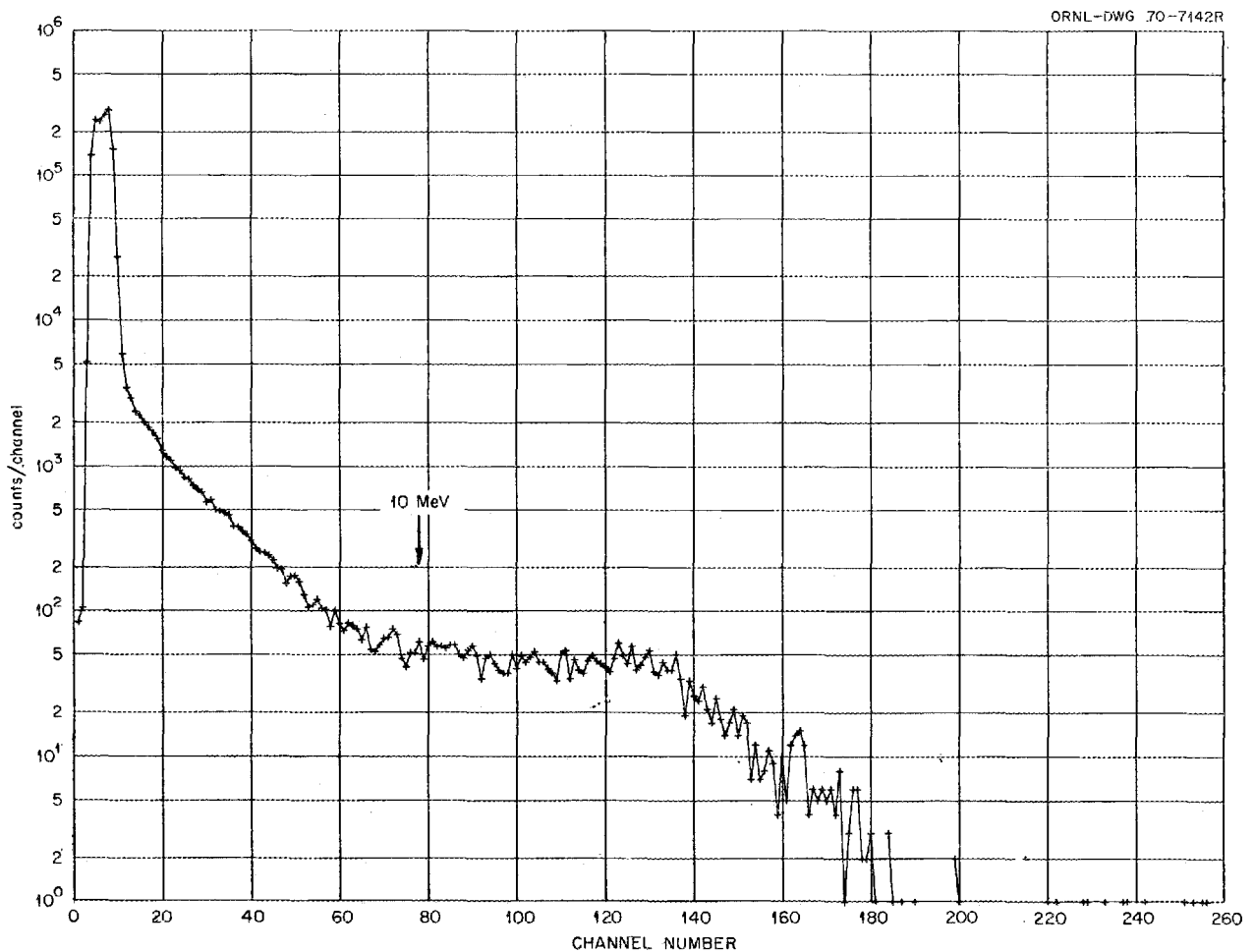


Fig. 5.1.2. Cumulative Gamma-Ray Spectrum from Balloon Flight 17, June 1969.

event that we will not be chosen to participate in the HEAO series, we expect to request consideration on other suitable spacecraft.

References

¹ Instrumentation and Controls Division.

² We wish to acknowledge the assistance for this flight of NASA which furnished the balloon and helium for the flight. In addition, through Mr. H. W. Parker and his assistants, the Marshall Space Flight Center furnished the telemetry and the battery power for all electrical equipment.

5.2 DIFFERENTIAL CROSS SECTIONS FOR HYDROGEN AND HELIUM PARTICLES FROM 30- TO 60-MeV PROTONS ON NUCLEI¹

R. W. Peelle F. E. Bertrand²

A series of experiments was performed to study the production spectra of hydrogen and helium isotopes resulting from bombardment of nuclei by incident 30- to 60-MeV protons.³ During this year major improvements have been made in the data analysis software, and a series of reports is being produced to make tabulated cross sections available.⁴ This report describes some of the qualitative findings which have become

evident from the results and from comparisons of the results against the intranuclear-cascade theory. The paragraphs below discuss the dependence of the observed cross sections on incident energy, the presence of quasifree scattering peaks, the integral spectra, the dependence on target mass number of the production of the various secondary hydrogen and helium particles, and the present ability of the cascade model with evaporation to predict the intensities of protons and alphas at low energy and at wide angles.

Figure 5.2.1 shows for a scattering angle of 30 deg from ⁵⁴Fe a comparison between experimental secondary proton differential cross sections and the predictions of the Bertini (MECC) cascade program with the consequent evaporation added in. The broad histograms are the theory. From left to right the incident proton energies are 29, 39, and 62 MeV. At the highest incident energy, the continuum regions agree very well except below 5 MeV, but at lower incident energies agreement is destroyed. This suggests the demise of the cascade + evaporation model in the 50-MeV region, a conclusion which would surprise no one. But other angles must be considered, and Fig. 5.2.2 does this by showing the differential energy spectra (integrated over angle) for the same cases. Elastic scattering has been removed. Theory is everywhere very high in the "evaporation" region and

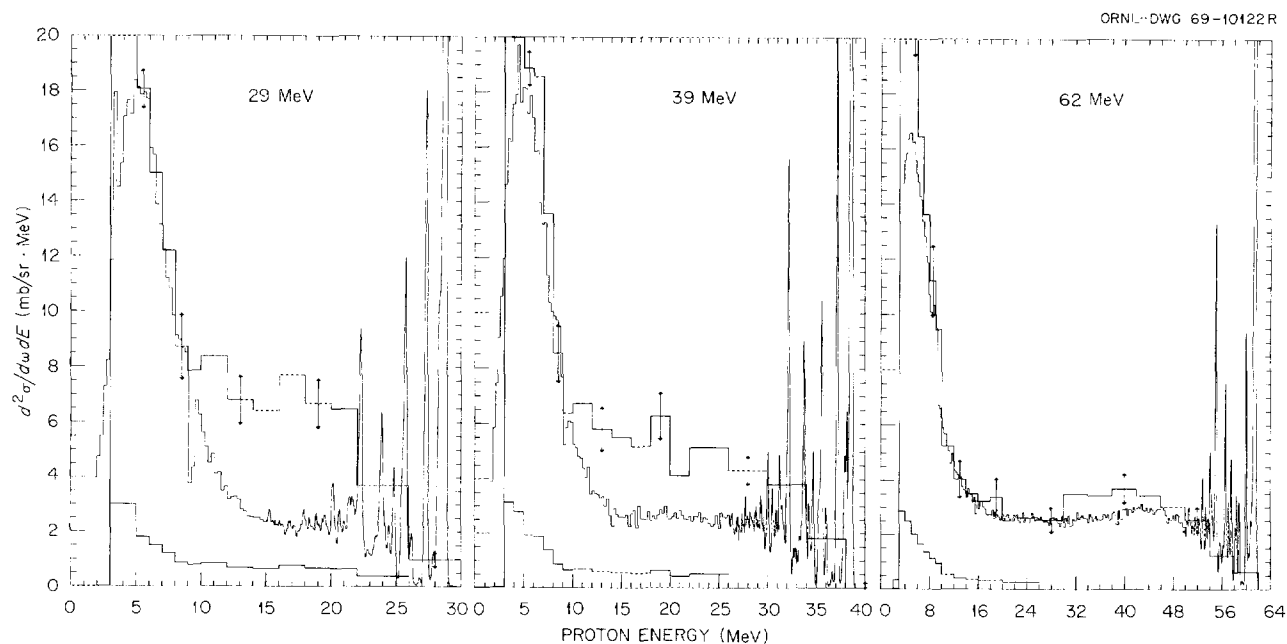


Fig. 5.2.1. Scattered Protons at 30 deg from ⁵⁴Fe for 29-, 39-, and 62-MeV Incident Protons. The histograms with the broader steps represent the Bertini cascade plus evaporation model (also shown divided by 10).

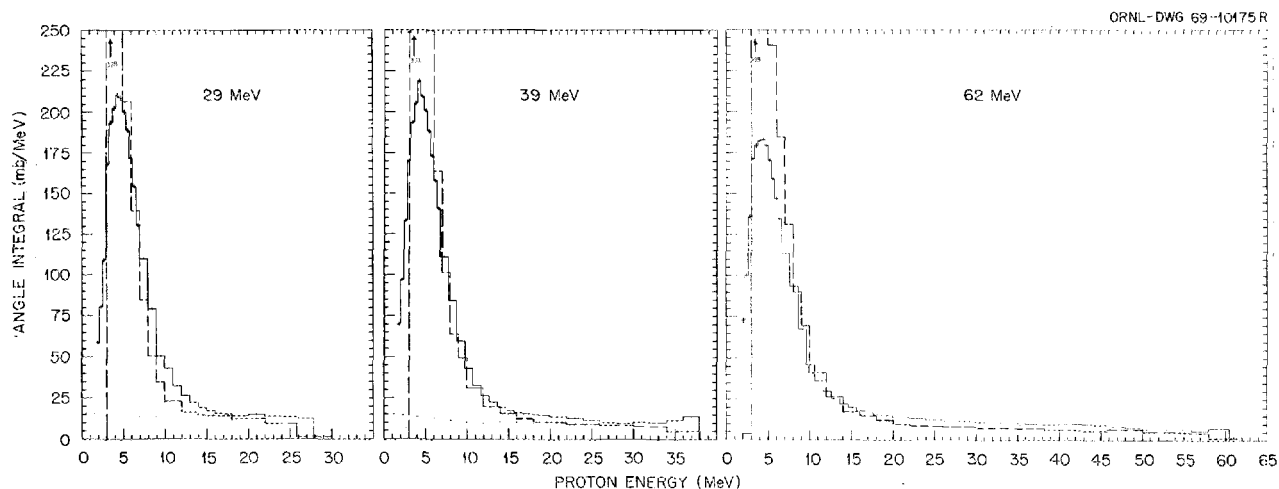


Fig. 5.2.2. Integrals over Angle of Protons Scattered from ^{54}Fe for Incident 29-, 39-, and 62-MeV Protons. The dashed histogram represents the result given by the Bertini cascade plus evaporation model.

slightly low in the continuum region, but any energy dependence of the disagreement is not marked. This pair of figures illustrates that the understanding of the energy dependence of the theory-experiment comparison will have to be approached with considerable care.

The cascade process in nuclei is based on elementary nucleon-nucleon scatterings within the nucleus, and the Bertini cascade model outputs always show the resulting quasifree scattering peaks at small angles, broadened by the momentum distribution within the nucleus. Quasifree scattering peaks have been clearly observed experimentally for incident proton energies above 300 MeV, and they appear in calculated results down to incident energies at least as low as 25 MeV. Figure 5.2.3 shows a typical comparison of our results with theory at 15 deg. The theory predicts a marked peak, while the experiment shows no sign of it. Generally, great imagination is required to see any trace of quasifree scattering in any of our data. Indeed, no experimenter has reported such a peak for incident proton energies below 100 MeV, but perhaps only two others have looked. The reason the predicted peak is "washed out" is unknown, but may be related to wave-mechanical effects of the average nuclear potential which are intentionally not included in the Bertini model.

Figure 5.2.4 shows comparisons between the cascade + evaporation model and differential energy spectra (integrated over angle) for the five observed secondary particles from 62-MeV protons on ^{27}Al . Elastic scattering has been removed. Note that the vertical scales are different for each type of outgoing particle. The proton

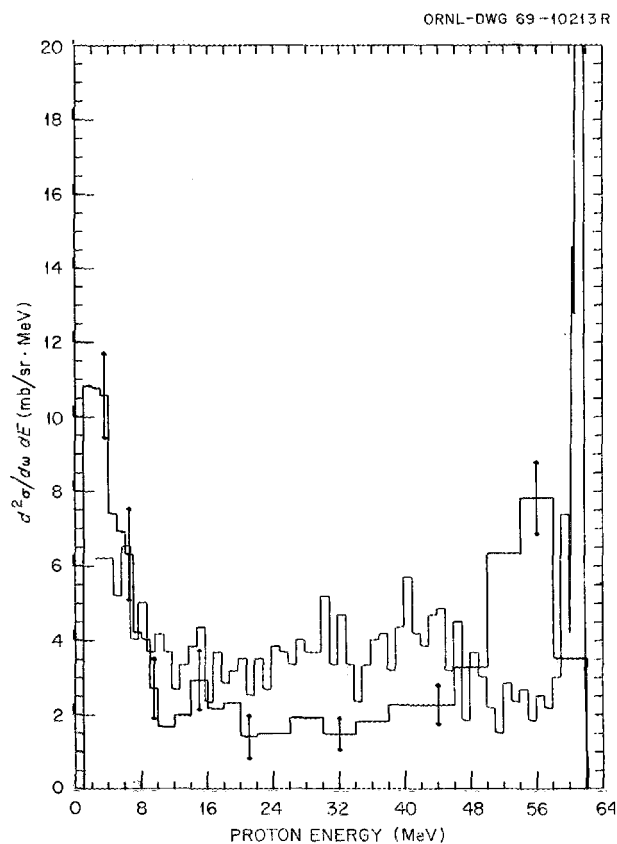


Fig. 5.2.3. Scattering of 62-MeV Protons at 15 deg from ^{27}Al Compared with Predictions of the Cascade Plus Evaporation Model Shown by the Broader-Stepped Histogram.

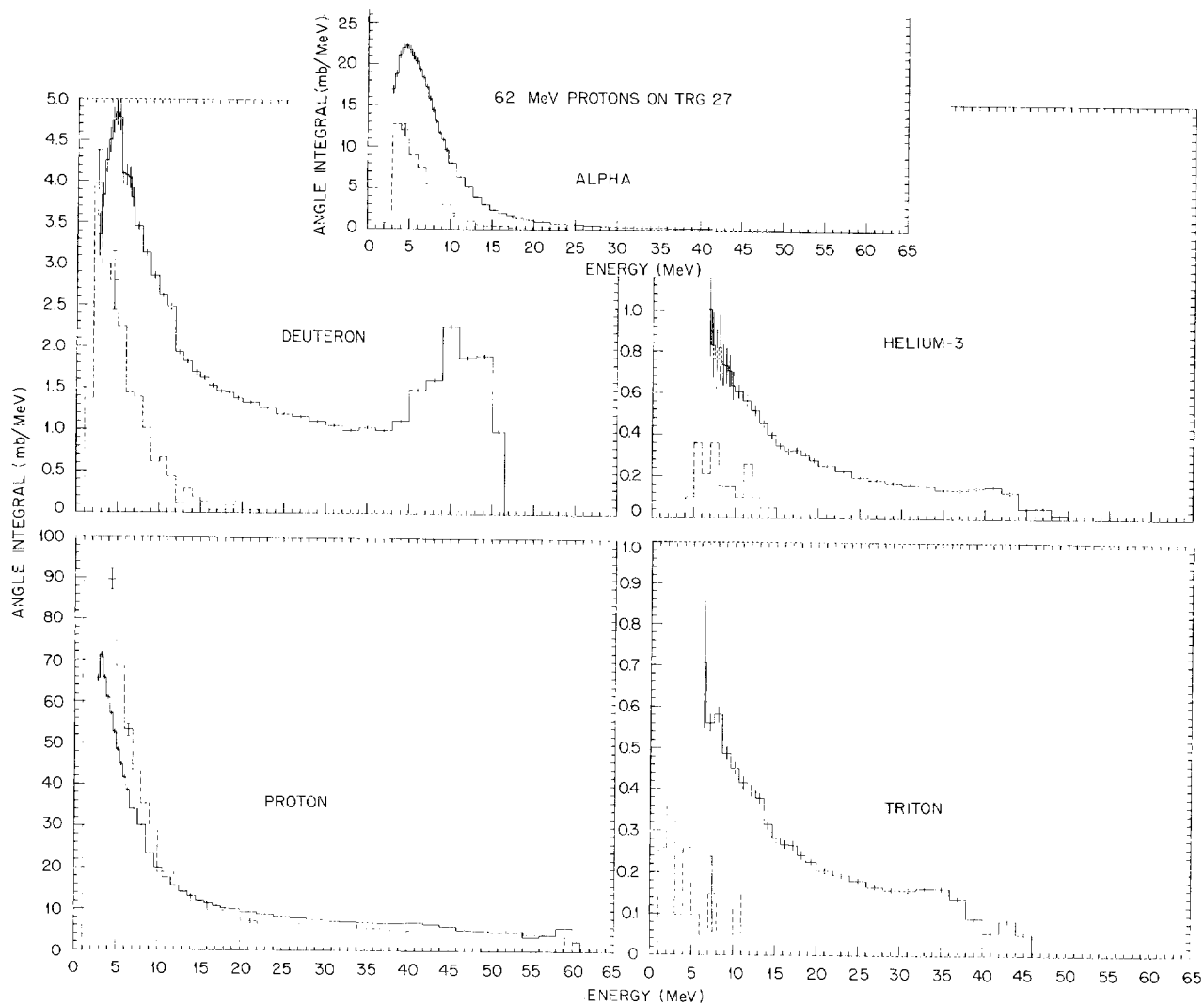


Fig. 5.2.4. Differential Energy Spectra for the Hydrogen and Helium Ions from 62-MeV Protons on ^{27}Al . The dashed distributions are from the cascade plus evaporation model.

spectrum is in better agreement than for ^{54}Fe , since there is a smaller surplus of predicted evaporation protons. For the other particles the present theory predicts only evaporation, while the experiment for ^2H , ^3H , and ^3He gives a completely different type of energy distribution. The alpha prediction is more reasonable in shape, but there is a high-energy tail in the experiment. Further, there is no easy way to bring the theory up to the experiment in the evaporation peak for any of the targets where evaporation is likely to be significant (below tin). (Since the proton and alpha-particle intensities disagree in opposite directions in the evaporation region, changes in the average post-cascade excitation energy cannot be helpful.) The low-energy deuteron peak is not seen from the heavier targets studied.

Figure 5.2.5 illustrates the dependence of the continuum cross sections on mass number for incident 62-MeV protons. For scattering at 30 deg, it shows the average observed cross section in the 20- to 30-MeV range. (This range avoids Coulomb effects and the high-energy cutoff, and the fixed detector angle was chosen because we have the greatest variety of data at 30 deg.) Note that there is some scatter in the points for a given mass region, often much larger than our estimated systematic uncertainties, but nevertheless the trends are clear. The proton cross section rises like $A^{1/3}$ up to tin (as if the length of the nuclear fringe determined the magnitude), and then becomes constant. Deuteron and alpha production cross sections are almost a fixed fraction of the proton cross section, while ^3He and ^3H show marked and opposite mass dependence. There has often been speculation about a neutron-rich "halo" around the nucleus -- could such a halo explain the observed relative A dependence for ^3H and ^3He ? The indirect pickup theory does postulate that these particles are produced largely in the nuclear fringe. The values in Fig. 5.2.5 would change if different energy and angle regions were chosen, but study so far indicates that the qualitative A dependence is relatively unchanged, at least for all forward angles.

The current cascade + evaporation theory has no mechanism for giving high-energy alpha particles. It gives some, but never enough, high-energy protons at backward angles. Figure 5.2.6 illustrates the situation for a target of ^{197}Au . At 50 deg the prediction has

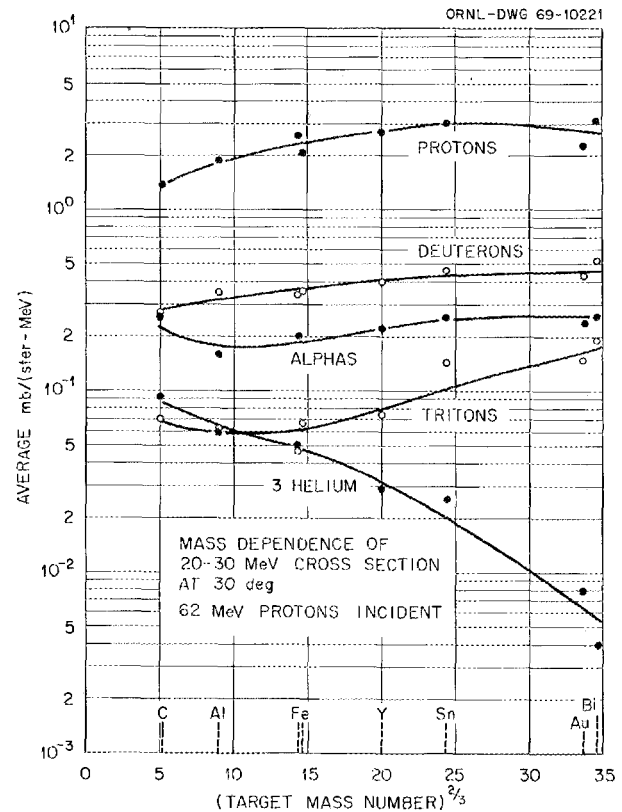


Fig. 5.2.5. A Dependence of the Observed Continuum Cross Section.

considerable validity except near the incident energy (a typical result too for other elements in this angle range), but at 100 deg the theory is "losing touch." The difference is more marked at large angles.

References

- ¹Work funded by the National Aeronautics and Space Administration under NASA Order L-12,186.
- ²Nuclear Data Group.
- ³F. E. Bertrand *et al.*, *Differential Cross Sections for the Charged Particles Produced by 60-MeV Protons on Carbon, Iron, and Bismuth*, ORNL-4274 (1968).
- ⁴See Sects. 5.4 through 5.9.

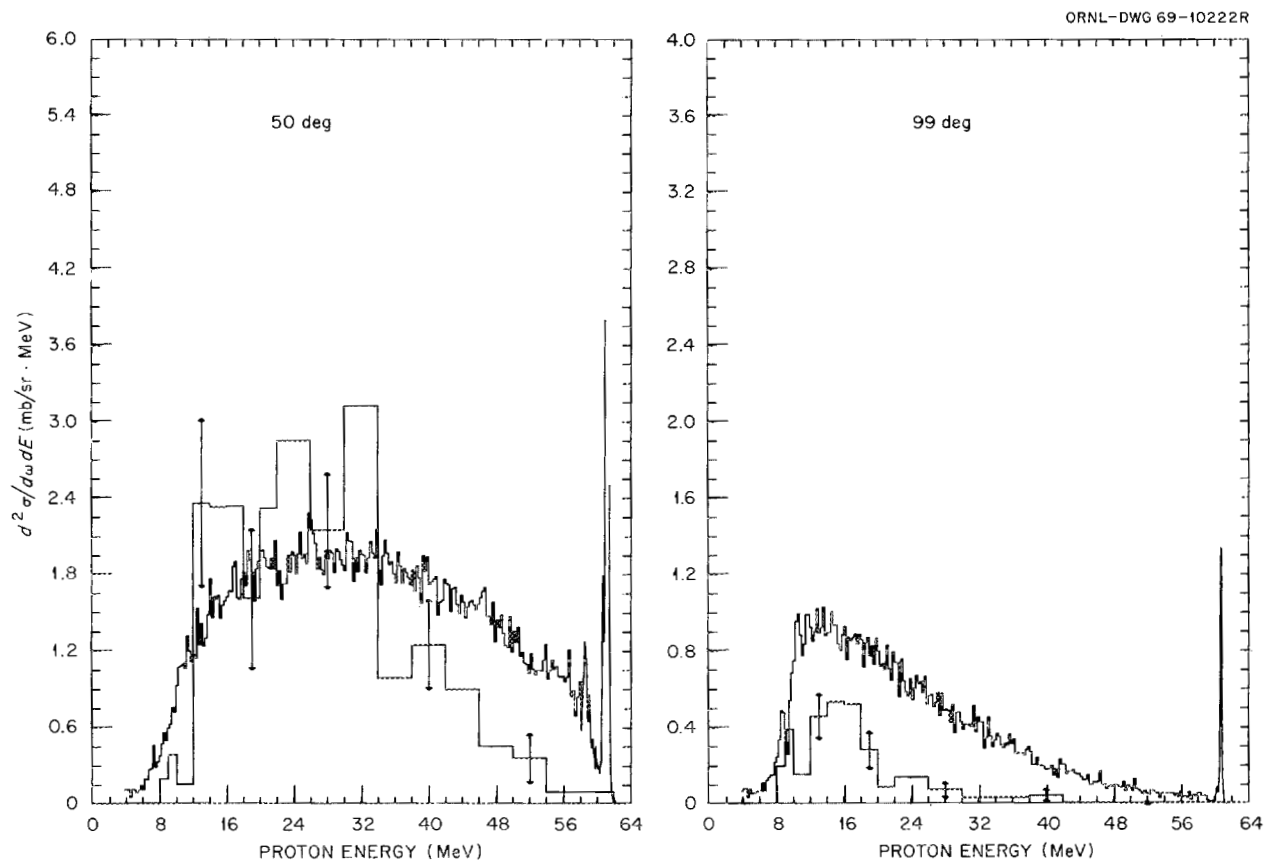


Fig. 5.2.6. Scattering of 62-MeV Protons on ^{197}Au at 50 and 99 deg. The broad histograms are given by the Bertini cascade plus evaporation model.

5.3 TABULATED CROSS SECTIONS FOR HYDROGEN AND HELIUM PARTICLES PRODUCED BY 62- AND 29-MeV PROTONS ON ^{197}Au ¹

F. E. Bertrand² R. W. Peelle

Tabulated differential cross sections are presented for the production spectra of proton, deuteron, triton, helium-3, and alpha particles from ^{197}Au bombarded by approximately 62- and 29-MeV protons. Continuum cross sections are given at six angles from 15 through 125 deg over the energy region down to a low-energy cutoff of 3 to 13 MeV which depends on particle type.

References

¹Work partially funded by the National Aeronautics and Space Administration under Order L-12,186; abstract of ORNL-4460 (December 1969).

²Nuclear Data Group.

5.4 TABULATED CROSS SECTIONS FOR HYDROGEN AND HELIUM PARTICLES PRODUCED BY 62- AND 29-MeV PROTONS ON ^{120}Sn ¹

F. E. Bertrand² R. W. Peelle

Tabulated differential cross sections are presented for the production spectra of proton, deuteron, triton, helium-3, and alpha particles from ^{120}Sn bombarded by 62- and 29-MeV protons. Continuum cross sections in ~ 1 -MeV bins are listed for 19 angles for 62-MeV incident protons and for 5 angles for 29-MeV protons. The low-energy cutoffs range from 2 to 6 MeV for the different exit particle types. Angular distributions are given for excitation by 62-MeV protons of states at 0, 1.17, and 2.38 MeV in ^{120}Sn and at 0, 0.73, 1.02, and 1.29 MeV in ^{119}Sn . Only the elastic scattering cross sections are given for incident 29-MeV protons, since there is an inadequate amount of data for angular distributions.

References

¹Work partially funded by the National Aeronautics and Space Administration under Order L-12,186; abstract of ORNL-4471 (July 1970).

²Nuclear Data Group.

**5.5 TABULATED CROSS SECTIONS FOR
HYDROGEN AND HELIUM PARTICLES
PRODUCED BY 62-MeV PROTONS
ON ⁸⁹Y¹**

F. E. Bertrand² R. W. Peelle

Tabulated differential cross sections are presented for the production spectra of proton, deuteron, triton, helium-3, and alpha particles from ⁸⁹Y bombardment by 61.5-MeV protons. Five detector angles were employed in the range 30 to 124 deg. The continuum cross sections are given from the maximum energy down to a cutoff (2 to 7 MeV) which depends on particle type. Some improvements in the analysis procedure are discussed.

References

¹Work partially funded by the National Aeronautics and Space Administration under Order L-12,186; abstract of ORNL-4450 (October 1969).

²Nuclear Data Group.

**5.6 TABULATED CROSS SECTIONS FOR
HYDROGEN AND HELIUM PARTICLES
PRODUCED BY 61-MeV PROTONS
ON ⁵⁶Fe¹**

F. E. Bertrand² R. W. Peelle

Tabulated differential cross sections are presented for the production of proton, deuteron, triton, helium-3, and alpha particles from ⁵⁶Fe bombarded by approximately 61-MeV protons. Continuum cross sections are listed at ten angles from 20 through 160 deg. Angular distributions are given for excitation of states at 0-, 0.85-, 2.66-, 3.11-, 4.55-, 5.26-, and 6.79-MeV in ⁵⁶Fe; 0-, 0.41-, 0.93-, 1.92-, 2.99-, 4.97-, and 7.86-MeV in ⁵⁵Fe; and the ground state in ⁵⁴Fe.

References

¹Work partially funded by the National Aeronautics and Space Administration under Order L-12,186; abstract of ORNL-4456 (November 1969).

²Nuclear Data Group.

**5.7 TABULATED CROSS SECTIONS FOR
HYDROGEN AND HELIUM PARTICLES
PRODUCED BY 62-, 39-, AND 29-MeV
PROTONS ON ⁵⁴Fe¹**

F. E. Bertrand² R. W. Peelle

Tabulated differential cross sections are presented for the production of protons, deuterons, tritons, helium-3, and alpha particles from ⁵⁴Fe bombarded by 62-, 39-, and 29-MeV protons. Continuum differential cross sections are listed at 20 angles for 62-MeV, 7 angles for 39-MeV, and 5 angles for 29-MeV incident protons. The low-energy cutoffs on the spectra range from 1.5 to 6 MeV for the different particle types. Angular distributions are given for excitation by 62-MeV protons of states at 0.0, 1.41, 2.55, 2.97, 3.3, 3.84, 4.28, 4.60, 4.81, 6.38, 7.25, 8.02, and 8.52 MeV in ⁵⁴Fe and at 0.0, 0.76, 1.39, 2.85, 2.99, 3.38, 3.58, 4.28, and 7.34 MeV in ⁵³Fe. Levels in ⁵²Fe at 0.0, 0.85, 4.43, 5.37, 6.1, 6.44, and 8.59 MeV were observed; however, no angular distributions are presented for these levels.

References

¹Work partially funded by the National Aeronautics and Space Administration under Order L-12,186; abstract of ORNL-4469 (February 1970).

²Nuclear Data Group.

**5.8 TABULATED CROSS SECTIONS FOR
HYDROGEN AND HELIUM PARTICLES
PRODUCED BY 62- AND 29-MeV
PROTONS ON ²⁷Al¹**

F. E. Bertrand² R. W. Peelle

Tabulated differential cross sections are presented for the production of proton, deuteron, triton, helium-3, and alpha particles from ²⁷Al bombarded by 62- and 29-MeV protons. At 62 MeV, continuum cross sections are listed at 18 angles from 12 through 160 deg, while at 29 MeV data are given at only three angles. The low-energy cutoffs on the spectra range from 3 to 6 MeV. Angular distributions are given for excitation by 62-MeV protons of states at 0, 2.2, 2.7, and 3.0 MeV in ²⁷Al and at 0, 1, 1.06, 2.07, and 4.7 MeV in ²⁶Al.

References

¹Work partially funded by the National Aeronautics and Space Administration under Order L-12,186; abstract of ORNL-4455 (November 1969).

²Nuclear Data Group.

5.9 DIFFERENTIAL CROSS SECTIONS FOR NEUTRONS FROM 40- AND 60-MeV PROTONS ON NUCLEI¹

J. W. Wachter T. A. Love
R. T. Santoro W. Zobel

The energy spectra of secondary neutrons with energies ranging from maximum down to 5 MeV emitted by targets bombarded by 40- or 63-MeV

protons were measured at the Oak Ridge Isochronous Cyclotron (ORIC) with a time-of-flight neutron spectrometer. The measurements were made on ^{12}C , ^{27}Al , ^{54}Fe , and ^{208}Pb at angles of observation of 0, 20, 45 (or 40), 60, 90, and 135 deg.

The experimental apparatus is shown schematically in Fig. 5.9.1. The pulsed proton beam from ORIC was directed through parallel metal plates which served as the capacitor of a resonant circuit. The frequency of

ORNL-DWG 70-8252

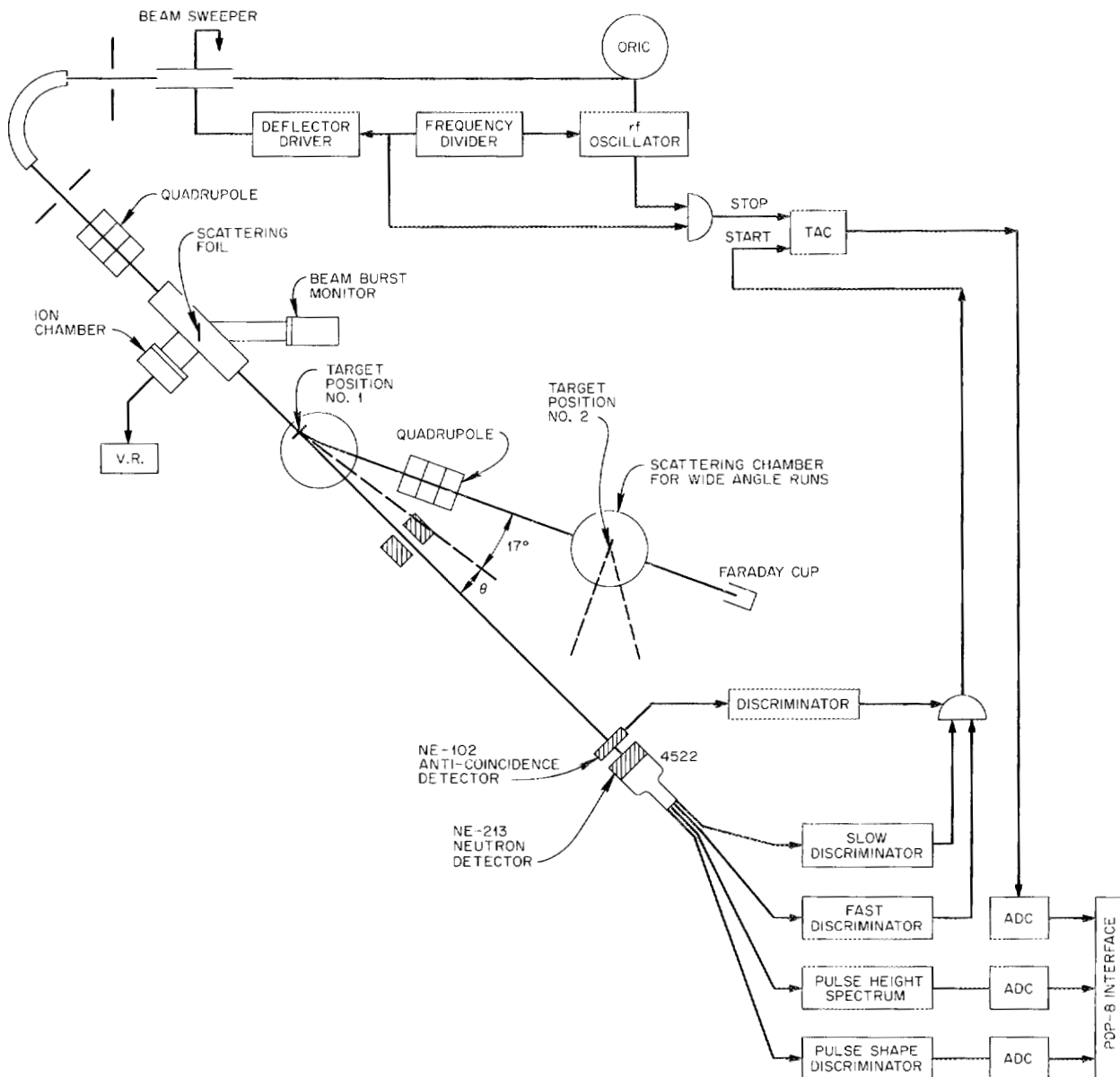


Fig. 5.9.1. Block Diagram of the Experimental Apparatus.

the circuit was a fixed fraction of the cyclotron rf frequency, so that the electric field of the capacitor deflected six of every seven proton bursts away from the entrance slit of the 153-deg analyzing magnet. The separation of successive proton bursts was thereby increased to 385 nsec for 40-MeV protons and to 308 nsec for 60-MeV protons. The analyzed beam was then focused onto the target at the entrance of a 17-deg deflection magnet. The primary proton beam was separated from the neutrons to be measured by this clearing magnet and was focused into a Faraday cup, where the integrated proton current was measured. This arrangement, with suitable shielding, was used for observation at detector angles in the range from 0 to 44 deg.

At angles greater than 44 deg, a second target position was located in the 7-m leg between the first target position and the Faraday cup. When this position was used, the target assembly at position 1 was removed and the beam refocused at position 2 by means of a quadrupole magnet between the target positions. Measurements were made at 45 deg and at all larger angles from position 2.

The proton current incident at either target position was measured by a beam intensity monitor located immediately in front of target position 1. This monitor consisted of a 0.6-mil plastic film, mounted at an angle of 45 deg to the incident proton beam, and an ion chamber located immediately below the beam pipe to measure the charged-particle flux scattered from the film. The ion-chamber charge was measured with an electrometer and integrator circuit. The total proton bombardment charge at the target was found by initial (target out) calibration against the Faraday cup. This monitor system enabled the use of thicker targets than was found possible with the Faraday cup alone. (When only the Faraday cup was used, multiple scattering had to be limited to ensure that all the primary beam was caught at the cup.)

Protons scattered at ~ 20 deg from the incident beam by the plastic foil were viewed by an NE-102² scintillator coupled to an RCA-8575 photomultiplier tube. The time distribution of the elastically scattered protons relative to the rf timing fiducial defined the time spread of the proton pulse incident on the target. This time spread, monitored during all the neutron angular distribution measurements, was observed to be of the order of 850 psec for 40-MeV protons and ~ 1.1 nsec for 60-MeV protons (including the contribution of the photomultiplier tube transit time). Therefore, the contribution to the overall timing uncertainty due to the beam was minimal. Observations of the total time

resolution for neutrons from the ${}^7\text{Li}(p,n)$ reaction indicate that the total timing uncertainty was of the order of 1 nsec, or 2% of the flight time at 40 MeV.

An additional benefit derived from this counter was that it served as a backup to the ion-chamber monitor; that is, the elastically scattered proton count rate was calibrated against the average Faraday cup current in the same manner as was the ion chamber.

As in preliminary experiments, the neutron spectrometer was a 3-in. by 3-in. NE-213² liquid scintillator centered on the face of an RCA-4522 photomultiplier tube. In this detector the light emitted by charged particles arising from interactions between the incident neutrons and the materials of the detector is measured. Charged particles incident on the face of the detector were rejected by means of a thin NE-102 detector that was mounted in front of the NE-213 neutron detector and operated in anticoincidence with it. Both neutrons and gamma rays are detected in the NE-213, and the slow light emission characteristics of the products of neutron reactions in the scintillator were used to distinguish between neutron and gamma-ray pulses. Pulse-shape discrimination was achieved with a cross-over timing circuit.

The neutron energy was inferred from its time of flight from the target. The output of a fast/slow coincidence circuit started a time-to-amplitude converter (TAC), which was subsequently stopped by a pulse derived from the rf oscillator of the cyclotron.

In order to minimize errors in the timing circuits and to facilitate data handling, the TAC output, the pulse height from the scintillator, and the output of the pulse-shape discriminator were fed to an on-line PDP-8 computer. Data were continuously recorded on magnetic tape and also displayed for monitoring during the experiment.

The computer retained all events in one-dimensional spectra for monitoring purposes but recorded on magnetic tape only a sample ($\sim 6\%$) of the gamma events so as to minimize tape-writing time. To guard against bias drifts in the electronics, all gamma events near the gamma-neutron decision line were retained. Likewise, all gamma events in which the pulse height corresponded to an energy greater than ~ 10 MeV were recorded, since high-energy protons produced by neutrons in the scintillator have slow/fast light characteristics more nearly like those of electrons than of lower-energy protons.

Postexperiment handling of the data tapes involves several distinct phases as the data are subjected to increasingly sophisticated analysis. Initially, the on-line experimental and calibrating data are scanned so as to

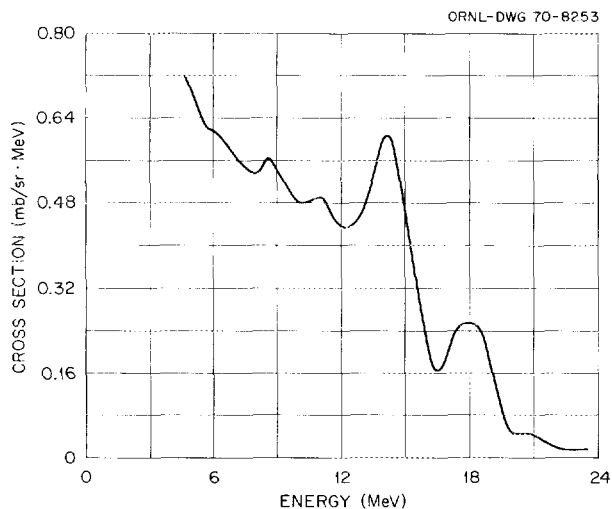


Fig. 5.9.2. Differential Cross Section for Secondary Neutrons from 39-MeV Protons on ^{12}C at 60 deg (Preliminary Data).

obtain pulse height, TAC, and slow/fast light distributions for both the neutron and the gamma samples. Analysis of these data enables correction factors to be determined for changes in the calibration and permits software bias levels to be determined for separation of neutrons and gammas on the basis of specific ranges of each of the three variables. The tapes are then re-analyzed to obtain neutron distributions in both time and pulse height.

Figure 5.9.2 shows a preliminary analysis of the $^{12}\text{C}(p,n)^{12}\text{N}$ data for 39-MeV protons. In this figure the neutron time of flight (TOF) has been inferred from the TAC data, without correction for walk, and the spectrometer efficiency has been estimated from a Monte Carlo calculation. In the figure, the peak at 18 MeV corresponds to the ground-state reaction ($Q = -18.3$). An improved efficiency estimate will be made by comparing the experimentally determined response spectra with the results of the OSS Monte Carlo calculations. Based on this comparison a lower pulse-height limit will be established for each flight time such that the experimental and theoretical responses above this limit are in agreement. The Monte Carlo results permit the estimation of the efficiency for any bias point; hence the TOF analysis can be based upon only those counts that fall in the pulse-height region for which the spectrometer efficiency is well established. Final cross sections will incorporate both walk corrections and this energy-dependent pulse-height bias.

References

¹Work funded by the National Aeronautics and Space Administration under Order L-12,186.

²Product of Nuclear Enterprises, Inc., San Carlos, Calif.

5.10 IBM-360 ROUTINES TO READ AND WRITE PDP-8 MAGNETIC TAPES^{1,2}

J. W. Wachter T. J. Tyrrell³

A package of FORTRAN IV and assembly language routines has been written to assist the IBM-360 programmer in the reading and writing of DEC type 580 seven-track magnetic tapes. The routine PDPIN reads a tape record generated by the PDP-8 computer, rearranges the bit structure so that each 12-bit PDP-8 word is deposited in a single half-integer word, and buffers in the next record while computation proceeds on the current record. The routine PDPOU reverses the process. Additional routines print the integer PDP-8 words in octal representation, convert between truncated ANSI and EBCDIC, and dissect each word into an integer of specified bit length and one-bit logical variables. End-of-file marks, long or short records, and parity errors are flagged, and provision is made for optional printout of error messages and of error summary tables.

References

¹Work partially funded by the National Aeronautics and Space Administration under Order L-12,186.

²Abstract of ORNL-TM-3057 (in preparation).

³Mathematics Division.

5.11 TEDIT – TAPE EDITING PROGRAM FOR THE PDP-8^{1,2}

J. W. Wachter

PDP-8 programs are described by which teletype input-output can be diverted to magnetic tape input-output by means of intermediate buffering routines TAPEI and TAPEO. An application to the DEC Symbolic Editor permits a designated file of ASCII card images to be called from the magnetic tape and appended to or inserted into the text buffer of the editor. Similarly, magnetic tape files can be updated from the editor. The PAL III assembler has been changed to read from magnetic tape and to allow an arbitrary number of such files to be processed as a single assembly.

References

¹Work funded by the National Aeronautics and Space Administration under Order L-12,186.

²Abstract of ORNL-TM-3058 (in preparation).

Publications and Papers Presented at Scientific Meetings

PUBLICATIONS

ABBOTT, L. S., H. C. CLAIBORNE, and C. E. CLIFFORD, Editors

Weapons Radiation Shielding Handbook

Chapter 6, "Methods for Predicting Radiation Fields Produced by Nuclear Weapons," by W. Selph and M. B. Wells, DASA-1892-4 (December 1969) (Classified).

Chapter 2, "Basic Concepts of Radiation Shield Analysis," by P. N. Stevens and H. C. Claiborne, DASA-1892-5 (June 1970).

ALSMILLER, R. G., Jr.

"Electromagnetic- and Nuclear-Cascade Calculations and Their Application in Shielding and Dosimetry," ORNL-TM-2722 (Aug. 15, 1969).

ALSMILLER, R. G., Jr., T. W. ARMSTRONG, and W. A. COLEMAN

"The Absorbed Dose and Dose Equivalent from Neutrons in the Energy Range 60 to 300 MeV and Protons in the Energy Range 400 to 3000 MeV," ORNL-TM-2924 (Mar. 20, 1970).

ALSMILLER, R. G., Jr., and J. BARISH

"High Energy (<18 GeV) Muon Transport Calculations and Comparison with Experiment - II," *Nucl. Instr. Methods Letters* **75**, 344 (1969); ORNL-TM- 2669 (July 21, 1969).

ALSMILLER, R. G., Jr., T. A. GABRIEL, and M. P. GUTHRIE

"The Energy Distribution of Photoneutrons Produced by 150-MeV Electrons in Thick Be and Ta Targets," *Nucl. Sci. Eng.* **40**, 365 (1970); ORNL-TM-2751 (Sept. 11, 1969).

ALSMILLER, R. G., Jr., and O. W. HERMANN

"Calculation of the Neutron Spectra from Proton-Nucleus Nonelastic Collisions in the Energy Range 15-18 MeV and Comparison with Experiment," *Nucl. Sci. Eng.* **40**, 254 (1970); ORNL-TM-2752 (Sept. 15, 1969).

ALSMILLER, R. G., Jr., and H. S. MORAN

"Calculation of the Energy Deposited in Thick Targets by High-Energy (1 GeV) Electron-Photon Cascades and Comparison with Experiment - II," *Nucl. Sci. Eng.* **40**, 483 (1970); ORNL-TM-2843 (Jan. 15, 1970).

ARMSTRONG, T. W. and R. G. ALSMILLER, Jr.

"An Approximate Density-Effect Correction for the Ionization Loss of Charged Particles," *Nucl. Instr. Methods* **82**, 289 (1970); ORNL-TM-2868 (Jan. 12, 1970).

"Calculation of the Residual Photon Dose Rate Around High-Energy Proton Accelerators," *Nucl. Sci. Eng.* **38**, 53 (1969).

ARMSTRONG, T. W., R. G. ALSMILLER, Jr., and J. BARISH

"Calculation of the Radiation Hazard at Supersonic Aircraft Altitudes Produced by an Energetic Solar Flare," *Nucl. Sci. Eng.* **37**(3), 337 (1969).

ARMSTRONG, T. W., and J. BARISH

"Calculation of the Residual Photon Dose Rate Due to the Activation of Concrete by Neutrons from a 3-GeV Proton Beam in Iron," *Nucl. Sci. Eng.* **38**, 365 (1970).

"Calculations Evaluating Several Methods for Reducing the Residual Photon Dose Rate Around High-Energy Proton Accelerators," ORNL-TM-2768 (Nov. 10, 1969).

"Calculated Activation of Copper and Iron by 3-GeV Protons," ORNL-TM-2902 (Feb. 16, 1970).

"Reduction of the Residual Photon Dose Around High-Energy Proton Accelerators," *Nucl. Sci. Eng.* **40**, 128 (1970).

ARMSTRONG, T. W., and H. S. MORAN

"Calculation of the Radiation Hazard at Supersonic Aircraft Altitudes Produced by an Energetic Solar Flare — II," ORNL-TM-2844 (Dec. 31, 1969).

BERTINI, H. W.

"The Masking Effect of Multiple Scattering on the Determination of the Two Nucleon Correlation from π^- Absorption Experiments," *Phys. Rev.* **30B**(5), (Oct. 27, 1969); ORNL-TM-2561 (July 25, 1969).

"Absorption Charge-Exchange and Double Charge-Exchange Reactions of Mesons with Complex Nuclei: Comparison of Theoretical Predictions with Experimental Results," *Phys. Rev.* **1**(2), 423 (February 1970); ORNL-TM-2699 (July 14, 1969).

"Intranuclear-Cascade Calculation of the Secondary Nucleon Spectra from Nucleon-Nucleon Interactions in the Energy Range 340 to 2900 MeV and Comparisons with Experiment," *Phys. Rev.* **185**, 1711 (1969).

BERTRAND, F. E., and R. W. PEELLE

"Tabulated Cross Sections for Hydrogen and Helium Particles Produced by 62-MeV Protons on ^{89}Y ," ORNL-4450 (October 1969).

"Tabulated Cross Sections for Hydrogen and Helium Particles Produced by 62-, 39-, and 29-MeV Protons on ^{54}Fe ," ORNL-4469 (February 1970).

"Tabulated Cross Sections for Hydrogen and Helium Particles Produced by 62- and 29-MeV Protons on ^{197}Au ," ORNL-4460 (November 1969).

"Tabulated Cross Sections for Hydrogen and Helium Particles Produced by 62- and 29-MeV Protons on ^{27}Al ," ORNL-4455 (November 1969).

"Tabulated Cross Sections for Hydrogen and Helium Particles Produced by 61-MeV Protons on ^{56}Fe ," ORNL-4456 (November 1969).

"Tabulated Cross Sections for Hydrogen and Helium Particles Produced by 62- and 29-MeV Protons on ^{120}Sn ," ORNL-4471 (July 1970).

BÈS, D. R., R. A. BROGLIA, R. P. J. PERAZZO, and K. KUMAR

"Collective Treatment of the Pairing Hamiltonian (I). Formulation of the Model," *Nucl. Phys.* **A143**, 1 (1970).

BOOTH, R. S.

"A Comparison of Folding and Unfolding Techniques for Determining the Gamma Spectrum from Thermal-Neutron Capture in Aluminum," ORNL-TM-2898 (Mar. 5, 1970).

"Design Considerations for an ORELA Target Using Tantalum Followed by Beryllium," ORNL-TM-2925 (Mar. 31, 1970).

BURGART, C. E., and P. N. STEVENS

"A General Method for Importance Sampling the Angle of Scattering in Monte Carlo Calculations," ORNL-TM-2890 (Mar. 3, 1970).

BURGART, C. E., E. A. STRAKER, T. A. LOVE, and R. M. FREESTONE, Jr.

"The Energy Spectrum of Photoneutrons Produced by 140-MeV Electrons Incident on Tantalum," ORNL-TM-3022 (June 17, 1970).

BURRUS, W. R., and R. M. FREESTONE, Jr.

"RESPMG, A Response Matrix Generation Code Package," ORNL-TM-2594 (Apr. 29, 1970).

CLAIBORNE, H. C., and D. K. TRUBEY

"Dose Rates in a Slab Phantom from Monoenergetic Gamma Rays," *Nucl. Appl.* **8**(5), 450 (May 1970).

COUCH, R. G., J. A. BIGGERSTAFF, F. G. PEREY, S. RAMAN, and K. K. SETH

"Spectroscopy of $^{65,67,69}\text{Ga}$ by (d,n) Reaction," *Phys. Div. Ann. Progr. Rept. Dec. 31, 1969*, p. 46, ORNL-4513.

COUCH, R. G., F. G. PEREY, J. A. BIGGERSTAFF, and K. K. SETH

"Isobaric Spin Dependence in Proton Transfer Reactions," *Phys. Letters* **29B**10 (Aug. 18, 1969).

de SAUSSURE, G.

"Analytical Description of the Neutron Cross Sections of ^{233}U Below 60 eV," ORNL-TM-2745 (Nov. 5, 1969).

de SAUSSURE, G., R. B. PEREZ, and W. N. MOORE

"Autocorrelation Technique for Determining the Average Level Spacing of the Intermediate Subthreshold Structure in the Fission Cross Section of ^{235}Pu ," *Phys. Letters* **31B**(7) (Mar. 30, 1970).

DICKENS, J. K.

" $^{28-30}\text{Si}(x,\gamma)$ Reaction for $5.3 \leq E_n \leq 9.0$ MeV," ORNL-TM-2883 (Feb. 23, 1970).

DICKENS, J. K., and R. D. BAYBARZ

"A Monoenergetic 6130-keV Gamma-Ray Source for Detector Calibration," ORNL-TM-2958 (Apr. 15, 1970).

DICKENS, J. K., and F. G. PEREY

"The $^{14}\text{N}(n,x\gamma)$ Reaction for $8.5 \leq E_n \leq 11$ MeV," *Nucl. Sci. Eng.* **40**, 346 (1970); ORNL-TM-2278 (Nov. 26, 1969).

"The $^{16}\text{O}(n,x\gamma)$ Reaction for $6.7 \leq E_n \leq 11$ MeV," *Nucl. Sci. Eng.* **40**, 283 (1970); ORNL-TM-2770 (Nov. 12, 1969).

DRESNER, L.

"A Note on the Application of Lie Groups to the Integration of First-Order Partial Differential Equations," ORNL-TM-2690 (Sept. 4, 1969).

"Motion of Elasto-Plastic Membranes Under Shock Loading," *J. Appl. Phys.* **41**(6), 25-52 (1970); ORNL-TM-2755 (Oct. 30, 1969).

"Variation of Shock Overpressure with Distance in a Shock Tube Driven by an Exploding Gas Mixture," *J. Appl. Phys.* **41**(2), 79-801 (February 1970).

FRENCH, R. L., and L. G. MOONEY

"Prediction of Nuclear Weapon Neutron Radiation Environments," RRA-M92 (Nov. 26, 1969).

FRENCH, R. L., and J. M. NEWELL

"Analysis of Initial Radiation Protection Aboard Ship," RRA-M91 (June 13, 1969).

FU, C. Y., and K. J. YOST

"A Unified Model of Deformed Odd-Odd Nuclei for Nuclear Data Generation and Analysis," ORNL-TM-2832 (Jan. 20, 1970).

GABRIEL, T. A.

"Analytic Representation of Photonucleon and Photopion Differential Yields Resulting from High-Energy Electrons ($50 \leq E_e \leq 400$ MeV) Incident on an Infinite Copper Target," ORNL-4442 (September 1969).

"Calculation of the Long-Lived Induced Activity in Soil Produced by 200-MeV Protons," ORNL-TM-2848 (Jan. 23, 1970).

GABRIEL, T. A., and R. G. ALSMILLER, Jr.

"Photonucleon and Photopion Production from High-Energy (50 to 400 MeV) Electrons in Thick Copper Targets," ORNL-4443 (September 1969).

"Photonucleon and Photopion Production from 400-MeV Electrons in Thick Copper Targets," *Nucl. Phys.* **B-14**, 303 (1969).

GABRIEL, T. A., R. G. ALSMILLER, Jr., and M. P. GUTHRIE

"An Extrapolation Method for Predicting Nucleon and Pion Differential Production Cross Sections from High-Energy (>3 GeV) Nucleon-Nucleus Collisions," ORNL-4542 (May 1970).

GWIN, R., L. W. WESTON, G. de SAUSSURE, R. W. INGLE, J. H. TODD, and F. E. GILLESPIE

"Measurements of the Neutron and Fission Absorption Cross Sections of ^{239}Pu over the Energy Region 0.02 eV to 30 keV," ORNL-TM-2598 (Oct. 7, 1969).

IRVING, D. C.

The Adjoint Boltzmann Equation and Its Simulation by Monte Carlo," ORNL-TM-2879 (May 18, 1970).

IRVING, D. C., R. G. ALSMILLER, Jr., and H. S. MORAN

"Calculation of the Energy Deposited by Nucleons in a Spherical Phantom and Comparison with Experiment," Technical Note, *Nucl. Sci. Eng.* 37, 304 (August 1969).

IRVING, D. C., and H. S. MORAN

"PLOTTER, A General-Purpose Plotting Routine," ORNL-TM-2873 (May 22, 1970).

IRVING, D. C., and G. W. MORRISON

"PICTURE: An Aid in Debugging GEOM Input Data," ORNL-TM-2892 (May 14, 1970).

JONES, G. J., D. K. TRUBEY, and J. GURNEY

"The 1969 RSIC Computer-Based Information Retrieval System in Brief," ORNL-TM-2719 (November 1969).

KINNEY, W. E.

"Finite-Sample Corrections to Scattering Data," *Nucl. Instr. Methods* 85, 15 (1970).

KINNEY, W. E., and F. G. PEREY

"Neutron Elastic- and Inelastic-Scattering Cross Sections for Co in the Energy Range 4.19 to 8.56 MeV," ORNL-4549 (June 1970).

"Neutron Elastic- and Inelastic-Scattering Cross Sections for Mg in the Energy Range 4.19 to 8.56 MeV," ORNL-4550 (June 1970).

"Neutron Elastic- and Inelastic-Scattering Cross Sections for Si in the Energy Range 4.19 to 8.56 MeV," ORNL-4517 (July 1970).

"Calculated ^{55}Fe Neutron Elastic and Inelastic Scattering and Gamma-Ray Production Cross Sections from 1.0 to 7.6 MeV," *Nucl. Sci. Eng.* 40, 396 (1970).

"Neutron Elastic- and Inelastic-Scattering Cross Sections for ^{56}Fe in the Energy Range 4.19 to 8.56 MeV," ORNL-4515 (June 1970).

KUMAR, K.

"The Prolate-Oblate Difference and Its Effect on Energy Levels and Quadrupole Moments," *Phys. Rev.* C1, 369 (1970).

KUMAR, K., and B. SORENSEN

"Derivation of the Radial Dependence of the Quadrupole Force from a Woods-Saxon Potential," *Nucl. Phys.* A146, 1 (1970).

MAERKER, R. E., and F. J. MUCKENTHALER

"Gamma-Ray Spectra Arising from Fast-Neutron Interactions in Elements Found in Soils, Concretes, and Structural Materials," ORNL-4475 (April 1970).

MARUSAK, A. L.

"Measurements of (d,n) Reactions on ^{58}Ni , ^{60}Ni , ^{62}Ni , ^{64}Ni at 5 and 10 MeV," ORNL-TM-2472 (February 1970).

MASKEWITZ, B. F., D. K. TRUBEY, H. E. COMOLANDER, H. R. HENDRICKSON, I. J. BROWN, R. W. ROUSSIN, V. A. JACOBS, C. M. ANTHONY, J. GURNEY, M. W. LANDAY, and A. B. GUSTIN

"The Information Analysis Center Concept as Developed by the Radiation Shielding Information Center in Its Computer Codes Activities," ORNL-TM-2973 (Apr. 28, 1970).

MOONEY, L. G.

"Calculations of Weapon Radiation Doses in Single-Compartment Above-Ground Concrete Structures," RRA-M93 (Nov. 26, 1969).

MOORE, N. M., R. S. BOOTH, and R. B. PEREZ

"Dispersion Relations Satisfied by the Neutron Wave Field," ORNL-TM-2942 (Apr. 9, 1970).

MYNATT, F. R.

"An Analysis of the Effect of Streaming Paths on the Radiation Shielding Capability of a Missile Silo Cover Shield," ORNL-TM-2824 (Jan. 13, 1970) (classified).

MYNATT, F. R., F. J. MUCKENTHALER, and P. N. STEVENS

"Development of Two-Dimensional Discrete Ordinates Transport Theory for Radiation Shielding," CTC-INF-952 (Aug. 11, 1969).

PEELLE, R. W., and F. C. MAIENSCHIN

"The Absolute Spectrum of Photons Emitted in Coincidence with Thermal-Neutron Fission of Uranium-235," ORNL-4457 (April 1970).

"Prompt Gamma Rays from Thermal Fission of Uranium-235," Technical Note, *Nucl. Sci. Eng.* **49**, 485 (June 1970).

PENNY, S. K.

"HELENE — A Computer Program to Calculate Nuclear Cross Sections Employing the Hauser-Feshbach Model, Porter-Thomas Width Fluctuations, and Continuum States," ORNL-TM-2590 (Aug. 18, 1969).

PEREY, C. M., R. J. SILVA, J. K. DICKENS, and F. G. PEREY

"11-MeV Proton Inelastic Scattering from Even-Even Medium Weight Nuclei," ORNL-TM-2861 (Jan. 29, 1970).

PEREY, F. G., and W. E. KINNEY

"Neutron Elastic and Inelastic Scattering Cross Sections for Na in the Energy Range of 5.4 to 8.5 MeV," ORNL-4518 (June 1970).

"Sulfur Neutron Elastic- and Inelastic-Scattering Cross Sections from 4.0 to 8.5 MeV," ORNL-4539 (June 1970).

"Calcium Neutron Elastic- and Inelastic-Scattering Cross Sections from 4.0 to 8.5 MeV," ORNL-4519 (April 1970).

"Carbon Neutron Elastic- and Inelastic-Scattering Cross Sections from 4.5 to 8.5 MeV," ORNL-4441 (December 1969).

PEREY, F. G., C. O. Le RIGOLEUR, and W. E. KINNEY

"Nickel-60 Neutron Elastic- and Inelastic-Scattering Cross Sections from 6.5 to 8.5 MeV," ORNL-4523 (April 1970).

MOCKEL, A. J., and R. B. PEREZ

"Variation of the R -Matrix," ORNL-TM-2816 (Jan. 9, 1970).

PROFIO, A. E., Editor

"Shielding Benchmark Problems," ORNL-RSIC-25 (ANS-SD-9) (1969).

RITTS, J. J., M. SOLOMITO, and P. N. STEVENS

"The Calculation of Neutron-Induced Physical Doses in Human Tissue," ORNL-TM-2991 (May 22, 1970).

"Calculation of Neutron Fluence-to-Kerma Factors for the Human Body," *Nucl. Appl.* **9**, 89 (1969).

RITTS, J. R., R. W. ROUSSIN, and I. J. BROWN

"JRMACRO: A Program for Converting Microscopic Multigroup, P_n Cross-Section Data into Corresponding Macroscopic Data for Mixtures or Compounds," ORNL-TM-3052 (March 1970).

ROUSSIN, R. W.

"Using ANISN to Reduce the DLC 100-Group Cross-Section Data to a Smaller Number of Groups," ORNL-TM-3049 (May 1969).

SANTORO, R. T., W. ZOBEL, and R. E. TEXTOR

"SMOOTHIE: A Program for Smoothing O5S Histogram Output," ORNL-TM-2597 (Nov. 5, 1969).

SCOTT, W. Wayne

"Comparisons of the Results Obtained with Several Electron-Penetration Codes," ORNL-RSIC-28 (March 1970).

SHIMA, Y., and R. G. ALSMILLER, Jr.

"Calculation of the Photon-Production Spectrum from Proton-Nucleus Collisions in the Energy Range 15 to 150 MeV and Comparison with Experiment," *Nucl. Sci. Eng.* **41**, 47 (1970); ORNL-TM-2908 (Nov. 20, 1969).

SOLOMITO, M., and H. C. CLAIBORNE

"A Simple Method for Determining a Combined Lead-Steel Shield for Shipping Casks That Is Equivalent to a Lead Shield," ORNL-TM-2591 (May 29, 1969).

STRAKER, E. A.

"Time-Dependent Neutron and Secondary Gamma-Ray Transport in Infinite Air and in Air Over Ground," ORNL-TM-2781 (Mar. 7, 1970).

"Sensitivity of Secondary Gamma-Ray Dose to Angular Distribution of Gamma Rays from Neutron Inelastic Scattering," Technical Note, *Nucl. Sci. Eng.* **41**, 147 (1970).

STRAKER, E. A., M. B. EMMETT, and C. L. THOMPSON

"Ground Heating Due to a Point Source of 12.2- to 15-MeV Neutrons at an Altitude of 50 Feet," ORNL-TM-2587 (Aug. 19, 1969).

TRUBEY, D. K.

"The Radiation Shielding Information Center --- A Technical Information Service for Nuclear Engineers," *Nucl. Eng. Design* **9**, 392 (1969).

TRUBEY, D. K., and B. F. MASKEWITZ

"Computer Codes for Shielding Calculations - 1969," *Nucl. Eng. Design* **10**, 505 (1969).

TRUBEY, D. K., and Jane GURNEY

"A Review of Multigroup Nuclear Cross Section Preparation --- Theory, Techniques, and Computer Codes," ORNL-RSIC-27 (1969).

TRUBEY, D. K., and H. E. FRANCIS

"OGRE MASTAPE --- Photon Interaction Cross Section Library and Data Handling Code," ORNL-TM-3046 (July 1969).

TRUBEY, D. K., and J. R. STOCKTON

"OGRE Cross Section Package for Using Photon Interaction Data in ENDF/B Format," ORNL-TM-2757 (Oct. 27, 1969).

WELLS, M. B., and J. D. MARSHALL

"Calculations of the Leakage into Missile Silos Exposed to Nuclear Weapons Initial Radiation," RRA-T96 (June 1969) (classified).

"Differential Neutron and Secondary Gamma-Ray Albedos for Steel-Covered Concrete Slabs: Vols. I-VI," RRA-T97-I-VI (July 10, 1969).

WESTON, L. W., and J. H. TODD

"Pulse-Shape Measurements for the Oak Ridge Electron Linear Accelerator with Gamma-Ray Detection Techniques," ORNL-TM-2833 (Jan. 20, 1970).

WRIGHT, R. A., S. N. CRAMER, and D. C. IRVING

"UKE --- A Computer Program for Translating Neutron Cross Section Data from the UKAEA Nuclear Data Library to the Evaluated Nuclear Data File Format," ORNL-TM-2880 (March 1970).

YOST, K. J., P. H. PITKANEN, and C. Y. FU

"The Calculation of Gamma-Ray Transition Probabilities in Odd-A Nuclei," *Nucl. Sci. Eng.* **39**, 379 (1970).

PAPERS

Second Symposium on the Physics and Chemistry of Fission, 28 July--1 August, 1969, Vienna, Austria.

R. B. PEREZ, G. de SAUSSURE, and W. N. MOORE: "Statistical Tests for the Detection of Intermediate Structures in the Fission Cross Sections of ^{235}U and ^{239}Pu "

International Conference on Properties of Nuclear States, August 25--30, 1969, Montreal, Canada; Proceedings published by Presses de l'Universite de Montreal, 1969.

K. KUMAR: "The Competition Between Prolate and Oblate Shapes in the $A = 190$ Region"

8th Annual ANL-AUA Faculty-Student Conference, Argonne National Laboratory, August 27, 1969, Argonne, Illinois.

J. W. WEBSTER: "Shielding Requirements of Space Flight"

RSIC Seminar Workshop, October 2, 1969, Oak Ridge, Tennessee.

W. E. FORD III, and D. H. WALLACE: "POPOP4 Multigroup Secondary Gamma-Ray Production Cross Sections -- What They Are and How to Use Them"

S. K. PENNY: "A Method for the Calculation of Multigroup Gamma-Ray Production Cross Sections"

E. A. STRAKER and D. C. IRVING: "Use of Multigroup Cross Sections in the MORSE Monte Carlo Code"

American Physical Society Meeting, October 30--November 1, 1969, Boulder, Colorado; Bull. Am. Phys. Soc. Ser. II 14(12) (1969).

Hugo W. BERTINI: "Calculation of Nuclear Reactions for Incident Nucleons and π -Mesons in the 300- to 2000-MeV Energy Range and Comparisons with Experiment"

R. W. PEELLE and F. E. BERTRAND: "Production of Hydrogen and Helium Ions by 30- to 60-MeV Protons on Nuclei"

Second International Conference on Accelerator Dosimetry and Experience, November 5--7, 1969, Stanford, California.

R. G. ALSMILLER, Jr.: "Electromagnetic- and Nuclear-Cascade Calculations and Their Application in Shielding and Dosimetry"

R. G. ALSMILLER, Jr. and H. S. MORAN: "Calculation of the Energy Deposited in Thick Targets by High-Energy (1 GeV) Electron-Photon Cascades and Comparison with Experiment"

R. G. ALSMILLER, Jr. and E. SOLOMITO: "The Transport of Neutrons Produced by 3-GeV Proton-Lead Nucleus Collisions Through a Labyrinth and Comparison with Experiment"

T. W. ARMSTRONG and J. BARISH: "Calculation of the Residual Photon Dose Rate Due to the Activation of Concrete by Neutrons from a 3-GeV Proton Beam in Iron"

T. W. ARMSTRONG and J. BARISH: "Calculation of the Residual Photon Dose Rate Induced in Iron by 200-MeV Protons"

Hugo W. BERTINI: "Calculation of Nuclear Reactions for Incident Nucleons and π -Mesons in the Energy Range 30 to 2700 MeV"

T. A. GABRIEL and R. G. ALSMILLER, Jr.: "Photonucleon and Photopion Production from High-Energy (50--400 MeV) Electrons in Thick Copper Targets"

American Nuclear Society Meeting, November 30--December 4, 1969, San Francisco, California; Trans. Am. Nucl. Soc. 12(2) (1969).

E. A. BERNARD and R. B. PEREZ: "Determination of Heterogeneous Parameters by the Neutron Wave Technique"

R. S. BOOTH and F. J. MUCKENTHALER: "The Gamma Energy Spectrum Above 1 MeV Caused by Thermal Neutron Absorption in ^{238}U "

R. S. BOOTH and W. A. SWANSIGER: "A Direct Determination of Continuum Mode Contamination in a Neutron Wave Experiment"

Calvin E. BURGART and P. N. STEVENS: "A General Method of Biasing the Angle of Scattering in Monte Carlo Calculations"

V. R. CAIN, P. N. STEVENS, and E. A. STRAKER: "The MORSE Monte Carlo Code and Its Applications"

S. N. CRAMER, V. R. CAIN, E. A. STRAKER: "Monte Carlo Graphite Benchmark Calculations Using S_n Adjoint Biasing"

G. de SAUSSURE and R. B. PEREZ: "Statistical Properties of the Resonance Parameters of the Fissile Isotopes"

W. W. ENGLE, Jr. and F. R. MYNATT: "A Shield Optimization Technique with Direct Utilization of Transport Calculations"

W. E. FORD III, and D. H. WALLACE: "The Calculation and Evaluation of POPOP4 Multigroup, Secondary Gamma-Ray Production Cross Sections"

R. L. FRENCH and L. G. MOONEY: "Prediction of Nuclear Weapon Neutron Radiation Environments"

D. C. IRVING and E. A. STRAKER: "Evaluation of the Total Cross Section of Iron"

R. E. MAERKER and F. J. MUCKENTHALER: "Gamma-Ray Spectra Arising from Thermal-Neutron Capture in Titanium, Nickel, Zinc, Chlorine, Sulfur, and a Stainless Steel"

L. G. MOONEY: "Calculations of Weapon Radiation Doses in Single-Compartment Above-Ground Concrete Structures"

F. R. MYNATT: "A Review of Some Recent Multidimensional Discrete Ordinates Shielding Calculations"

S. K. PENNY: "The Thrust of Cross-Section Data Requirements for Reactor Shielding Calculations"

R. B. PEREZ and G. de SAUSSURE: "The Calculation of the Generalized Kapur-Peierls Parameters by Expansion of the Reich-Moore Multilevel Formula"

J. J. RITTS, M. SOLOMITO, and P. N. STEVENS: "Neutron (15 MeV to Thermal) Flux-to-Dose Rate Conversion Factors for the 'Standard Man' "

E. G. SILVER: "A Brief Description of the Oak Ridge Electron Linear Accelerator"

E. G. SILVER, J. H. TODD, and J. LEWIN: "A Large Scintillation Detector for Neutron Time-of-Flight Measurements"

E. A. STRAKER, M. B. EMMETT, and C. L. THOMPSON: "Ground Heating Due to a Point Source of 12.2- to 15-MeV Neutrons at an Altitude of 50 Feet"

D. K. TRUBEY: "Kernel Methods for Radiation Shielding Calculations"

K. J. YOST: "Nuclear Data Generation and Analysis for Shielding Applications"

K. J. YOST, P. H. PITKANEN, and C. Y. FU: "Low-Energy Gamma-Ray Yields in ^{23}Na and ^{57}Fe "

American Physical Society Meeting, December 29-31, 1969, Los Angeles, California; Bull. Am. Phys. Soc., Ser. II 14(12) (December 1969).

K. KUMAR and K. J. YOST: "Preliminary Report on the Core-Quasi-Particle Coupling Scheme for Odd-A Nuclei"

American Physical Society Meeting, January 26-29, 1970, Chicago, Illinois; Bull. Am. Phys. Soc., Ser. II 15(1) (January 1970).

K. KUMAR and K. J. YOST: "The Core-Quasi-Particle Coupling in ^{13}C and ^{209}Pb "

American Physical Society Spring Meeting, April 27-30, 1970, Washington, D.C.; Bull. Am. Phys. Soc., Ser. II 15(4) (April 1970).

K. KUMAR: "The Non-Conservation of the Number of Particles in the Pairing Theory"

Semi-Annual AEC Computer Information Meeting, April 30-May 1, 1970, Washington, D.C.

B. F. MASKEWITZ: "Dissemination of Information, Codes - The Radiation Shielding Information Center"

INTERNAL DISTRIBUTION

1. L. S. Abbott
2. F. S. Alsmiller
3. R. G. Alsmiller, Jr.
4. T. W. Armstrong
5. J. Ashe
6. J. Barish (K-25)
7. R. D. Baybarz
8. H. W. Bertini
9. F. E. Bertrand
10. N. A. Betz
11. J. A. Biggerstaff
12. B. L. Bishop
13. A. L. Boch
14. R. S. Booth
15. R. T. Boughner
16. I. J. Brown
17. C. E. Burgart
18. V. R. Cain
19. K. C. Chandler
20. G. T. Chapman
21. R. O. Chester
22. H. C. Claiborne
23. F. H. S. Clark
24. C. E. Clifford
25. H. E. Comolander
26. R. G. Couch
27. R. R. Coveyou
28. S. N. Cramer (K-25)
29. C. W. Craven
30. F. L. Culler, Jr.
31. J. T. DeLorenzo
32. G. de Saussure
33. J. K. Dickens
34. L. Dresner
35. E. Eichler
36. M. B. Emmett
37. W. W. Engle, Jr. (K-25)
38. W. E. Ford III (K-25)
39. J. L. Fowler
40. K. D. Franz (K-25)
41. R. M. Freestone, Jr.
42. C. Y. Fu
43. T. A. Gabriel
44. F. E. Gillespie
45. L. W. Gilley
46. J. H. Gillette
47. N. M. Greene (K-25)
48. M. L. Gritzner (K-25)
49. Jane Gurney
50. M. P. Guthrie
51. R. Gwin
52. J. A. Harvey
53. H. R. Hendrickson
54. K. M. Henry, Jr.
55. W. O. Hermann (K-25)
56. R. F. Hibbs
57. N. W. Hill
58. L. B. Holland
59. J. L. Hull
60. R. W. Ingle
61. J. G. Jones (K-25)
62. W. H. Jordan
63. R. Keubbing
64. W. E. Kinney
65. K. Kumar
66. C. O. Le Rigoleur
67. J. Lewin
68. T. A. Lewis
69. E. C. Long (K-25)
70. T. A. Love
71. H. G. MacPherson
72. E. Madden
73. R. E. Maerker
- 74--125. F. C. Maienschein
126. J. J. Manning
127. B. F. Maskewitz
128. J. W. McConnell
129. C. O. McNew
130. J. K. Millard
131. F. J. Muckenthaler
132. F. R. Mynatt (K-25)
133. D. O. Nellis
134. C. E. Newlon
135. J. V. Pace (K-25)
- 136--137. R. B. Parker
138. J. W. Paul
139. R. W. Peelle
140. S. K. Penny
141. C. M. Perey
142. F. G. Perey
143. R. Perez
144. P. H. Pitkanen
145. H. P. Ramon
147. J. W. Reynolds

- | | |
|---------------------------|---|
| 148. R. J. Rodgers (K-25) | 173. D. H. Wallace (K-25) |
| 149. R. W. Roussin | 174. D. R. Ward |
| 150. B. W. Rust (K-25) | 175. H. Weaver |
| 151. R. D. Sabin | 176. A. M. Weinberg |
| 152. R. T. Santoro | 177. L. W. Weston |
| 153. G. R. Satchler | 178. J. E. White |
| 154. W. W. Scott | 179. L. R. Williams |
| 155. R. J. Silva | 180. D. R. Winkler |
| 156. E. G. Silver | 181. H. Q. Wright |
| 157. M. J. Skinner | 182. R. Q. Wright |
| 158. G. G. Slaughter | 183. K. Yamada |
| 159. A. H. Snell | 184. G. Young |
| 160. E. Solomito | 185. K. J. Yost |
| 161. P. H. Stelson | 186. W. Zobel |
| 162. P. N. Stevens | 187. E. R. Cohen (consultant) |
| 163. J. R. Stockton | 188. H. Feshbach (consultant) |
| 164. E. A. Straker | 189. H. Goldstein (consultant) |
| 165. D. A. Sundberg | 190. C. R. Mehl (consultant) |
| 166. R. Textor (K-25) | 191. RSIC Library |
| 167. C. L. Thompson | 192. Biology Library |
| 168. H. A. Todd | 193–196. Central Research Library |
| 169. J. H. Todd | 197–198. ORNL -- Y-12 Technical Library
Document Reference Section |
| 170. D. K. Trubey | 199--238. Laboratory Records Department |
| 171. T. J. Tyrell | 239. Laboratory Records, ORNL RC |
| 172. J. W. Wachter | |

EXTERNAL DISTRIBUTION

- 240--558. Given external Distribution
559. P. B. Hemmig, Division of Reactor Development, U.S. Atomic Energy Commission, Washington, D.C.
560. W. H. Hannum, Reactor Physics Branch, U.S. Atomic Energy Commission, Washington, D.C.
561. W. W. Grigoreiff, Assistant to the Executive Director, Oak Ridge Associated Universities, Oak Ridge, Tennessee
562. K. O. Laughon, AEC Site Representative, ORNL
563. J. A. Swartout, Union Carbide Corporation, New York, N.Y.
564. A. E. Profio, University of California, Santa Barbara, Calif.
565. F. A. R. Schmidt, Institute fur Kerenergetik, Stuttgart, Germany
566. J. J. Ritts, Westinghouse Advanced Reactor Division, Waltz Mill Site, Madison, Pa. 15663
567. A. L. Marusak, University of California, Los Alamos Scientific Laboratory, P.O. Box 1663, Los Alamos, New Mexico 87544
- 568--569. R. W. Hockenbury and R. C. Block, Rensselaer Polytechnic Institute, Troy, New York
570. D. C. Irving, 816 Legare Road, Aiken, South Carolina 29801
- 571--573. D. R. Bès, R. A. Broglia, and R. P. J. Perazzo, University of Minnesota, Minneapolis
- 574--582. N. M. Schaeffer, R. L. French, M. B. Wells, J. D. Marshall, J. M. Newell, L. G. Mooney, R. Kimmell, and J. K. Workentin; Radiation Research Associates, Inc., 3550 Hulen Street, Fort Worth, Texas 76107
583. E. A. Bernard, Los Alamos Scientific Laboratory
584. K. K. Seth, Northwestern University, Evanston, Ill.
585. M. N. Moore, San Fernando State College, Department of Physics, Northridge, Calif.
586. A. J. Mockel, University of Florida, Gainesville
587. Laboratory and University Division, AEC, ORO
588. Patent Office, AEC, ORO
- 589--820. Given distribution as shown in TID-4500 under Physics category (25 copies -- CFSTI)